IN SITU IMPULSE TEST
AN EXPERIMENTAL AND ANALYTICAL EVALUATION OF DATA INTERPRETATION PROCEDURES

DISCLAIMER

DISCLAIMER

Portions of this document may be illegible in electronic image products. Images are produced from the best available original document.

IN SITU IMPULSE TEST
AN EXPERIMENTAL AND ANALYTICAL
EVALUATION OF DATA
INTERPRETATION PROCEDURES

Manuscript Completed: August 1975
Date Published: September 1976

Shannon & Wilson, Inc. and Agbabian Associates
Seattle, Washington 98103
El Segundo, California 90245

Prepared for the U.S. Nuclear Regulatory Commission
Under Contract No. AT(04-3)-954

MASTER

ABSTRACT

Special experimental field testing and analytical studies were undertaken at Fort Lawton in Seattle, Wasington, to study "close-in" wave propagation and evaluate data interpretation procedures for a new in situ impulse test. This test was developed to determine the shear wave velocity and dynamic modulus of soils underlying potential nuclear power plant sites. The test is different from conventional geophysical testing in that the velocity variation with strain is determined for each test. In general, strains between 10^{-1} and 10^{-3} percent are achieved.

The experimental field work consisted of performing special tests in a large test sand fill to obtain detailed "close-in" data. Six recording transducers were placed at various points on the energy source, while approximately 37 different transducers were installed within the soil fill, all within 7 feet of the energy source. Velocity measurements were then taken simultaneously under controlled test conditions to study shear wave propagation phenomenology and help evaluate data interpretation procedures. Typical test data are presented along with detailed descriptions of the results. These data show that both compression and shear waves separate into two distinct repeatable waves at a distance of about 1.8 feet from the energy source. Beyond this point, wave characterististics such as amplitude, frequency, and arrival times of both P and S waves can be studied as the wave travels outward into the surrounding soil mass.

The analytical work supported the field experimentation with calculations to simulate the same "close-in" conditions and results of the experimental program. Both linear elastic and non-linear finite element calculations were carried out under this program, in which different interpretation procedures were applied to the results, in order to establish the most suitable procedure.

Additional tests were also performed to study repeatability, effects of symmetry and "shadow", prior load history, variations in hammer weight and drop height, jacking pressure, casing, P-wave, and anchor coupling.

This report presents the results of combined experimental
and analytical studies undertaken to continue development of
an in situ impulse test for the determination of the soil shear
modulus. Emphasis of the field work was directed toward making
simultaneous "close-in" field measurements at various points in
the soil surrounding the test's energy input source. From these
data, test characteristics, general soil behavior, and the wave
propagation phenomenon could be studied under ideal test con-
ditions and at shear strains in the strong motion earthquake
range. The analytical work was oriented toward supporting the
field effort through evaluation of the experimental results
combined with additional calculations to study the same close-in
behavior as the experimental test program. Both sets of results
could then be compared and together provide insight into data
interpretation procedures for this test. This work represents a
part of continuing studies to evaluate in situ soil behavior
under earthquake loading conditions. This and the other related
studies each provide important steps in the overall project for
determination of the best methods of evaluation and prediction of
soil behavior of potential nuclear power plant sites under
seismic loading conditions.

This is the fifth report prepared by the joint venture of
Shannon & Wilson, Inc., (SW), and Agbabian Associates, (AA), on
the in situ test development project. The current work was
conducted under Contract No. AT(04-3)-954 between the joint
venture (SW-AA) and the Nuclear Regulatory Commission.

A number of contributions by both members of the joint
venture assisted in conducting these research studies and in
the preparation of this report. For Shannon & Wilson, Inc. the
primary contributors were Mr. S. D. Wilson, Mr. F. R. Brown and
Mr. J. H. Troncoso. Dr. R. P. Miller was the Project Engineer

for Shannon & Wilson and is also the Project Manager for the joint venture. For Agbabian Associates, Mr. S. D. Werner was the Project Engineer, assisted by Mr. D. Van Dillen and Mr. K. Boisen. Dr. Lydik S. Jacobsen, special consultant to the joint venture, also provided valuable guidance in these studies.

IN SITU IMPULSE TEST
AN EXPERIMENTAL AND ANALYTICAL
EVALUATION OF
DATA INTERPRETATION PROCEDURES

CHAPTER 1

INTRODUCTION

1.1 STATEMENT OF PROBLEM

As more sophisticated analytical techniques are developed
to predict soil behavior under seismic loading conditions, more
accurate input parameters must likewise be provided. One of
the more important of these properties is the dynamic shear
modulus. This is determined either in the laboratory or in situ,
and its numerical value varies not only with the soil type and
its physical characteristics but also with the magnitude of the
imposed vibratory forces. The procedures for these existing
tests together with the limitations of each test are described in
a previous report (SW-AJA, 1972).

In situ measurements presently are made at strains smaller
than those produced by earthquakes, while conventional laboratory
tests are performed at strains either higher or lower than those
produced by most earthquakes. However, laboratory results may
be complicated by sample disturbance, imperfect duplication of in
situ stress conditions, and effects of stress history, structure
and cementation. In either case, extrapolation of the measured
data is required to adjust the modulus to the strains of interest.
To assure that laboratory values of moduli are consistent with
field values during large earthquakes and that extrapolation of
test data is correctly done, there existed a need to develop
an in situ test procedure to obtain moduli data at frequent depth
intervals and at strains in the strong motion earthquake range.

To address this problem, a new in situ impulse test procedure has been developed (SW-AA, 1974). This test employs a cross-hole wave propagation procedure with velocity sensors located in closely spaced adjacent borings. A schematic drawing of the basic system is shown in Fig. 1-1. The signal generating system consists of an in-hole anchor and hammer assembly which imparts an impulsive shearing load to the soil. The shape of the generated pulse is controlled by a spring located between the anchor system and the hammer, and the magnitude by the mass of the hammer and the height of drop.

With this new procedure, consistent repeatable test data at the strains of interest were obtained on a production basis from velocity transducers positioned on the anchor and in the free field soil in adjacent borings. Studies of this data provided reasonably rational procedures for interpreting the results even though all aspects of the test were not clear. However, further attempts to understand 1) the wave propagation phenomenon between the energy source and the free field sensors, 2) the motions of the anchor, and 3) the cause of minor distortions in the recorded velocity signatures revealed the "real" complexities in this seemingly simple test procedure. Therefore to provide the best and most rational interpretation of future test results, further research to develop a better understanding of the test and the data obtained was considered necessary.

1.2   APPROACH TO THE PROBLEM

To further evaluate the details of the test procedure, a research program was first developed. This program approached the problem both theoretically and experimentally. From available literature, closed form solutions of idealized cases of the test setup were reviewed primarily to establish likely attenuation rates in the near vicinity of the anchor. This was then followed by two numerical computations of the "close-in" test setup using
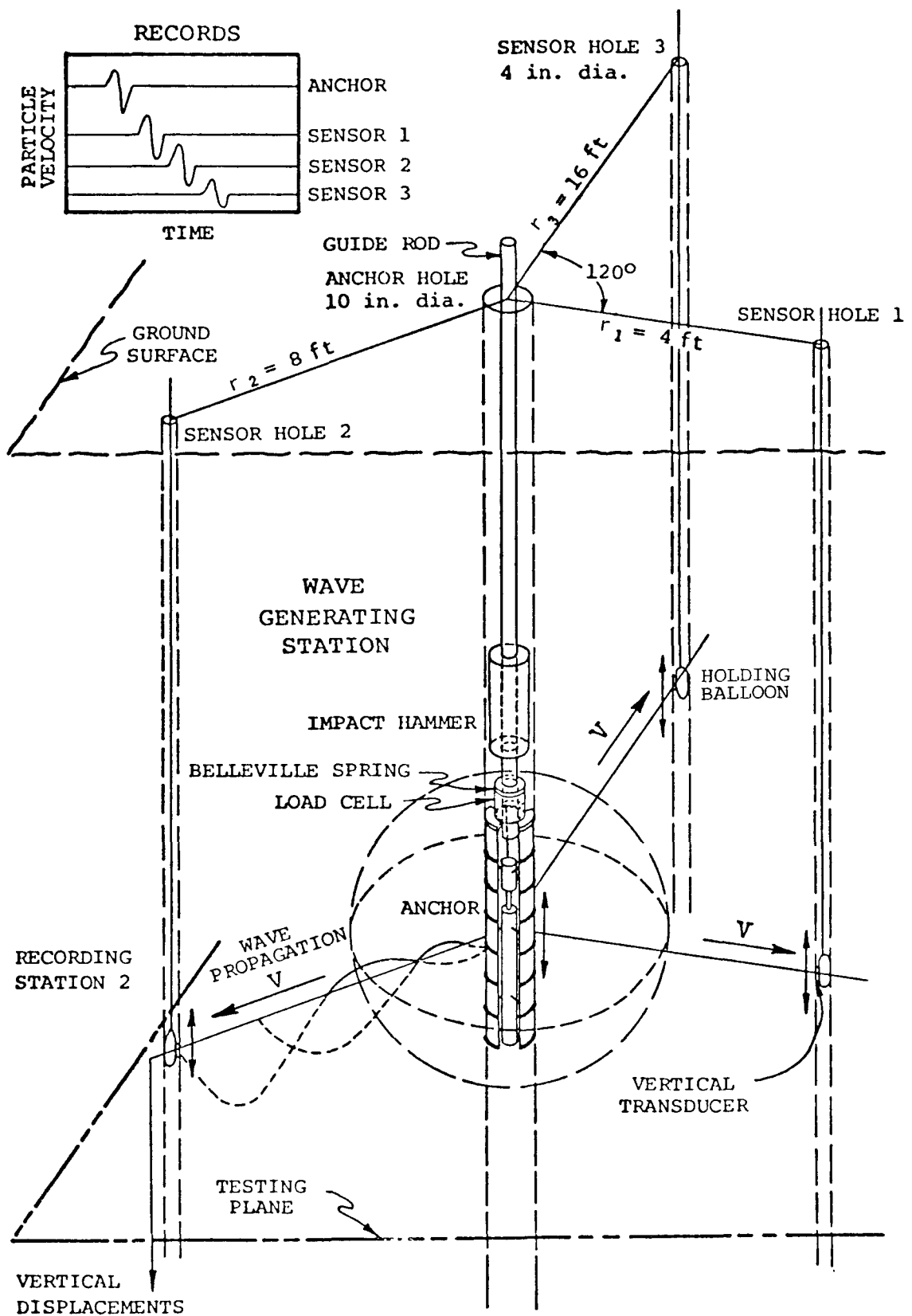
FIGURE 1-1 SCHEMATIC REPRESENTATION OF IN SITU IMPULSE TEST

finite element procedures. The first calculation was performed using linear elastic soil properties. This work was then followed by one using non-linear properties. The primary purpose of these calculations was to evaluate procedures for obtaining in situ soil properties from the test data. While these calculations cannot duplicate field test conditions exactly, they nevertheless provide important information which is used to assist in understanding the entire problem. The primary advantage of such calculations is that the input material properties provided a consistent basis for evaluating those properties obtained by applying various data processing techniques to the node point velocity histories.

A second phase of this program consisted of the measurement of detailed test data from additional tests conducted under controlled conditions in an artificial fill, constructed and instrumented for this work. This silty sand fill was placed in a 10-foot deep by 30-foot diameter pit, and manually compacted around the wave-generating station (anchor and hammer assembly) and 32 receiving stations. These stations, consisting of vertically and horizontally-oriented velocity transducers and accelerometers, were laid out in select configurations at different elevations all within seven feet from the energy source. Simultaneous tests consisting of four measurements at a time were accomplished under constant test conditions such that the propagating pulse could be studied as it travels from the source through the free-field soil. Of particular concern was the appropriate treatment of the velocity record obtained from the transducer mounted on the anchor. This record is unlike the free field sensor records in that it represents the motion of the anchor or a part of it and not necessarily the motion of the surrounding soil. Also this record is affected by 1) a stress relief due to a larger hole size, 2) slip at the anchor soil interface during the impact, and 3) the radial jacking stress exerted by the anchor against the soil wall. These results

together with the analytical calculations provide the necessary
base for an appropriate interpretation to be made and used at
production test sites.

The positioning of each of the sensors was selected such
that a number of other test parameters could be evaluated.
These include:

1) Casing effects
2) Jacking pressure effects
3) Assymmetry effects
4) P-wave effects and characteristics
5) Repeatability
6) Prior load history

Motion and force characteristics of the anchor system
were also investigated with velocity transducers, accelerometers
and a load cell. The velocity transducers and accelerometers
were installed at several different points on the anchor while
the load cell monitored the force applied by the hammer to the
top of the anchor.

The combined results of this research effort together with
a recommended simplified procedure for data interpretation,
based on these results, are presented in the chapters that follow.

1.3 SCOPE

The report is organized into six chapters with appendices.
Following this introductory section describing the extent of the
work accomplished is Chapter 2 discussing the basic test equip-
ment and procedures for obtaining and reducing production in situ
test data. Emphasis is placed on describing the test and
procedures, such that anyone interested in performing this test

would know exactly how it is done.

An analytical description of the in situ impulse test is presented in Chapter 3. This chapter attempts to identify practical problems associated with the collection of field data together with theoretical problems, inherent to the wave generation and wave propagation phenomenon.

Chapter 4 is devoted to analytical studies of the test system. This work includes two finite element calculations performed to provide realistic "close in" velocity time histories for soils with known properties. With this computed data, various procedures used to estimate strain-dependent shear moduli could be applied to check the general validity of various data interpretation procedures.

The fifth chapter discusses the results of a special experimental test program conducted in an artificial sand fill. Emphasis of the tests, like Chapter 4, was to obtain "close in" results which could be evaluated to establish rational data interpretation procedures for processing production test information. This chapter evaluates these results.

The final chapter, Chapter 6, provides a recommended procedure for interpreting production data. This information is based on the results and studies presented in Chapters 4 and 5. Also included is a brief discussion of planned future work on this particular project.

Seven appendices accompany the main text. Appendix A includes a description of the non-linear soil model used in the finite element calculations described in Chapter 4. Appendix B presents typical experimental results obtained using the pneumatic anchor described in Chapter 2. The soil properties, fill construction procedures and equipment installations at the Fort Lawton

experimental test site are included in Appendices C and D.
These appendices describe much of the details of the soil con-
ditions and test equipment installations not described in
Chapter 5.

Appendix E presents the results of a small literature review
to establish sensor spacing requirements for the experimental
test program. The final appendices, F & G, are a comprehensive
coverage of the special experimental tests and subsequent com-
parative and statistical studies conducted to evaluate the
effects of various in situ test parameters on the in situ soil
response measurements. This evaluation of the data was obtained
as a major part of the special experimental program conducted at
Fort Lawton and supplements that data provided in Chapter 5.

CHAPTER 2
IN SITU IMPULSE TEST

The development of the in situ impulse test involved
1) development of the basic test set up, 2) design and fabri-
cation of test equipment, 3) development of field testing pro-
cedures and 4) development of data processing techniques. In
previous studies, the test set-up was established through
experimentation and bench testing in shallow borings with more
simplified equipment. This testing was conducted to first check
the feasibility of the procedure and in general establish boring
spacing requirements, clarity of signature and the mechanics of
the equipment. From these efforts, the impulse test as presently
accomplished on a production basis is described in Section 2.1.

Design and fabrication of test equipment also followed a
line of progressive advancement in sophistication. In-hole equip-
ment was improved and modified through testing to achieve
optimum workability. Recording equipment originally consisting
of strip chart recorders and oscilloscopes was updated by incor-
porating a magnetic tape recorder into a single console unit.
This current equipment has greater resolution, greater recording
flexibility, computer compatibility and greatly simplifies field
recording procedures. The details of the test equipment are
presented in Section 2.2.

.With reasonably well-established testing techniques and
refined test equipment, current efforts have been concentrated
on obtaining production data at different sites with different
soil types. During this period six sites have been tested by
this procedure to depths approaching 100 feet or greater. From
this field testing, considerable experience has been gained.
Based on this experience, Section 2.3 describes in sequence the
general field exploration equipment and procedures used for
exploring and testing these sites with this new test procedure.

Finally the test data had to be processed in a consistent manner. Computer programs were developed for extracting the pertinent data points from each signature. The procedures for this are described in Section 2.4.

2.1 TEST DESCRIPTION

The in situ impulse test is similar in some respects to the cross-hole technique used in conventional geophysical explorations, in that it is based on the generation and recording of the propagation of shear waves through a mass of soil between two or more boreholes. A schematic of the test, shown in Fig. 1-1, includes a generating source and three or more recording stations arranged in a horizontal plane at a given depth, inside vertical boreholes. This arrangement may be radial as shown in the figure, or in an array in which the source and sensors are in a line. Borings containing free-field sensors may be either cased or uncased.

The primary difference between this test and other cross-hole impulse-type tests is in the generation, magnitude and control of the shear waves. This test utilizes a controlled in-hole energy source in which shear waves dominate. The resultant recorded velocity-time signatures therefore have a distinct amplitude and shape as the shear pulse travels through the soil to successive recording stations. A consistent shape enables the identification of characteristic points on each pulse marking the time of passage of a wave through each recording station. The desired large amplitudes of the shear pulse are obtained by adjusting the spacing of the borings. For the general strains of interest (10^{-3} to 10^{-1} percent), sensors have generally been positioned in boreholes spaced about 4, 8 and 16 feet from the energy source. These are considerably closer spacings than used in the conventional cross-hole procedures. Thus the close spacing minimizes the inherent limitations

in the cross-hole procedure of having waves reflecting or
traveling over paths greatly different than assumed.

2.2 TEST EQUIPMENT

Major development efforts of testing equipment were accom-
plished in previous work and the results presented in previous
progress reports (SW-AA, 1973 & 1974). However, since this
equipment has been gradually updated through minor improvements
and modifications, the main features are summarized below.

2.2.1 Anchor and Hammer Assembly

Two anchor and hammer assemblies have been developed
to transmit the applied impact energy to the soil. The primary
anchor used in the program to date consists of a heavy hydraulic
system designed to operate in a 9 to 10 inch diameter borehole.
This anchor is four feet long, weighs 195 pounds and is formed
by three aluminum curved plate segments. The details of this
anchor are shown in Fig. 2-1a. The vertically oriented piston
shown in this photograph is a 25-ton capacity double acting
hydraulic ram. This ram, when expanded, extends through a system
of arms, forcing the curved plates outward and pressing them
tightly against the walls of the borehole. A hand operated
pump and gage is located at the ground surface to control and
maintain the hydraulic pressure in this ram.

On top of the anchor plate segments as shown in
Fig. 2-1b a striking plate, load cell, and two Belleville springs
in series form the cushion. This cushion receives and transmits
the impact of the hammer to the anchor assembly. The Belleville
springs have a stiffness of about 300,000 lbs/in. The load cell
is waterproofed, has a maximum capacity of 60 kips and is
designed to respond to high frequency motions. Auxiliary equip-
ment with the load cell enables the load cell output to be
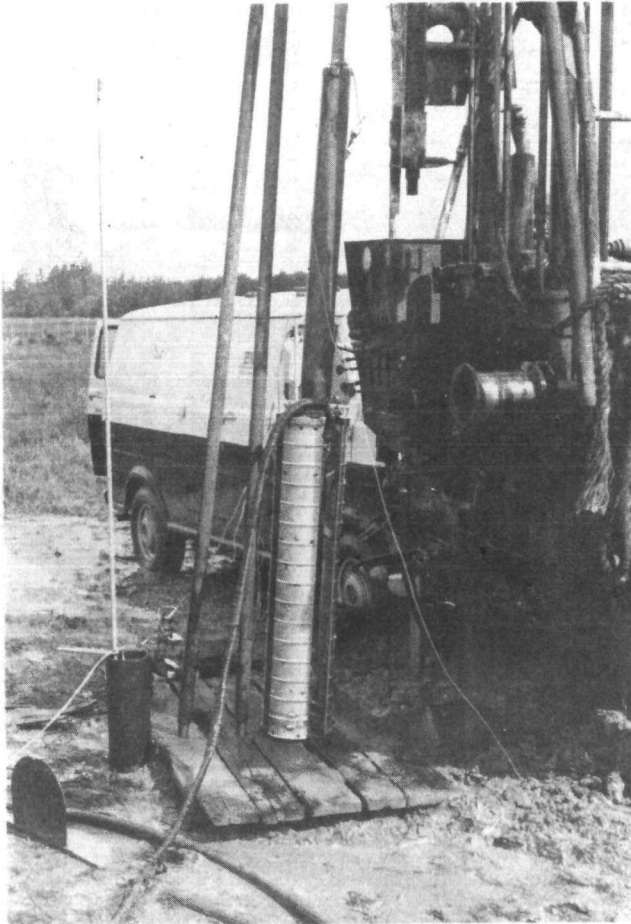
(a) Anchor and Hammer Assembly
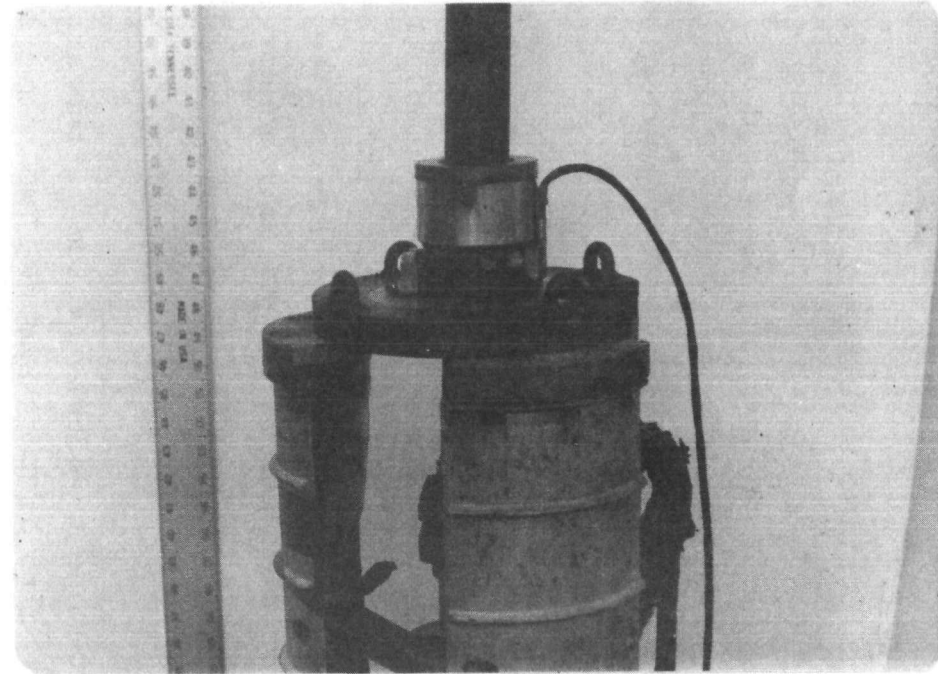
(b) Detail of Top of Anchor

FIGURE 2-1   HYDRAULIC ANCHOR DETAILS

recorded as a function of time simultaneously with the velocity measurements. Standard BW drill rod extends through the center of the springs, load cell, and striking plate and is fastened to the anchor by a yoke. This rod maintains alignment of the striking plate in the center of the anchor and also is used to raise and lower the entire assembly in the borehole.

During testing, the diameter of the expanded anchor can be determined at the ground surface by measuring, with a special key system on the bottom end of the BW rod, the stroke of the piston. If the hydraulic pressure in the ram and the diameter of the anchor are determined; by appropriate calibration, the radial horizontal stress at the soil/anchor interface also can be determined. Procedures for determining this value are described in Section 3.1.3.

The last component in this system is the striking mass itself, herein referred to as the hammer. Two hammers were used and consisted of different size steel cylindrical weights, tapered slightly on the lower end. These weights are controlled from the ground surface by a thin steel hoisting cable. The hammers each have a 2-inch diameter hole through their center to be guided and centered in the hole by the BW drill rod. For production testing, 58 and 150 pound hammers were used. With these weights, a wide variation in energies was achieved by varying the height of drop.

The second anchor, tested to a lesser extent, was designed to operate in a 4-inch diameter borehole. This pneumatic anchor is five feet long, weighs about 150 pounds, and is formed by three steel plates surrounding an inflatable packer. The details of this anchor are shown in Fig. 2-2. The curved plates are made from double extra strong pipe cut into three curved segments. The inner core of this system consists of a high pressure packer unit (Burst pressure of 1300 psi). The
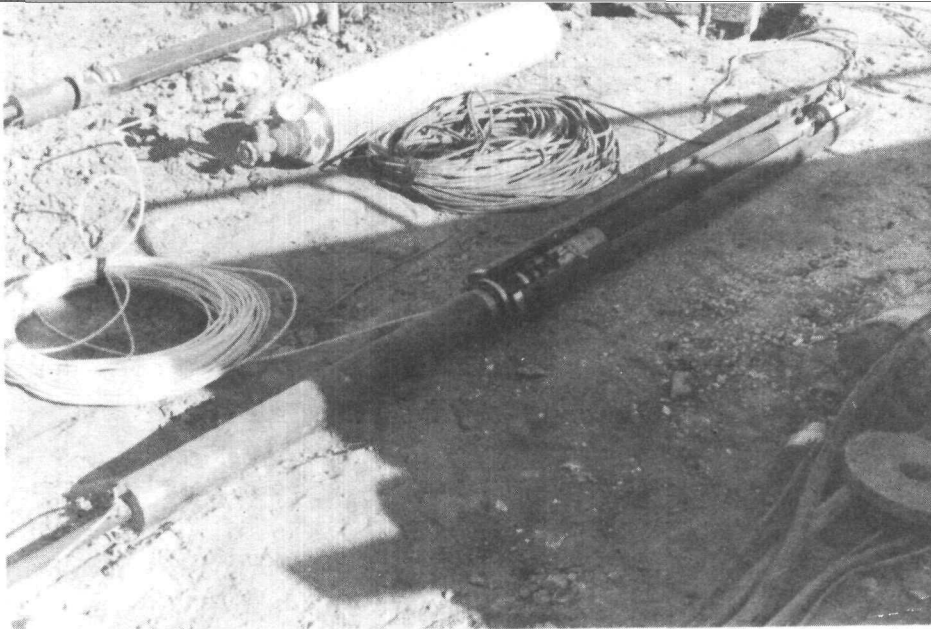
(a) Anchor and Hammer Assembly
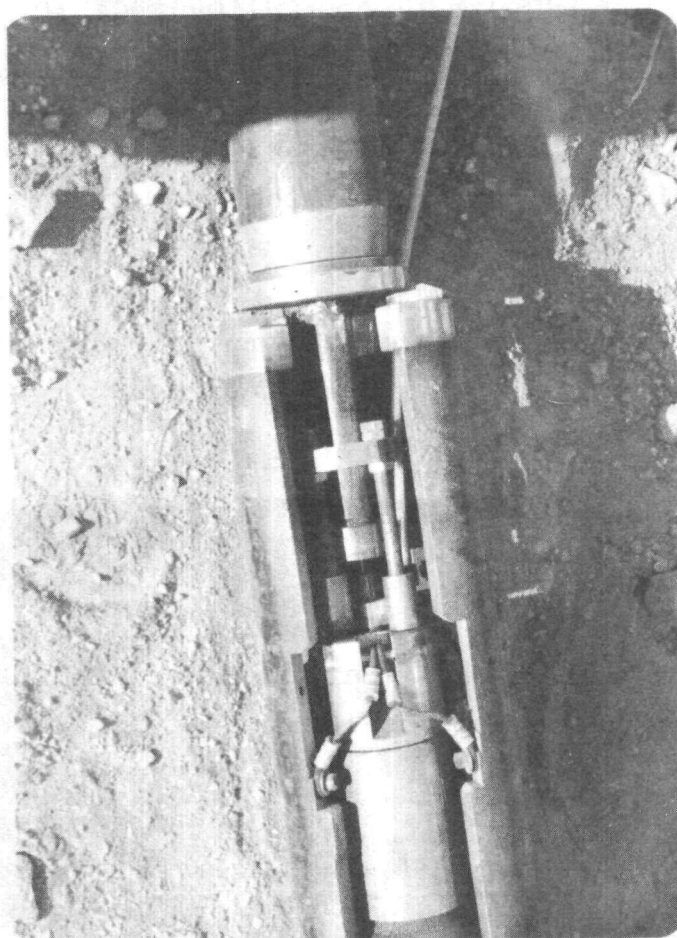
(b) Detail of Top of Anchor

FIGURE 2-2 PNEUMATIC ANCHOR DETAILS

packer contains a 2½-inch O.D. steel wire reinforced rubber unit
which expands up to about 6 inches in diameter under high air
pressures. Coupling is achieved by expanding this unit outward
pressing the plate segments tightly against the borehole walls.
As the unit expands, the lower end of the packer contracts on
an inner rod as a piston. This relieves the longitudinal stresses
in the packer.

The entire anchor is held together by a system of
eighteen short cables. When the anchor is expanded the cables
compress or loosen causing the plates to hang in the borehole.
Vertical alignment of the plates is maintained by this hanging
action. When the air pressure is released the piston action of
the packer pulls the system of cables together retracting the
curved plates tightly against the inner packer.

The striking plate, springs, yoke and hammer systems
shown in Fig. 2-2b, all operate on the same principal as the
first anchor. The hammer for this system weighs about 90 pounds.

Both anchor and hammer assemblies are raised and
lowered in the borehole by the drill rig used to advance the
borings.

2.2.2   Sensors

The sensor units for this test consisted of vertically
oriented velocity transducers (Mark Products L-10AK). These
particular sensors have a natural frequency of 30 cycles per
second. For these tests, each velocity transducer was placed
in water-tight casings and fixed to a sensor holder. These
holders consist of a strong, 1½-inch diameter inflatable, rubber,
cylindrical balloon with two short aluminum heads fastened in
each end. To make the holder act as a rigid element vertically,

a thin solid steel rod extends through the rubber unit and is fixed to the two aluminum heads. The balloons are pressurized by compressed air and can be expanded to about 6 inches in diameter, if required, to achieve adequate coupling of the sensors with the walls of the boreholes. Orientation of the sensors was maintained at the ground surface through interconnecting 1/2-inch diameter, 10-foot long steel rods fixed to the aluminum head of the balloons. Details of the sensor and sensor holder are shown in Fig. 2-3.

2.2.3   Recording Equipment

The recording console used in the field to acquire velocity time histories from each sensor and load cell measurements is shown in Fig. 2-4. The console contains four basic units. The waveform recorder (Biomation Model 1015 Waveform Recorder) is the primary central data acquisition unit. This unit is capable of recording simultaneously and storing in memory, the velocity or load time histories independently from four sources. This stored data can be withdrawn from the recorder in either analog or digital form.

In analog form, the entire signal from each of the four channels is displayed simultaneously on the screen of the oscilloscope (lower right unit in Fig. 2-4). Because the information displayed on the oscilloscope is being taken from a memory bank, adjustments in time and amplitude of the signals are possible after the event. This feature enables small or critical data parts on any channel to be studied separately in detail or compared with critical parts on other channels. The oscilloscope was equipped with a camera mounted in front of the screen. Photographs, taken of the continuous display, provided not only a back up recording system but also valuable additional graphical records used for determining visually which tests were the best and should undergo further study and processing.

FIGURE 2-3   SENSOR AND SENSOR HOLDER
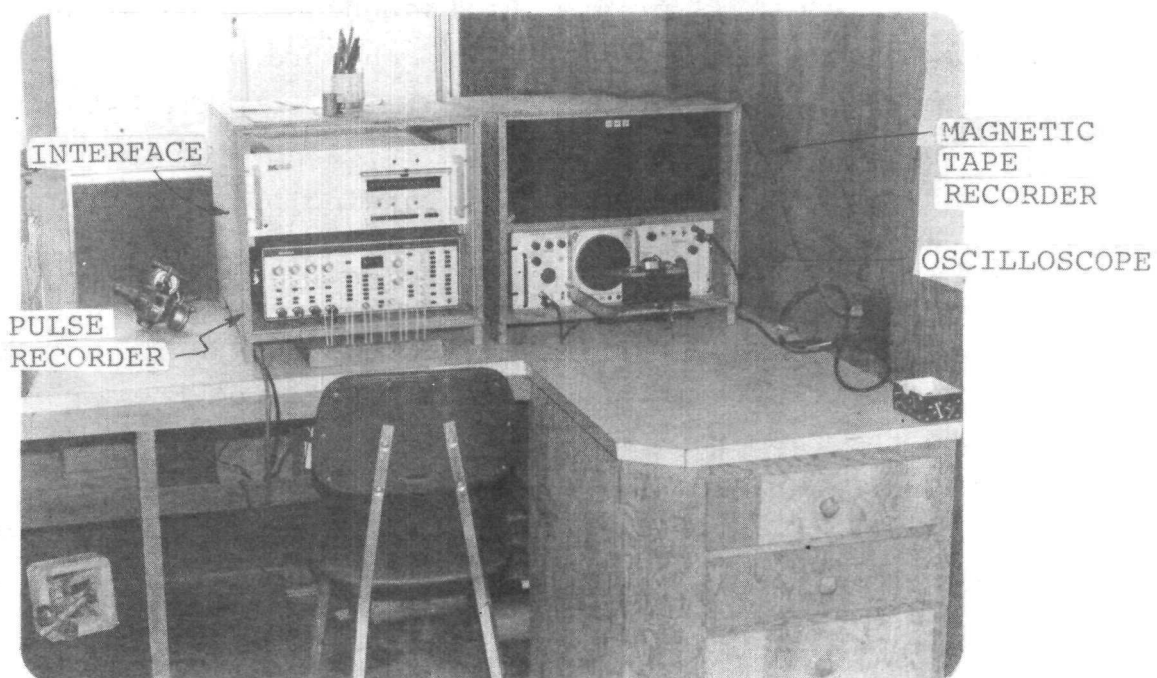
FIGURE 2-4 RECORDING EQUIPMENT

In digital form, the data is withdrawn from the waveform recorder and placed directly on computer compatible digital magnetic tape. The top right unit in Fig. 2-4 is a Cipher Model 70M magnetic tape recorder. Records for each test can be digitally placed on the tape in about 30 seconds. Each of the four channels is printed in sequence as 1024 words or 4096 words in total. In most cases each word is printed with a time and amplitude resolution of 0.05 milliseconds and one part in 1024, respectively. The recorder is capable of achieving a minimum and maximum time resolution ranging between 0.01 milliseconds and 10 seconds per word.

The interface unit provides the necessary electrical circuitry for transferring the digital data from the waveform recorder to the tape recorder. Also the interface unit contains manual control and automatic options which enable the test data, test labels, and both time and amplitude scales for each of the four channels to be organized systematically on the magnetic tape. This greatly simplifies data reduction, because the computer can read the necessary scaling information and test data on the tapes such that very little other data need be entered into the computer manually for complete processing.

2.2.4   Surveying Equipment

The precise horizontal distances between the velocity transducers in adjacent borings is determined with two electrical instruments, a spiral checking device and an inclinometer. These instruments are separately lowered into plastic casings either temporarily or permanently installed in each boring. Guide wheels on each instrument track in special continuous vertical slots grooved in the plastic casing. These slots assure accurate alignment and orientation of the instruments. The spiral checking device measures at five foot intervals any minor rotation of the grooves in the casing. By knowing the rotational

position of the grooves at the ground surface, the change in rotation relative to the surface position can also be determined at any depth.

The inclinometer sensor also follows in the same slots and accurately determines the inclination of the sensor from the vertical. Inclinations are recorded on perpendicular planes at two foot intervals for the entire depth of the boring. With both inclination and rotational surveys combined, the horizontal displacements of the borehole at any depth relative to the top of the borehole can be established. By measuring the surface displacements with a tape, the distance (within an accuracy of about 0.1 ft) between respective holes at any depth can be computed.

2.3 FIELD EXPLORATIONS AND TESTING PROCEDURES

From past and current testing efforts at production sites, rather well established drilling and testing procedures have evolved. A small trailer and the necessary drilling equipment are first mobilized to each test site. The trailer transports the in situ equipment to each site and serves as a data acquisition center during field drilling and testing operations. Drilling rigs utilized to advance the borings and perform the in situ testing are conventional equipment and have consisted of either hollow stem auger rigs and/or rotary rigs.

The following paragraphs describe in sequence the general field exploration and testing program recommended for use in evaluating the variation in the in situ dynamic shear modulus with strain and depth at a potential nuclear power plant site. This work would generally supplement that normally performed on a routine basis.

2.3.1   Field Exploration and Surveying Procedures

At each site four borings are drilled and tests performed to depths on the order of 100 to 200 feet. These borings are aligned in a straight line or in an array indicated in Fig. 1-1. The three sensor borings, spaced 4, 8 and 16 feet from the fourth anchor boring, are usually about 4 inches in diameter. The anchor boring is either 4 or 9 inches in diameter depending upon the anchor used.

Drilling is usually initiated by advancing and sampling one sensor boring for the entire (usually 200 feet) depth. This boring serves as an early base for defining the subsurface materials and assessing the likely performance of this hole to caving or deterioration. If caving is apparent, casing (plastic) should be installed in this as well as the remaining sensor borings. Otherwise testing can be accomplished in uncased holes. The anchor boring is usually drilled last, because it must be maintained and testing performed in an uncased hole.

As soon as each boring is completed three inch diameter casing is lowered into the hole through the drilling fluid for the full depth and rigidly fixed at the surface. The hole is then surveyed by lowering the two surveying probes inside the casing and recording the inclination and rotation characteristics of the casing. The casing is then removed from the hole shortly after the survey is completed. This entire operation usually takes about two to three hours per hole. If casing is required to prevent caving, the surveying operation of the sensor borings can be accomplished any time during the test program.

Surveying requirements for the anchor boring depend upon the anchor and drilling equipment being used. If the 4-inch pneumatic anchor is used, the survey described above can be either accomplished before or at the completion of testing. If the larger 9-inch hole is required, it must be accomplished in one of two ways. If this hole is advanced by a continuous flight 3-3/8-inch I.D. hollow stem auger, the casing can be installed in the hollow stem. The hole can then be surveyed and the casing removed prior to pulling the auger.

If rotary procedures are used, a two-step operation is accomplished. First a pilot hole 4 inches in diameter is advanced for the full depth of the boring. This hole is then surveyed using the temporarily installed casing described previously. The pilot hole is then reamed to its full diameter. To prevent drift from the surveyed hole, the reaming bit should be aligned and guided with a pilot bit advancing at least five feet in front. Reaming can be accomplished in steps concurrent with testing or for the full depth. By drilling and testing in steps, borehole disturbances are minimized and the walls of the borehole are left exposed for shorter periods of time. This is an especially important consideration when caving or deterioration of the walls is a problem.

In advancing the four borings, care must be taken to assure reasonable verticality of the holes especially the two nearest the anchor. Excessive drift in the alignment can result in holes converging to a common distance from the anchor. This, in effect, causes two potential data stations to act as one. This may require the drilling of extra holes. If initial care is taken to properly align the drilling rig and long heavy drill collars are used in the drilling operation, this problem is minimized.

2.3.2   Field In Situ Testing

Once all holes have been completed and surveyed, in
situ testing is conducted usually at 5-foot intervals. Testing
usually starts at the top of the boreholes and progresses downward.

The anchor and hammer assembly is raised and lowered
on BW drill rod to the prescribed test depth by the drilling rig.
The rig is needed for this operation because it is capable of
1) flushing the hole prior to the start of testing, 2) pushing
the anchor assembly through bridges or tight spots, 3) pulling
the anchor assembly loose from the borehole walls following
testing, and 4) pumping water or drilling fluid through the center
of the assembly to wash out soil particles that have collected
during the testing operation.

Coupling of the anchor is accomplished by gradually
increasing the hydraulic pressure in the 25 ton ram until a stable
value is reached. To monitor the coupling of this anchor
assembly, measurements of jacking pressure and the vertical
stroke of the ram (using the special key system) are checked
periodically during the jacking process and during the test itself.
With appropriate calibration, these two values enable the diameter
of the anchor and the resulting radial stress being applied to
be monitored. As will be indicated in Section 3.1.3 and
Appendix G, achieving optimum coupling is very important. Either
too high or too low a pressure can affect the strains achieved.
The number of strokes applied to the hydraulic pump and the
general resistance to pumping provide another satisfactory index
of the increasing soil resistance to jacking forces.

For the pneumatic anchor, air pressure is used to
expand the anchor assembly and couple it to the sides of the bore-
hole wall. Initial coupling of this system is checked by pulling
slightly on the rods with the drill rig. Immediate resistance

will indicate coupling.

Free-field sensors and their holders are lightweight (less than 3 pounds) and can be raised and lowered usually with interconnecting 1/2-inch diameter, 10-foot long, thin steel rods. The pin connecting ends of the rods are designed such that proper orientation or positioning of the sensors within the borehole could be quickly and easily established.

Coupling of each sensor is achieved by inflating the rubber packer holder with compressed nitrogen. Firm coupling is verified by pulling or pushing manually on the interconnecting rods. Also to assure continued coupling during testing, the rods are left free standing above the ground surface. Thus their weight is supported entirely by the sensor holder providing a simple monitor of the coupling effectiveness. If the coupling becomes loose, the rods would drop several inches and catch a horizontal clamp on the top of surface casing.

For each depth, a trial impact is first applied. From this impact, velocity time histories are recorded from four vertically oriented sensors, (i.e., where shear waves were the dominant particle motion). These records are displayed continuously on the screen of the oscilloscope. This display is then inspected by the field engineer to determine if all equipment is operating properly (i.e., proper coupling of both anchor and sensors, clear impact, and proper scales on recording equipment). The impact is then repeated and other records obtained the same way until four clear properly scaled time history signatures are obtained from one impact. Two or three tentative trials is usually sufficient to obtain a good test. This last test is made a permanent record by first taking photographs of the display on the oscilloscope. Because portions of each signature may be expanded or the scale changed after the event, more than one photograph is often justified. The information is then recorded

on a basic data sheet and in digital form on a computer compatible magnetic tape recorder for the later study and evaluation. The photographs enable the overall signatures to be studied and assessed qualitatively while the digital records provide the necessary time and amplitude resolution needed in this test.

At a given test depth, about six tests are taken; usually three tests at two different energy levels. The different energy levels are achieved by varying the height of drop of the one of the two hammers. For most soils, the drop commonly varies between six inches and two feet. In addition to measurements of vertical particle velocities, measurements of load applied to the anchor and horizontal particle velocities from free field sensors are also recorded. The load provides for partial inter-pretation of the shear wave velocity at the anchor and the hori-zontal velocity measurements enable the P-wave velocity and the water table to be determined.

2.4 DATA PROCESSING

In order to determine the shear modulus, G, (or shear wave velocity, V_s) as a function of strain, four basic measurements are obtained in the performance of the test as listed below:

1) the distances between the anchor and the free field sensors
2) the arrival time at each sensor
3) the peak particle velocity at each sensor
4) the time of first impact of the hammer to the anchor

In addition, to study the response of the anchor, the peak force amplitude recorded on the load cell, as well as various time points that define the shape of the recorded load impulse have been processed.

The distance between borings at corresponding depths is determined by precise field surveys of each hole. The remaining parameters are obtained from time history measurements using a load cell and velocity transducers positioned on and within the anchor respectively, and vertically-oriented velocity transducers located in adjacent borings. A sample of the particle velocity versus time records for a test is shown in Fig. 2-5. This photograph shows the analog signals as displayed on the screen of an oscilloscope. The data actually processed and reduced are in digital form on magnetic tape. In general, data processing for production tests can be divided into three phases: 1) initial checkout of the data, 2) computer processing of the response measurements, and 3) final determination of the velocity (or modulus) strain relationships.

2.4.1   Initial Checkout Phase

The initial step in this phase, upon receipt of the magnetic tapes, oscilloscope photographs, and summary data sheets, was to copy the data from the field tapes onto separate magnetic tapes. The purpose of this step was threefold. First, the computer facilities were able to transcribe the data onto a separate tape at a much higher voltage level than was possible from the field recorder. This greatly facilitated subsequent data processing operations. Second, the original field tapes provided backup data storage, in the event the tapes generated were damaged. Finally, any portions of the field tapes that contained unrecoverable data could be quickly identified. If these portions were small, they were skipped so that the remainder of the tapes could be processed. In the unlikely event that a major portion of the data was unrecoverable, the engineers could be notified while still in the field, and the measurements corresponding to the unrecoverable data could be repeated.
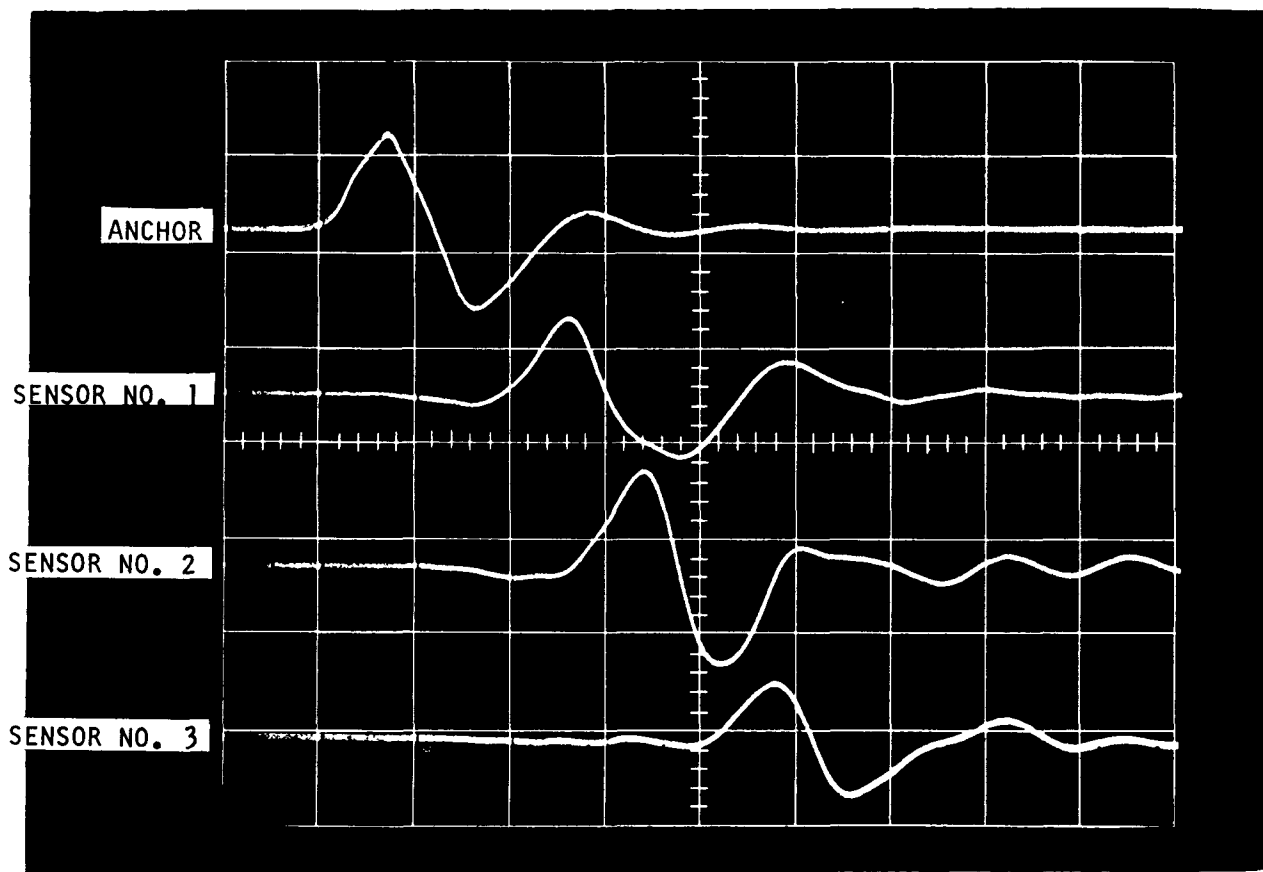
FIGURE 2-5   TYPICAL VELOCITY TIME SIGNATURES DISPLAYED
ON THE SCREEN OF THE OSCILLOSCOPE

Once the tapes were copied, further processing of the data was initiated. The copied tapes were dumped and the listings were checked for bad tape records and improper data or labels. Then the following data on the test summary sheets were compared with the tape dumps, where appropriate, and were used as input to the processing program described in the next section.

a. Test sequence number
b. Test depth
c. Sensors used
d. Recorder scale setting for each sensor
e. Recorder triggering scheme
f. Test loading (hammer weight and drop height)
g. Anchor jacking pressure
h. Data sample rate
i. Oscilloscope/photo number and scaling

The above comparison served to indicate whether any changes would be required to the data processing programs and also provided a basis for noting in advance those tests that were duplicates or missing and those that did not require subsequent processing. Only vertical velocity records and load cell measurements were processed according to the procedures described herein. Horizontal time of arrival measurements for determining P-wave velocities were determined manually from the initial tape listings.

2.4.2   Computer Processing Phase

Once the initial checkout phase was completed, the data were then read into a specially developed computer program which processed the data according to the following steps:

a. Reformat data
b. Scale data into engineering units

c.   Label tests and test channels

d.   Detect peaks and zero crossings

e.   Compute time delays

f.   Store and manage results for easy reaccess

g.   Print results in suitable report format

The first step in this final processing (Step a) involved the proper reading and decoding of the binary coded decimal formatted data into four digit integers in the digitizer range of 0 to 1024 counts. Then, in Step b, the 12-character test label preceding each test was decoded into six 2-character parameters which represented the test sequence number, the sampling interval and the recorder scale setting for each of the four data channels recorded in each test. In addition, the computer program was designed to automatically decode the label for scaling purposes and also corrected for zero-amplitude offsets in the data.* The recorder scale setting was combined with the transducer sensitivity factor to produce a resultant scale factor. The zero-amplitude offset level was subtracted from the data prior to scaling.

Step c of the final processing involved labeling the test channels with appropriate sensor names, test numbers, and test sites. This data was stored for future identification of the data processed in subsequent steps.

---

* The Recording system used in the field identified only positive integers (0 to 1024 counts) when recording the velocity histories. Therefore, the zero level of the velocity history was assigned a positive integer value by the Biomation Recorder; this integer value had to be sufficiently large so that the largest-amplitude negative velocities could be recorded using a positive integer. In processing the data, corrections for this zero-amplitude offset had to be made; in providing these corrections, the first data value from each channel was assumed to correspond to this offset level.

In Step d, key amplitude and time points of the velocity and load cell data were identified. These points corresponded to those considered significant for subsequent assessment of the velocity-strain relationships (Fig. 2-6). The times of arrival at adjacent sensors of the first downward velocity peak and the first crossing ("TPOS PK" and "TZEROX" respectively in Fig. 2-6a) were then used to compute time delays in Step e. Further discussion and evaluation of various methods for computing shear velocities is presented in Chapters 4, 5 and 6.

The final steps in this phase (Steps f and g) consisted of storage of the processed data so that it could be easily retrieved and, in addition, a printout of the summary information developed in Steps d and e. A sample of the pertinent data extracted from these tapes is summarized in Fig. 2-7. For each test at each depth, this printout included the energy level, jacking pressure, test number, the time and amplitude measurements identified in Fig. 2-6, and the various time delays between adjacent sensors.

2.4.3   Determination of Velocity-Strain Relationships

Having determined the above parameters from the data tapes, the time data are next plotted with distance as shown in Fig. 2-8. As discussed in Chapter 6, the time of first crossing (TZEROX) is most commonly used to identify the arrival time in the free field sensors. This time point from each sensor record, together with the measured position of each sensor relative to the anchor, was used to construct the position versus time curve shown in Fig. 2-8. The slope of this curve at each sensor was used to estimate the shear wave velocity at that location. Since the wave decays rapidly in the near-anchor regions, the soil strains likewise attenuate with increasing distance from the energy source. The strains in the free field are then computed assuming the wave travels as a
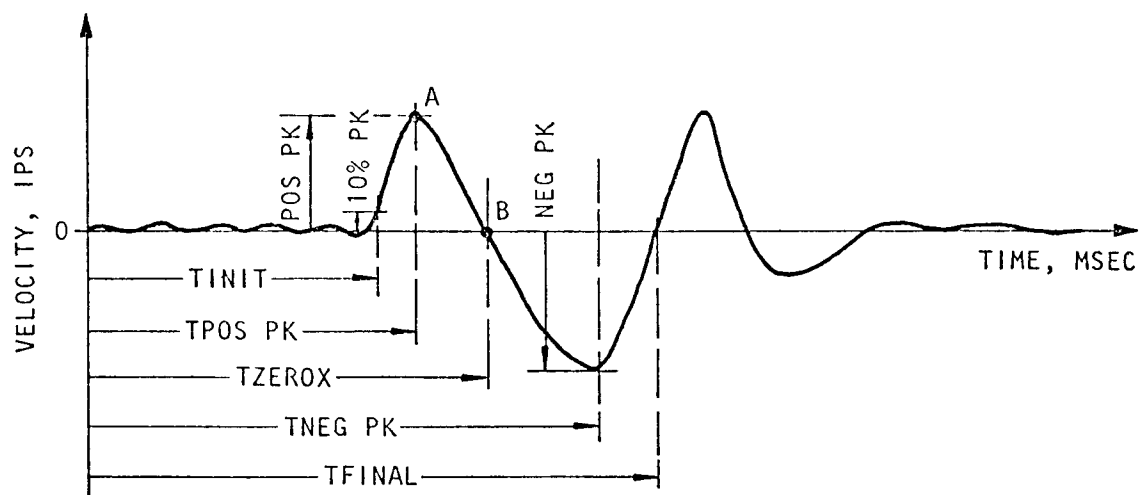
TIME DELAYS: POSITIVE PEAK -- BASED ON ARRIVAL TIME OF POINT A
               ZERO CROSSING -- BASED ON ARRIVAL TIME OF POINT B

(a)   Vertical velocity measurements
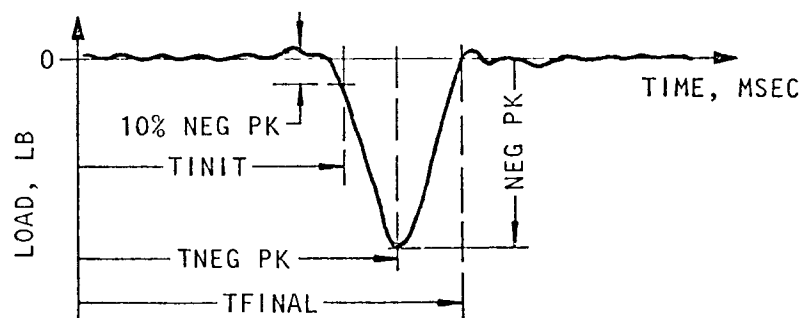
NOTE (FOR BOTH VERTICAL VELOCITY AND LOAD CELL MEASUREMENTS):

    ZERO TIME REPRESENTS FIRST RECORDED DATA VALUE
    ZERO AMPLITUDE BASED ON BIAS OF FIRST RECORDED DATA

(b)   Load cell measurements

FIGURE 2-6   DATA REQUIRED FROM PRODUCTION TESTS

-30-

PRODUCTION TESTS EL CENTRO SITE   DEPTH = 8 FEET
(TIME IN MSEC, VELOCITY IN IPS, LOAD IN LB)

    TESTS 27 AND 28 (TAPE C-3)   ENERGY LEVEL = 150 LB X 2.0 IN
                                          JACKING PRESSURE = 1500 PSI

    TEST 27   TINIT   TPOS PK   TZEROX   TNEG PK   TFINAL   POS PK   NEG PK
    ANCHOR 3V   2.05   2.85   4.55   6.90   10.15   17.2738   -17.2738
    HOLE 1V   10.65   13.05   16.10   19.35   24.25   .4171   -.4537
    HOLE 2V   19.10   24.85   27.50   31.30   35.20   .0645   -.1417
    HOLE 3V   39.35   43.30   45.55   48.75   51.05   .0643   -.0952
    TEST 28
    ANCHOR 3V   10.80   11.60   13.00   15.35   18.50   18.7066   -18.0698
    ANCHOR 4V   10.70   11.60   12.00   14.50   14.85   29.2938   -32.0799
    LOAD CELL   10.15   11.00   13.20   -8566.2

    TIME DELAYS(MSEC)   POSITIVE   ZERO
    TEST 27   PEAK   CROSSING
    ANCHOR 3V TO HOLE 1V   10.20   11.55
    HOLE 1V   TO HOLE 2V   11.80   11.40
    HOLE 2V   TO HOLE 3V   18.45   18.05

    TESTS 30 AND 31 (TAPE C-3)   ENERGY LEVEL = 150 LB X 1.0 FT
                                          JACKING PRESSURE = 1500 PSI

    TEST 30   TINIT   TPOS PK   TZEROX   TNEG PK   TFINAL   POS PK   NEG PK
    ANCHOR 3V   1.95   2.85   3.40   6.30   7.15   26.1893   -28.8161
    HOLE 1V   10.70   13.60   16.80   20.50   25.55   .5891   -.7132
    HOLE 2V   20.00   25.25   28.45   32.70   36.70   .0939   -.2269
    HOLE 3V   39.65   43.65   46.25   49.80   51.05   .0904   -.1433
    TEST 31
    ANCHOR 3V   10.85   11.75   12.40   15.40   16.30   23.3236   -27.3037
    ANCHOR 4V   10.75   11.40   11.75   13.50   13.20   33.8311   -47.6024
    LOAD CELL   10.20   11.25   13.65   -13986.5

    TIME DELAYS(MSEC)   POSITIVE   ZERO
    TEST 30   PEAK   CROSSING
    ANCHOR 3V TO HOLE 1V   10.75   13.40
    HOLE 1V   TO HOLE 2V   11.65   11.65
    HOLE 2V   TO HOLE 3V   18.40   17.80
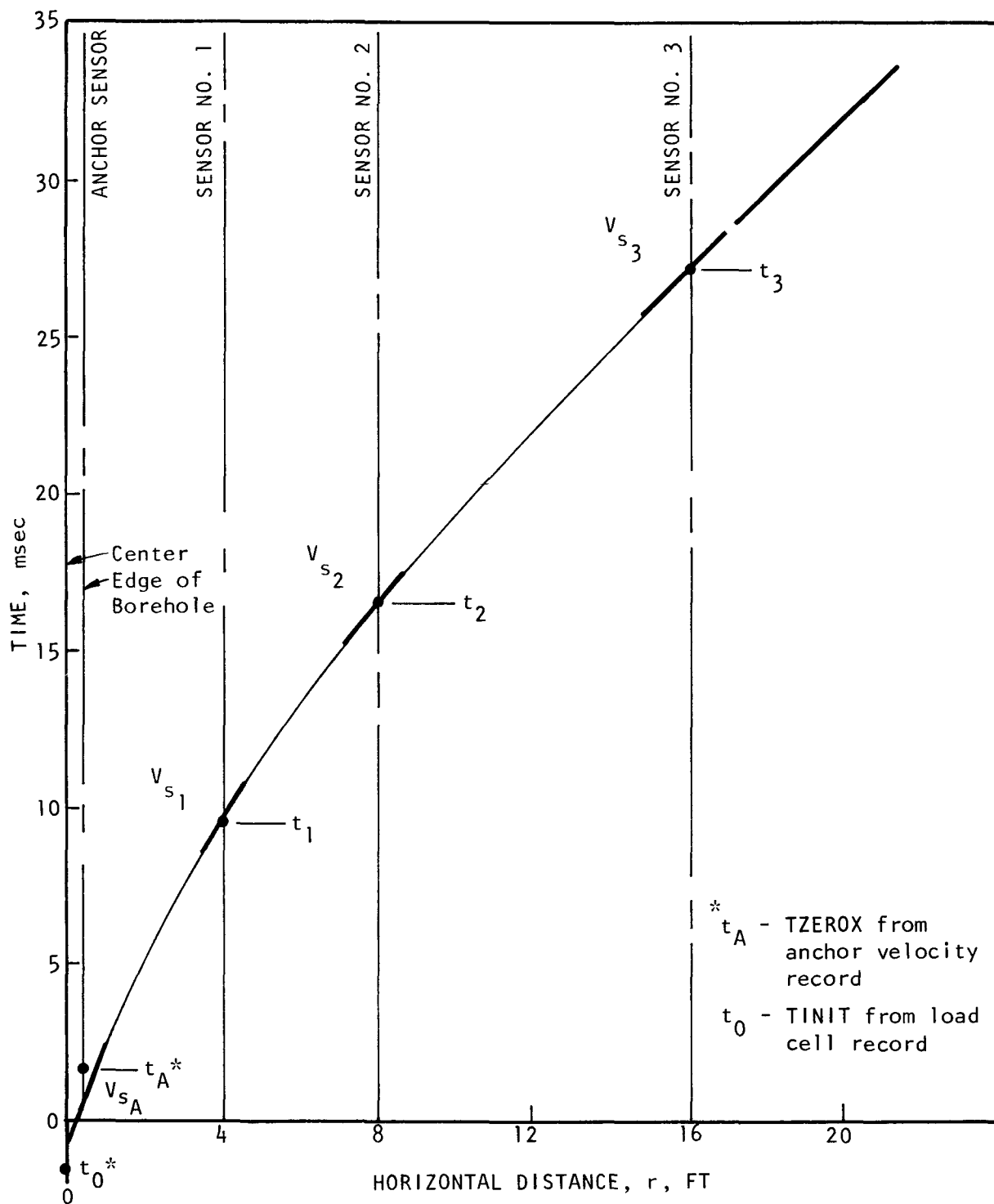

            FIGURE 2-7   SAMPLE OUTPUT FROM PRODUCTION TESTS

FIGURE 2-8   TIME OF ARRIVAL AT PEAK STRESS VS DISTANCE FROM ANCHOR

plane wave (i.e., $\gamma = \dfrac{V_p}{V_s}$). The procedures for determination
of shear-wave velocity and strains at the anchor are not
as straightforward. A fuller treatment of the meaning and con-
struction procedures of individual points at the anchor, based
on the results of this special study are presented in Chapters
5 and 6.

Having determined the shear wave velocity and corres-
ponding shear strain for each station, the shear modulus is
computed by:

$$G = \rho \, V_s^2 \qquad\qquad\qquad (2.1)$$

where ρ is the mass density of the soil.

Both G and V_s can then be plotted with strain as shown in
Fig. 2-9. This procedure is repeated for each test depth,
from which profiles of shear modulus at specific strain levels
can be estimated (Fig. 2-10). These profiles can be used to
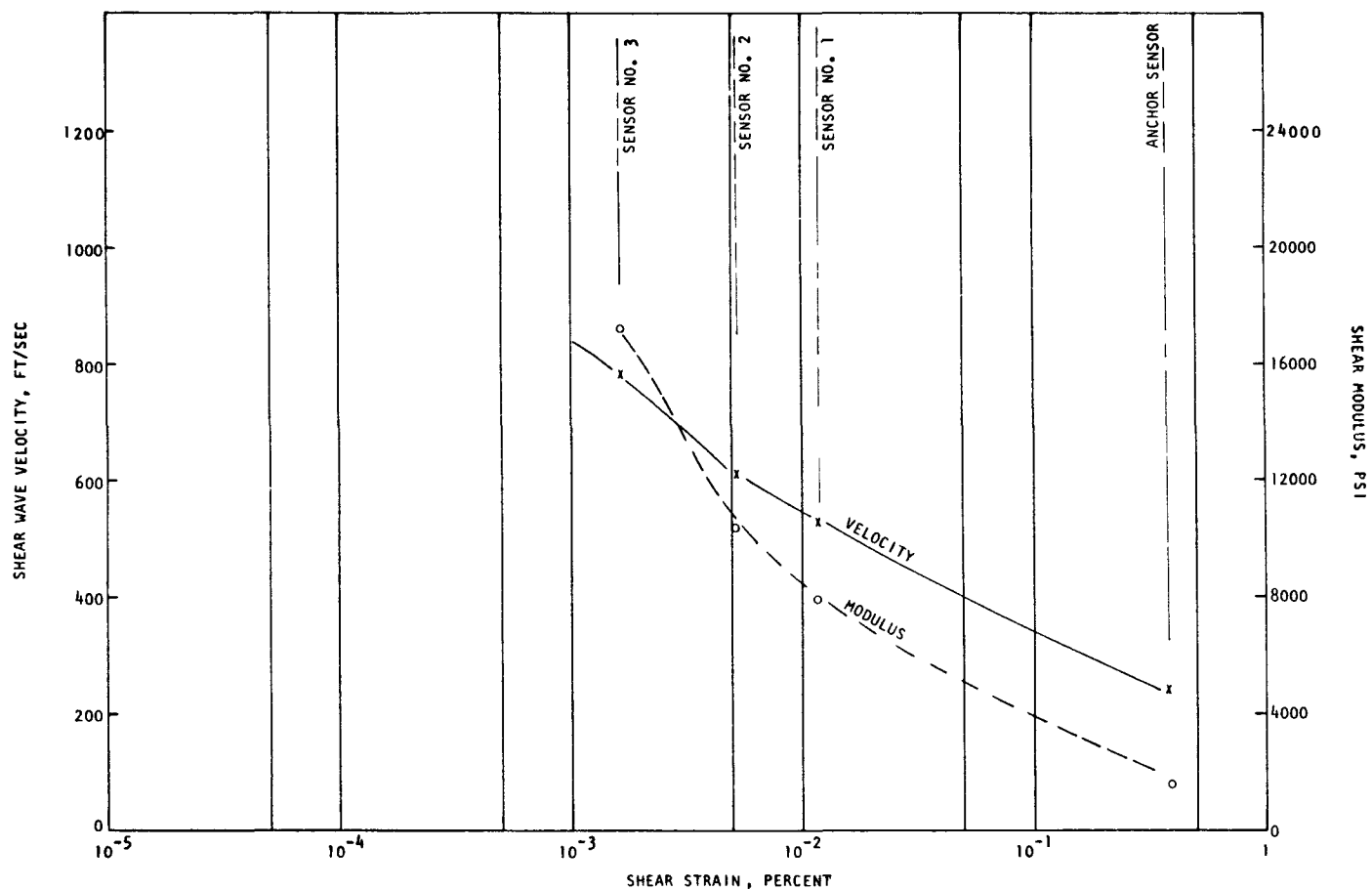represent soil material properties for use as input to site
response studies.

FIGURE 2-9   EXAMPLE PLOT OF MODULUS AND VELOCITY VS STRAIN

-34-

SOIL
LOG

DEPTH

PERCENT
SHEAR STRAIN
10^{-1}
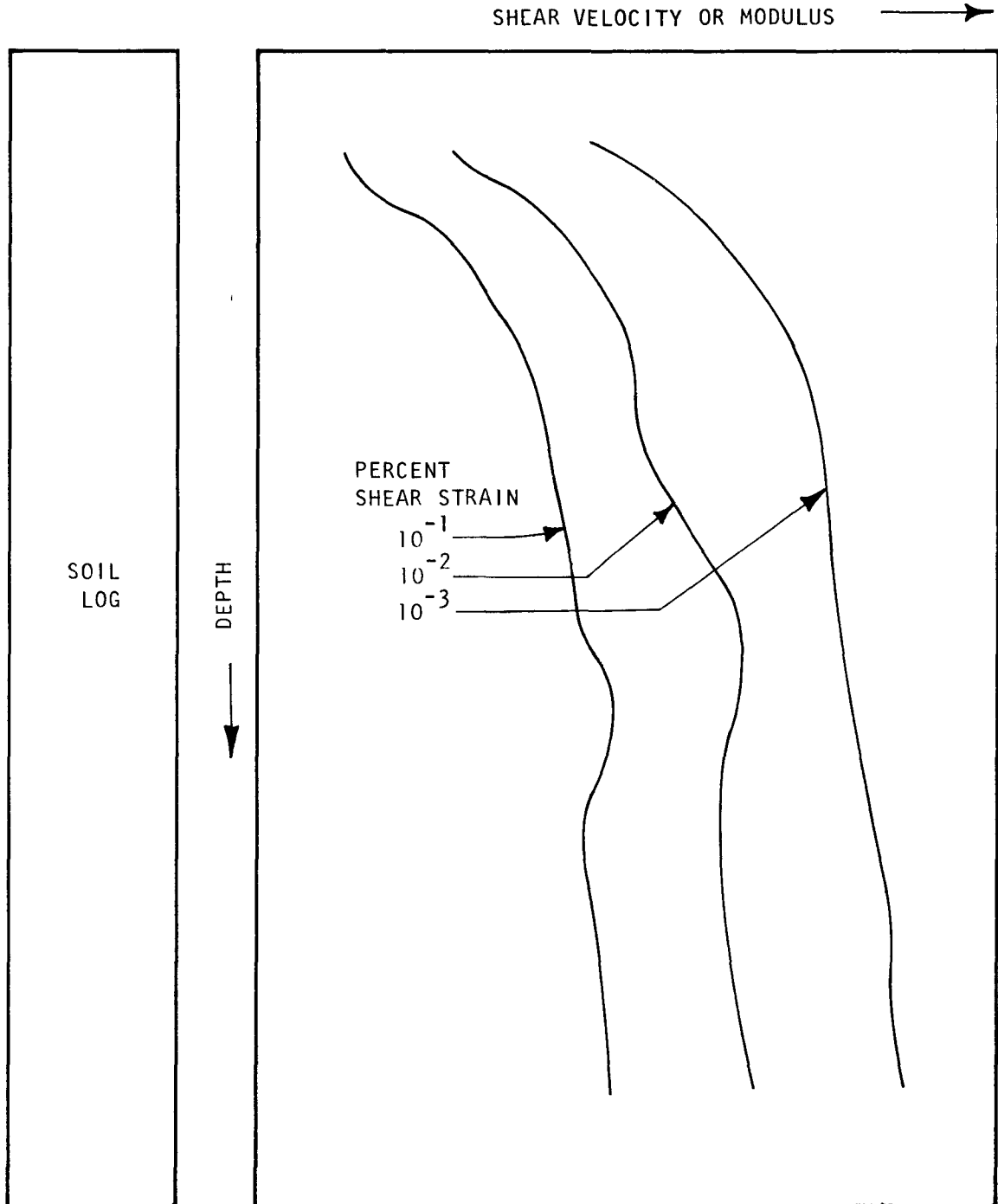10^{-2}
10^{-3}

FIGURE 2-10   SCHEMATIC OF TYPICAL IN SITU TEST RESULTS

CHAPTER 3

ANALYTICAL DESCRIPTION OF THE

IN SITU IMPULSE TEST

The purpose of this chapter is to present an analytical
discussion of the wave propagation phenomena and the test
conditions of the in situ test procedure. To carry this out,
the chapter is divided into three sections. Section 3.1
considers potential effects of such factors as drilling of the
boreholes and installation of the anchor and sensors on the
in situ soil properties. The dynamics of the coupled anchor-soil
system are briefly discussed in Section 3.2, while Section 3.3
develops those particular fundamentals of basic wave theory
that are associated with the in situ test approach.

3.1 ANALYSIS OF TEST CONDITIONS

Three conditions exist during the drilling and testing
operation which may cause changes within the soil mass being
tested. These are 1) stress relief around borings, 2) disturbance
caused by advancing borings through the medium and 3) horizontal
jacking stresses applied in coupling the anchor to the borehole
wall. The following sections discuss the likely qualitative
effect of each condition.

3.1.1   Conditions Caused by Stress Relief

The change in the state of stress caused by the removal
of the soil in a drill hole has been studied by Terzaghi, 1943
and Westergaard, 1940. As a result of stress relief, a zone of
plastic equilibrium develops around the opening. For a soil
whose shearing strength is given by:

$$S = c + \bar{\sigma} \tan \phi \tag{3.1}$$

where: c is the cohesion, $\bar{\sigma}$ the effective normal stress on the plane of shear, and ϕ the angle of internal friction, the boundary between the plastic zone and the surrounding elastic zone, is located at a radius r_e, from the center of the hole. This distance is given by the following equation (Terzaghi, 1943).

$$r_e = r_o \left\{ \frac{2[(N_\phi - 1)\gamma z + 2c\sqrt{N_\phi}]}{(N_\phi+1)[(N_\phi-1)\sigma_{ro}+2c\sqrt{N_\phi}]} \right\}^{\frac{1}{(N_\phi - 1)}} \quad (3.2)$$

where: r_o is the radius of the hole

σ_{ro} is the normal stress applied at the walls of the hole at a depth z

γ is the unit weight of the soil

$N_\phi = \tan^2(45^\circ + \frac{\phi}{2})$

From this equation, if no supporting normal stress is provided, ($\sigma_{ro}=0$), failure will occur at any depth for a cohesionless soil. For a clay with $\phi=0$, the equation indicates that no plastic zone will develop for depths z smaller than:

$$z = \frac{c}{\gamma} \quad (3.3)$$

In the normal drilling procedures for the in situ test, drilling mud is used to remove drill cutting, to counterbalance the hydrostatic head of groundwater, and to create a "mud jacket" around the walls. These last two features produce a counteracting normal stress, σ_{ro}, which minimizes the plastic zone created. The actual extent of the plastic zone depends on the ratio between the free field stress and the applied supporting stress, (σ_{ro}), together with the shear strength of the soil, at each depth.

To illustrate the importance of the thickness of the

plastic zone, consider a sand deposit with c=0, $\phi=30^O$, $N_\phi=3$. Equation 3.2 becomes:

$$\frac{r_e}{r_o} = \left(\frac{\gamma z}{2\sigma_{ro}}\right)^{\frac{1}{2}} ,$$

(3.4)

and the following values are computed:

Table 3.1

Extent of Plastic Zone for Sand, $\phi=30^O$

$\dfrac{\sigma_{ro}}{\gamma z}$	$\dfrac{r_e}{r_o}$	Result
1	.71	No plastic zone developed
.5	1	No plastic zone developed
.25	1.41	Plastic zone, thickness = .41 r_o
.1	2.24	Plastic zone, thickness = 1.24 r_o
.05	3.16	Plastic zone, thickness = 2.16 r_o

Determination of the effective supporting stresses of drilling muds is difficult. However, local sloughing of bore-hole walls is an indication that the plastic zone is enlarging. To maintain the drill hole, use of increasingly heavier muds is required. This increase in mud thickness, in effect, automatically increases this supporting stress keeping the plastic zone to a minimum. As a rough estimate the ratio of $\sigma_{ro}/\gamma z$ for a reasonably thick mud is probably of the order of .1 to .25. Based on this, and realizing that even if caving does not occur; for average test depths of 100 to 200 feet, a plastic zone affecting a concentric area around a 9 to 10-inch anchor bore-hole and 4-inch sensor borehole is probably about one-half to

one foot and several inches thick, respectively. This zone is
considered negligible for the smaller holes. For the large
anchor, this zone if maintained, by using heavy drilling muds
should produce only a minor difference in measured data. The
difference is probably well within the accuracy of other test
measurements (especially those made at the anchor).

3.1.2   Disturbances Caused by Drilling

Drilling operations produce disturbances of the soils
around a borehole. The degree of disturbance depends on the
size of the hole, the properties of the materials, the equipment
and procedures, and the experience of the drillers. Published
information relative to the degree of disturbance of the walls
of boreholes is difficult to find.

Using rotary methods or the hollow-stem auger excessive
disturbances can occur in about four ways. Excessive water
pressures and turbulent flow of the drilling mud, especially
at the bottom of the borehole, can locally erode or deteriorate
surrounding soils rapidly. Rapid withdrawal or lowering of
drilling tools can gouge and smear walls. The rotation of
drilling tools at one depth for excessive periods can cause
enlarged zones. Finally use of flexible tools and no drill
collar can cause not only crooked holes but also irregular cylin-
drical shapes with possible protrusions, cavities and local dis-
continuities. In all cases, these effects of disturbances of
the soil especially for the larger anchor hole are important
field considerations for the field inspector and driller per-
forming the test and can be minimized with due care. For the
soils tested, the zone of excessive disturbance caused by drilling
operations is estimated to be confined probably to a thickness
of one to two inches.

3.1.3   Conditions Caused by Coupling

The most important operation of the installation of the wave generating station is coupling of the anchor plates with the soil mass. In this operation, both the effectiveness of coupling and the radial jacking stresses must be determined. The effectiveness of coupling is a field consideration and requires close tolerances in control of the shape and diameter of the borehole. If the hole size is maintained (i.e., is less than 11 inches for the hydraulic anchor and 6 inches for the pneumatic anchor), the lateral travel of the equipment components is usually sufficient to press through the mud jacket and the concentric layer of soils disturbed by drilling and firmly grip the undisturbed soils.

Further gripping power is achieved at the interface of the large diameter anchor through evenly spaced horizontal wedges protruding from the contact surface of the anchor plates. These wedges, spaced vertically every three inches, have a triangular shape 1/4 inch at the base by 1/4 inch high. These wedges, when pressed into the soil increase the friction coefficient from one corresponding to smooth contact between aluminum and soil to that of soil to soil. Also the wedges provide some confinement to limit the spreading of local bearing failure zones which may result from stress concentrations caused by minor irregularities in the shape of the hole.

Proper selection of an optimum radial jacking stress is also a field consideration in establishing the effectiveness of coupling. The optimum value should be large enough to minimize slippage and thus avoid the creation of distorted signatures due to this slippage. On the other hand, this stress should not exceed a limit value as discussed in Appendix G. If this jacking stress combined with the stresses from the impact exceeds the bearing capacity of the soil, local shear failure results. This

condition, while not distorting recorded signal shapes, reduces greatly the energy transmitted to the soil and thus the strains achieved in the free field. By experimental testing at the first few test depths in a production test program, this optimum stress can be readily estimated.

For close control of coupling in the field, the numerical values of radial jacking stress on the anchor plates can be determined and is required for later use in data interpretation procedures. As discussed earlier (Section 2.2.1) measurement of the stroke of the hydraulic ram made from the ground surface, and the jack pressure enable the determination of both the radial stress and the diameter of the anchor during testing.

The radial stress is determined by the equation:

$$\sigma_r = \frac{2}{3} \sigma_j \frac{\Omega}{A_L} \cot \alpha \qquad (3.5)$$

where: σ_r radial stress

σ_j jack or ram pressure

Ω effective area of the piston of the hydraulic ram

A_L lateral area of one anchor plate

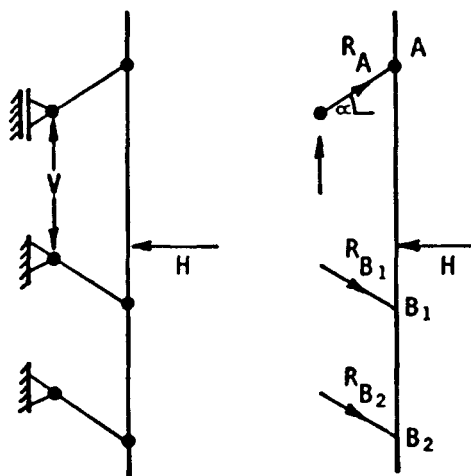α angle of the arms of the anchor with the horizontal plane

The above symbols in this equation are also identified in Fig. 3-1. The diameter of the anchor is determined by the following equation.

$$D = d + 2a \sqrt{1 - \left(\frac{L - [(1-g) - t]}{2a} \right)^2} \qquad (3.6)$$

a. Anchor

$$l = t + q + s$$

$$\sin \alpha = \frac{L-s}{2a}$$

$$\cos \alpha = \frac{D-d}{2a}$$

$$\frac{D-d}{2a} = \sqrt{1 - \left\{ \frac{L - (1-q) + t}{2a} \right\}^2}$$
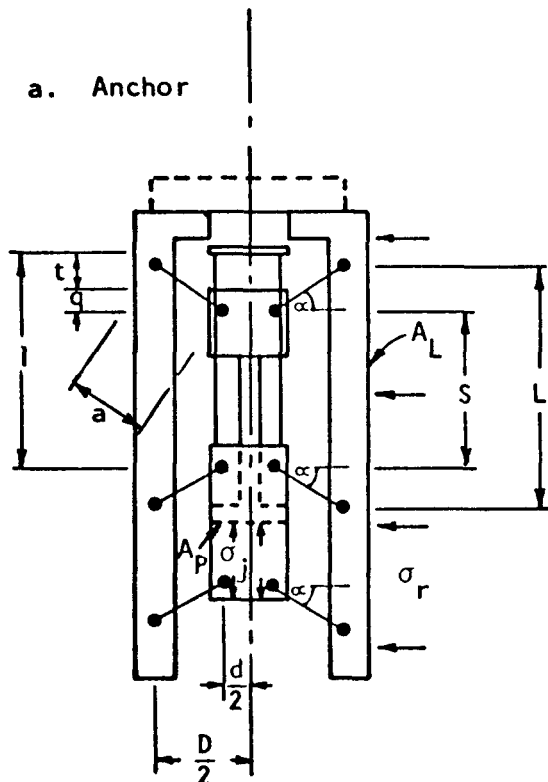
b. Equilibrium of one Plate

since: $V = \frac{1}{3} \sigma_j A_P$

and be: $H = \sigma_r A_L$

$$\boxed{\sigma_r = \frac{2}{3} \sigma_j \frac{A_P}{A_L} \cot \alpha}$$

c. Radial Stress Versus Diameter

FIGURE 3-1. INSTALLATION OF THE ANCHOR. RELATIONSHIPS FOR MONITORING COUPLING

where: D = equivalent external diameter of the anchor

t = complement of stroke displacement

d, a, L, l, q = constants of the anchor, as shown in Fig. 3-1

The radial stress applied by the anchor changes the state of stress of the soils in the vicinity of the anchor. Since the confining stress has an important influence on the modulus, (SW-AA, 1972) the numerical value of jacking stress is needed in interpreting the test data and accounting for this variation in stress conditions from the free field state of stress. The use for the radial stress is included in Chapters 5 and 6.

3.2   ANALYSIS OF THE GENERATING STATION

The generating station may be schematically represented as shown in Fig. 3-2. The purpose of this simplified representation is to describe the main elements of the dynamic system and to introduce the basic relationships of motion. The symbols in this figure are:

m_H the mass of the striking hammer

m_A the mass of the anchor

k_c the stiffness of the loading head
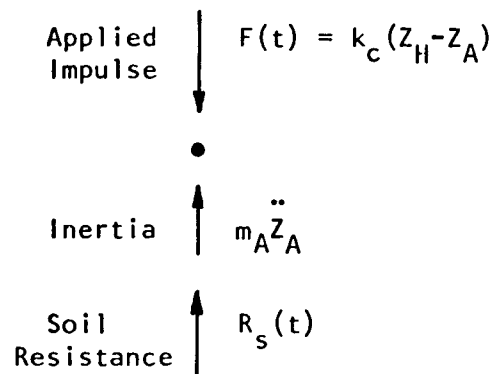
R_s the resistance of the supporting soil

The impulse loading of the anchor, resulting from the impact applied by one blow of the striking hammer has an energy, W, given by:

$$W = m_H \, g \, h \tag{3.7}$$

where: h   the height of free fall of the hammer

g   the acceleration of gravity
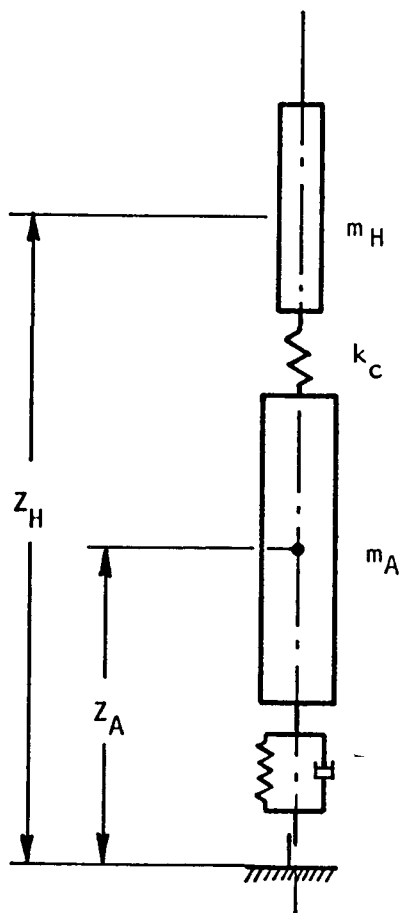
Free Body Equilibrium for Anchor:

Applied Impulse $F(t) = k_c(Z_H - Z_A)$

Inertia $m_A \ddot{Z}_A$

Soil Resistance $R_s(t)$

Equations of motion for 2-degree of freedom ANCHOR-SOIL STRUCTURE:

$$m_H \ddot{Z}_H + k\,(Z_H - Z_A) = 0$$

$$m_A \ddot{Z}_A - k_c(Z_H - Z_A) + R_s = 0$$

FIGURE 3-2. SIMPLIFIED MODEL OF THE WAVE GENERATING STATION

The velocity of the hammer at the instant when it strikes the anchor assembly is:

$$v_o = \sqrt{2gh} \qquad (3.8)$$

The applied force, as measured at the top of the anchor, is:

$$F(t) = F_1 [f(t)] = k_c (z_H - z_A) \qquad (3.9)$$

Where: z_H and z_A are the displacement time histories of the hammer and the anchor respectively, F_1 is the maximum applied force and $f(t)$ is a function which defines the shape of the load pulse.

The equations of motion of the simplified system, assuming 1) that the anchor and the hammer are rigid bodies, 2) that the loading head is a linear elastic element, and 3) that only vertical motions occur, are:

$$m_H \ddot{z}_H + k_c (z_H - z_A) = 0 \qquad (3.10)$$

$$m_A \ddot{z}_A + R_s (t) - k_c (z_H - z_A) = 0 \qquad (3.11)$$

In an actual test, the force $F(t)$ applied to the anchor is measured by means of a load cell attached to the striking plate. By substitution Equation 3.11 becomes:

$$m_A \ddot{z}_A + R_s (t) - F(t) = 0 \qquad (3.12)$$

The resisting function, $R_s (t)$, represents the supporting force applied by the surrounding soil. Solution for this equation requires defining the resisting function in terms of the soil properties, the variables of motion, and the geometry of the

problem. Although mechanical models exist for the behavior of the soil in terms of stiffness and viscous damping, it is not possible to determine the values of the corresponding constants which pertain to the boundary conditions of the problem (i.e., a short segment of a long cylindrical opening in a semi-infinite mass). The general problem is further complicated when considering the changed state of stress created in the surrounding soil by applying large radial stresses with the anchor. As discussed in the previous section, the different degrees of coupling can also result in the possibility of reaching failure condition, slippage at the anchor soil interface or local shear failure from excessive jack pressures. All of these variables make it difficult to model "real" conditions at the generating station.

Because of the impossibility of finding a closed form solution to analyze the response of the anchor in the in situ test, finite element methods and special experimental tests have been employed for the development of the procedures for data interpretation. The results of this work are treated in detail in Chapters 4 and 5.

3.3 DISCUSSION OF WAVE PROPAGATION PHENOMENA

Anchor motion, excited by a falling hammer (see Fig. 1-1), is transmitted as transient stress waves to the three-dimensional soil mass. These stress waves can exist as either P-waves or S-waves. P-waves (also termed primary or compressional waves) are characterized by particle motions along the direction in which the wave propagates, while S-waves (also termed secondary or shear waves) involve particle motions transverse to the direction of wave propagation. The anchor constitutes the origin of the disturbance during the in situ test; the direction of propagation for an element of soil, therefore, is approximately aligned with the line connecting the element with the anchor, provided the soil mass is locally homogeneous. Although the

design of the anchor, shown schematically in Fig. 3-1, results in the generation of some horizontal motions in the soil, the predominant soil response is expected to be vertical. For soil elements located on the midplane of the anchor, therefore, for which the direction of propagation is horizontal and the predominant direction of particle motion is vertical, the S-wave component of the propagating stress wave should have a larger amplitude than the P-wave component, even though the P-waves may still be significant in the near-anchor region (Chapter 5). Furthermore, since S-waves and P-waves propagate at different characteristic wave velocities, the two components will separate at a distance from the anchor which depends on the two characteristic wave velocities and the duration and magnitude of the impulse load applied to the anchor.* Beyond this distance the S-wave component of the propagating stress wave is unaffected by the P-wave component.

The task of determining the strain-dependent in situ properties of the soil medium from a finite number of free-field particle velocity records requires that shear wave velocity and shear strain be determined from these records. Since the S-wave propagates at the shear wave velocity, a first approximation to the shear wave velocity of the soil medium can be obtained by observing the propagation of any identifiable feature of the S-wave. Due to dispersion of the S-wave as it propagates away from its nearly axisymmetric source, the various identifiable features do not all propagate at the same velocity as the wave itself. Furthermore, since the properties of the soil medium are strain-dependent, the shear wave velocity of an element of soil varies from instant to instant as the stress wave propagates through. For these reasons, the value of shear wave velocity obtained by observing a particular feature of the

---

* For the special field tests described in Chapter 5, the distance was about 2 feet.

propagating S-wave is not necessarily related to the strain-
dependent soil properties in a straightforward way. Therefore,
special studies have been carried out, using finite element
procedures (Chapter 4) and special field tests (Chapter 5) to
investigate this problem.

Once the shear wave velocity has been determined, a first
approximation of the peak shear strain occurring in a given
element of soil can be obtained through the relation

$$\gamma = \left| \frac{\dot{w}}{V_s} \right| \tag{3.13}$$

in which γ is the magnitude of the peak shear strain, $\dot{w}$ is the
peak particle velocity of the soil element, and V_s is the shear
wave velocity. Equation 3.13 was originally developed for the
case of plane S-waves propagating in an infinite elastic medium.
This relation can be shown to be valid for elements at large
distances from the anchor for an in situ test. This can be done
using a solution developed by C. C. Mow, 1965, to determine the
free-field response of an infinite elastic medium to the arbi-
trary motion of a rigid spherical inclusion along a vertical axis.
Equation 3.13 holds, in this case, for elements located along
the midplane of the sphere at large distances from the sphere.
At these large distances, the shape of the anchor (i.e., whether
cylindrical or spherical) is not particularly important; further-
more, the shear strains in soil elements located at large
distances from an actual anchor in an in situ test will be
sufficiently small so that these particular elements can be
considered to behave elastically. Therefore, the results from
the above indicated closed form solution can be considered to
be representative of the behavior of actual soil elements located
at large radial distances from the anchor. For these particular
elements, Equation 3.13 was shown to be applicable, as indicated
above.

The behavior of soil elements located in the immediate vicinity of the anchor is quite different from that represented by Equation 3.13. For such elements in an infinite elastic medium, the response may be more nearly represented by cylindrical waves; however in an in situ test of actual soil materials these waves are further complicated by the boundary effects at the anchor-soil interface (i.e., slippage, jacking pressures, the finite length of the anchor, etc.) and the inelastic behavior of the near-anchor soil elements. Such complex response characteristics cannot possibly be represented by closed form solution based on elementary wave propagation principles, as described above. However, these near-anchor response characteristics can be investigated by using nonlinear finite element techniques and by special field test procedures, as described in Chapters 4 and 5, respectively.

CHAPTER 4
FINITE ELEMENT ANALYSES

4.1 INTRODUCTION

The in situ test to determine the shear properties of
soils has undergone considerable development in previous efforts;
however, various aspects of the data reduction procedures for
these tests still require further evaluation. For example,
current procedures for defining shear wave velocities between
adjacent sensors have not yet been fully verified. In addition,
current techniques for establishing shear strains from the
measured soil motions are based on certain assumptions that
require further assessment when applied to the complex response
conditions that exist during the in situ test.

4.1.1 Purpose of Calculations

The purpose of the finite element calculations des-
cribed in this chapter is to evaluate procedures for obtaining
in situ soil properties from the test data. This is carried out
by treating each nodal point in the finite element grid as a
sensor, and the velocity histories obtained from the calculations
as field measurements. Data processing procedures used to
estimate strain-dependent shear moduli from actual field data
are applied to these computed velocity histories. The shear
moduli estimates obtained using these procedures are then com-
pared to the shear moduli actually used as input to the finite
element model.

The use of finite element calculations in this manner
offers several important advantages when assessing data processing
procedures. First of all, the soil properties incorporated as
input data for the finite element model provide a basis for
evaluation of the results of the various data processing methods.

In addition, the closely spaced nodal points that comprise the finite element grid represent a much finer network of soil response "sensors" than is ordinarily available under field production test conditions. Finally, these nodal points monitor the soil response not only in the vicinity of the middepth of the anchor, as per the actual field tests, but throughout a two-dimensional array of locations encompassing the entire near-anchor region of soil.

While the above advantages show the finite element approach to be a potentially powerful means of assessing the data processing procedures, there are also certain limitations that must be considered. These are associated with the fact that it is impractical to incorporate every detail of an actual in situ test into the finite element model. For example, the details of the anchor, including the nonaxisymmetric bearing of the individual plates against the sides of the borehole, have been omitted from the finite element calculations discussed herein. In addition, the effects of the jacking pressure and possible slippage of the anchor along its interface with the soil have not been considered. Such limitations in the finite element model do not represent deficiencies in the method itself; rather they have been introduced to keep computational costs within reason. It is anticipated that the inaccuracies arising due to these limitations are small and confined to the immediate vicinity of the anchor. Furthermore, slight differences between calculation and experiment are not severely detrimental to the goal of evaluating data processing techniques. The evaluation procedure is entirely self-contained within the finite element calculation, and is independent of experimental results. It is for the purpose of extrapolating conclusions from analytical checkout into actual field practice that good correlation between calculation and experiment is desirable.

4.1.2   Scope of Calculations

Once dynamic soil responses are measured during the in situ tests, data processing techniques must be used to convert these response measurements to corresponding dynamic soil properties in shear. The principal objective, that of determining a relationship between shear modulus and level of shear strain in the in situ medium, involves two phases of data interpretation. First, the shear wave velocity, which determines the shear modulus, must be obtained; and then the strain level corresponding to that value of shear wave velocity must be determined. Initially, it is best to consider these phases separately; however, before the final recommendations can be formulated, the various methods for estimating shear moduli and strains, by themselves, must be tested in combinations suitable for the construction of modulus/strain relationships. It is on the basis of how well these modulus/strain relationships approximate the known relationships that the recommendations will be made. Two calculations have been included in the present study: one in which the soil has been modeled as a linear elastic medium, and one in which the soil has been described as a nonlinear, hysteretic material.

The elastic finite element calculation is of great value in assessing each phase of data reduction separately. The shear wave velocity is constant in this case, thus simplifying the evaluation of those data reduction techniques intended to determine shear wave velocity. Furthermore, since the method of estimating shear strain depends on the shear wave velocity, an a priori knowledge of shear wave velocity uncouples the strain calculation from the shear-wave-velocity phase of the data reduction. Any problems encountered in estimating shear strain, therefore, can be traced to the shear-strain phase of the data reduction.

The nonlinear finite-element calculation allows the various data processing methods to be applied under conditions more nearly simulating the actual conditions of an in situ test. In fact, the nonlinear soil properties, hammer weight, Belleville spring constant, and anchor weight used in the nonlinear calculation correspond as nearly as possible to those parameters from the experimental tests in Chapter 5. Therefore the nonlinear finite element results can be compared directly to the special test results (Section 4.3.1) and can serve to provide further insight into results from that test program. In addition, the nonlinear finite element calculation is of value in evaluating both phases of data reduction acting together. In the elastic case, the shear wave velocity is independent of strain level, making it meaningless to attempt to construct a modulus/strain relationship. In the nonlinear case, however, a nontrivial modulus/strain relationship does exist and, more importantly, is known from the input data to the calculation. Because of this, combinations of data reduction techniques intended to determine the modulus/strain relationship can be verified against the input data.

4.2   FINITE ELEMENT MODEL

The calculations described in this chapter were carried out using FEDIA, a dynamic, two-dimensional, continuum finite element computer code developed at AA. The material properties that can be accommodated in FEDIA range from linear elastic to highly complex nonlinear properties representative of soils or reinforced concrete and based on variable bulk and/or shear moduli and plastic yield functions. The boundary conditions available include time-varying pressures, time-varying velocities, fixed or free conditions along either global axis, and energy absorbing boundaries. The memory usage is dynamically allocated, and when necessary, data is stored on peripheral units so that larger problems may be solved than would otherwise be possible.

4.2.1   Finite Element Grid

The finite element grid used in both the elastic and the nonlinear calculations is shown in Fig. 4-1. The grid is axisymmetric and contains a total of 954 elements and 1020 nodal points, with the greatest mesh refinement in the vicinity of the anchor. The upper boundary of the grid is modeled as a free surface, 20 feet above the center of the anchor. To simulate a soil medium of infinite extent, the bottom and right boundaries were assigned energy-absorbing properties, thereby minimizing any signals reflecting back into the interior of the grid from these boundary locations. The left boundary of the grid, which corresponds to the borehole, was subjected to stress-free boundary conditions along that portion of the hole wall not in contact with the anchor.

It can be seen from Fig. 4-1 that the finite element grid employs an especially fine array of elements and nodal points in the vicinity of the anchor, which is the region of primary interest in both of these calculations. The nodal-point spacing is as small as 2 inches at the anchor/soil interface, and gradually increases with increasing distance from the anchor to a maximum of 24 inches at the right boundary of the grid. However, the spacing never exceeds 10 inches within 10 feet of the anchor/soil interface.

The ability of the grid to accurately transmit shear waves depends on the nodal-point spacing and the shear wave velocity of the soil medium. In the elastic calculation, in which the shear wave velocity is 1000 fps, the fineness of the grid allows the undistorted transmission of shear waves with
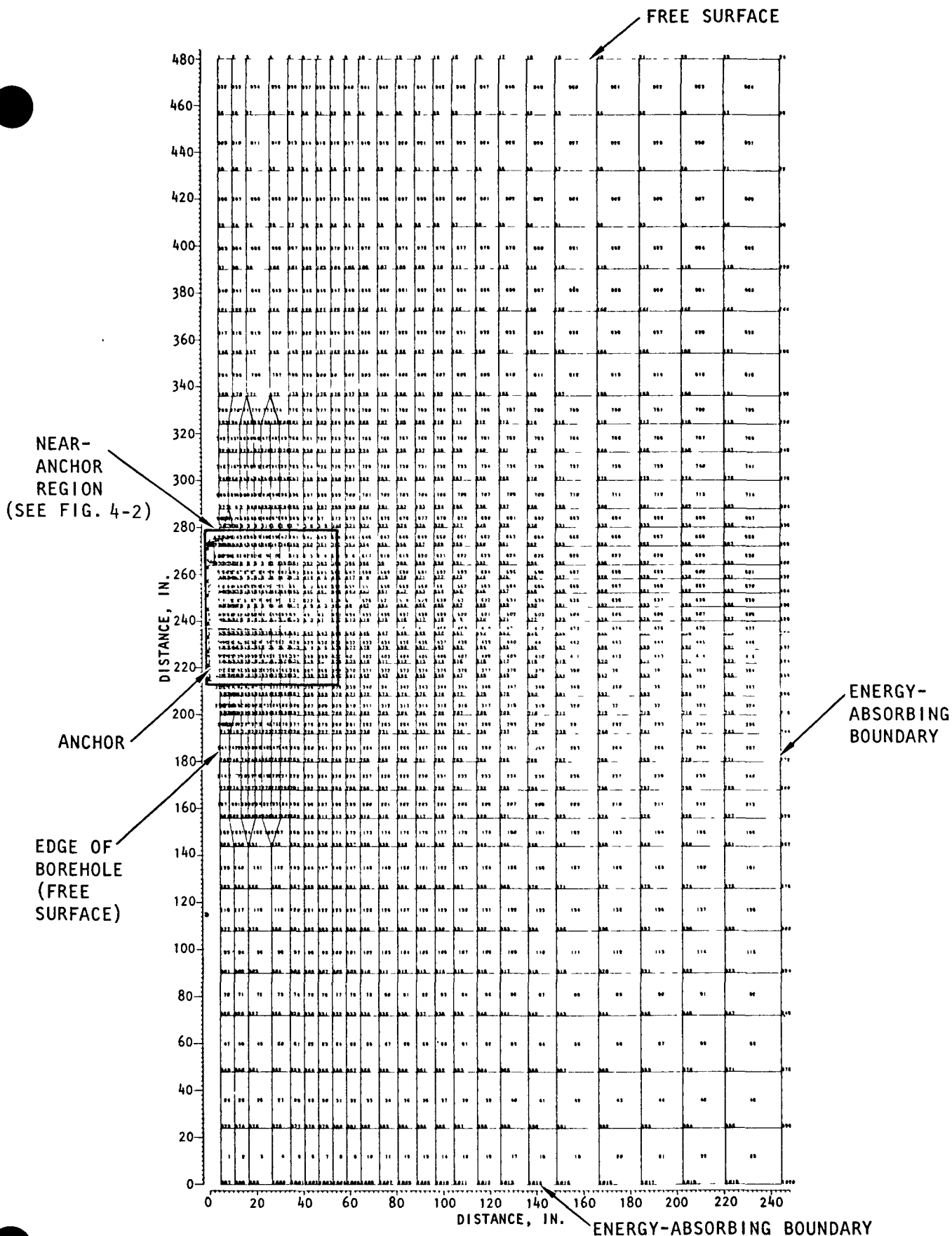
FIGURE 4-1. FINITE ELEMENT GRID

-55-

a frequency content of up to 500 Hz* out to a distance of 5 feet from the anchor. Furthermore, in the near-anchor region, shear waves with frequency components of up to 1500 Hz can be propagated without distortion. In the nonlinear calculation, in which the shear wave velocity varies but is typically between 400 and 500 fps, shear waves having frequencies of up to 200 Hz can be accurately transmitted to a distance of 5 feet from the anchor and signals of up to 600 Hz are permissible near the anchor. Typical free-field velocity histories for a soil medium in which the material properties are virtually the same as those of the nonlinear finite element calculation are available from the special tests. The upper bounds of the frequencies contained in these velocity histories are about 300 Hz near the anchor and about 200 Hz at about 5 feet from the anchor. These values are well within the transmission capabilities of the finite element grid.

4.2.2   Application of Dynamic Loading

In the in situ test, loads are applied by means of a freely falling hammer, which strikes Belleville springs attached to the top of a relatively rigid anchor. The hammer, Belleville springs, anchor, and soil then form a coupled dynamic system through which loads are applied to the soil along the vertical anchor/soil interface. As shown in Fig. 4-2, this dynamic system is incorporated as completely as possible into the finite

---

* It is assumed that good resolution of a frequency component of a shear wave is assured if the ratio of wave length, L, to mesh size equals or exceeds 4. The highest frequency component compatible with a given nodal-point spacing, d, can then be computed from the formula

$$f = \frac{V_s}{L} = \frac{V_s}{4d}$$

where V_s is the shear wave velocity of the medium, and f is the maximum frequency in Hz.
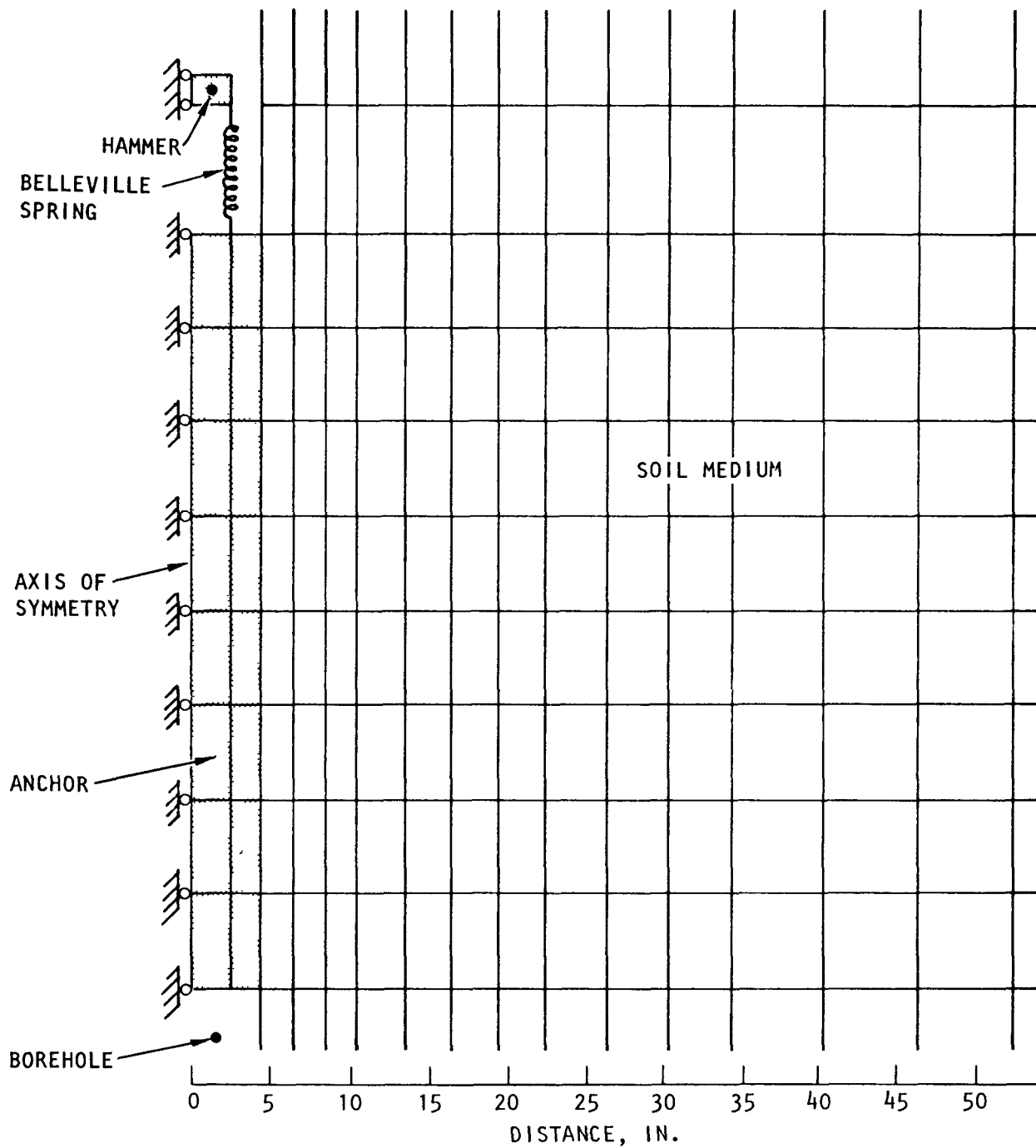
FIGURE 4-2. ENLARGED VIEW OF THE NEAR-ANCHOR REGION OF GRID

element model. The Belleville springs are represented as a
one-dimensional massless element with a finite compression
stiffness of 322 kip/in. This element has no tension stiffness
in order to allow for possible uplift of the hammer. The top
of the spring element of Fig. 4-2 is connected to a single
element which simulates the dropped hammer. The weight of this
element was taken to be 150 lb for the elastic calculation, and
58 lb for the nonlinear calculation. The anchor is modeled
using axisymmetric elements that are very stiff when compared
to the soil. The total weight of these elements corresponds
to the actual weight of the anchor (195 lb). The anchor elements
are considered to be fully bonded to the adjacent soil elements.

Time-zero of each calculation is taken to be the
time at which the freely falling hammer makes initial contact
with the Belleville spring. The drop height of the hammer is
entered into the calculation in the form of an initial velocity
corresponding to the velocity of the hammer immediately prior
to initial contact with the Belleville spring when released
from the specified drop height. The initial conditions are as
follows:

$$x(0) = 0$$

$$\dot{x}(0) = \sqrt{2gh}$$

where: $x(0)$, $\dot{x}(0)$ = initial displacement and velocity
                    of the hammer
            g = acceleration due to gravity =
                32.2 ft/sec^2
            h = height above Belleville spring from
                which hammer is dropped

In the elastic case the drop height was 2 feet, resulting in
an initial velocity of 11.35 fps. In the nonlinear case the

drop height was 6 inches, corresponding to an initial velo-
city of 5.67 fps.

4.2.3   Representation of Soil Materials

        The properties of the soil in the elastic finite
element calculation are as follows: the shear wave velocity
is 1000 fps, Poisson's ratio is 0.3, and the unit weight is
100 pcf. The material model used in the nonlinear finite element
calculation was designed to fit cyclic triaxial test data
obtained from the sand used in the special pit tests. The
material model used is of the variable-modulus type in which
the instantaneous tangent shear and bulk moduli are computed,
for each integration step of the calculation, as a function of
the current state of stress and the stress history of each
element of the grid. Hysteresis is incorporated into the
shear modulus by distinguishing, on the basis of stress history,
between the conditions of virgin loading and of unloading/reloading.
Virgin loading exists if the current principal component of shear
stress exceeds all previous values. Otherwise the element is
undergoing unloading/reloading. A thorough description of the
soil model, along with numerical values of the parameters used
and curves comparing the model with the cyclic triaxial data,
is contained in Appendix A.

4.2.4   Integration Time Step

        The integration time-step schedule for the elastic
calculation is 0.05 msec for the first 7 msec, 0.1 msec for
the next 5 msec, and 0.2 msec thereafter, resulting in a total
record length of 20 msec. This time increment schedule is much
finer than that required merely to satisfy the dynamic stability
criteria of the finite element method. The fineness of the time
increment arises from the necessity of knowing the time of
arrival, at a particular location, of various key features of

the response signature, such as the first peak of the particle velocity. In computing the travel times of these key features across distances as small as 2 inches, for which the transit time of a pulse propagating at 1000 fps is 0.167 msec, it is necessary to know the arrival times of these features to within a margin of error which is small compared to this transit time. While the time increment of 0.05 msec may not be small enough to allow satisfactory resolution over a 2 inch interval, inter-polation techniques can be applied to the data, if necessary, to improve the resolution.

A similar line of reasoning was used to select a time-increment schedule for the nonlinear calculation. Although the shear wave velocity in this case is not constant, its average value is about half as large as the shear wave velocity of the elastic calculation. Therefore transit times between adjacent nodal points are approximately twice as long in the nonlinear calculation as in the elastic case. For this reason the nonlinear calculation consisted of time increments twice the size of those of the elastic calculation. The schedule is as follows: 0.1 msec for the first 14 msec, 0.2 msec for the next 10 msec, and 0.4 msec thereafter, resulting in a total time span of 40 msec.

4.3 RESULTS OF ANALYSIS

Results of the dynamic analyses are obtained in the form of motion time histories for each nodal point in the grid, and stress and strain time histories for each element. As noted in Section 4.1.1, these results are used to assess data pro-cessing techniques currently used in the in situ soil test program. In addition, the results are used to study the characteristics of the waveforms generated in the soil during the in situ tests. These assessments and studies are summarized in the remainder of this section.

4.3.1   Comparison with Experiment

It was pointed out in Section 4.1.1 that the finite element calculations can be used to evaluate the data processing procedures without comparing the calculations with experimental results. In fact the elastic calculation is used exactly this way, in that there has been no experiment conducted in an elastic medium. However, since the nonlinear finite element calculation more nearly simulates the special test conditions, its comparison with experimental results is possible. The application of the results of the evaluations of data processing procedures to the processing of actual field data would be greatly facilitated if good correlation between calculation and experiment were to be obtained. For the sake of credibility, therefore, it seems appropriate that the discussion of the analytical results should begin with a comparison of the nonlinear finite element results with the results from the special experimental pit tests. The sensors from the special pit tests used in this comparison are shown in Fig. 4-3.

The velocity histories recorded from the special pit tests were obtained using velocity transducers having the frequency-response spectrum of Fig. 4-4. The experimental displacement histories were obtained by integration of the velocity histories. In order to provide a consistent comparison between calculation and experiment, it is necessary to adjust the calculated free-field response in a manner that simulates the effect of the transducers. This is accomplished by operating on the calculated velocities with a transfer function having the frequency response of Fig. 4-4. Adjusted displacements are then obtained from the adjusted velocities by integration. Both the original calculated response and the adjusted response are shown in the comparison plots which follow.
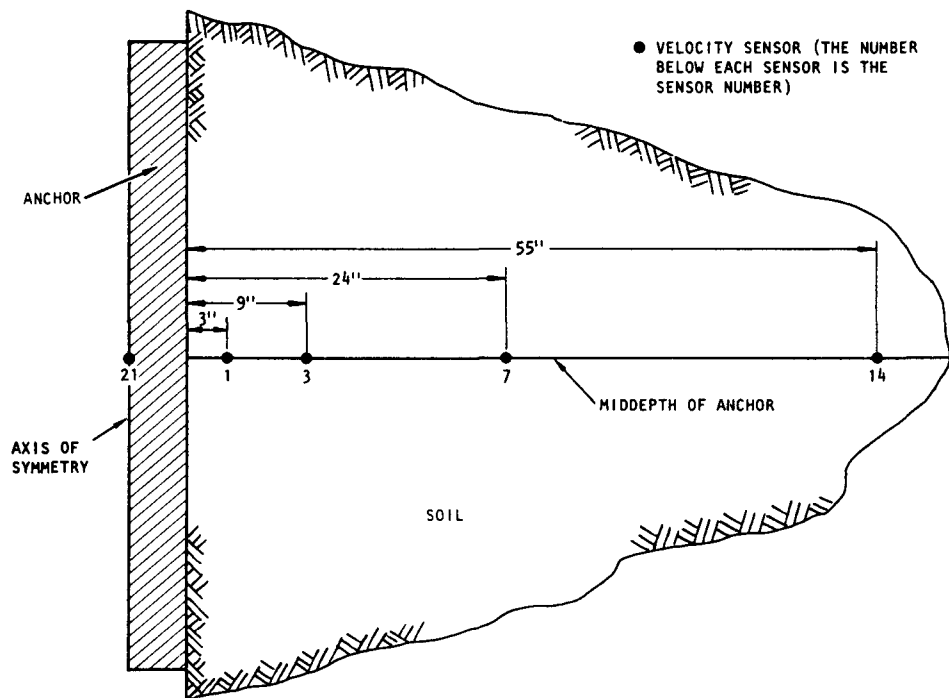
FIGURE 4-3. NOMINAL LOCATIONS OF SPECIAL TEST VELOCITY SENSORS USED IN COMPARISON WITH CALCULATED RESULTS
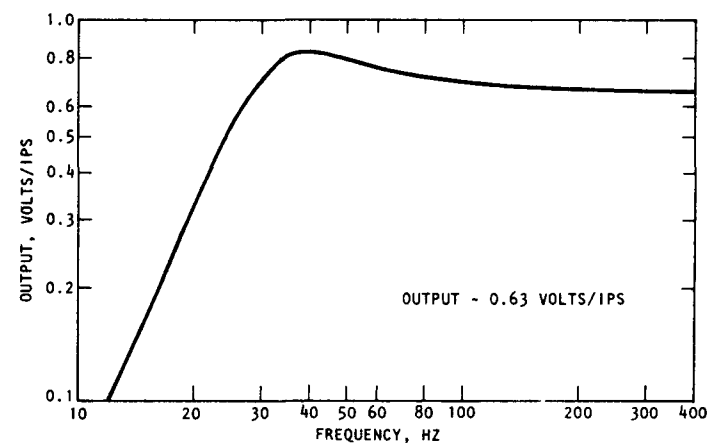
FIGURE 4-4. FREQUENCY-DEPENDENT OUTPUT FROM GEOPHONE -- S&W/AA FY 75 FIELD TESTS

Figs. 4-5 to 4-9 show comparisons between the experimental and the calculated response during an in situ test. Since there is no way to correlate the starting time of the experimental time histories with the starting time of the calculated time histories, arbitrary time shifts have been employed. For any given nodal point, the velocity and displacement histories have been shifted by equal amounts. The experimental results, plotted as solid lines, correspond to mean response curves taken over several repetitions of the test. The calculated results shown are from nodal points located the same distances from the anchor as the sensors to which they are being compared. In cases where no nodal point occurs at the approximate location of a particular sensor, responses of the two nearest neighboring nodal points on either side of the actual sensor location are shown.

Comparisons of the unadjusted calculated responses with the experimental responses indicate an excellent agreement among the velocities. The computed peaks tend to be slightly low at the anchor and slightly high at large distances from the anchor, suggesting that the calculation may have slightly underestimated the dissipative properties of the soil. But the general form of the calculated velocity response appears to be accurate throughout the entire time span of the experiment. The displacement histories show less agreement. A noticeable difference between calculation and experiment involves the occurrence of permanent displacements in the near-anchor region of the finite element results. There is no evidence of permanent displacements in the experimental data.

Reasons for this difference between the computed and measured displacement histories can be attributed, at least in part, to the frequency characteristics of the sensor. As noted in Fig. 4-4, the sensor has extremely low output at low frequencies. This suggests that any permanent displacements, which essentially
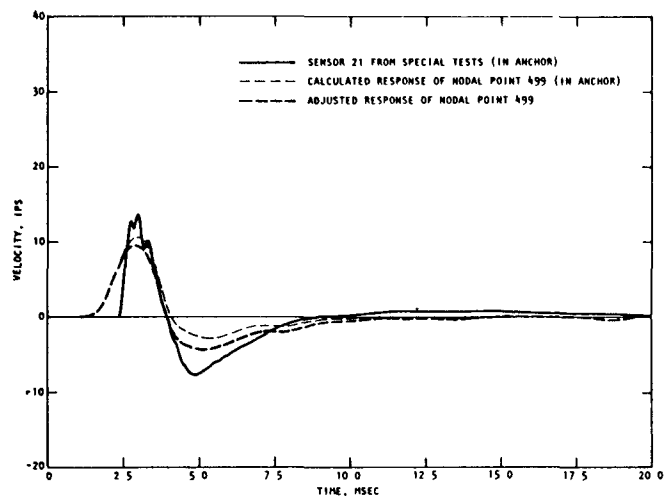
(a) Vertical velocity (positive downward)
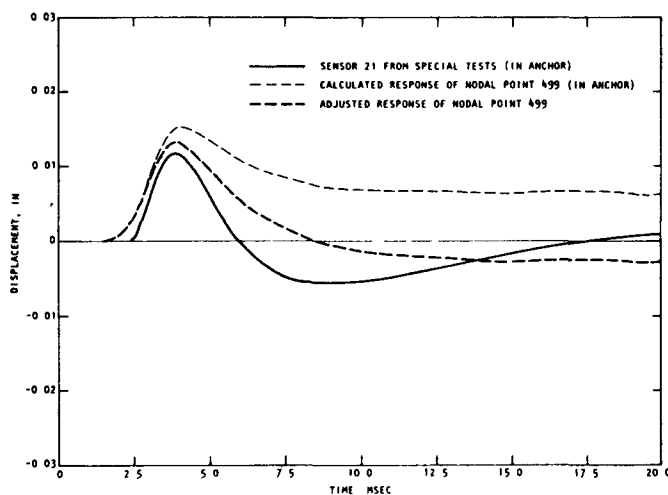
(b) Vertical displacement (positive downward)

FIGURE 4-5.   COMPARISON BETWEEN EXPERIMENT AND
CALCULATION OF ANCHOR RESPONSE
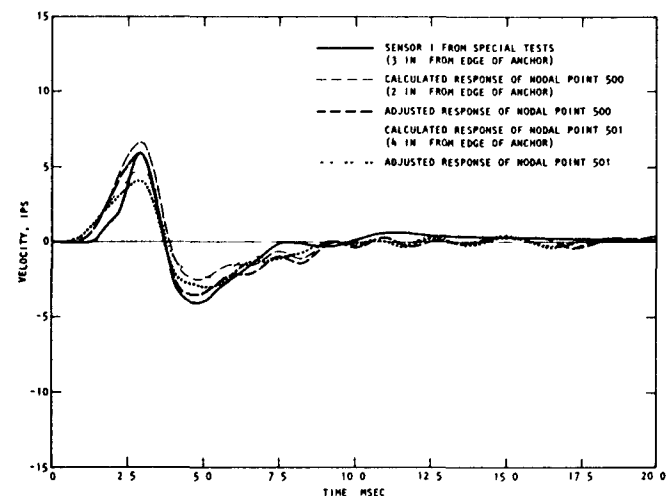
(a) Vertical velocity (positive downward)
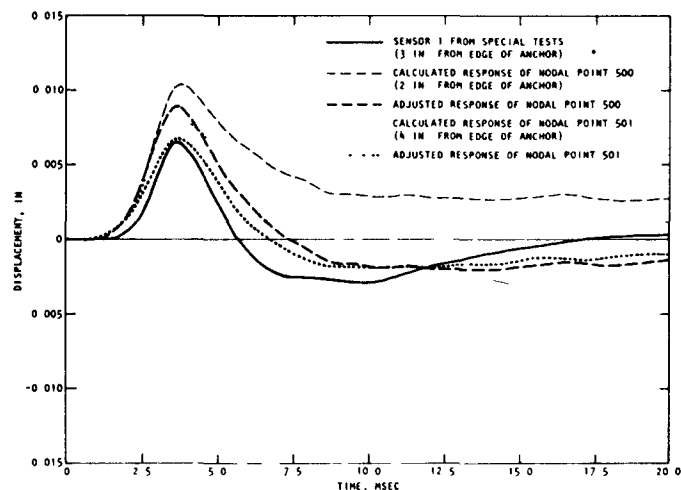
(b) Vertical displacement (positive downward)

FIGURE 4-6.   COMPARISON BETWEEN EXPERIMENT AND
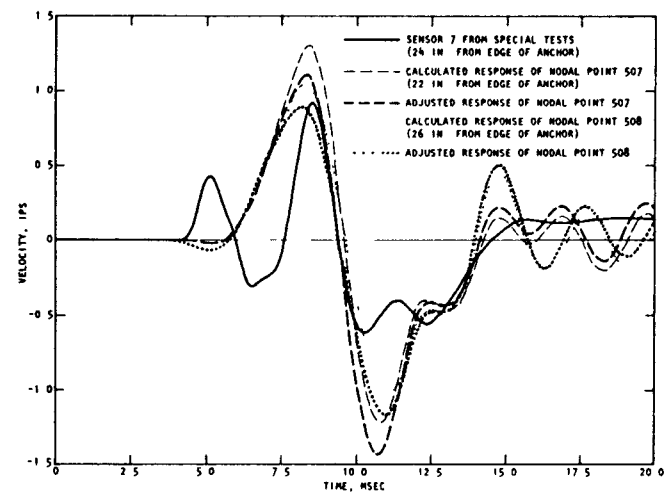CALCULATION OF RESPONSE 3 IN.
FROM EDGE OF ANCHOR
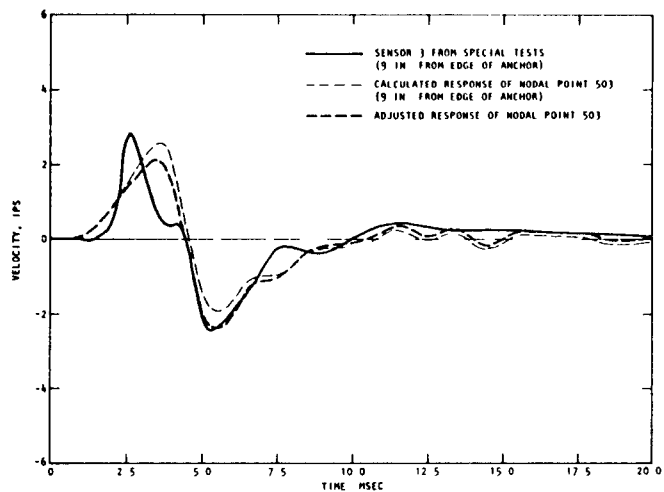
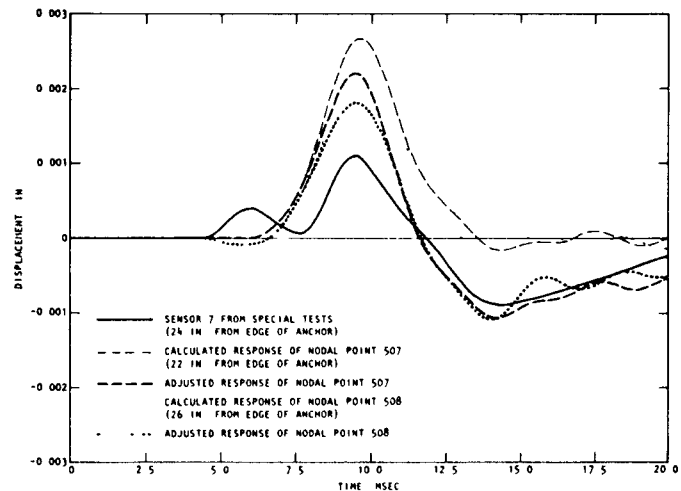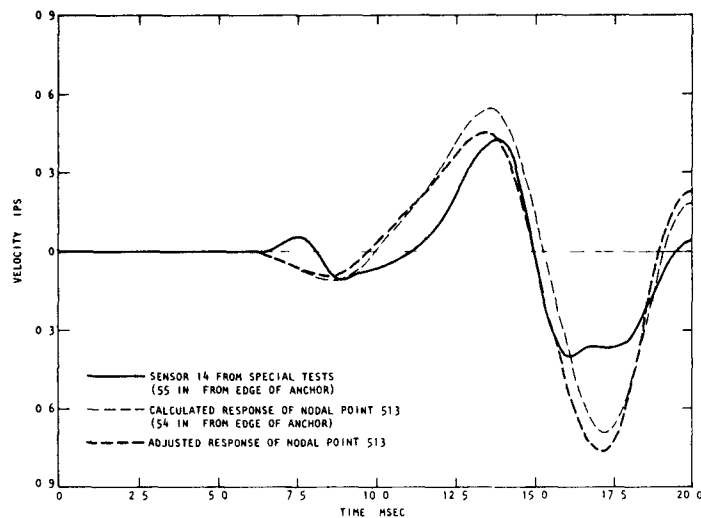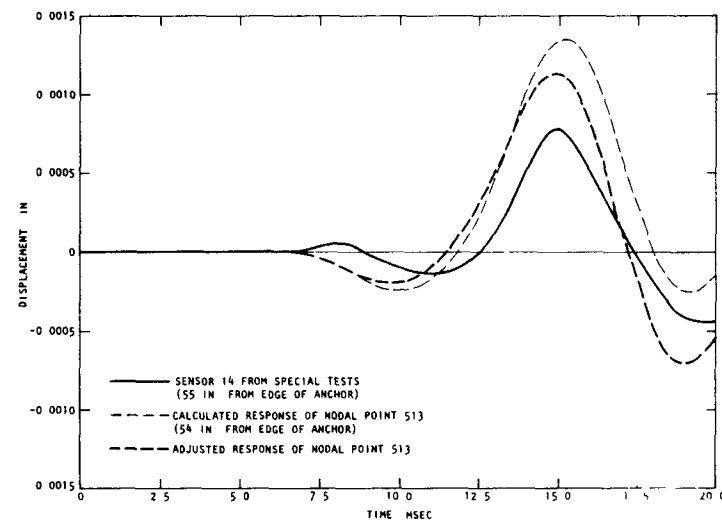(a) Vertical velocity (positive downward)
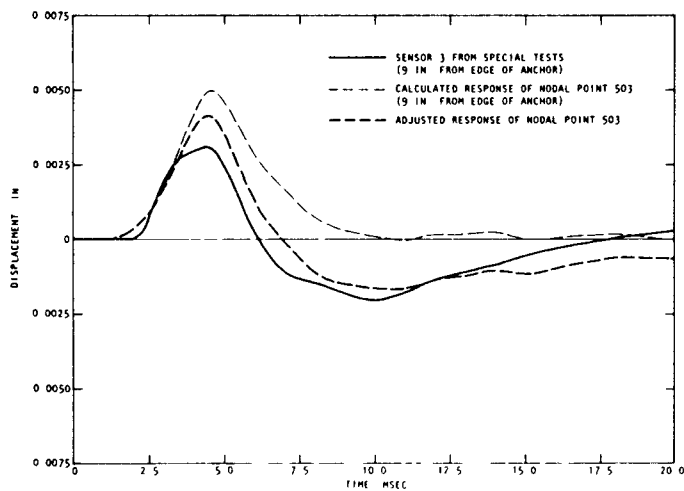
(b) Vertical displacement (positive downward)

FIGURE 4-7. COMPARISON BETWEEN EXPERIMENT AND
CALCULATION OF RESPONSE 9 IN.
FROM EDGE OF ANCHOR

(a) Vertical velocity (positive downward)

(b) Vertical displacement (positive downward)

FIGURE 4-8. COMPARISON BETWEEN EXPERIMENT
AND CALCULATION OF RESPONSE
24 IN. FROM EDGE OF ANCHOR

(a) Vertical velocity (positive downward)

(b) Vertical displacement (positive downward)

FIGURE 4-9. COMPARISON BETWEEN EXPERIMENT AND CALCULATION
OF RESPONSE 55 IN. FROM EDGE OF ANCHOR

correspond to a zero-frequency response, are filtered out by
the sensor. Therefore, it is most consistent to compare the
experimental response histories with the computed response
histories that have been adjusted to account for the presence
of the sensor. These comparisons, as shown in Figs. 4-5 to 4-9,
indicate a significantly improved correlation between the com-
puted and measured displacement histories. In fact, it can be
concluded that the adjusted finite element results provide a
generally excellent comparison with the experimental results
over the entire time frame of the computations. This high level
of correlation justifies the application of the conclusions of
this analytical study to actual field data.

Note that the adjusted displacements of the finite
element calculation show no indication of permanent displacements,
even though the unadjusted displacement histories show them
to be present near the anchor. This shows that these velocity
transducers though all matched to respond the same, may not
accurately measure permanent displacements, as explained above.
This observation together with the observation that the adjusted
finite element response has been quite successful at representing
the transducer output, indicates that permanent displacements
probably occur in the near-anchor region of actual in situ tests.

4.3.2   General Nature of Waves Generated During In Situ
        Soil Tests

The nature of the wave propagating away from the anchor
is of great importance to the success of the in situ soil test
program. For example, if the shear wave velocity is to be
successfully determined, it must be shown that the wave, or
some identifiable portion of it, is a shear wave. Furthermore,
the formulae used in determining the shear strain require the
stress field to be nearly uniform in the vertical direction.
Since the finite element results contain a vast quantity of

information pertaining to motions, stresses, and strains in the near-anchor region, systematic examination of these results can provide valuable insight as to the nature of the propagating wave.

Fig. 4-10 shows contour plots of the vertical component of particle velocity in the vicinity of the anchor at several instants of time. The contour plots show only the portion of the near-anchor region which lies above the middepth of the anchor. The velocity and stress fields shown in these figures are nearly symmetric with respect to the middepth. Essentially no information has been omitted, therefore, by showing only half of the near-anchor region. By comparing the position of the crest of the velocity wave of Fig. 4-10 with the position of the crest of the shear stress wave of Fig. 4-11, it can be seen that the two travel together. This indicates that the disturbance identified in the response of the velocity transducers of an in situ soil test is especially rich in shear and its propagation is governed by the shear properties of the soil medium. Furthermore, both Figs. 4-10 and 4-11 show that the variation of velocity and stress in the vertical direction is negligible compared with the variation in the radial direction. This observation validates the assumption that only radial gradients of vertical displacement need be considered in estimating shear strain.

Fig. 4-12 shows the shear stress vs. shear strain paths of several elements along the middepth of the anchor for the nonlinear finite element calculation. These elements are located at distances of 1 inch, 10.5 inches, 24 inches, and 57 inches from the edge of the anchor. The values of the secant shear modulus, G, and the damping ratio, λ, are shown for each element. It can be seen from this figure that both the modulus and the damping are significantly different for elements near the anchor, where strains are large, than for elements far from
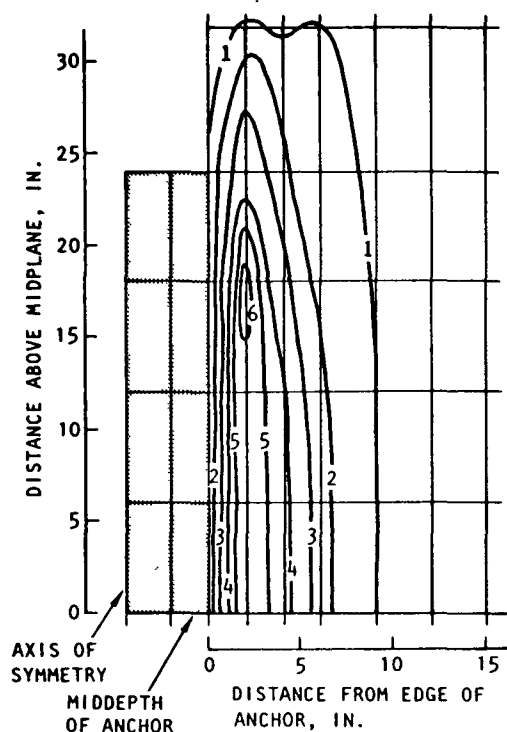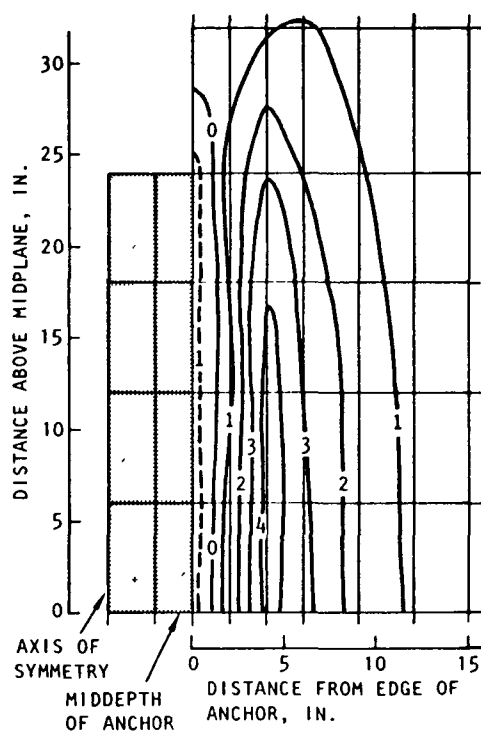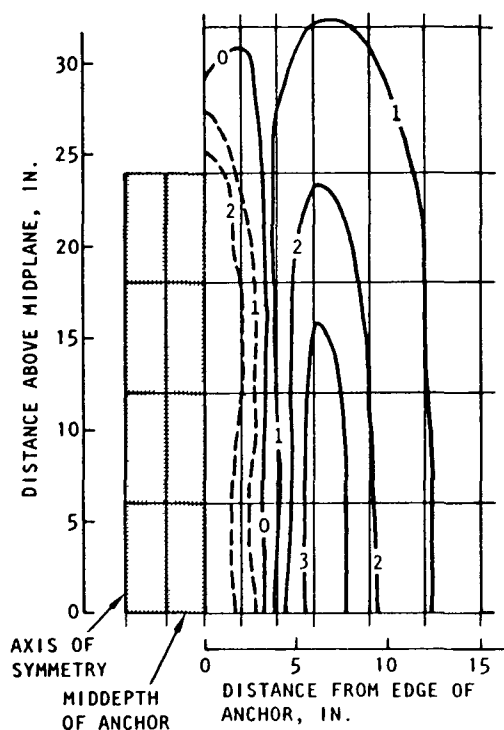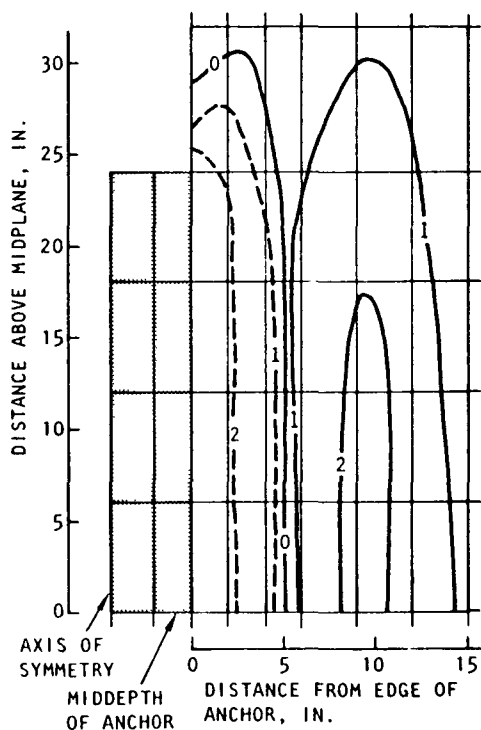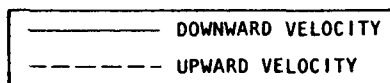
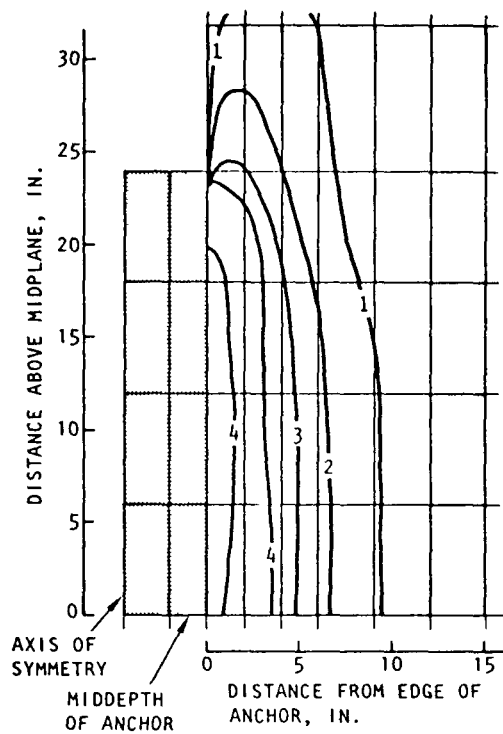FIGURE 4-10. CONTOUR PLOTS OF VERTICAL VELOCITY (IPS) IN THE NEAR-ANCHOR REGION

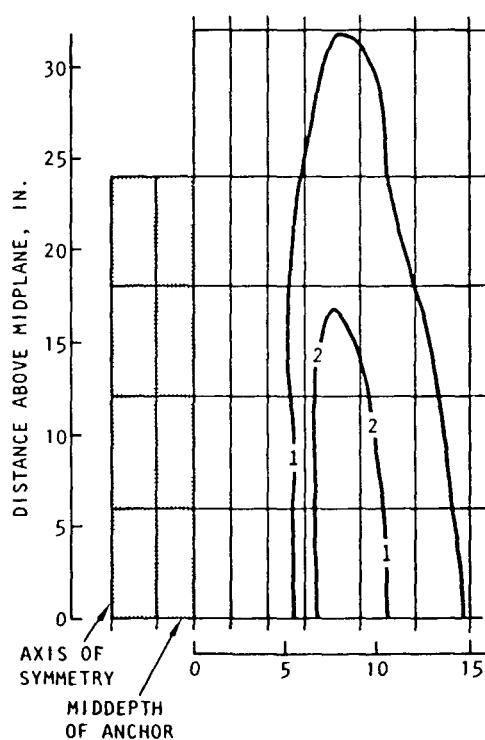-69-
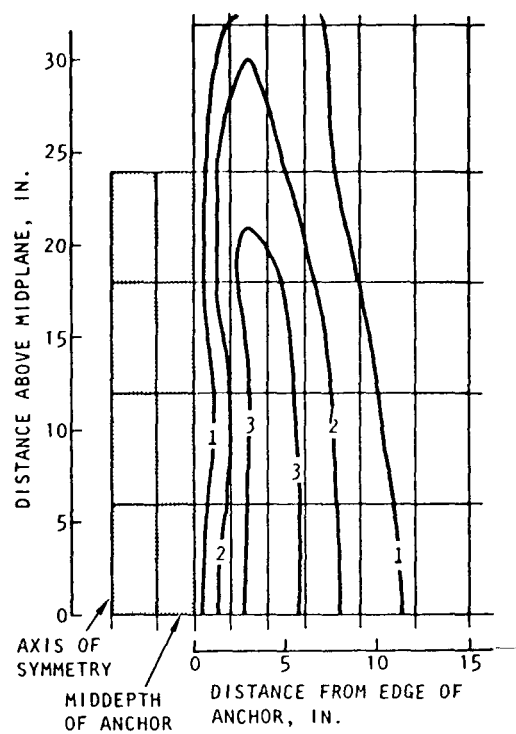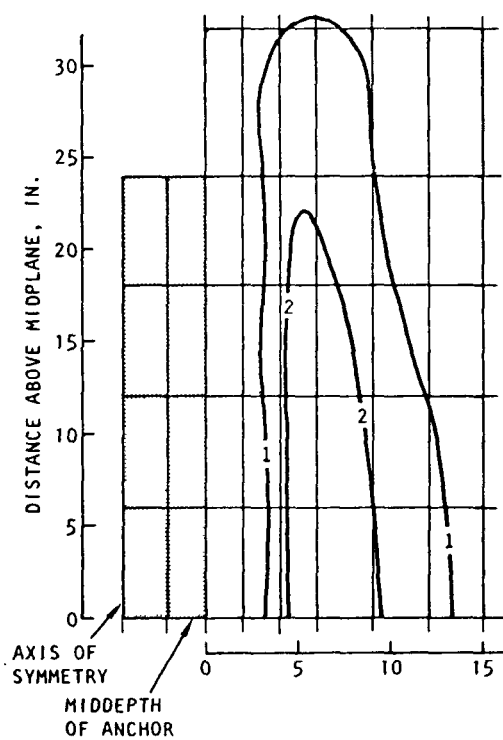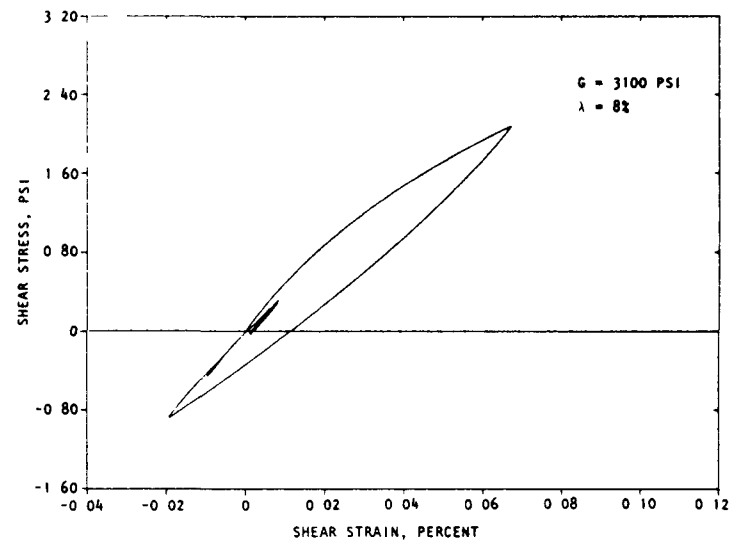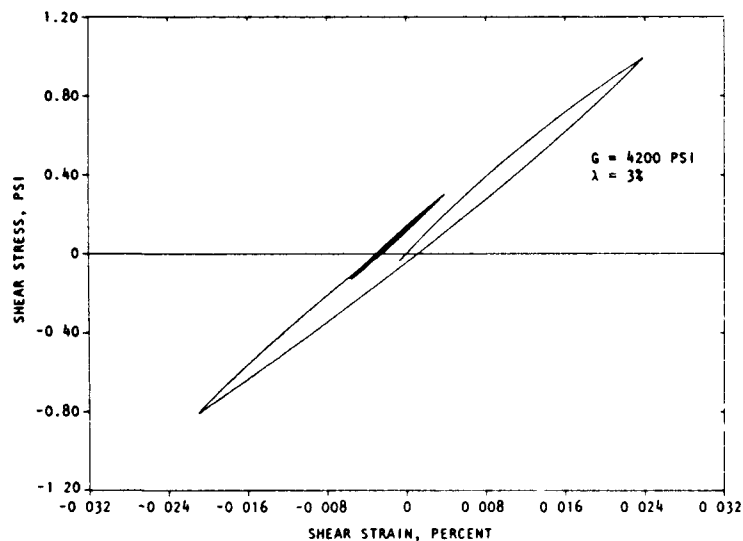
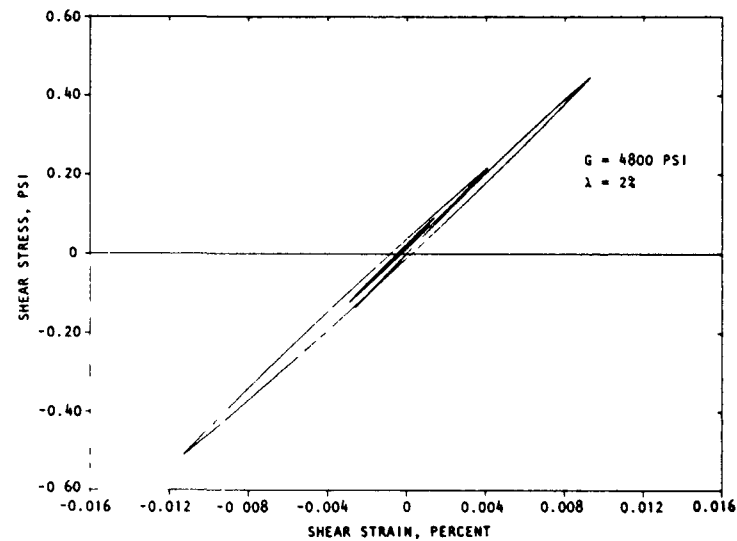FIGURE 4-11. CONTOUR PLOTS OF SHEAR STRESS (PSI) IN THE NEAR-ANCHOR REGION
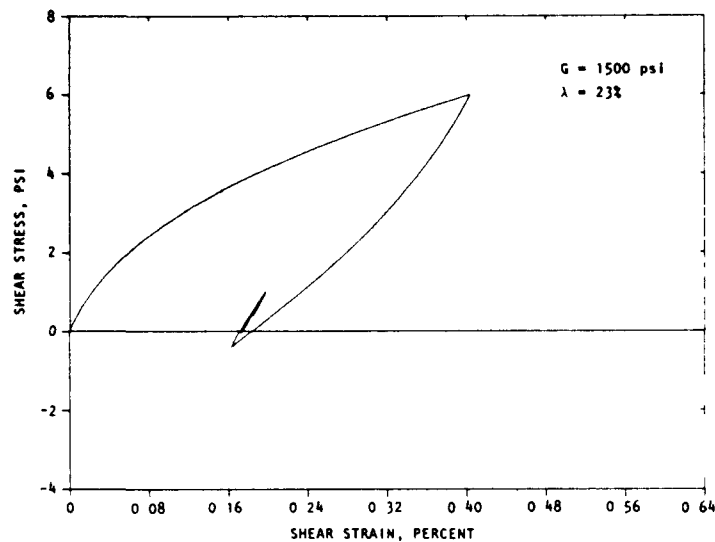
(a) Element 480, 1 in. from edge of anchor

(b) Element 484, 10.5 in. from edge of anchor

(c) Element 488, 24 in. from edge of anchor

(d) Element 494, 57 in. from edge of anchor

FIGURE 4-12. SHEAR STRESS VS. SHEAR STRAIN CURVES FOR SELECTED SOIL
ELEMENTS -- NONLINEAR FINITE ELEMENT RESULTS

the anchor. The most rapid changes in both G and λ occur near the anchor. The changes in both parameters become much more gradual with increasing distance from the anchor.

Due to the hysteretic nature of the soil material, permanent distortions of elements near the anchor remain after the excitation has quieted down. This effect can be seen most clearly in Fig. 4-12a. These permanent strains can be explained by making the observation that equilibrium is a condition requiring zero shear stress. The return to equilibrium from the state of maximum stress follows a stress/strain path different from that by which maximum stress was originally attained; therefore, the strain at which zero stress prevails is nonvanishing. As seen in Fig. 4-12, this phenomenon quickly disappears with increasing distance from the anchor.

4.3.3   Assessment of Data Processing Procedures for
         Determination of In Situ Shear Wave Velocities

The shear wave velocity is an important property of the soil medium in that it leads directly to the shear modulus by way of the relationship

$$G = \rho \, V_s^{\,2} \tag{4.1}$$

where G is the shear modulus, ρ is the mass density, and V_s is the shear wave velocity, all expressed in a consistent set of units. In addition, the shear wave velocity is required for the estimation of shear strain, as discussed in Section 4.3.4.

Thus far in the in situ test program, two different approaches have been used to estimate shear wave velocities. The first approach is termed the time-history method and identifies a particular feature within the measured velocity histories

recorded at adjacent sensors. The delay time associated with that feature, i.e., differences in the time of occurrence of the feature at adjacent sensors, is determined from the sensor records. The shear wave velocity of the soil medium between these sensors is then computed as the ratio of the sensor spacing and the delay time.

A second approach is termed the waveform method and utilizes the displacements at the various sensors (obtained by integrating the velocity histories) to define wave profiles at different discrete times. A specific feature on each displacement profile, such as the crest of the wave, is then identified, and its location within the soil medium is noted. The distance traveled by this feature during a given time interval is used to estimate the shear wave velocity.
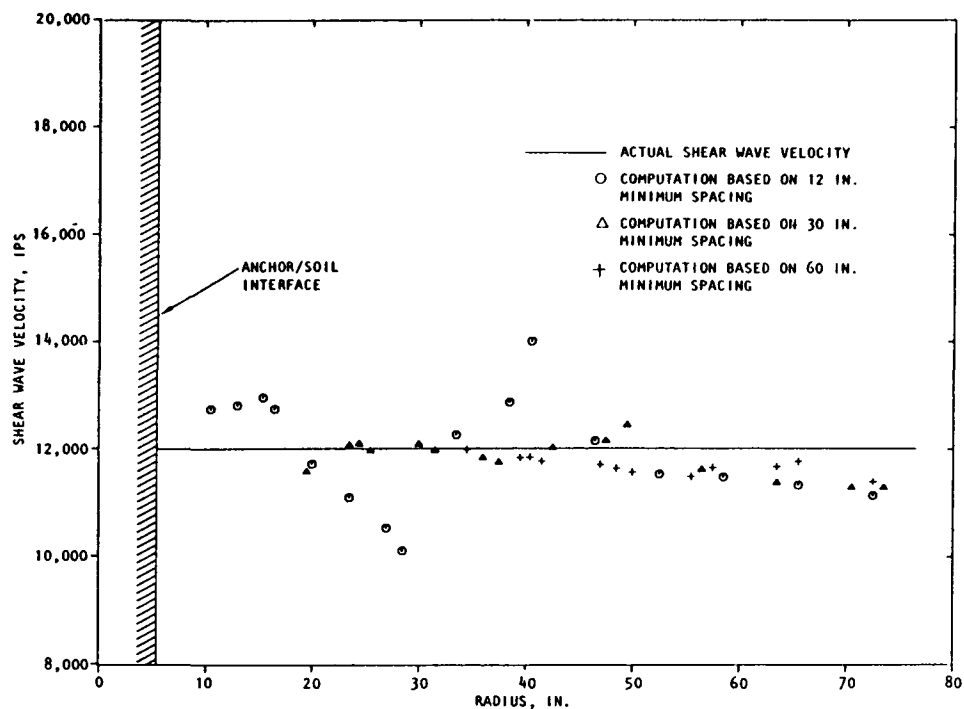
a. Time-History Methods

The time-history methods primarily used thus far for estimating shear wave velocities from in situ response measurements have been based on the first downward peak of the velocity history and the zero crossing of the velocity history after this peak (which corresponds to the first downward peak of the displacement history). These features were identified in the velocity histories for nodal points located along the middepth of the anchor. The resulting shear wave velocity computations were then compared to the original soil properties used as input to both the elastic and the nonlinear finite element calculations.

When computing shear wave velocities using time-history methods the time required for a feature of the velocity signal to propagate a given distance is first noted. The shear wave velocity is then computed as the ratio of the given distance

to this propagation time. Geometrically, this process amounts
to computing the slope of the position-time diagram of the
feature being observed. Thus, the computation of shear wave
velocity involves a process of numerical differentiation, a
process which is well known for its tendency to magnify the
fluctuations of a time-history record. This tendency to exag-
gerate local fluctuations can be counteracted somewhat by choosing
large distances or time intervals over which the differentiation
is performed. However, this carries with it a penalty in
sensitivity.

Fig. 4-13a shows the shear wave velocities as
computed by the method of zero crossing of the velocity histories
for the elastic case. Fig. 4-13b shows the shear wave velocities
as calculated by the method of peak velocities. In both cases
the actual shear wave velocity is indicated by a solid line.
Minimum sensor spacings of 12 inches, 30 inches, and 60 inches
have been used in these figures. The calculations involving 12
inches minimum spacing show an objectionable amount of scatter,
while those corresponding to 30 inches and 60 inches are rela-
tively scatter free. The results of the zero-crossing method
agree remarkably well with the actual shear wave velocity. The
results of the peak-velocity method are less accurate near the
anchor, and improve with increasing distance from the anchor.
However the results are acceptable throughout the entire radius
range shown in the figure.

Fig. 4-14a shows the zero-crossing method applied
to the results of the nonlinear calculation, while Fig. 4-14b
shows the results of the peak-velocity method. The solid line
in each figure shows the shear wave velocity based on the secant
shear modulus of each element of soil. The secant shear modulus
is computed as the peak shear stress divided by the peak shear
strain of each element. For the 12-inch minimum spacing, there
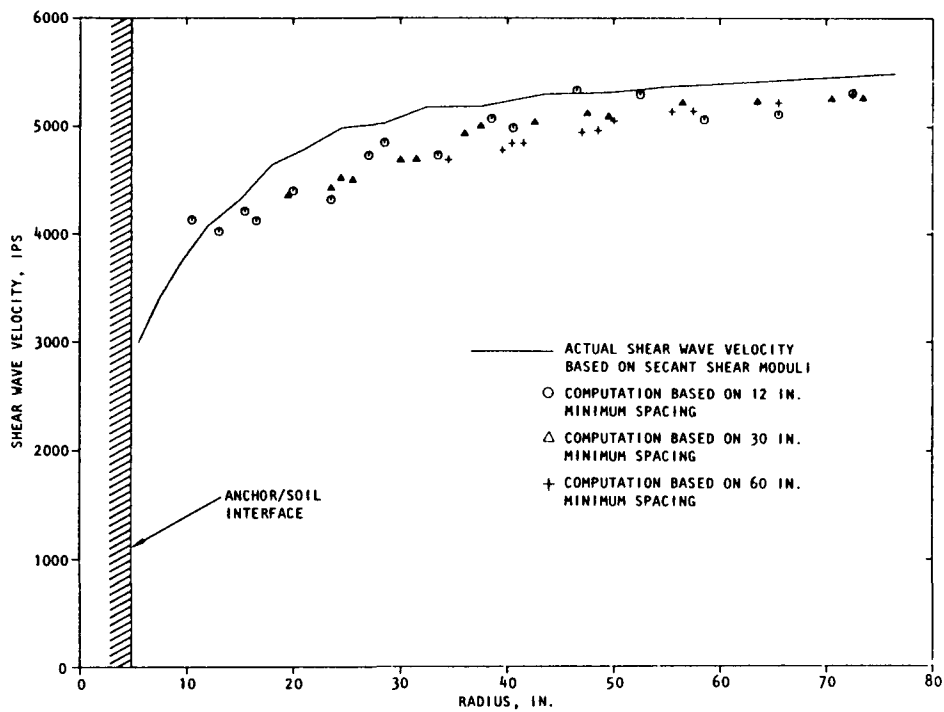is an objectionable amount of scatter associated with the peak-
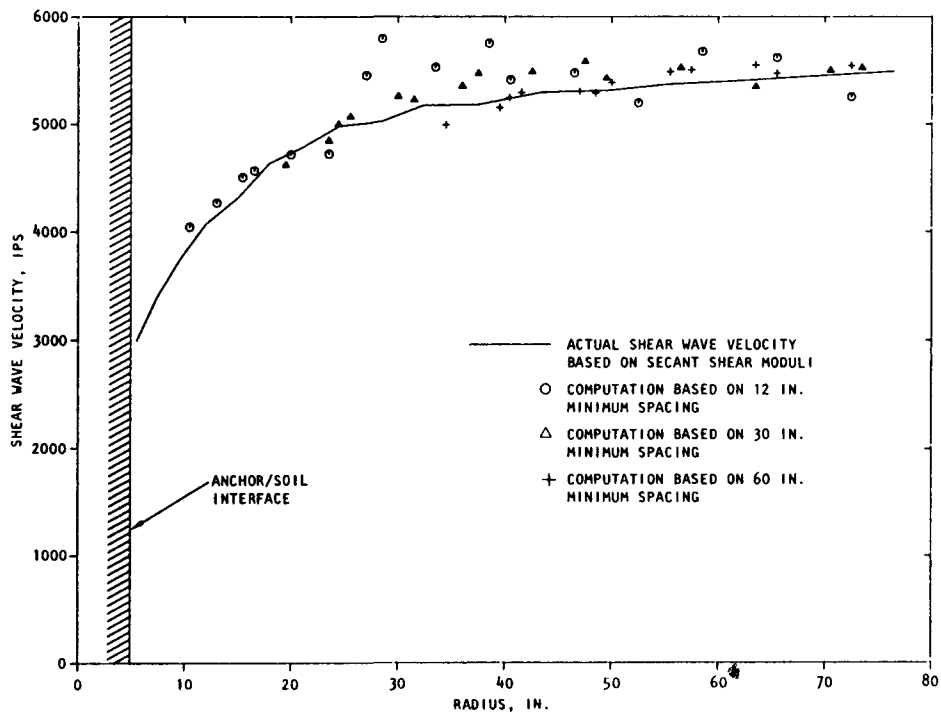
(a)   Zero crossing of velocity history
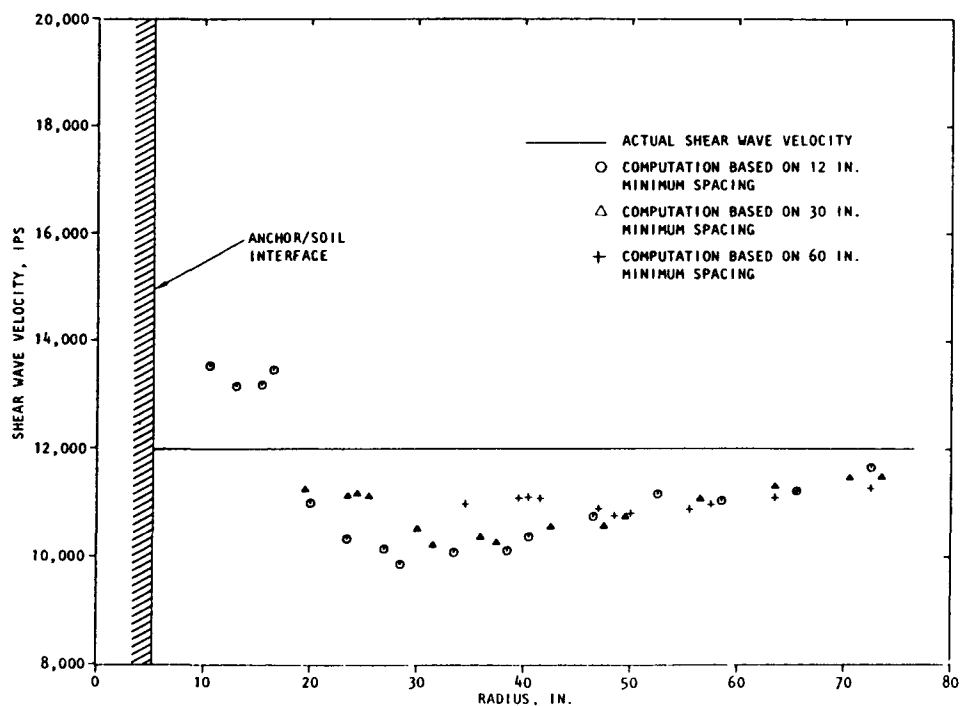
(b)   First peak of velocity history

FIGURE 4-13.   SHEAR WAVE VELOCITIES COMPUTED USING TIME-HISTORY
METHODS -- ELASTIC FINITE ELEMENT RESULTS

(a) Zero crossing of velocity history

(b) First peak of velocity history

FIGURE 4-14.   SHEAR WAVE VELOCITIES COMPUTED USING TIME-HISTORY
METHODS -- NONLINEAR FINITE ELEMENT RESULTS

velocity method. In fact, the peak-velocity method seems to show more scatter at all sensor spacings than does the zero-crossing method. On the other hand, disregarding the results obtained using 12-inch minimum spacing, the peak-velocity method seems to fall slightly closer to the actual shear wave velocity. The difference between the results of the two methods may be related to the trend whereby the peak velocity occurs while the element is undergoing peak shear stress, whereas peak displacement occurs during unloading under conditions of low stress. Due to nonlinearity, therefore, the shear wave velocities involved in the propagation of the peak velocity and the zero crossing are slightly different. In the case of the nonlinear finite element calculation, the peak-velocity method produced slightly superior results. However, it cannot be concluded that this method will prove to be superior in all cases. In spite of the slight difference in results, both methods provide acceptable accuracy for the more distant stations (i.e., for distance greater than 20 inches from the anchor).

The above methods for determining shear wave velocity involve measurement of the travel time of some feature of the wave as it propagates from one sensor to another. The shear wave velocity computed in this manner is an average value for the region between the sensors. An alternative approach, referred to as the curve-fit approach, enables the determination of shear wave velocity at a point, rather than for a region between sensors. To apply this approach, time-of-occurrence data for the wave feature under observation are required at several locations. A curve of the form

$$T(r) = \frac{a_1}{r} + a_2 + a_3 r \qquad\qquad (4.2)$$

is then fitted to these data, where $T(r)$ is the time-of-occurrence function, r is the distance from the axis of symmetry, and a_1, a_2, and a_3 are undetermined coefficients. The slope of the curve

at any point determines the shear wave velocity at that point. Since this can be computed analytically, there is no numerical differentiation associated with this approach. Reduced scatter, therefore, is one of its advantages.

Fig. 4-15 shows time-of-occurrence data for zero crossing and peak velocity for nodal points along the middepth of the anchor in the nonlinear finite element calculation. These data have been fitted, using a least-squares procedure, with curves having the form of Eq. 4.2. These curves are shown in the figure as solid lines. It is seen that the comparison between the analytical approximation of Eq. 4.2 and the raw data is excellent. It can be concluded, therefore, that Eq. 4.2 is an appropriate form with which to seek an analytical approximation of the time-of-occurrence data. Eq. 4.2 can be used to fit these data as long as there are at least three data points.

Fig. 4-16 shows the shear wave velocity of the nonlinear finite element calculation as computed by the zero-crossing and peak-velocity curve-fit methods. The time-of-occurrence functions, Eq. 4.2, were fitted based on data from all of the nodal points at the middepth of the anchor. Shear wave velocity was then computed at each nodal point location. The resulting data sets show no scatter at all. In fact, since the time-of-occurrence function is represented analytically, it would have been possible to plot the shear wave velocity calculations as continuous curves. It is evident from Fig. 4-16 that shear wave velocity measurements at the anchor-soil interface are possible, using the curve-fit approach. This was not the case using the original approaches for estimating travel times. Furthermore, the accuracy seems to be acceptable throughout the range of Fig. 4-16 for both methods. Had fewer points been available for fitting the time-of-occurrence function, a slightly different analytical fit would, most likely, have been obtained. However, the results would have been equally free of
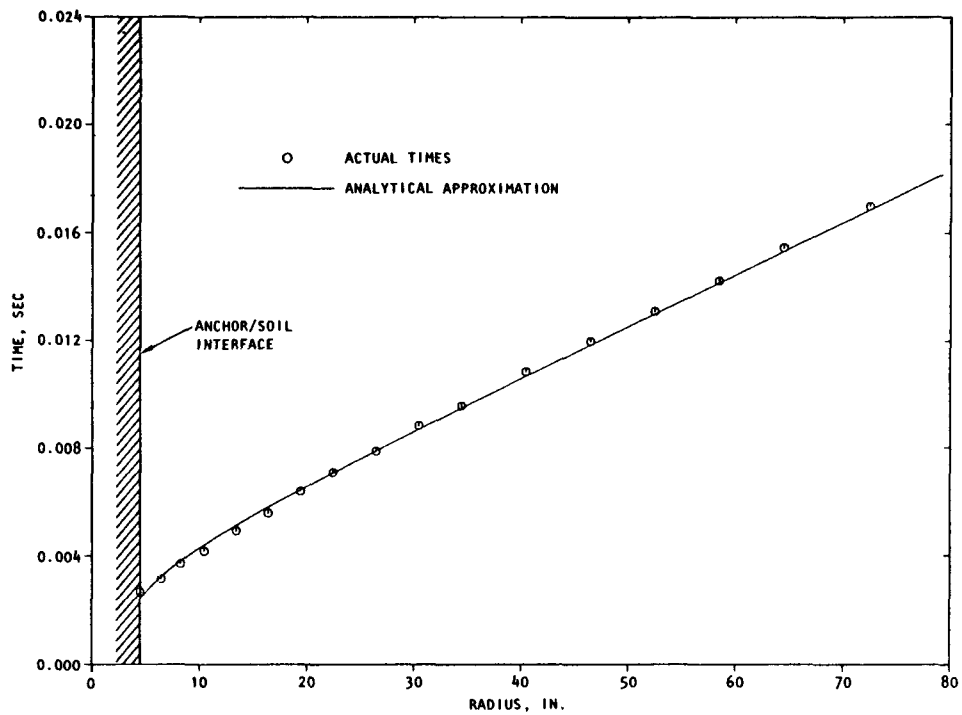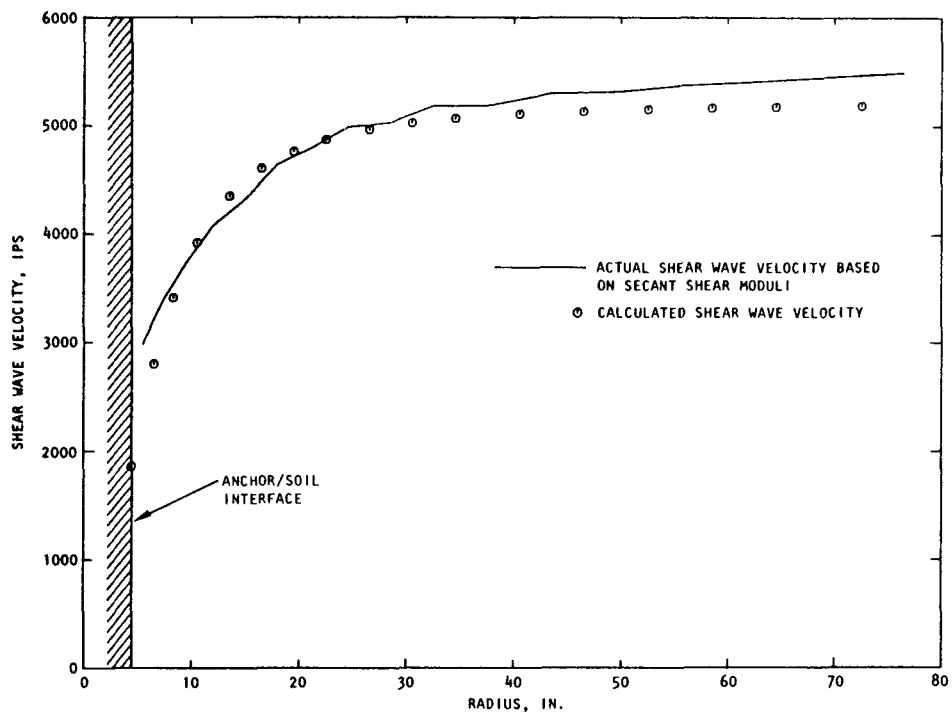
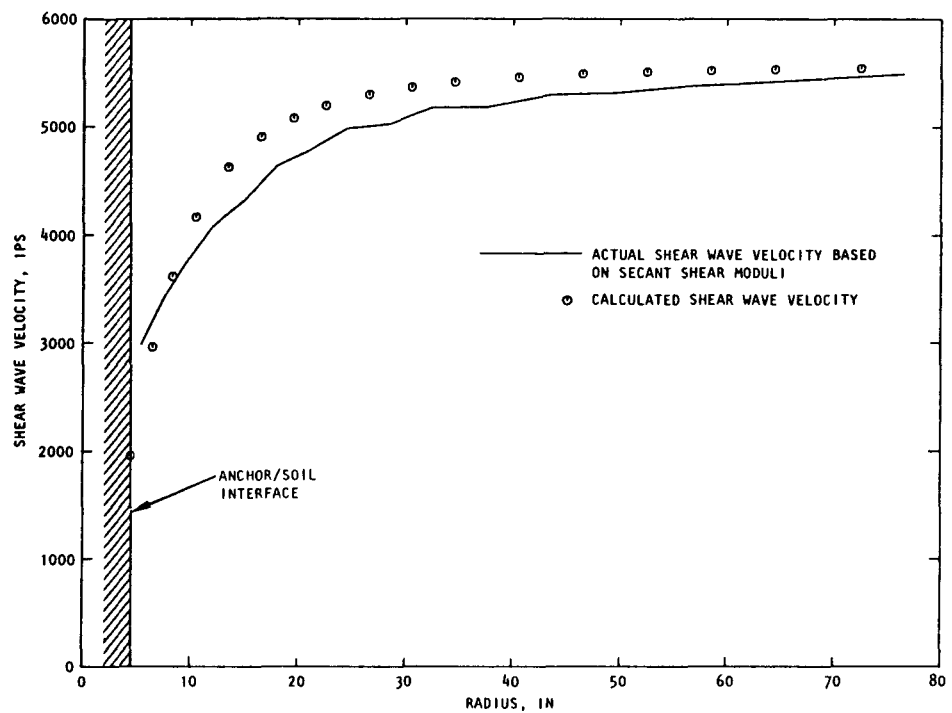(a) Arrival times of zero crossing of velocity
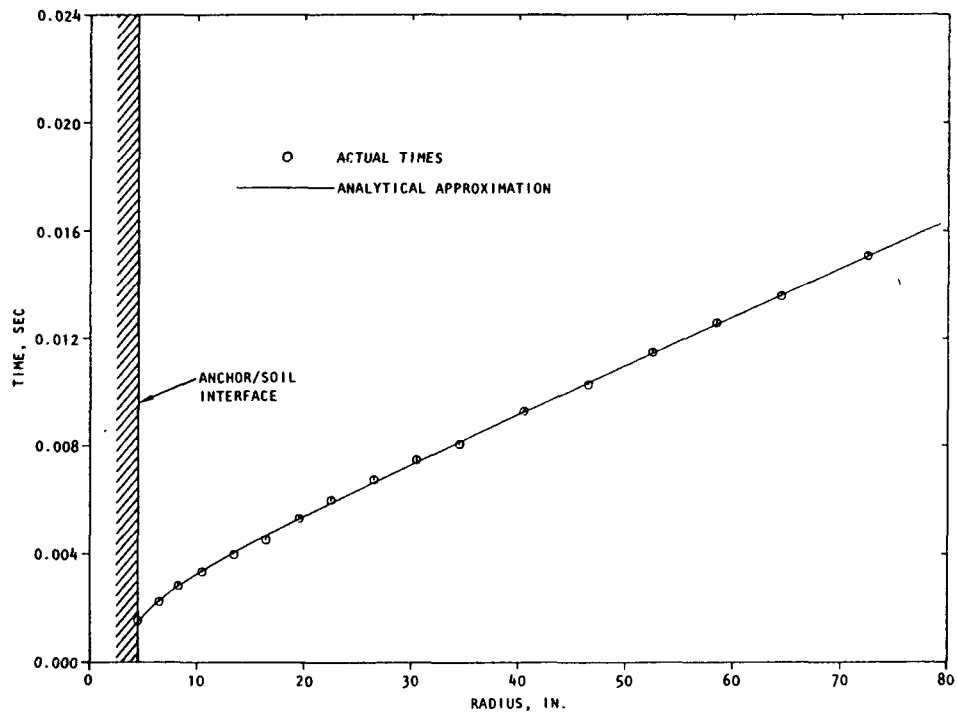
(b) Arrival times of peak velocity

FIGURE 4-15. TIMES OF PEAK AND ZERO CROSSING OF COMPUTED VELOCITY
HISTORIES -- NONLINEAR FINITE ELEMENT RESULTS

(a) Zero-crossing curve-fit method

(b) Peak-velocity curve-fit method

FIGURE 4-16. SHEAR WAVE VELOCITIES COMPUTED USING CURVE-FIT APPROACH --
NONLINEAR FINITE ELEMENT RESULTS

scatter and the amount of error would probably not have been
much greater.

b.   Waveform Methods

The time-history methods of computing shear wave
velocity in the soil medium are based on the propagation of
distinctive features of the response history observed at isolated
points in the soil medium. The waveform methods, on the other
hand, are based on the propagation of distinctive features of
the spatial distribution of free-field response observed at
isolated instants of time. The waveform methods employed in
the in situ test program thus far have been based primarily on
observations of the crest of the displacement wave. Although,
in theory, the shear wave velocity can be determined through the
observation of any feature of the wave, the displacement crest
has been selected primarily because it is easily identified
and relatively simple to work with. Furthermore, it has the
physical significance that it is a point of zero shear strain
and peak displacement, and occurs as the first identifiable
point on the velocity history measurement after the peak strain
has occurred. Thus it is more than merely an identifiable label
on the response profile; it is a significant feature of the
propagating shear disturbance.

Application of the waveform methods to in situ
data is hampered by a shortage of sensors in typical production
tests. The spatial resolution of velocity gages ordinarily
used in in situ production tests is inadequate for accurately
constructing the response profile at a given instant of time.
On the other hand, application of waveform methods to the finite
element results, due to the abundance of nodal points distributed
along the midplane of the anchor, does not suffer due to inade-
quate spatial resolution. Several displacement profiles,
constructed from the elastic finite element results, are shown

in Fig. 4-17a. The propagation of the crest of the displacement profiles is an easily recognized feature of this figure. The envelope of peak displacements is also shown in Fig. 4-17a. The peak displacement at a given location occurs when the displacement profile is tangent to the peak-displacement envelope at that point. It is obvious from the figure that when this occurs, the crest of the displacement profile occupies a different position, closer to the anchor than the point which is under-going its peak displacement. Thus, at points close to the anchor, the peak displacement at a point and the crest of the displacement profile at that point do not correspond to the same event. This is the basic difference between the time-history methods and the wave-form methods. However, beyond several feet from the anchor, the rate of attenuation of dis-placement with distance is small, and the crest of the wave-forms is identical to the zero-crossing point in the time-history method.

Fig. 4-17b shows several displacement profiles constructed from the nonlinear finite element results. The permanent displacements of near-anchor soil elements, which were discussed in Section 4.3.1, are evident in these profiles. These permanent displacements are of such magnitude that the displacement of a given nodal point near the anchor is never exceeded by the displacement of any other nodal points near the anchor at which the crest of the displacement profile never occurs. Even at several nodal points where there is a local maximum of the displacement profile, this feature is indistinct, making it difficult to determine the precise location of the crest. These problems render the wave-form methods ineffective in determining the shear wave velocity for the nonlinear case, particularly near the anchor. Although this phenomenon of permanent displacements near the anchor was not observed experi-mentally, it was pointed out in Section 4.3.1 that permanent displacements probably were present.
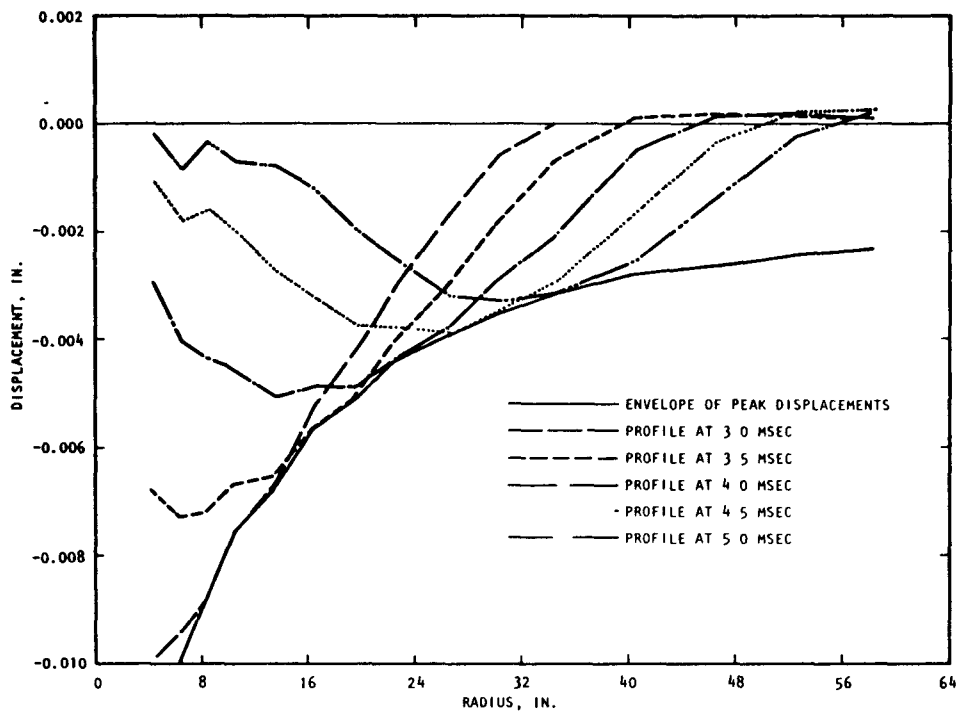
(a) Elastic finite element results
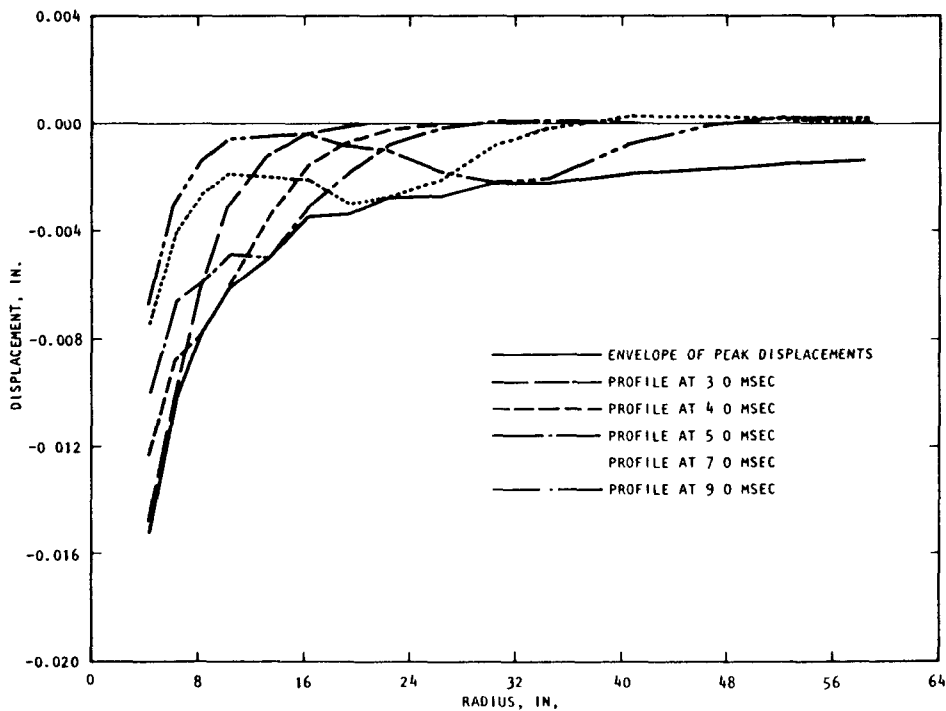
(b) Nonlinear finite element results

FIGURE 4-17. DISPLACEMENT PROFILES AT VARIOUS INSTANTS OF TIME
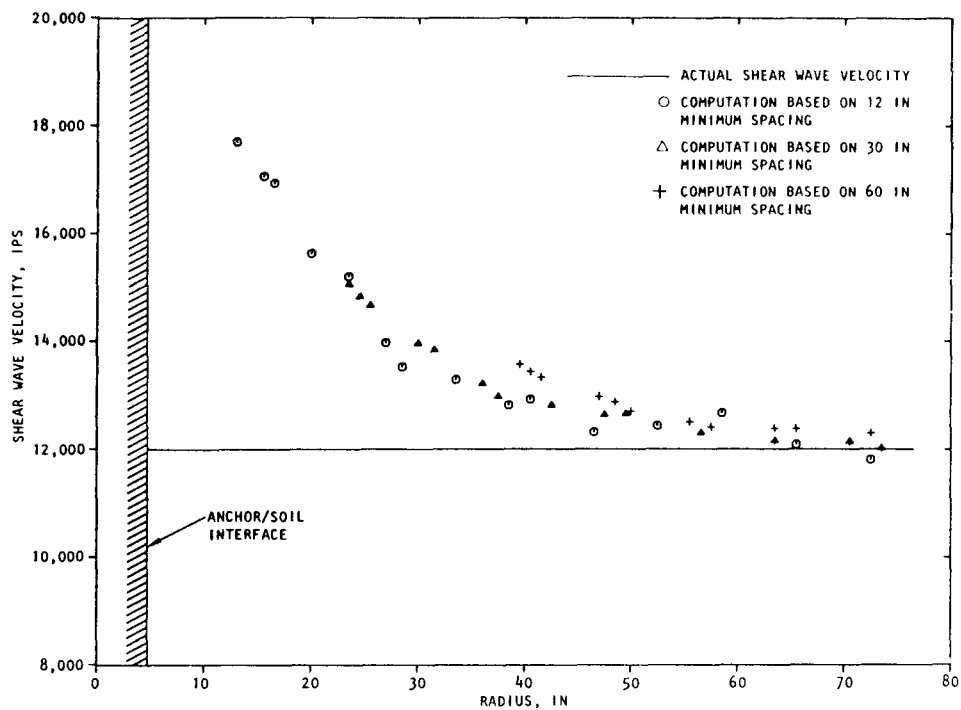ALONG THE MIDDEPTH OF THE ANCHOR

FIGURE 4-18. SHEAR WAVE VELOCITIES COMPUTED USING WAVE FORM METHODS --
ELASTIC FINITE ELEMENT CALCULATION

The displacement profiles of the elastic finite
element calculation can be used to determine the position of the
crest of the displacement wave at any given instant of time.
In order to improve the precision with which the position of
the wave crest can be determined, a parabolic interpolation scheme
has been used. Using this method, the displacements at several
points in the vicinity of the crest of the profile are represented
analytically using a parabola in which the coefficients are chosen
by a least-squares procedure. The crest of the profile is taken
to the point at which the parabola has zero slope.

Results of this procedure are presented in Fig.
4-18 in which the sensor spacings of 12 inches, 30 inches, and
60 inches have again been used. The lack of scatter, even for
the 12 inch sensor spacing, as well as the fact that crest
locations obtained by parabolic interpolation are consistent
with profile plots, indicates that the degree of precision with
which this method has been applied must have been high. An
obvious trend whereby excessively high wave speeds are recorded
near the anchor suggests that the crest of the displacement
profile propagates at a velocity different from the shear wave
velocity near the anchor. This observation implies that wave-
form methods based on the crest of the displacement profile
are not well suited for determining shear wave velocities in
the near-anchor region. As a result, it is recommended that
subsequent data reduction be performed using time-history methods,
and that the wave-form methods be dropped from further consi-
deration for computing shear wave velocities.

4.3.4   Assessment of Data Processing Procedures for
         Determination of In Situ Shear Strain

The present approach used for estimating shear strains
from the in situ response measurements is based on an analogy
with the propagation of plane shear waves in an elastic medium

of infinite extent. The resulting formula is:

$$\gamma_{rz} = \frac{\dot{w}}{V_s} \tag{4.3}$$

where: γ_{rz} shear strain at the point under consideration

$\dot{w}$ particle velocity at the point under consideration

V_s shear wave velocity of the soil medium at the point under consideration

A discussion of the validity of Eq. 4.3 is given in Chapter 3. This discussion indicates that Eq. 4.3 can be expected to yield accurate results at large distances from the anchor; however, near the anchor, the soil behavior becomes more complex and Eq. 4.3 no longer applies.

The implementation of Eq. 4.3 first requires an estimate of the shear wave velocity of the soil medium. Procedures for estimating this parameter have been described and assessed in Section 4.3.3. Once the shear wave velocity has been obtained for a given location, the peak shear strain at that location can be determined by using the peak particle velocity in Eq. 4.3. The results are likely to vary slightly, depending on the particular method used to estimate the shear wave velocity. Fig. 4-19 shows comparisons between actual peak shear strains obtained in the finite element calculations and peak shear strains computed by using the peak-velocity curve-fit method in conjunction with Eq. 4.3. Fig. 4-19a shows this comparison for the elastic finite element calculation, while Fig. 4-19b shows the results of the nonlinear finite element calculation. As previously indicated in Chapter 3, good agreement has been obtained away from the anchor (in general, 20 to 25 inches away). Near the anchor, the agreement is not quite as good.
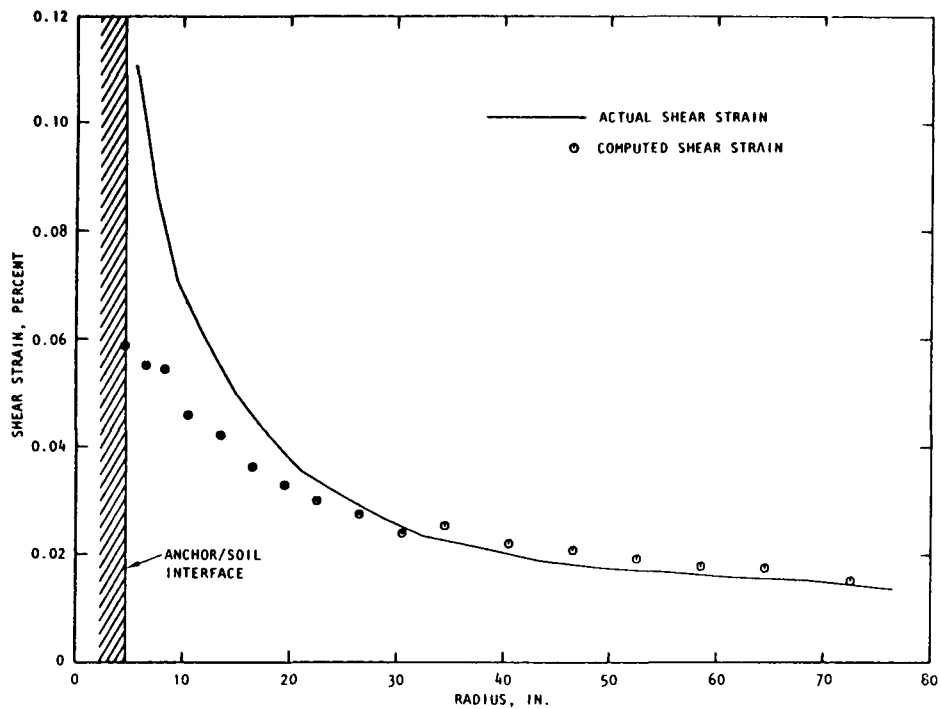
(a) Elastic case
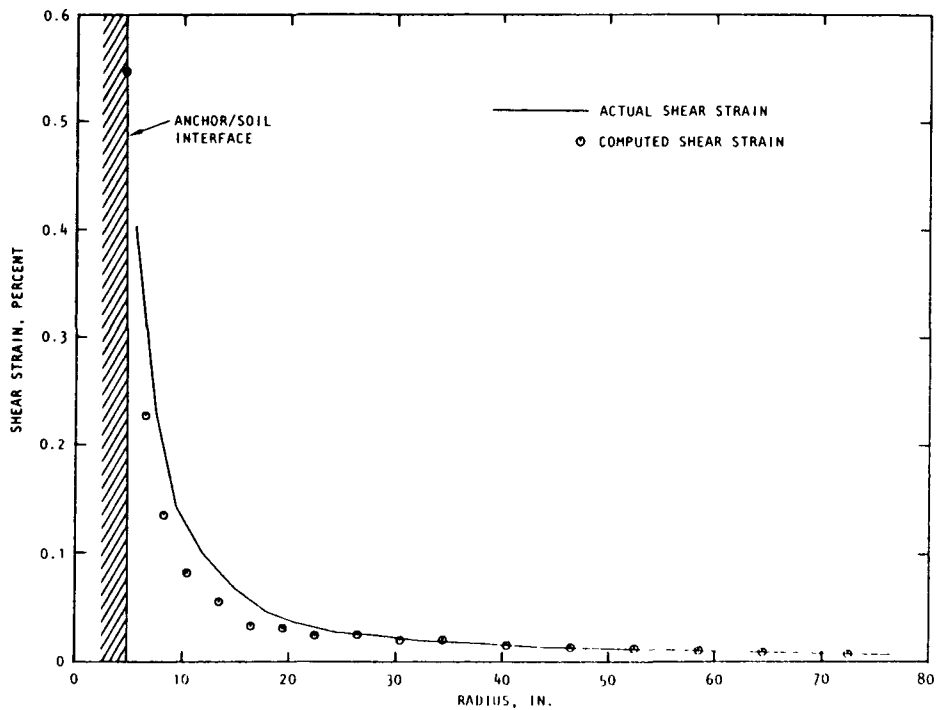
(b) Nonlinear case

FIGURE 4-19. COMPARISON OF ACTUAL PEAK STRAINS FROM THE FINITE ELEMENT CALCULATIONS
WITH PEAK STRAINS COMPUTED USING EQUATION 4-3

-87-

When the shear wave velocity has been estimated using a method involving the travel time between sensors, the resulting value is an average value for the region between the sensors. The shear strain associated with this average value of shear wave velocity must also be an average value for the region. Three methods of computing an average shear strain for the region between two sensors are studied below. The test as to which of these methods is most compatible with the value of shear wave velocity obtained is considered in Section 4.3.5.

The first proposed method of computing the average shear strain in the interval between two sensors is to estimate the shear strain at the midpoint between the two sensors. This method is referred to as the midpoint method. In order to estimate the shear strain at the midpoint of the region, the approximate distribution of shear strain between the sensors must be known. Fig. 4-20, which shows the distribution of peak shear strain obtained from the nonlinear finite element calculation, indicates that the relationship between peak shear strain and radius is nearly linear on a log/log grid. This suggests that the shear strain distribution between two sensors can be approximated by the expression:

$$\gamma_{rz} = Ar^{\alpha} \hspace{4cm} (4.4)$$

where: γ_{rz} shear strain

      r   distance from axis of symmetry

    A, α arbitrary parameters

The shear wave velocity for the region between the sensors, and the peak particle velocity at each sensor can be used to estimate the peak shear strains at the two sensors. By enforcing the conditions that Eq. 4.4 should assume these values of strain when r equals the coordinates of the sensors, the values of A and α for the interval between the sensors can be computed. By
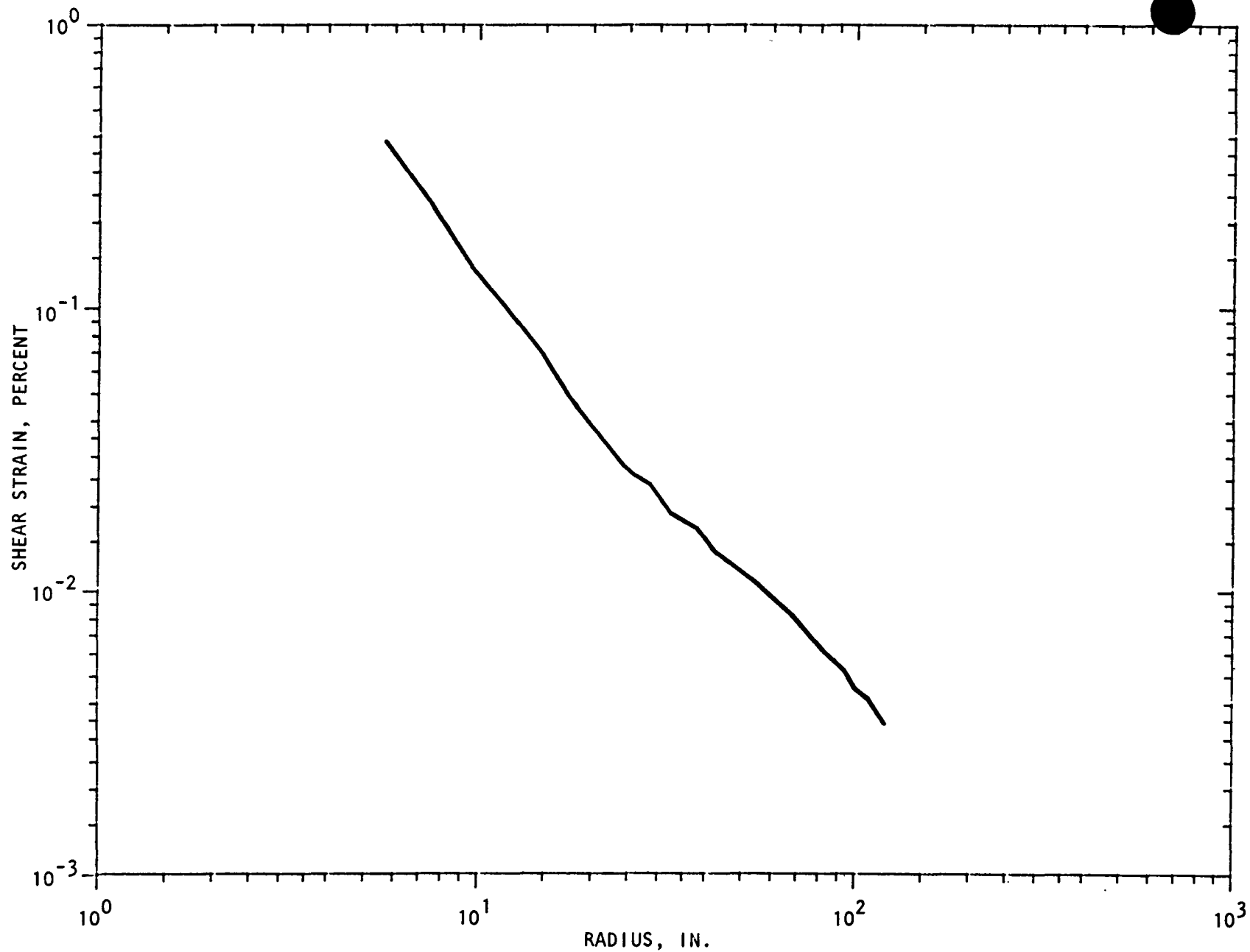
FIGURE 4-20. PEAK SHEAR STRAIN VS. DISTANCE FROM THE AXIS OF SYMMETRY -- NONLINEAR FINITE ELEMENT RESULTS

setting r equal to the coordinate of the midpoint between the sensors, Eq. 4.4 gives the average strain determined by the midpoint method.

The second method of computing the average shear strain for the region between two sensors is referred to as the integration method. In this method, the distribution of shear strain between the two sensors is represented by Eq. 4.4, in which A and α are determined in the same manner as was done in the case of the midpoint method. Eq. 4.4 is then integrated with respect to r, with limits corresponding to the coordinates of the two sensors involved. The result of this integration is then divided by the distance between the sensors to obtain the integrated average shear strain.

The third method of estimating the average shear strain for the region between the sensors is referred to as the end-average method. In this method, the shear strains at the two sensors are estimated as was done in the case of the midpoint method. The straight numerical average of these two values is used as the average shear strain.

These methods of estimating shear strain, which are associated with the travel-time approach to estimating shear wave velocity, do not have as wide a range as the method used in Fig. 4-19. The region nearest the anchor escapes evaluation using these methods. The accuracy and range obtainable using these methods are considered in Section 4.3.5.

4.3.5   Evaluation of Total Data Reduction Systems

Several methods of computing shear wave velocity from in situ data have been investigated in Section 4.3.3. All of the time-history methods, including those which involve analytical curve fits as well as those which involve travel time between

-90-

sensors, have survived the initial evaluation. The wave-form
methods have been eliminated from further consideration because
of practical limitations in working with this data and because
of the apparent limitations of these methods in evaluating near-
anchor soil responses (Section 4.3.3). In addition, several
variations of the manner in which shear strains can be estimated,
related particularly to the travel-time methods, have been
proposed. These various methods for computing shear wave velo-
city and shear strain must be combined into total data reduction
systems, and evaluated as such. The various combinations under
consideration are identified in Table 4-1. The nonlinear finite
element calculation is used to evaluate each of these procedures,
based on the accuracy within which each procedure can reproduce
the original shear modulus vs. shear strain relationship used as
input to the finite element analysis. The shear modulus is
obtained from the shear wave velocity using Eq. 4.1.

Fig. 4-21 shows the midpoint method for averaging
shear strains used in conjunction with each of the travel-time
methods for computing shear wave velocity to construct modulus/
strain relationships. Fig. 4-22 shows the integration method,
while Fig. 4-23 shows the end-average method used along with
the travel-time methods to compute modulus/strain relationships.
In each of the figures, the relationships between secant shear
modulus and shear strain actually obtained from the nonlinear
finite element calculation is shown as the solid line. Minimum
sensor spacings of 12 inches, 30 inches, and 60 inches were
used in obtaining the computed modulus/strain relationships.

In each of the figures, the zero-crossing method for
computing shear wave velocity resulted in less scatter than the
peak-velocity method; however the results were less accurate.
This may be due to the fact that peak velocity occurs when the
shear stress is at a maximum, while the zero crossing does not.
The end-average method for estimating strain is seen to be badly

TABLE 4-1. KEY TO DATA REDUCTION PROCEDURES FOR DEVELOPMENT
OF SHEAR MODULUS VS. SHEAR STRAIN RELATIONSHIPS

Method of Calculating Shear Wave Velocity*		Method of Calculating Shear Strain			
		Analytical Curve-Fit	Midpoint Method	Integration Method	End-Average Method
Analytical Curve-Fit	Peak Velocity	Peak-Velocity/ Fit Method			
	Zero Crossing of Velocity	Zero-Crossing/ Fit Method			
Travel Time Between Sensors	Peak Velocity		Peak-Velocity/ Midpoint Method	Peak-Velocity/ Integration Method	Peak-Velocity/ End-Average Method
	Zero Crossing of Velocity		Zero-Crossing/ Midpoint Method	Zero-Crossing/ Integration Method	Zero-Crossing/ End-Average Method

*Shear modulus is obtained from shear wave velocity using Equation 4-1.
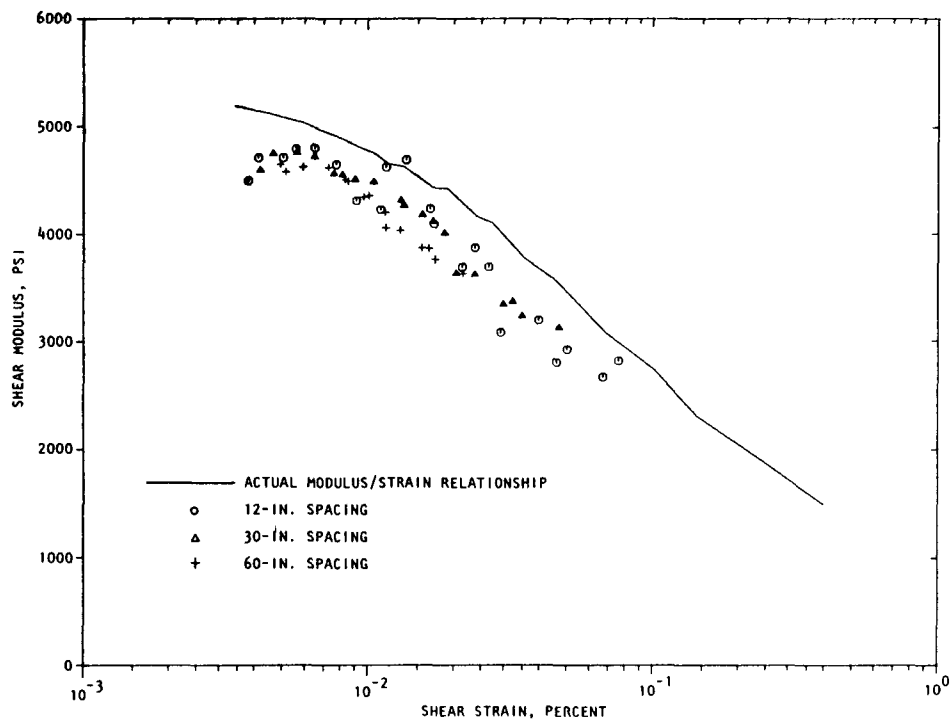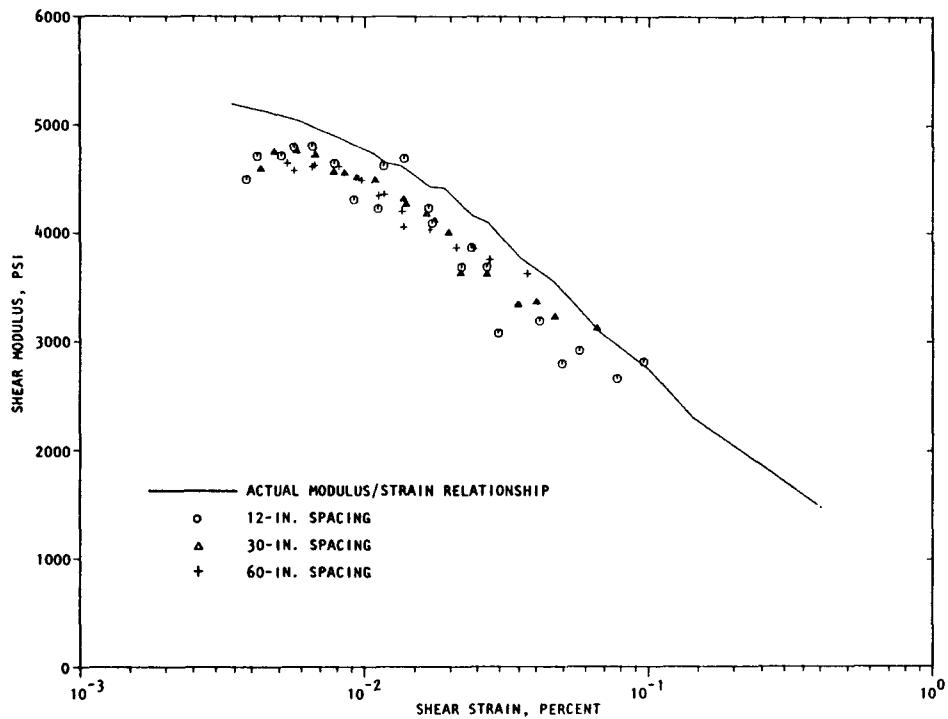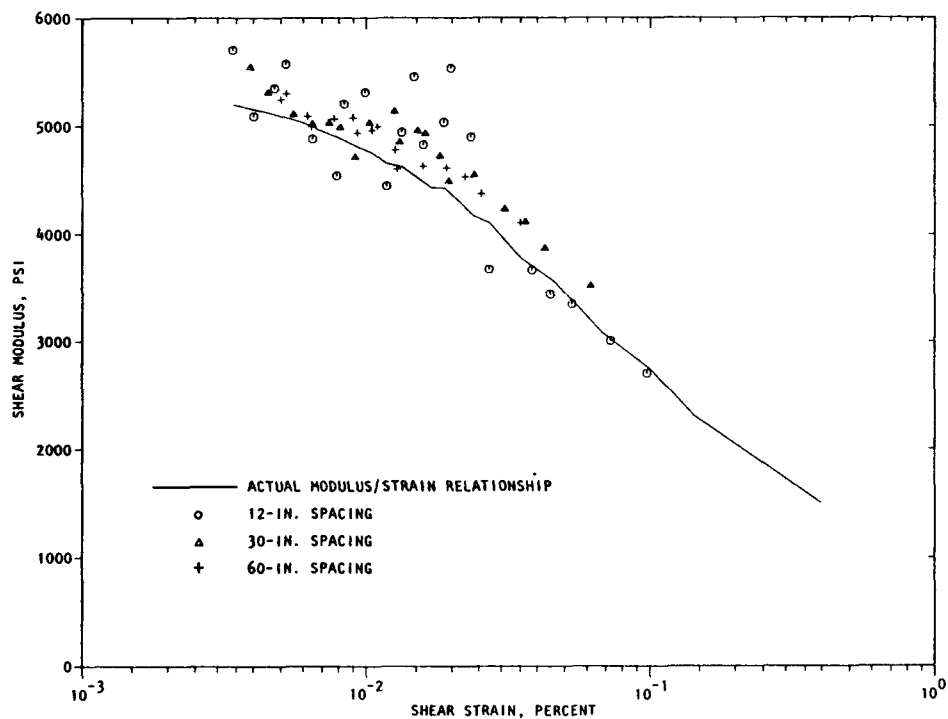
(a)   Zero-crossing/midpoint method
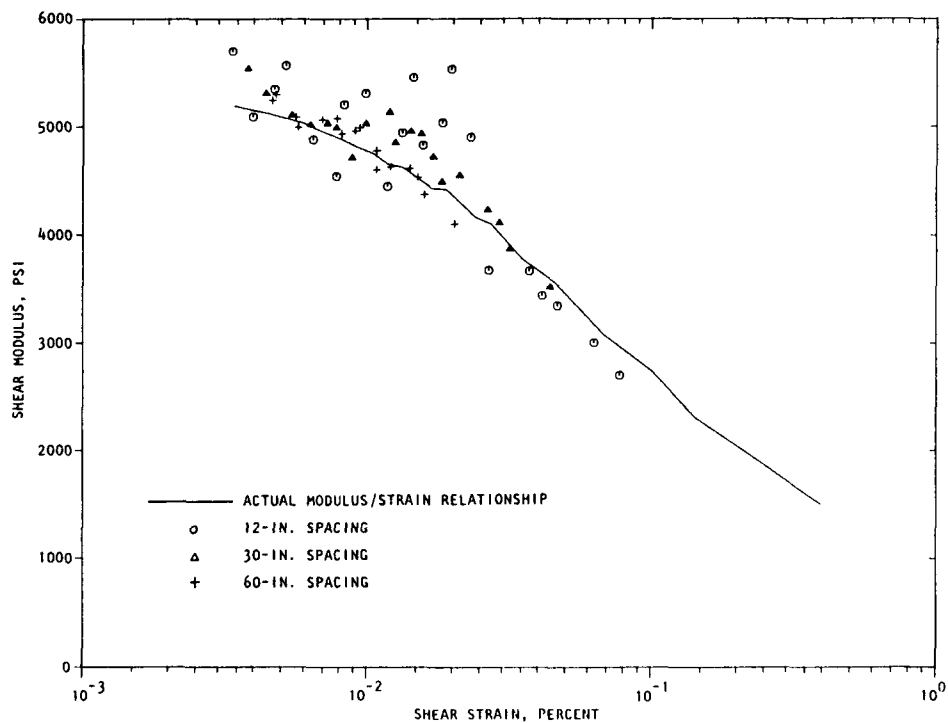
(b)   Peak-velocity/midpoint method

FIGURE 4-21.   USE OF MIDPOINT METHOD TO ESTIMATE SHEAR MODULUS VS. STRAIN
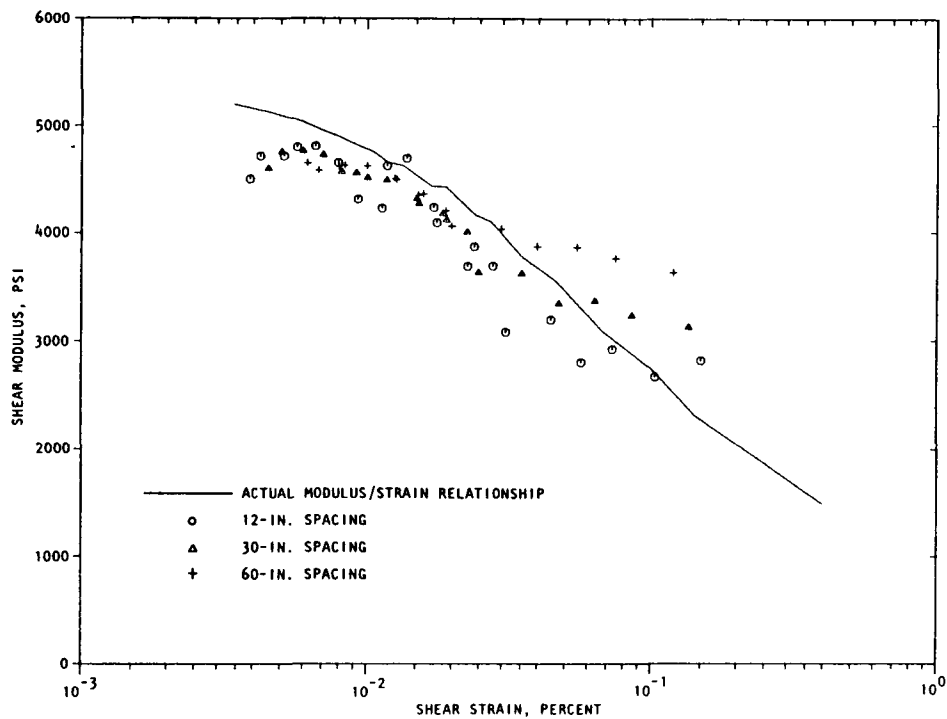RELATIONSHIP -- NONLINEAR FINITE ELEMENT RESULTS
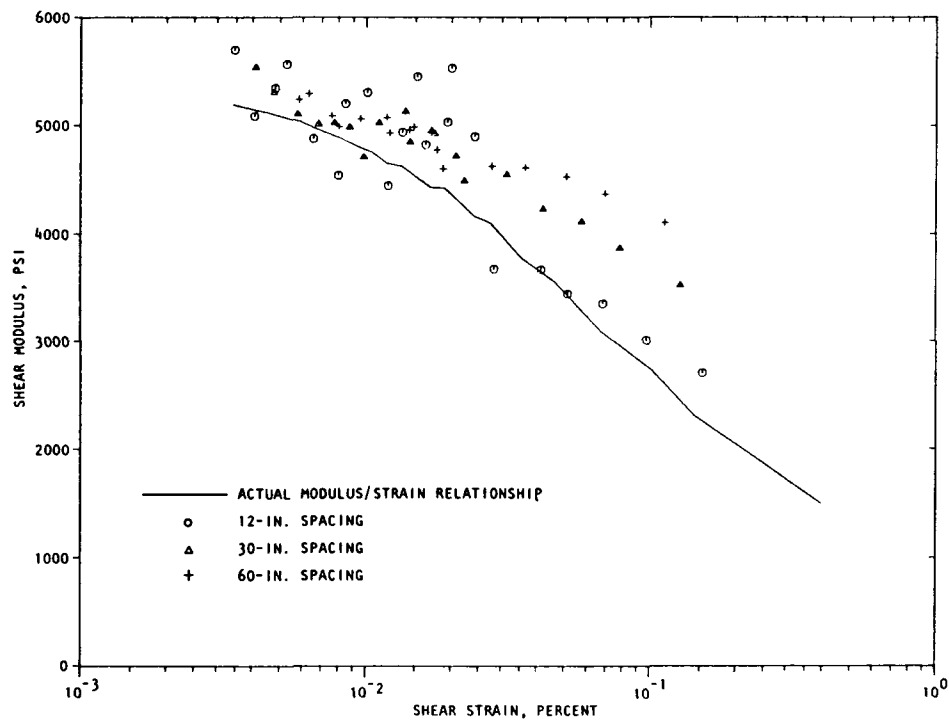
(a)   Zero-crossing/integration method

(b)   Peak-velocity/integration method

FIGURE 4-22.   USE OF INTEGRATION METHOD TO ESTIMATE SHEAR MODULUS VS. STRAIN
RELATIONSHIP -- NONLINEAR FINITE ELEMENT RESULTS

(a)   Zero-crossing/end-average method

(b)   Peak-velocity/end-average method

FIGURE 4-23.   USE OF END AVERAGE METHOD TO ESTIMATE SHEAR MODULUS VS. STRAIN
RELATIONSHIP -- NONLINEAR FINITE ELEMENT RESULTS

in error, particularly for large strains. The other two methods appear to be reasonably good.

Fig. 4-24a shows the zero-crossing/fit method applied to a group of four nodal points spaced in a manner which might be considered for use in an actual in situ test.[1] The times of zero crossing of velocity at each of the four points were used to fit the analytical approximation of Eq. 4.2. The resulting values of the undetermined coefficients are not as optimized as they would have been had all the available position-time data of zero crossing been considered in fitting the equation. However, the use of four data points is more consistent with the amount of data ordinarily available during an in situ soil test.

The availability of an analytical approximation to the propagation of the zero crossing of velocity makes possible the estimation of shear wave velocity, and hence shear modulus, at any desired distance from the anchor. The estimation of peak shear strain, on the other hand, requires also a knowledge of the peak particle velocity which occurred at the point of interest. This information is available only at the four locations for which the velocity histories are known. Only four strain values can be estimated, therefore, and as a result only four points can be plotted on the modulus/strain graph, Fig. 4-24a.

In an actual in situ test, there would be a multiple of repetitions of the test loaded under a wide range of different

_____

[1] One of these nodal points, located on the anchor, records the anchor motion. Due to the idealization of the finite element model whereby no slippage occurs between the anchor and the soil, this anchor motion is interpreted, in the data reduction procedures, as the motion of the soil along the anchor/soil interface. During an actual in situ test, where slippage may be present, this type of interpretation of the anchor motion in the data reduction procedure may not be possible.
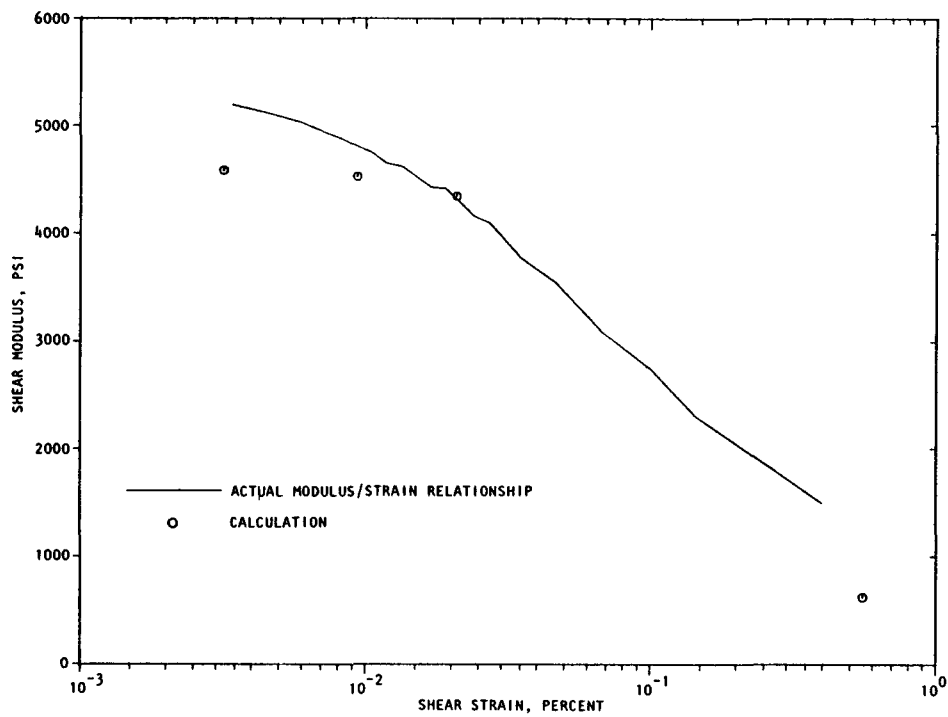
(a) Nodal points located in anchor and 30 in., 60 in., and 120 in. from the anchor
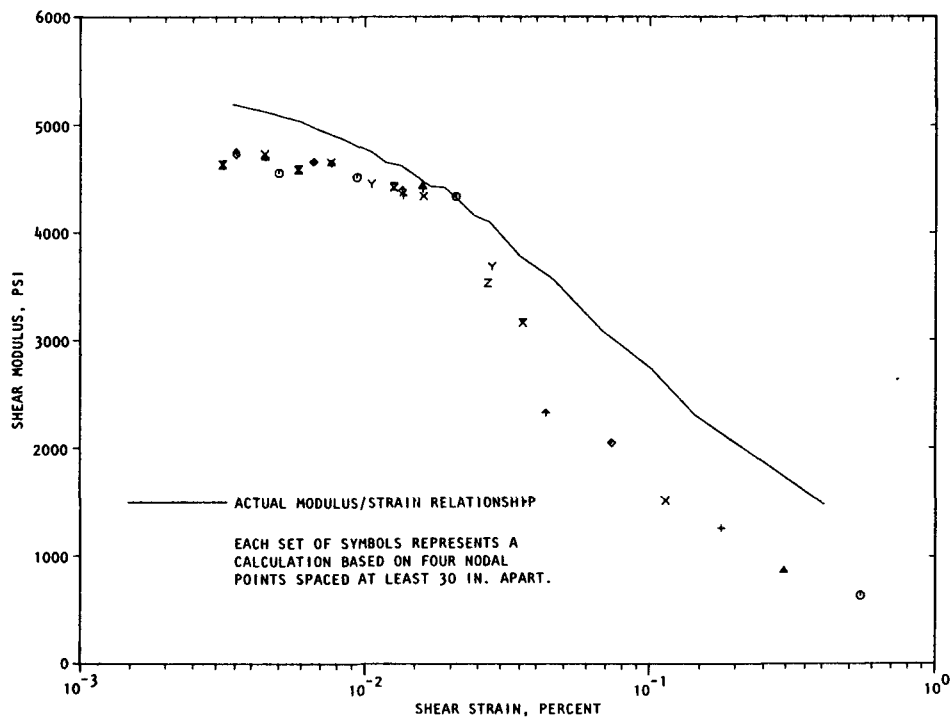
(b) Accumulation of many sets of data

FIGURE 4-24. APPLICATION OF ZERO-CROSSING/FIT METHOD TO NONLINEAR FINITE ELEMENT CALCULATION

energy levels. This would cause a variety of strain levels to occur at the various sensor locations (which are constant from test to test), thus allowing accumulation of a large quantity of shear modulus vs. strain data distributed uniformly over a large strain range. This accumulation of data, when plotted on a single graph, would result in the modulus/strain relationship. In order to simulate such a sequence of tests it was proposed that a similar accumulation of modulus/strain data could be obtained by considering several different groups of four sensor locations spaced about 30 inches apart. The results of such a consideration of the zero-crossing data of the nonlinear finite element calculation are shown in Fig. 4-24b.

An interesting feature of Fig. 4-24 is the small discrepancy between the data reduction technique and the actual modulus/strain relationship for small values of peak shear strain. The small values of shear strain occur at large distances from the anchor, where the method of computing shear strain has been shown to give excellent results (see Fig. 4-19). This suggests that the method for computing shear wave velocity (from which the shear modulus is computed) may be in error.

Due to the nonlinearity of the soil medium, the velocity of propagation of shear waves at a given location in the soil is constantly changing according to the changing state of stress at that location. At any given instant of time, the relation:

$$V_s = \sqrt{G/\rho} \tag{4.5}$$

which is obtained by rearranging Eq. 4.1, holds true. The solid curves of Fig. 4-24, which are labeled "actual", show the relationship between secant shear modulus and peak shear strain. In order to obtain wave propagation data which agree with these curves, the feature being observed would have to be propagating

at the secant shear wave velocity, which is obtained by using the secant shear modulus in place of G in Eq. 4.5.   It is evident from Fig. 4-24 that the zero crossing of velocity propagates at a velocity slower than the secant shear wave velocity at large distances from the anchor.   This observation is confirmed in Figs. 4-14a and 4-16a.

Fig. 4-25a shows the peak-velocity/fit method applied to the same sensors used in Fig. 4-24a.   Fig. 4-25b shows an accumulation of peak-velocity/fit data.   By comparison with Figs. 4-21b, 4-22b, and 4-23b the scatter is greatly reduced using the fit methods.   Furthermore, the strain range is much more extensive.   Otherwise the modulus/strain relationships obtained from the two sets of data are very much in agreement. Fig. 4-25b shows that there is a range of locations for which the velocity of propagation of the peak velocity exceeds the secant shear wave velocity, but that the two approach each other toward the outermost locations considered in the calculation. This observation is consistent with Figs. 4-14b and 4-16b.

4.4   CONCLUSIONS

Based on the results presented in this chapter, a number of conclusions are listed below.   When interpreting these conclusions, the inherent advantages and limitations of the finite element procedures, as discussed in Section 4.1.1, should be kept in mind.   Furthermore, to aid in this interpretation, certain comments based on experimental results from the special tests are provided as footnotes.   These experimental results are described in more detail in Chapter 5.

With this as background, the conclusions regarding the finite element analysis results are as follows:
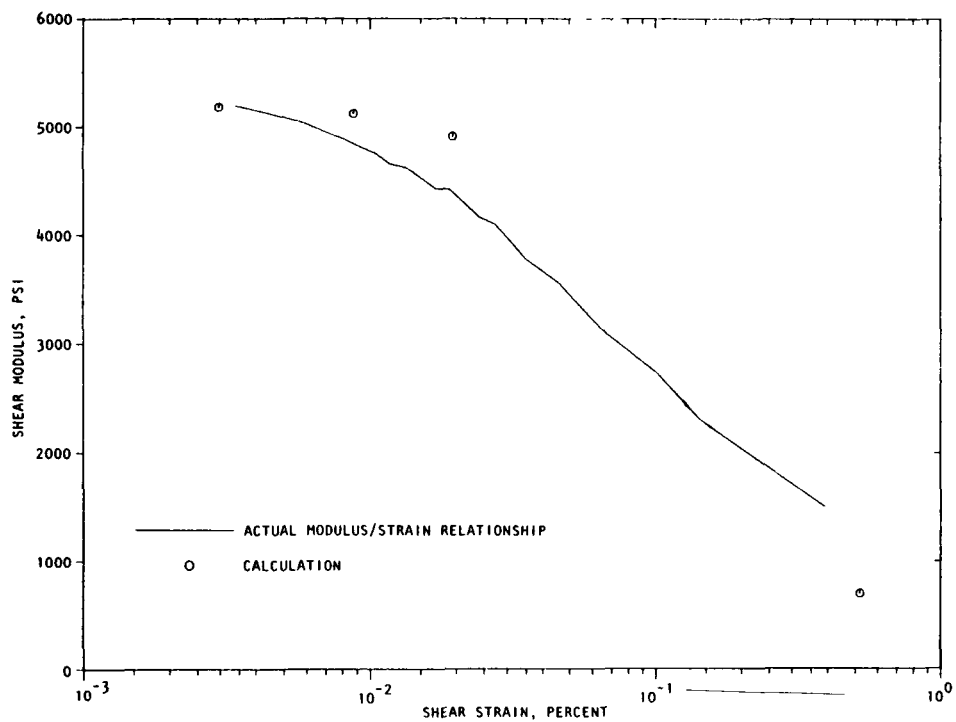
(a) Nodal points located in anchor and 30 in., 60 in., and
     120 in. from the anchor
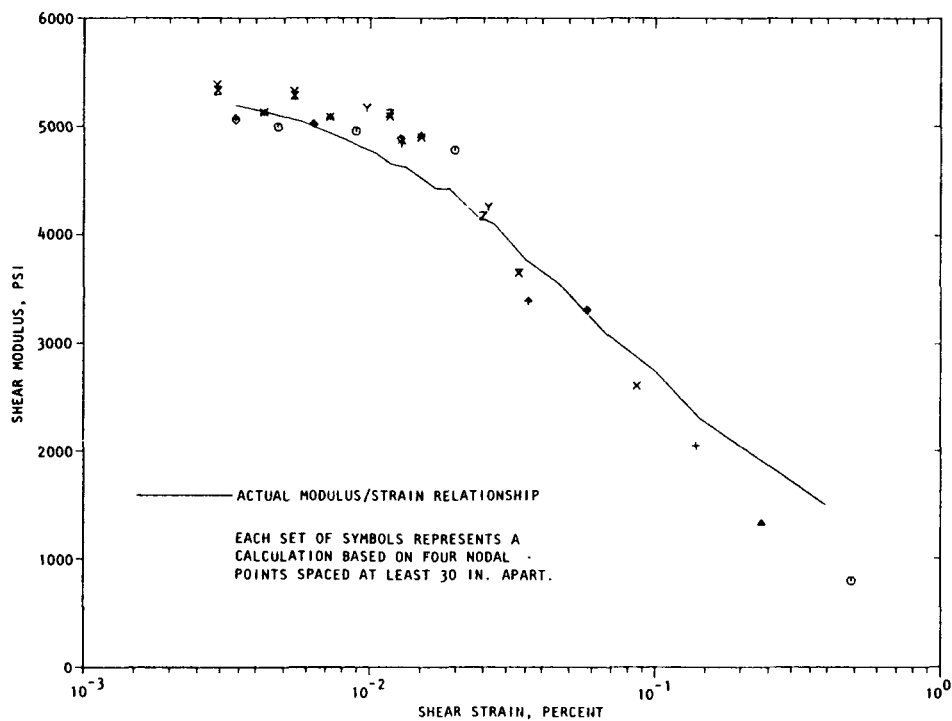
(b) Accumulation of many sets of data

FIGURE 4-25. APPLICATION OF PEAK-VELOCITY/FIT METHOD TO NONLINEAR FINITE
              ELEMENT CALCULATION

a. Although time-history methods involving zero-crossing and peak-velocity produce slightly different results, both methods are satisfactorily accurate. The results of the peak-velocity methods appeared to be slightly more accurate in the particular nonlinear calculations described in this chapter; however this may not necessarily be true for other soil conditions or input loads. In fact the zero-crossing method was superior in analyzing the data from the elastic case.*

b. The time-history methods include both curve-fit methods and travel-time methods, as shown in Table 4-1. The curve-fit methods are able to extract a wider range of data from the experiments by making use of the near-anchor soil region. The various data processing techniques have been shown to be some-what less reliable near the anchor than far from it. Despite these potential near-anchor problems, the modulus/strain comparisons for the curve-fit methods were found to be satisfactory near the anchor in the case of the nonlinear finite element calculation.

c. The travel-time methods are subject to excessive scatter, due to numerical differentiation incorporated within the methods. The nonlinear finite element calculations show that the sensor spacing must be about 30 inches or more in order to reduce the scatter to acceptable levels. This minimum allowable sensor spacing will probably vary from test to test depending upon such factors as shear wave velocity, input energy level, etc. It is evident from the modulus/strain comparisons that increased sensor spacing reduces the range of data obtainable. Thus, these methods are judged to be less useful than the curve-fit methods.

---

* It was observed in Section 5.3 that the zero-crossing data can be somewhat more precisely resolved from the special test measurements than peak velocity data. The two methods, when applied to production tests, gave nearly the same results.

d.   The wave-form methods were shown to be inappropriate for the calculation of the shear wave velocity in the near-anchor region.* Away from the anchor, these methods were shown to produce satisfactory results which agree with those of the time-history methods. However, because of the importance of the near-anchor region and the uncertainties associated with the application of wave-form methods for estimating shear wave velocities in this region, these methods are not recommended for use in production tests.

e.   The use of Eq. 4.3 to estimate peak shear strain is extremely successful away from the anchor.** In the near-anchor region, the performance of these formulae is only moderately successful. Errors in the near-anchor region evidently do not exceed 50%, and are often much smaller. The end-average method of determining the average strain for a region between sensors is not recommended.

f.   On the basis of the modulus vs. strain comparisons, the curve-fit methods are recommended for processing of in situ data. Referring to Table 4-1, these methods include the zero-crossing/fit method and the peak-velocity/fit method.

---

*   As noted in Section 5.3.2, wave-form methods have an additional disadvantage when used to estimate near-anchor shear wave velocities during typical production tests -- namely, the spatial resolution of the near-anchor soil sensors is not sufficient to provide an adequate representation of the crest of the wave in this region. However, the special tests described in Chapter 5 were different from typical production tests in that they provided an extremely fine spacing of near-anchor sensors that permitted an adequate representation of the displacement wave shape in this region. Therefore, the slopes of these displacement profiles were used in Chapter 5 to determine shear strains generated in the soil during the special tests. Such a treatment follows directly from the definition of shear strain and is valid even though the wave-form methods may be inappropriate for use in estimating near-anchor shear wave velocities.

** As discussed in Section 5.4 of Chapter 5, analysis of the special test data confirms the validity of the current methods for estimating shear strain.

CHAPTER 5
EXPERIMENTAL STUDY OF WAVE
PROPAGATION IN AN ARTIFICIAL SOIL FILL

Special field tests were carried out to provide additional
insight into the wave propagation phenomenology of the "real"
in situ test condition particularly for the region close to the
anchor. This work was accomplished by installing the anchor
assembly and extensive monitoring equipment within a soil fill
built for this purpose and conducting tests under a variety of
controlled test conditions. The results of these studies are
described in this section. While many tests were performed and
much data was reduced and studied as part of this effort, for
clarity, data for only representative cases are included in
this chapter. More detailed treatment of this data has been
presented in Troncoso, 1975.

5.1   TEST DESCRIPTION

The testing program was conducted in soils at a site on
the Fort Lawton Military Reservation in Seattle, Washington.
The soils used in the test fill consisted of a relatively uniform
deposit of silty fine to medium SAND. The index, mechanical
and dynamic properties of this material, based on a number of
laboratory tests are provided in Appendix C.

At this site, a large circular pit was first excavated to
the dimensions shown in Figure 5-1. These dimensions were
selected to avoid interference of reflected waves from the boun-
daries. The pit was then backfilled, and the materials densely
compacted in thin layers for the entire depth of the pit. During
the backfilling operation, the anchor assembly (Fig. 5-1) and
a number of recording sensors consisting of four accelerometers,
34 velocity transducers and one load cell, were hand placed at
predetermined locations in the soil fill. Six of these sensors
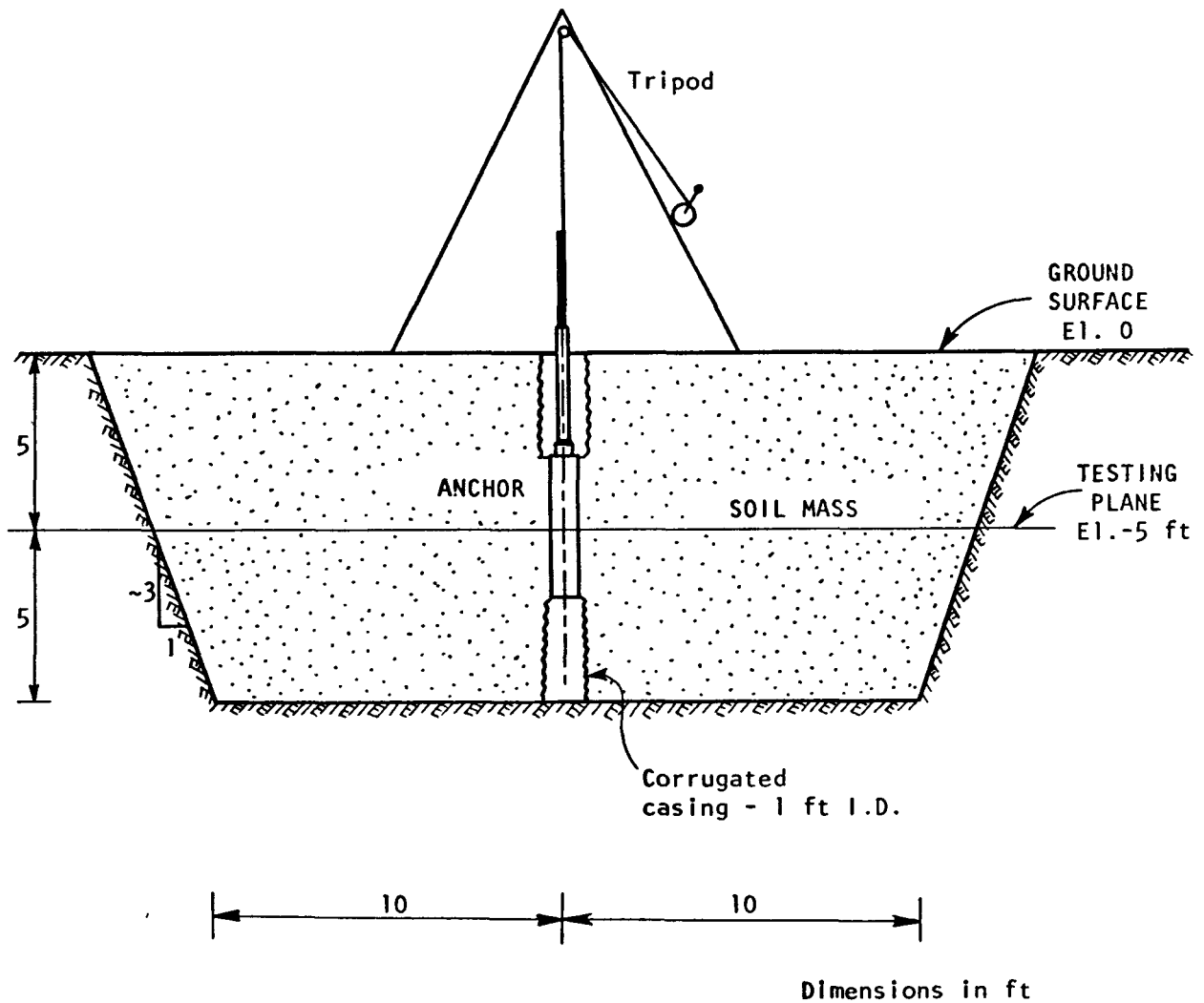
FIGURE 5-1 TESTING SET UP IN ARTIFICIAL SOIL FILL

Labels in figure:

Tripod

GROUND
SURFACE
El. 0

ANCHOR   SOIL MASS

TESTING
PLANE
El.-5 ft

~3
1

5

5

Corrugated
casing - 1 ft I.D.

10   10

Dimensions in ft

were placed on the anchor assembly. Most of the remaining sensors were located at the mid-depth of the pit (elevation -5 feet). The type and location of these sensors are identified in Fig. 5-2. Further details of fill construction and equipment installation procedures including photographs are provided in Appendix D.

The band of sensors in Fig. 5-2 was placed primarily to study wave propagation characteristics, and to provide insight into data interpretation procedures. As indicated in Appendix E, these sensors were staggered to avoid possible interaction effects between adjacent sensors. Also from this same band of sensors, test parameters such as P-wave effects (from the horizontally oriented sensors), and repeatability, could be studied. The remaining array of free field sensors together with the band provided data for study of symmetry and casing effects. Simultaneous measurements of motion and forces at the anchor and the close-in free field stations provided data for better understanding anchor behavior characteristics particularly for establishing empirical relationships relating measurements made at the anchor to those recorded in the free field. Also the importance of radial jacking stresses, and hammer weight and height of drop effects could be assessed. Most of these test parameter effects are discussed and evaluated in Appendices F and G.

Because the recording equipment is capable of monitoring only four sensors at a time, any test involving more than four measurements had to be repeated in order to collect sufficient data. By re-recording in every two tests at least one data station, normalization of times and amplitudes could be readily accomplished. The observed variations in amplitude and shape were almost always small and time shift adjustments between successive records were easily accomplished. With repeated tests, under constant test conditions, the response characteristics as
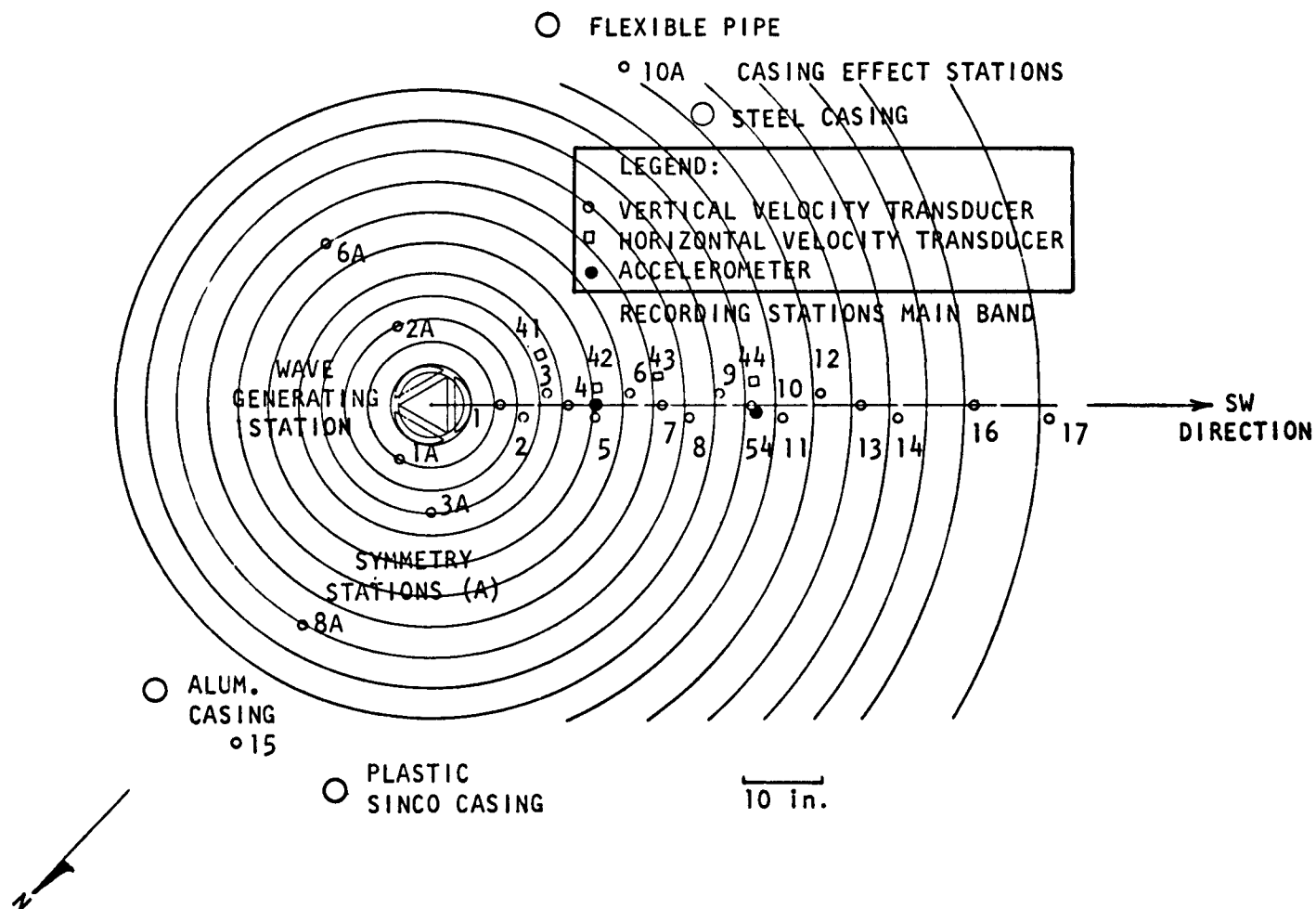
FIGURE 5-2   SENSOR LOCATION PLAN AT ELEVATION - 5 ft

the wave travels from the source through the band of sensors could be studied as if the data had all been obtained from one impact.

Test results for all sensors were obtained as time-histories of loads, accelerations and both horizontal and vertical particle velocities at different points in the soil and in the anchor. Through integration and other mathematical manipulations of the test data together with accurate distance measurements, displacements were determined and related as wave-forms both in terms of time and distance. This data provided a clear picture of changing wave characteristics and enabled actual wave velocities and shear strains to be computed. The data also enabled the laws of attenuation to be studied to a limited extent and provided for relating free field and anchor motion data.

5.2 WAVE PROPAGATION CHARACTERISTICS

5.2.1   Particle Velocity Characteristics

Wave propagation was mainly studied by measurements of the responses of 16 vertical velocity sensors arranged along the principal band shown in Fig. 5-2. A complete series of tests performed at a constant drop height, hammer weight, and jack pressure, σ_j, are shown in Fig. 5-3 as 16 velocity time measurements as the wave passes outward from the energy source. The most characteristic points of the velocity measurement are defined as shown in the idealized time history in Fig. 5-4. This idealized pulse is a superposition of vertical particle velocities generated by the passage of both compressional or P waves and shear or S waves. The first part of the pulse will be defined primary pulse and the second main pulse.

The curves in Fig. 5-3 illustrate progressive changes in the shape of the pulses as they travel outward through the
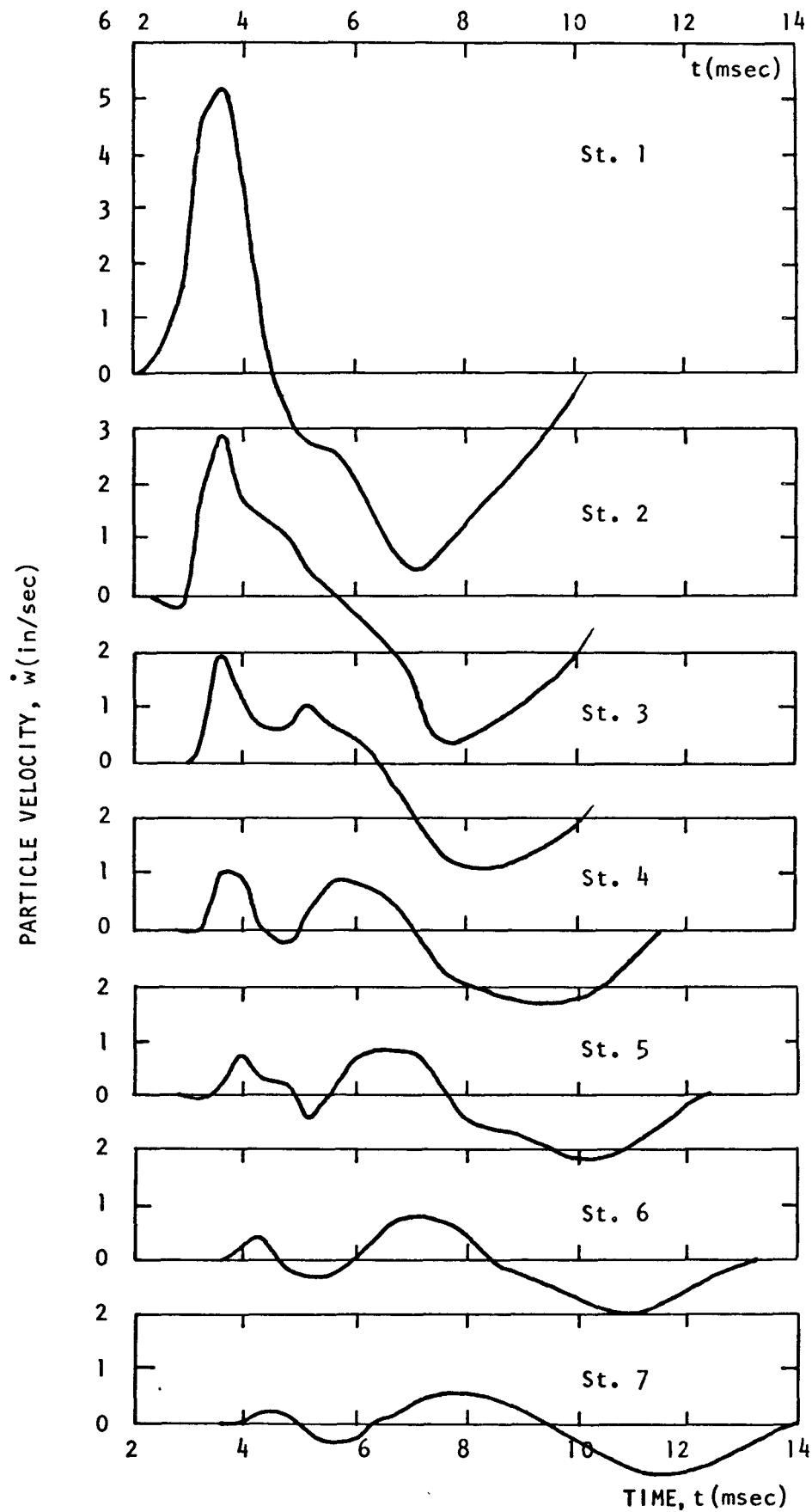
FIGURE 5-3a   PARTICLE VELOCITY - TIME HISTORIES
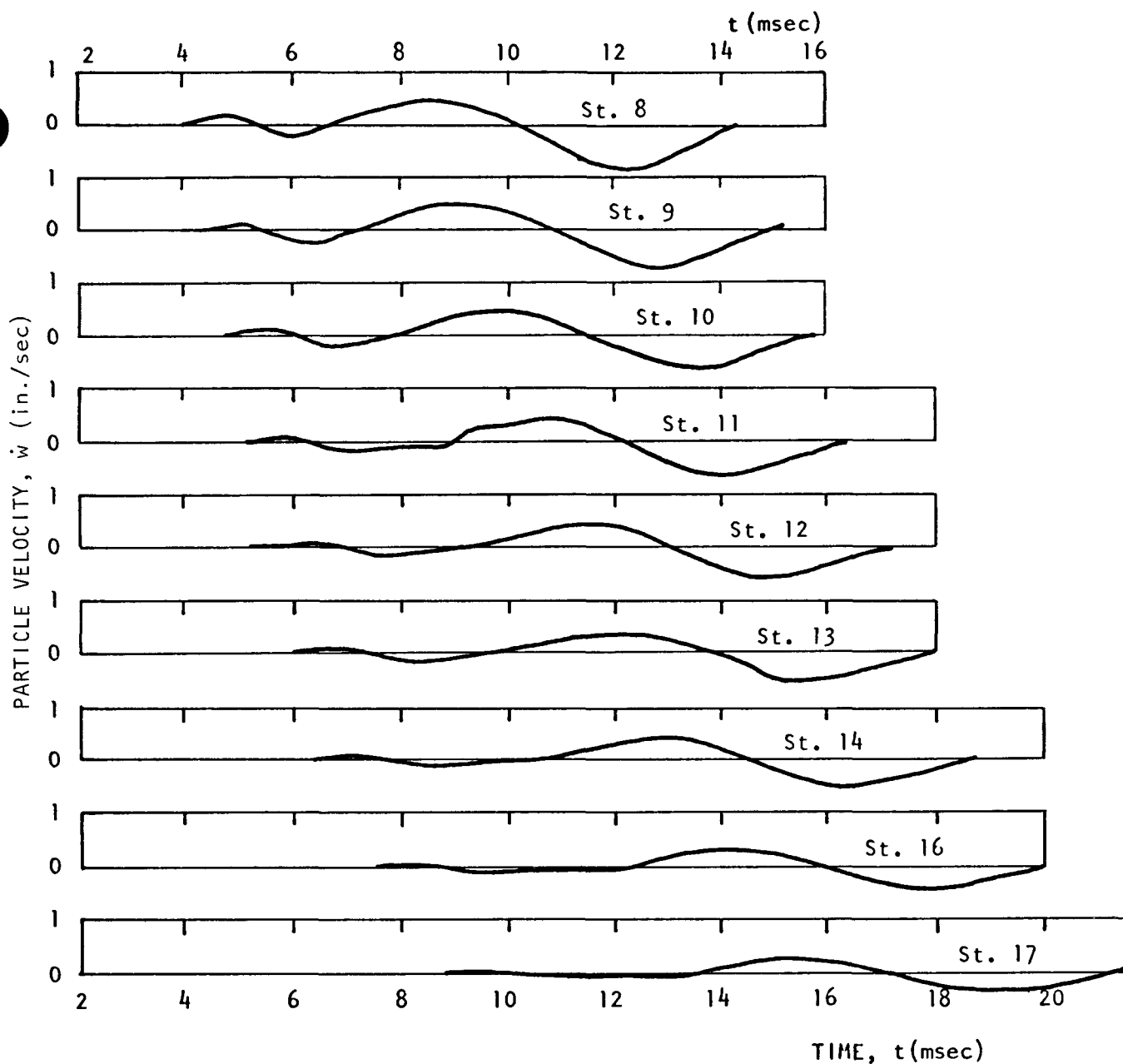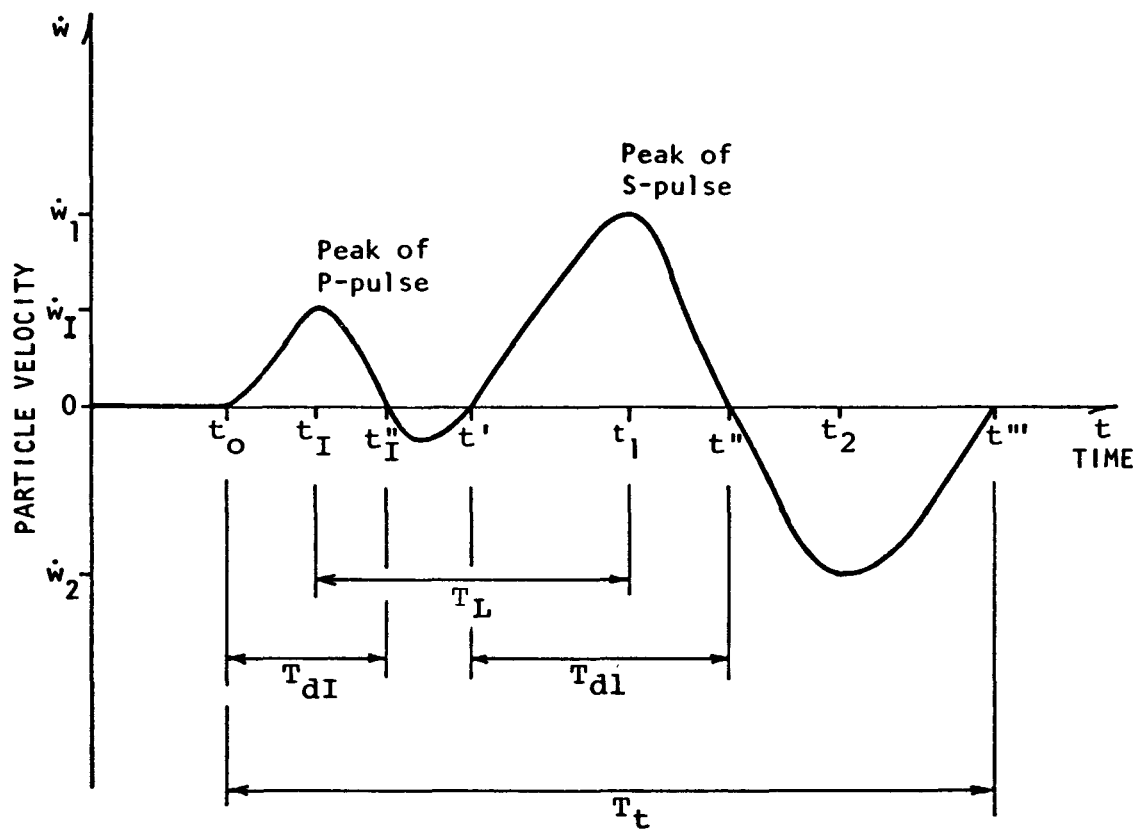   TESTS 2.2A-2.8   W = 58 lb x .5 ft, σ_j = 2,000 psi

FIGURE 5-3b   PARTICLE VELOCITY - TIME HISTORIES
TESTS 2.2A-2.8 W = 58 1b x .5 ft, σ_j = 2,000 psi

Sign Convention:
   Positive for downward motion

Time definitions:

t_o: first arrival

t_I'': second crossing of P-pulse

t': arrival of S-pulse

t''': end of S-pulse

$T_{dI} = t_I'' - t_o$: duration time of positive part of P-pulse

$T_{d1} = t'' - t'$: duration time of positive part of S-pulse

$T_L = t_1 - t_I$: time lag between P and S pulses

$T_t = t''' - t_o$: total duration time of complete pulse

FIGURE 5-4   TYPICAL PARTICLE VELOCITY - TIME HISTORY

soil mass. In general the particle velocity signatures change
from one composite pulse to the two distinct primary and main
components defined in the idealized curve (Fig. 5-4). As this
change or separation is taking place, there is also an increase
in the time durations of both the main pulse and the total pulse.
This indicates that the two components are traveling at different
speeds. The primary component is traveling the fastest and is
therefore the P-wave while the slower traveling main component
represents shear wave motion. Appropriate substitution of
Poisson's ratio in the theoretical equation:

$$\frac{V_p}{V_s} = \sqrt{\frac{2(1 - \mu)}{1 - 2\mu}} \qquad (5.1)$$

will always produce a ratio greater than 1 (i.e., the P-wave
is always the faster of the two body waves).

Further examination of the set of waves reveals that
the primary pulse is dominant in the "close in" zone around the
anchor, but becomes much smaller at greater distance. This
indicates that for these distances, the primary component
(P-wave) attenuates much faster (about 10 times) than the main
component (S-wave).

To estimate the point in this set of curves where the
two components separate, the following example is provided.

For a soil with an average S-wave velocity of 400
ft/sec and μ = .3, the P-wave velocity V_p is computed to be
750 ft/sec. Using the terms in Fig. 5-4, approximate conditions
for no overlap of the pulses may be expressed as:

$$\Delta t = t_1 - t_I \geq \frac{T_{d1} + T_{d1}}{2}$$

For: $t_1 = \dfrac{r}{V_s}$ and: $t_I = \dfrac{r}{V_p}$

where r is the radial distance of the points of no overlap,

$$r \geq \frac{1}{2} \; \frac{(T_{d1} + T_{d1})}{(\dfrac{1}{V_s} - \dfrac{1}{V_p})} \qquad\qquad (5.2)$$

Using this relationship and assuming both T_{ds} and T_{d1} are 2 msec, the radial distance of no overlap is 1.8 feet. This corresponds to a point located between stations 5 and 6, in Fig. 5-2. Based on this example calculation and study of other test series, the zone of no overlap generally occurs at a distance from the edge of the anchor varying between about 1.5 to 2.0 feet. Thus at distances greater than this, the main pulse is clearly dominant and unaffected by large P-wave effects. This outer zone may be defined as the "free field".

5.2.2   Displacement Characteristics

The displacement characteristics for studying wave propagation can be presented in two ways, either in relation to time or distance. Direct integration of the velocity-time histories produces pulses of displacement or displacement-time histories. Fig. 5-5 shows a typical set of displacement pulses obtained for a 58 pound weight falling 0.5 feet, and a constant jack pressure, σ_j = 3,500 psi. The sign convention is negative for a downward displacement. The figure shows only the negative parts of the pulses for both the anchor and the 16 vertical velocity transducers along the main band. In the "close in" zone (i.e., inside Station 5) the primary pulse has a strong influence on both the positive and negative side of the dis-placement curve. Because of this overlapping effect, interpre-
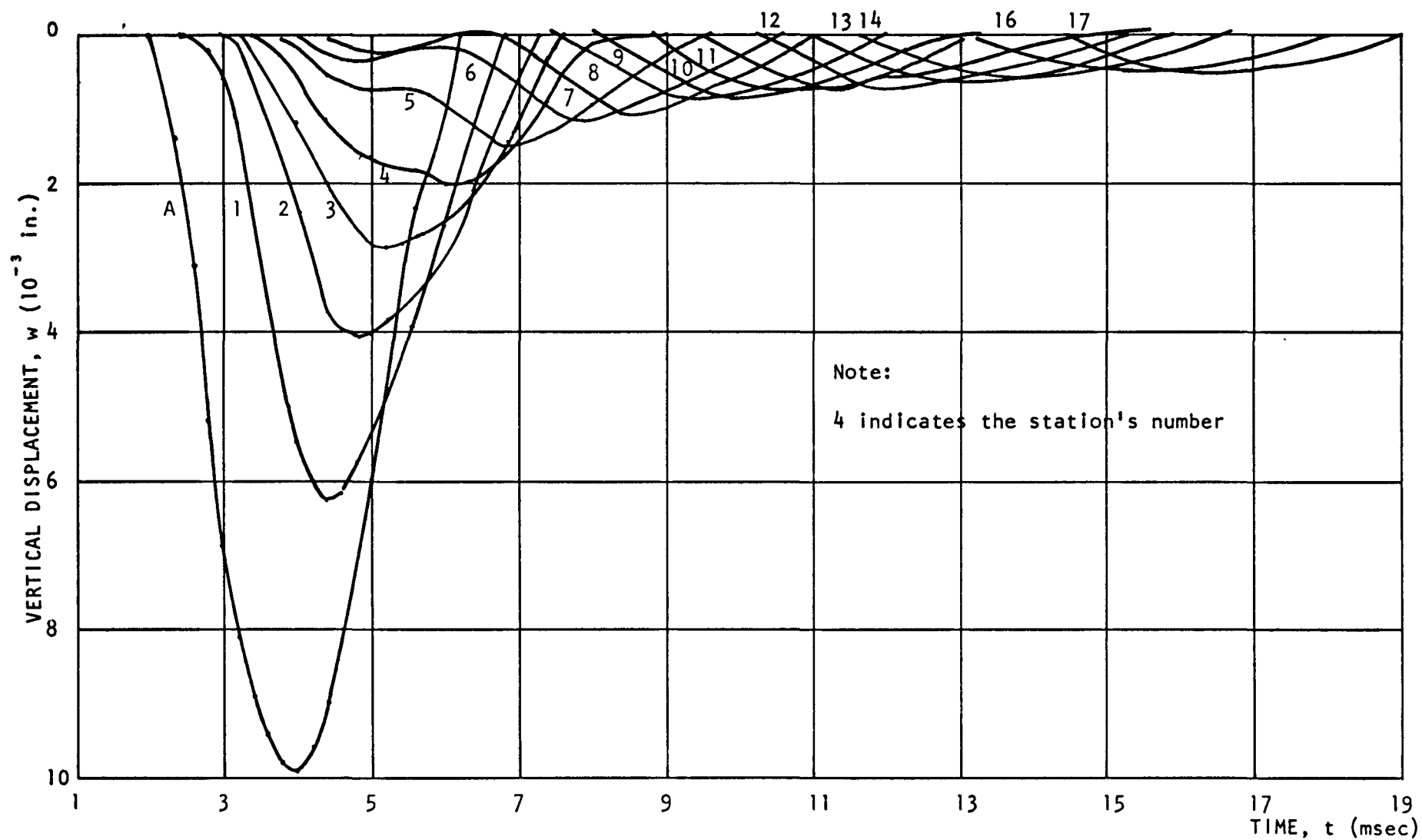
FIGURE 5-5   ATTENUATION OF DISPLACEMENTS — TESTS 6.1 to 6.7, W = 58 lb x .5 ft, σ_j = 3,500 psi

tation of the shear characteristics of the wave are difficult to isolate in this region. This pulse because it is composite and is rapidly separating in the "close in" region, produces distortions also in the displacement pulse as noted in Fig. 5-5.

The data obtained from Fig. 5-5 can be revised, and presented as waveforms or isochrone curves of displacement distance plots. Fig. 5-6 illustrates the waveforms obtained from this same test data. The zone of strong attenuation corresponds to the "close in" zone (i.e., Stations 1 to 5). The rate of attenuation decreases between Stations 5 and 12 and becomes very small beyond 12. This rapid change in displacement and attenuation together with the gradual increase in the length of the wave, in effect, produces a skewed wave shape.

Except in near-anchor regions where the waveform is distorted, the waveforms provide two factors essential for "free field" data interpretations. First it shows the physical vertical shearing distortions taking place at any interval of time. They also provide a means for estimating the maximum shear strains, since the waveform itself is a curve which satisfies the equation of displacement:

$$w = f(r,t) \tag{5.3}$$

If the small horizontal displacements are disregarded, the slopes of these curves therefore represent the shear strains at a certain point and time or:

$$\gamma = \frac{\partial w}{\partial r} \, t \tag{5.4}$$

Thus a maximum strain value is determined for each time isochrone at a point (or distance) corresponding to the maximum slope of that curve. This relationship is especially valid for
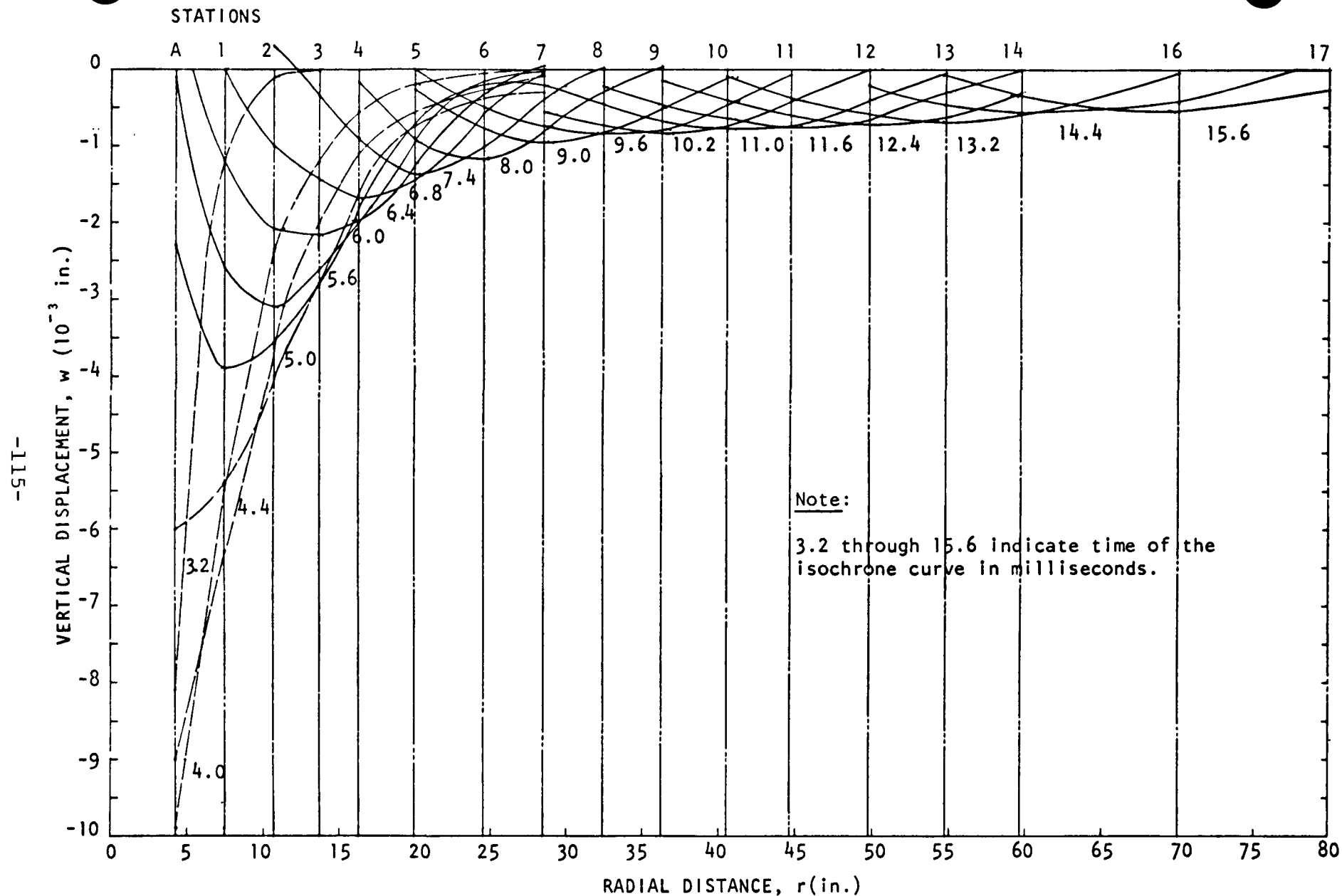
FIGURE 5-6   WAVEFORMS.   TESTS 6.1 to 6.7, W = 58 lb × .5 ft, σ_j = 3,500 psi

-115-

the free field sensors where the primary pulse is unimportant.
It also provides a check of the validity of using plane wave
theory to compute strains at the anchor. Further discussion
of this strain relationship is presented in Section 5.4.

5.3 SHEAR WAVE VELOCITY IN FREE FIELD SOIL

The waveforms in general indicate that the most readily
recognizable single point on each curve for determining propa-
gation velocities in the free field corresponds to the crest
of the wave, r_c. This crest, in general, is defined as the
point of maximum displacement at a given time, t, or:

$$w_{max} = f(r_c, t) \tag{5.5}$$

where: $\left(\dfrac{\partial w}{\partial r}\right)_{r_c, t} = 0$ and $\dfrac{dr_c}{dt} = V_s$

The crest displacement at a given time and at a certain
station is not always the absolute maximum that the station may
undergo. In fact, because of the "close in", rapid geometrical
attenuation of the waves in the near-anchor region (Section 3.3),
the absolute maximum displacement in the time history of
motions of a "close in" station occurs earlier than the passage
of the crest of the wave. However, as the wave moves further
away and into the free field, the rate of attenuation decreases,
the wave front advances as a plane wave and, therefore, the time
of maximum displacement in the time history coincides with the
time of the passage of the crest of the wave. Fig. 5-6 illus-
trates that Station 5 is the approximate boundary for the zone
closer to the anchor where the passage of the crest of the wave
does not coincide with the absolute maximum displacement. Station
5 is located approximately 20 inches from the anchor.

On the particle velocity-time record, the point is also
readily identified as the time of second crossing of the main
pulse or t" in Fig. 5-4.

This particular point has been chosen to identify the time
for computing the propagation velocity because:

1.   It corresponds to a well defined physical charac-
teristic of the wave propagation phenomena.

2.   It occurs after the soil has been subjected to
maximum strain, therefore being a good indicator of the strain
dependent benavior of the material.

3.   It can be used in zones closer to the anchor, since
it is less likely to be altered, by the primary pulses, than
points which precede it, as would be the case of the times
of first arrival and positive peak of the main pulse.

5.3.1   Velocities from Waveforms

From Figs. 5-6 and 5-7, several complications or
limitations appear apparent when using the crest of the wave-
forms to determine propagation velocity. The spacing of the
receiving stations and the time resolution control the precision
with which the crest of the wave can be defined. Also the
displacements include a component of primary wave which dis-
torts the main wave in the "close in" region. Finally the
anchor record cannot be used to define the waveforms in the
"close in' range primarily because it measures anchor movements
and slippage at the soil anchor interface as well as motions of
the surrounding soil.

In Fig. 5-7 the radial distance is measured from the
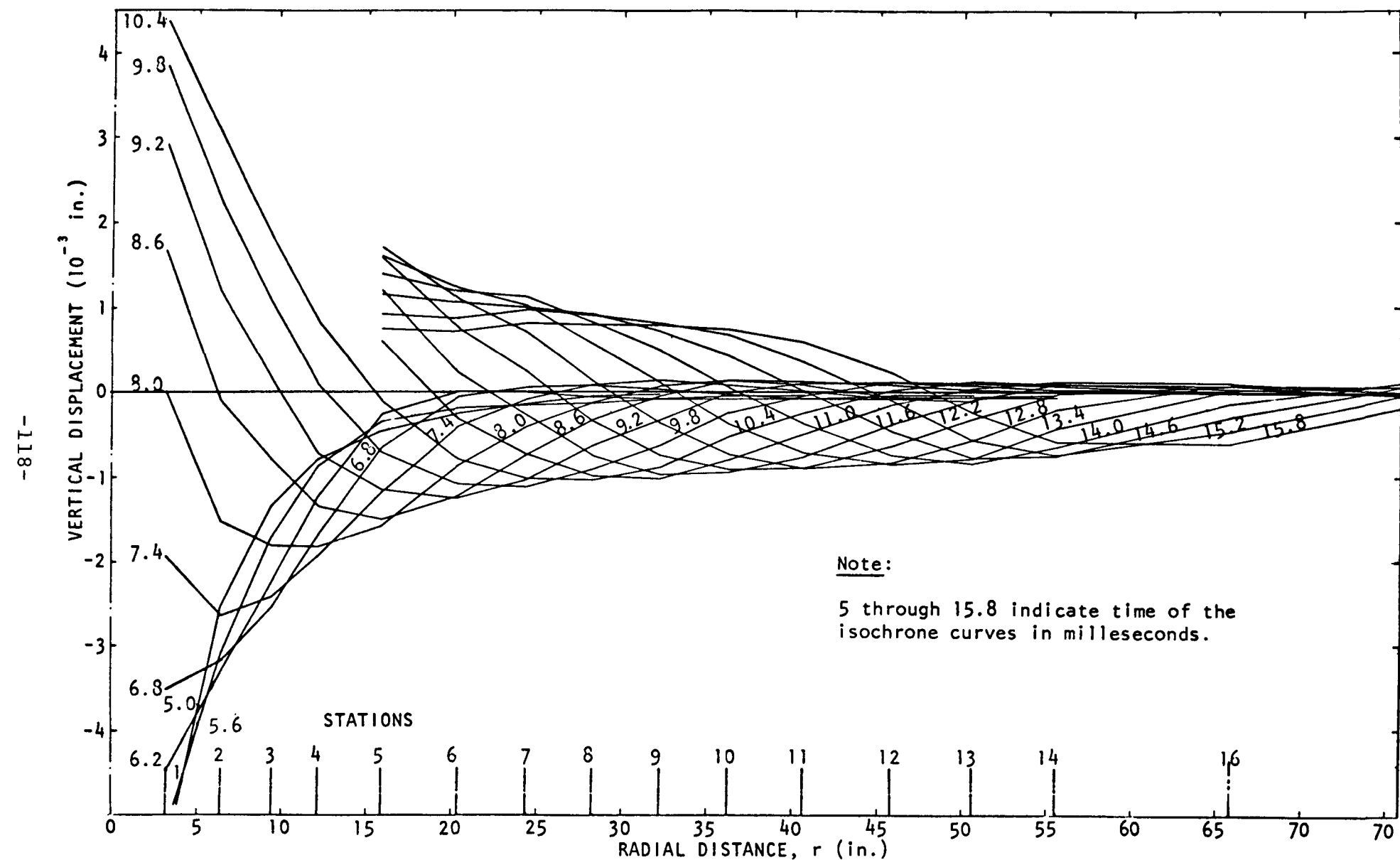edge of the anchor. From this figure and Fig. 5-6, the shear

FIGURE 5-7   WAVEFORMS.   TESTS 2.2A TO 2.8 ENERGY W = 68 lb × .5 ft,
JACK PRESSURE σ_j = 2,000 psi

wave velocity has been computed as shown in Tables 5.1 and 5.2, for the free field zone, between Stations 6 and 17. The point to point computations give results which vary considerably while the average velocities for distances in the order of every 10 inches vary to a lesser extent. The precision of point to point measurements is dependent on the definition of the location of the crest of the wave. Since only a few points, spaced at distances of 4 to 10 inches, are available, this definition of the crest in this region may be inaccurate. Velocities determined in Table 5.1 close to the anchor are generally higher than the rest, which is opposite to the trend of decreasing modulus with increasing strain. This anomaly may be due to the higher confining pressure caused by the effect of the radial stress of the anchor or to the component of primary wave pulses. It may also be due to the presence of a local dense lense of soil or to the inaccuracy of the waveform method near the anchor as indicated by the finite element results (Fig. 4-18). The proximity to the close range zone may also have influenced the first points of the Table 5.1, since parts of the waves are in that range. All other average velocities in these two tables agree with generally accepted soil behavior characteristics (i.e., to decrease in stiffness as the strain level increases).

Finally, it is also pertinent to note that these average velocities agree well quantitatively with the velocities determined from cyclic triaxial tests summarized in Appendix C, Fig. C-5. This is especially important when considering that both the in situ mass of soil and the laboratory samples were prepared as remolded materials.

5.3.2   Comparison of Several Methods for Determining Velocity

For production tests, it is not possible to construct waveform curves, because there is an insufficient number of free field recording stations. However, for the special tests, it is

Table 5.1

Shear Wave Velocity
For Waveforms in Fig. 5-7

Location of Crest of Wave r_c (in)	Time of Waveform t (msec)	Travel Distance Δr (in)	Travel Time Δt (msec)	Shear Wave Velocity V_s ($\frac{ft}{sec}$)	
				Point to Point	Average
22.8	9.8				
26.3	10.4	3.5	.6	486	
30.6	11.0	4.3	.6	597	542
33.6	11.6	3.0	.6	417	
37.3	12.2	3.7	.6	514	
41.2	12.8	3.9	.6	541	490
45.0	13.4	3.8	.6	523	
48.6	14.0	3.6	.6	500	
52.3	14.6	3.7	.6	514	514
55.5	15.2	3.2	.6	444	
60.6	15.8	5.1	.6	708	577

Table 5.2

Shear Wave Velocity
From Times t_1 of Peak Particle Velocity from Fig. 5-3

Sensor Station	t_1 (msec)	Δ r (in)	Δ t_1 (msec)	Shear Wave Velocity (fps) Station to Station	Average
6	7.54	/			
7	8.34	3.94	.8	410	
8	9.1	3.94	.76	432	421
9	9.68	3.87	.58	556	
10	10.42	4.06	.74	457	
11	11.12	4.32	.7	514	509
12	11.98	5.12	.86	496	
13	12.68	5.0	.7	595	
14	13.38	4.38	.7	581	557
16	14.62	10.37	1.24	697	
17	15.9	9.88	1.28	643	670

possible to use this data as a tool to compare velocities deter-
mined from the waveforms with recognizable points on the velocity
histories to aid in evaluating procedures for data reduction.
Ideally, for the "free field" stations, the crest point
generally corresponds to the point of zero crossing (t" in
Fig. 5-4). However, finite element results indicate that the
first peak velocity point (t_1) may be an equally acceptable point.
Therefore, as a first test, the three most identifiable points
on the main velocity time record (t_1, t", t_2) were determined
for all stations for a typical test series, the results of
which are plotted as Fig. 5-8. The three curves generally
parallel each other indicating that any of the three points pro-
vide reasonable values of shear wave velocity especially for
the more distant sensors. However, comparison of the two lower
curves show that the second crossing times, t", provide a
smoother curve than the first peak times, t_1. This is probably
because the particle velocity is changing more rapidly at t"
and is therefore less affected by minor distortions in the
wave shape itself. Also in the "close in" region, the first
peak time is probably more affected or contaminated by the
separating primary pulse. The smooth curvature of the second
crossing points in this region indicate that this time point
is less affected by strong primary pulses. Based on this com-
parison, it therefore appears that the zero crossing is the most
identifiable point of the three time points for use in computing
shear wave velocities especially for the "close in" region.
The third point, t_2, is often distorted in actual production
tests and therefore has received only minimal attention.

Before comparing these time points with the points
corresponding to the wave crest, it was considered desirable
to refine the waveforms for this example case by removing the
primary pulse from each velocity time signature prior to inte-
grating and constructing the waveform curves. Also to provide
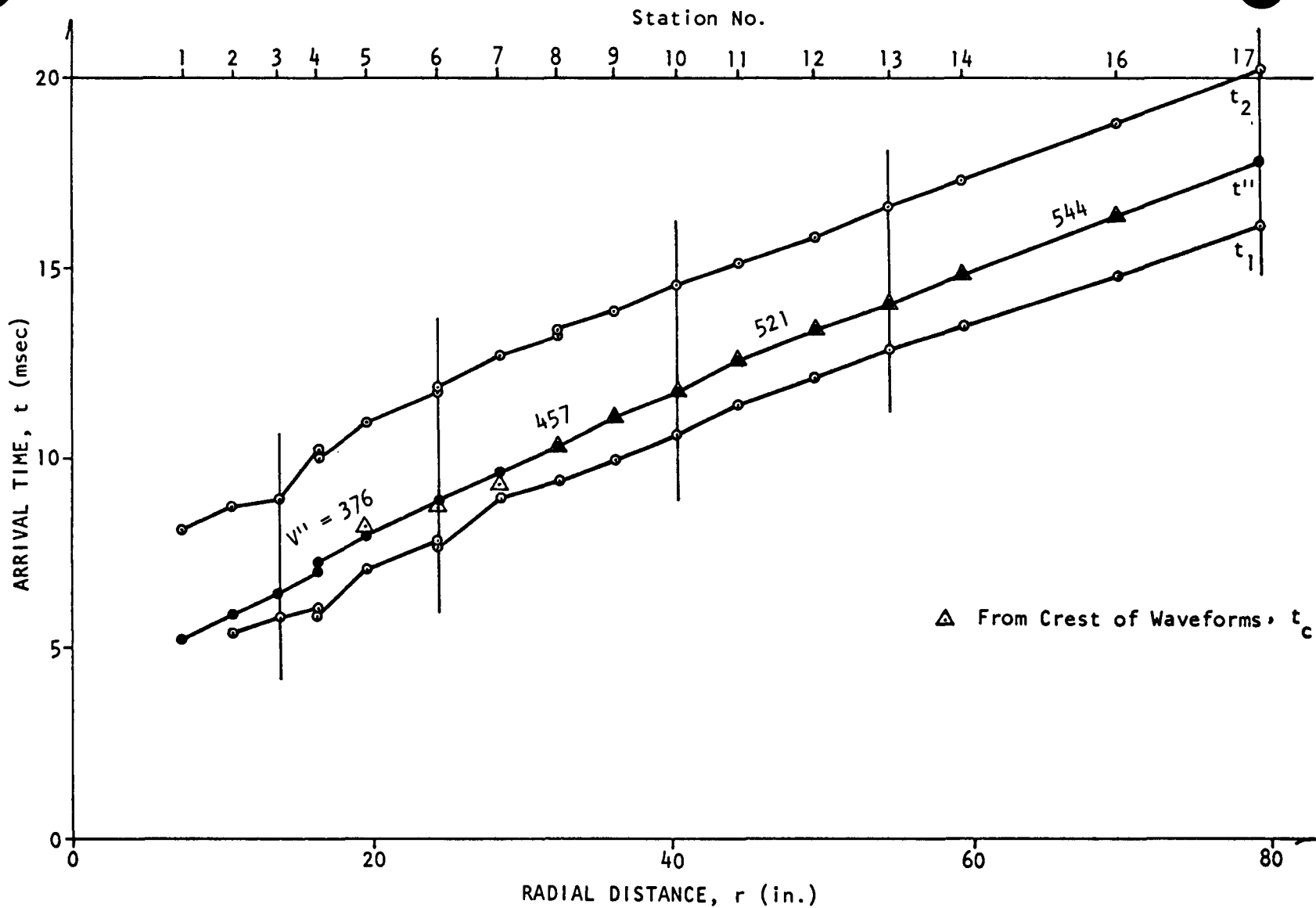a clearer definition of the crest of the waves, the displacements

FIGURE 5-8   TIME-DISTANCE PLOTS.   TESTS 2.10 TO 2.17A
ENERGY OF IMPACT, W = 58 lb x 1 ft.   JACK PRESSURE, σ_j = 2,500 psi

were greatly amplified. The time points obtained from this refinement of the waveforms have also been superimposed on Fig. 5-8. As indicated in this figure, data in the "close in" range is not included primarily because of the difficulties described earlier in this section and the inaccuracies noted in Chapter 4. The excellent agreement between this procedure for the indicated free field range when compared with time points on each velocity record indicate that the point corresponding to the zero crossing is indeed a proper point for identifying the arrival time of the shear wave at free field stations in production testing.

To further study the dependency of measurements of velocity on different energies of impact, three series of tests were performed at a constant jack pressure of 3,500 psi and different energies. A summary of the computed point to point velocities and average velocities using the time of zero crossing (t") is presented in Table 5.3.

The point to point data has its normal erratic variations, however the average values indicate reasonable soil behavior characteristics. Not only does the wave velocity increase as the wave propagates outward (i.e., increase in velocity with a decrease in strains) but also for respective stations a reduction in velocities with increasing energies is also evident. This data thus demonstrates in two ways that the shear wave velocity and thus the modulus is not only strain dependent but that this strain dependency can be assessed with in situ measurements.

5.4   SHEAR STRAINS IN FREE FIELD SOILS

Methods for the determination of shear strains in the free field have been tested using the analytical test results and are discussed in detail in Chapter 4. Shear strains were

Table 5.3

Shear Wave Velocity, V" (fps), Versus Energy

| Stations | W (lb x ft) | | |
No.	58 x .5	150 x .5	58 x 1.5
A-1	566	350	253
1-2	832	290	443
2-3	625	521	455
3-4	218	390	364
4-5	352	387	274
5-6	459	393	458
6-7	430	443	434
7-8	442	390	410
8-9	474	474	471
9-10	589	521	473
10-11	505	441	500
11-12	485	502	566
12-13	550	514	457
13-14	535	484	500
14-16	534	527	551
16-17	542	521	526

Average V" (fps) from t-r Curves

| Stations | W (lb x ft) | | |
No.	58 x .5	150 x .5	58 x 1.5
21-5	426	371	333
5-12	483	452	473
12-17	539	512	509

computed from the distortion of individual finite elements and then compared with maximum strains determined from the ratio of $\dot{w}/V_s$ (Eq. 3.13). The data, Fig. 4-18, showed that shear strains determined from $\dot{w}/V_s$ ratio agree well with computed values at distances greater than 20 inches, while for the cases and computational techniques considered in the figure, the "close in" values were about 30 to 50 percent too low. This large variation in the strains from the ratio equation is not surprising, it is known that this equation is not theoretically applicable in the near-anchor region.

Since the finite element calculations do not duplicate all aspects of the "real" in situ conditions, a similar comparison was made with the experimental data. A sample of test data comparing the strains determined from the waveforms (Eq. 5.4) with those calculated from the $\dot{w}/V_s$ ratio is presented in Fig. 5-9. This figure shows good agreement and further supports the validity of the analytical calculations and the comparison of this test data. This data further shows that, for the distance range shown, the strains determined from the waveforms agree well with the strains determined from the particle velocity shear wave velocity ratio. This is the same range where the finite element computed strains also agreed well with the strains computed from the velocity ratio. "Close in" strain data is neither shown nor compared because of uncertainties in interpreting the correct particle velocity value for the latter case. The strong primary wave present in this region could greatly influence the value of the peak particle velocity and thus the computed $\dot{w}/V_s$ ratio. Approximate strains determined from waveforms from the finite element calculations of Chapter 4, in which there were no primary waves, agreed within about 10 percent with the exact strain values computed during the calculations. This agreement was obtained in spite of the failure of the wave-form methods to provide good estimates of the shear wave velocity in the near-anchor region.
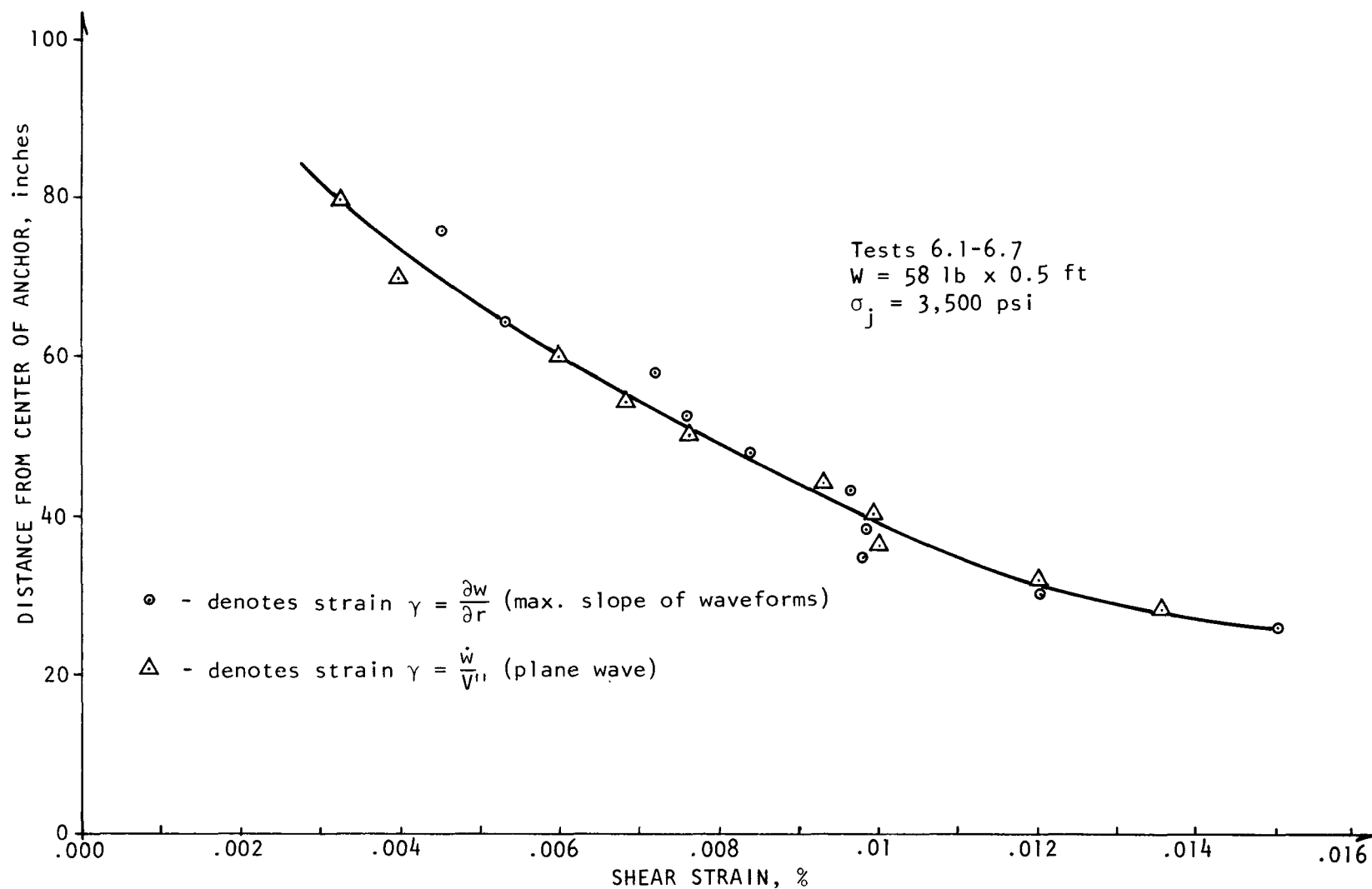
FIGURE 5-9   COMPARISONS OF STRAINS DETERMINED BY DIFFERENT METHODS

The figure plots DISTANCE FROM CENTER OF ANCHOR, inches (vertical axis, 0 to 100) against SHEAR STRAIN, % (horizontal axis, .000 to .016).

Tests 6.1-6.7
W = 58 lb x 0.5 ft
σ_j = 3,500 psi

⊙ – denotes strain $\gamma = \dfrac{\partial w}{\partial r}$ (max. slope of waveforms)

△ – denotes strain $\gamma = \dfrac{\dot{w}}{V''}$ (plane wave)

Since the waveforms provide reasonable approximations of the shear strain (but not necessarily wave velocities) in the "close in" region, both the influence of jack pressure and energy level on the strain in this region can be studied more closely. For this assessment four series of tests were compared, three at a constant jack pressure and varying impact energies and one with a variable jack pressure but the same energy as one of the previous three series. The strains computed from these series of tests from constructed waveforms are summarized in Table 5.4. Strain plots of the three series of tests with variable impact energies are presented as Fig. 5-10. The very strong attenuation in strain in the first 18 to 20 inches is clearly evident. The increase in strain with increased energies is also consistent. However, because of the rapid rate of attenuation "close in", actual strain values in the free field under various energy conditions are changed only a small amount and in fact appear only important in the closer range. Since the first free field sensor in production tests is located at an approximate radial distance of 48 inches, it is apparent that significantly larger strains cannot be achieved with larger energies and therefore the use of excessively strong equipment with very heavy hammers is not warranted for this test.

A comparison of the two series of tests at different jack pressures in Table 5.4 also indicates that increased jack pressures produce larger strains which are only significant in the closer range. This comparison would indicate that variations in jack pressure do not produce significantly different strains in the free field and therefore is not likely to significantly affect measured test values. The effects of jack pressure and energies (hammer weight and height of drop) are treated in greater detail in Appendices F and G.

Table 5.4

Shear Strain, γ (%), Versus Energy and Jack Pressure

		σ_j = 3,500 psi			σ_j = 2,000 psi
		W (lb x ft)			W (lb x ft)
r(in)	Sta. #	58 x .5	150 x .5	58 x 1.5	58 x .5
5.9	A-1	2.16×10^{-1}	4.36×10^{-1}	6.3×10^{-1}	
9.1	1-2	9.7×10^{-2}	1.69×10^{-1}	1.97×10^{-1}	9.2×10^{-2}
12.2	2-3	5.9×10^{-2}	9.2×10^{-2}	1.1×10^{-1}	4.6×10^{-2}
14.9	3-4	4.4×10^{-2}	8.4×10^{-2}	8.5×10^{-2}	4.0×10^{-2}
17.1	4-5	3.4×10^{-2}	5.7×10^{-2}	6.0×10^{-2}	2.96×10^{-2}
22.2	5-6	2.0×10^{-2}	3.5×10^{-2}	3.1×10^{-2}	1.73×10^{-2}
26.4	6-7	1.5×10^{-2}	2.8×10^{-2}	2.5×10^{-2}	1.32×10^{-2}
30.5	7-8	1.2×10^{-2}	2.2×10^{-2}	2.0×10^{-2}	1.09×10^{-2}
34.4	8-9	9.8×10^{-3}	1.5×10^{-2}	1.6×10^{-2}	8.01×10^{-3}
38.5	9-10	9.9×10^{-3}	1.44×10^{-2}	1.4×10^{-2}	9.41×10^{-3}
43.0	10-11	9.7×10^{-3}	1.45×10^{-2}	1.2×10^{-2}	7.75×10^{-3}
48.0	11-12	8.4×10^{-3}	1.2×10^{-2}	1.1×10^{-2}	7.62×10^{-3}
53.0	12-13	7.6×10^{-3}	1.1×10^{-2}	1.06×10^{-2}	6.4×10^{-3}
58.0	13-14	7.2×10^{-3}	8.6×10^{-3}	9.0×10^{-3}	7.58×10^{-3}
65.3	14-16	5.3×10^{-3}	7.4×10^{-3}	7.0×10^{-3}	5.11×10^{-3}
75.6	16-17	4.5×10^{-3}	6.2×10^{-3}	6.0×10^{-3}	4.45×10^{-3}
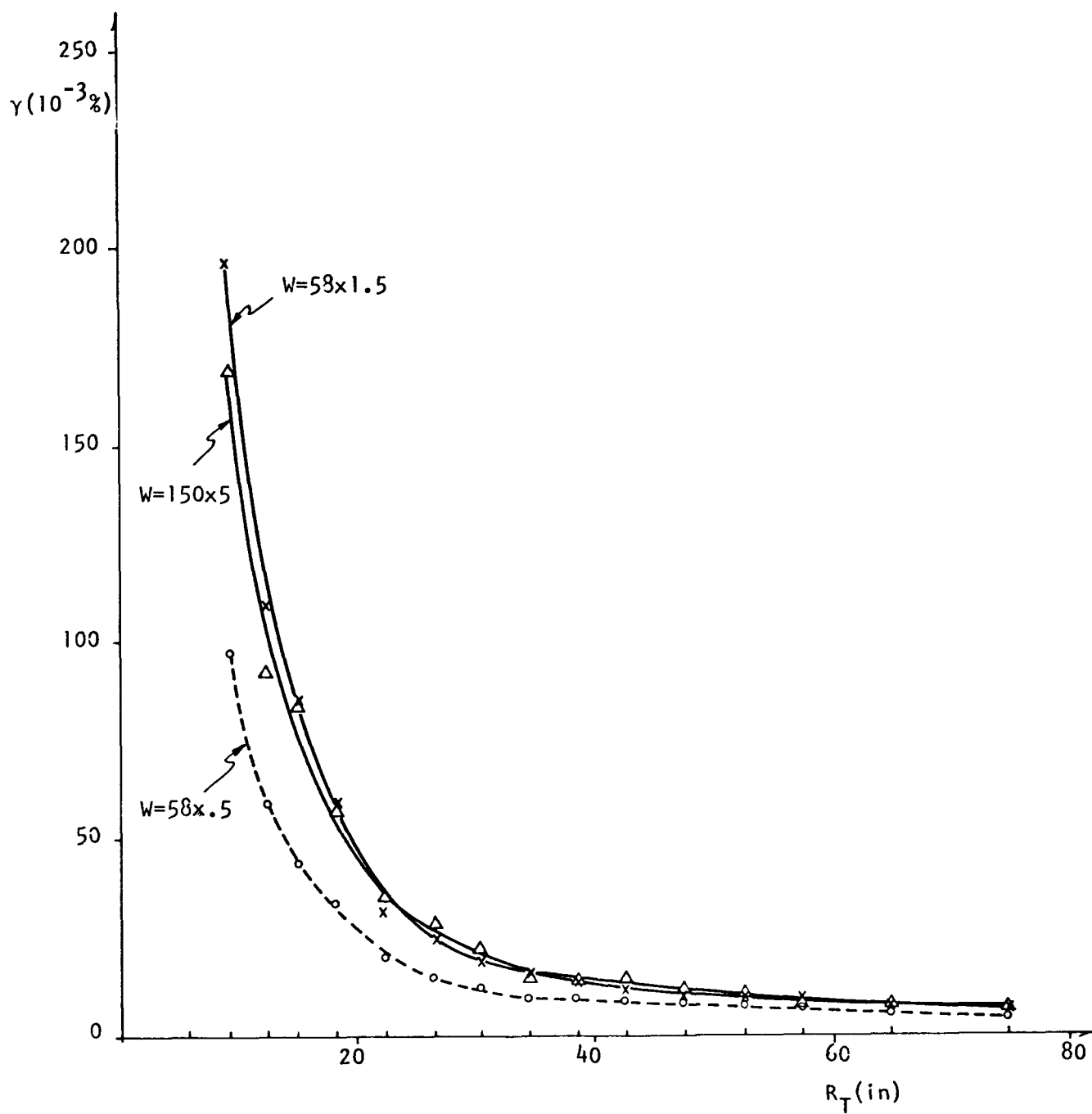
FIGURE 5-10   SHEAR STRAIN FROM WAVEFORMS
VERSUS RADIAL DISTANCE σ_j = 3,500 psi

5.5 SHEAR WAVE VELOCITY AND STRAINS IN SOILS
ADJACENT TO THE ANCHOR

The in situ impulse test provides accurate measurements for
the determination of shear moduli and shear strains in the free
field. The region adjacent to the anchor cannot be incorporated
in these measurements because of the special conditions in the
surroundings of the anchor source. However, approximate values
of wave velocities and shear strains could be obtained in this
region, if the records of loads and motions of the anchor could
be used to estimate the response of the adjacent soils. In
order to investigate the possibilities of this approach, under
the controlled conditions in the compacted fill, detailed
measurements of anchor loads and motions were recorded in
different special tests. This enabled the "real" test con-
ditions to be studied in relation to the more simplified
theoretical models defined in Chapters 3 and 4. As described
in Appendix D, the anchor was instrumented with a load cell to
measure the force applied to the anchor, and several velocity
transducers and accelerometers to measure anchor motion
characteristics. Simultaneous measurements of these character-
istics together with adjacent sensors in the soil would provide
sufficient information to obtain the shear wave velocity and
the corresponding strain at the anchor.

5.5.1   Anchor Records

A sample of records made from transducers on the anchor
and in the adjacent sensor are presented in Fig. 5-11 to illus-
trate characteristic shapes and points of each time history.
The applied load pulse has a slightly irregular triangular or
parabolic shape while the acceleration is a very random erratic
series of spikes. The latter two velocity curves except for
differences in amplitude in general exhibit amazingly similar
shapes. The three anchor measurements, although possessing a
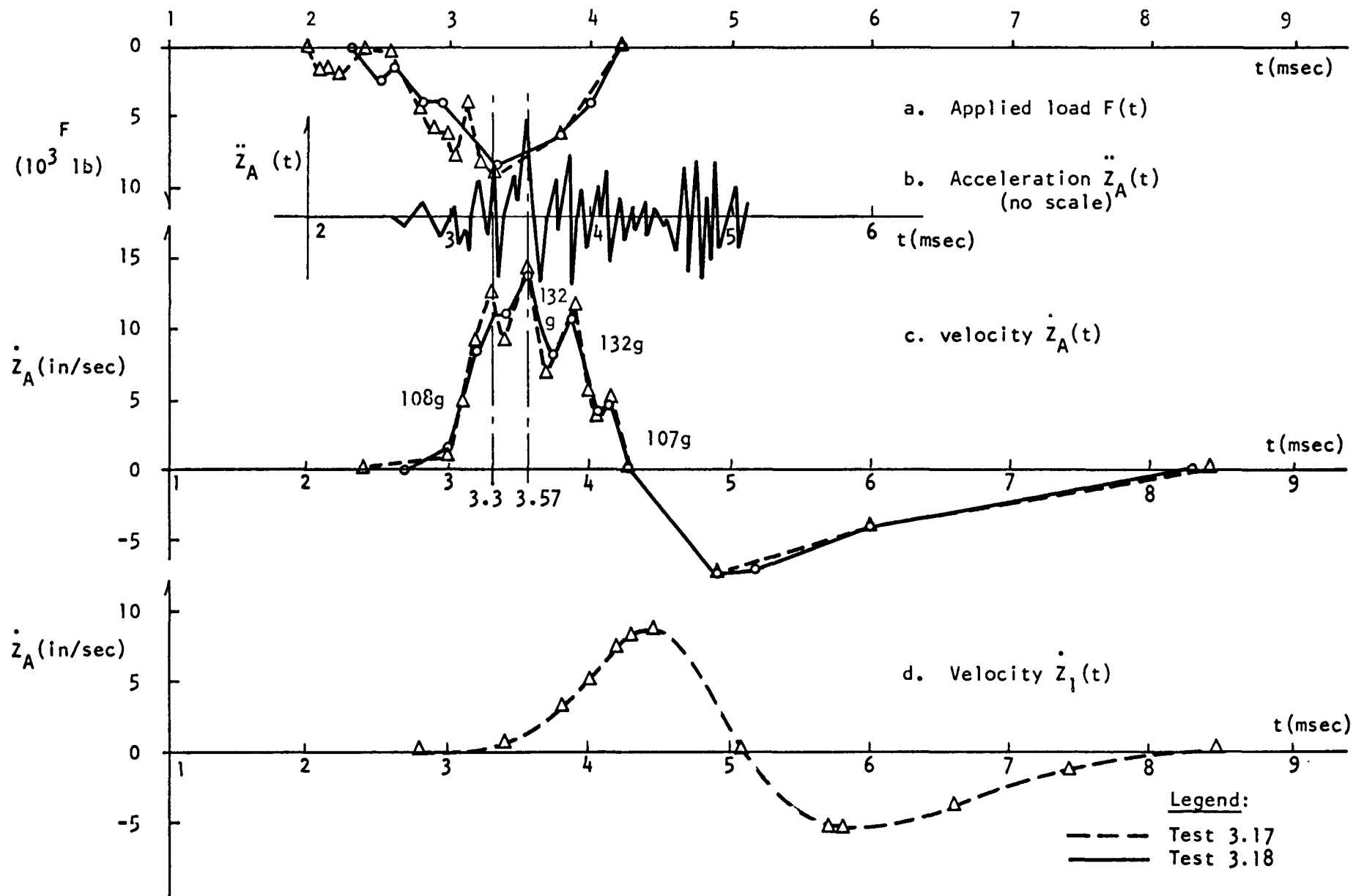
FIGURE 5-11   LOAD AND MOTIONS OF THE ANCHOR AND STATION 1
TESTS 3.17 and 3.18, W = 58 lb x .5 ft, σ_j = 6,000 psi

wide variety of shapes, all show a common time referring to the start of the event (or impact). This characteristic time is a lower bound value and if plotted on a time distance graph with free field points as in Fig. 2-1 defines a slope corresponding to a lower bound value of shear wave velocity. While this point does not define a true shear wave velocity in the soil, it provides a reference lower bound value at the location of the anchor.

The force time history was used primarily in this experimental study as a base for correlating the effect of jack pressure and for studying force characteristics at the adjacent soil anchor interface. For the range of jack pressures, hammer weights and drop heights used in these tests, force values of the order of 5,000 to 30,000 pounds were generally obtained. Force shape, magnitude, and signal duration, and rise time characteristics are discussed and related to jack pressure in Appendix G. These measurements and a comparison of various relationships in this appendix demonstrate the importance of achieving optimum anchor coupling.

Measurements of acceleration in the anchor were limited to one transducer, as the lower unit became damaged and did not operate. The data from this source was somewhat limited primarily because the measured motion was a registration of the passes of stress waves traveling up and down the high velocity metals of the anchor (i.e., propagation velocity of aluminum is 16,000 ft/sec). The records obtained were therefore a superposition of high frequency pulses which represent the stress changes in an element of a plate on the anchor and not entirely the motion of the anchor as a whole. These high frequency measurements, in general, masked out the lower frequency motions typical of the total motion of the anchor. The accelerometers were placed such that R_s (the resisting force in the soil - Eq. 3.12) could be computed from direct measurements. One other

less direct approach for estimating the acceleration of the anchor is from the slope of the velocity time history. Minor time shifts between the different recording transducers, however, did not produce any seemingly meaningful relationships. These relationships will be studied further in future efforts described in Chapter 6.

Particle velocity records of the anchor and records several inches away in the surrounding soil enabled relative transfer motion characteristics across the soil anchor interface to also be studied. As indicated in the Fig. 5-11, the shapes of the two curves were generally quite similar when excessive slippage did not occur. As the wave passed between these two stations, there was an attenuation in signal amplitude and a general filtering of the high frequency components in the anchor record. Where slippage was excessive, the anchor record became greatly distorted primarily because the input motion to the anchor exceeded the capacity of the transducer to record it correctly.

While the measured motion and force characteristics provided little additional theoretical understanding of the test phenomenology, they nevertheless provided additional definition of magnitude and forces acting on the anchor and transfer and stress characteristics (slippage and coupling) at the anchor soil interface. The data also provided consistent time and signal amplitude on the anchor records, to enable both the shear wave velocity and its strain to be estimated using characteristic points.

The approach for data interpretation of the anchor record was thus one of comparing free field velocities and strains determined from the experimental tests with those estimated in the anchor region. Once this was accomplished with the closer spaced special test measurements, empirical

methods could be developed for use with production test data.

5.5.2   Dimensional Analysis Procedures

Dimensional analysis procedures were used to find a relationship between the main variables of the test. The dimensional analysis procedure permits definition of dimensionless products formed by the variables of the test. These variables are:

W   the energy of impact of a test in (lb-ft)

ρ the mass density of the soil in $(lb \cdot sec^2/ft^4)$

V_s the shear wave velocity of the soil in (ft/sec)

r   the distance from the center of the anchor to the center of the element of soil in (ft)

$\dot{w}_1$ the average maximum particle velocity in the element of soil in (ft/sec)

Dimensionless products can then be related to represent a physical equation as φ (π_1, π_2) = 0 as long as all of the variables are included. Convenient dimensionless products for this equation are:

$$\pi_1 = \frac{\dot{w}_1}{V_s}$$

$$\pi_2 = \frac{(\rho V_s^2)^{\frac{1}{3}} r}{W^{\frac{1}{3}}}$$

where $\rho V_s^2 = G$, especially since π_1 represents the equation for strain γ of plane waves and π_2 is an indication of modulus.

Fig. 5-12 is the dimensional analysis log-log plot
of the dimensionless parameters for three series of tests
including only the free field stations. These tests were per-
formed with the same jack pressure and different hammer weights
and heights of drop. The narrow band of data from this plot
shows that for these soils, there is a unique relationship
between the variables of the test. Relationships of this
type may be used to estimate the variation of strain with
distance from the source. If the natural stress conditions were
the same in the close range, as in the free field, the free
field relationship could be extrapolated to verify strain values
close to the anchor. Unfortunately, the static radial stresses,
applied by coupling of the anchor, produce changes in the state
of stress, which are difficult to evaluate. Nevertheless,
these relationships may be used to verify measurements resulting
from impulse tests.

5.5.3   Shear Wave Velocity at Anchor

Shear wave velocities in the close range are difficult
to estimate because of superposition of pulses from P and S
waves and differences in states of stress around the anchor.
Characteristic time-distance curves, obtained from a complete
series of tests, are shown on Fig. 5-13. These curves are
formed using times of maximum displacement, t", and maximum
particle velocity, t_1, for all stations including the anchor
record. In the upper curve formed by using the t" times, it
is observed that, while free field points plot in fairly well
defined curves, close range points are erratic, because of the
reasons mentioned above.

Average wave velocities, estimated as average slopes
of the time distance curves, are 483 fps between stations 5
and 12, and 539 fps between stations 12 and 17. An approximate
upper value of wave velocity between the anchor and station 5 is

-136-
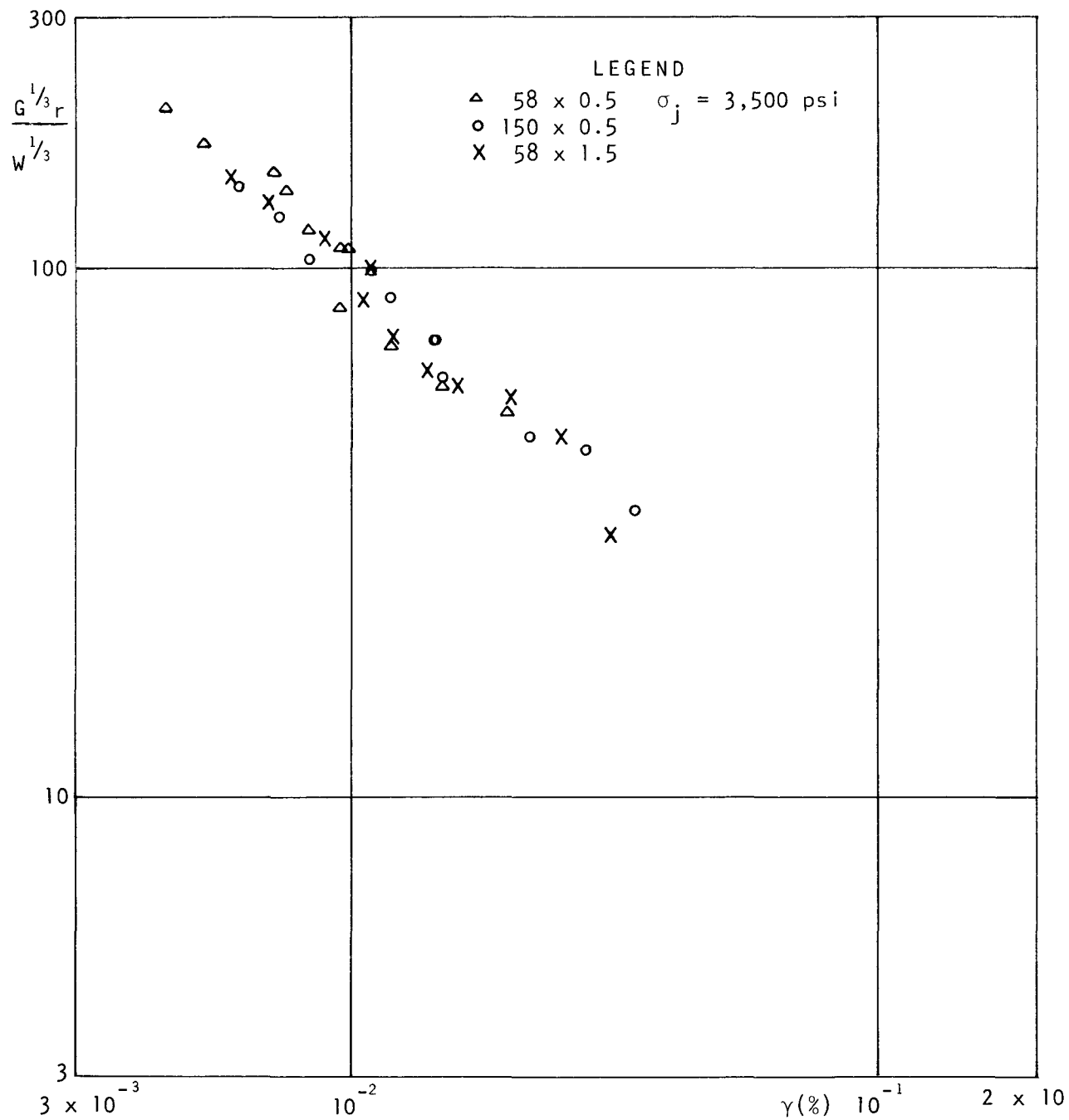
FIGURE 5-12   SOIL MODULUS VERSUS SHEAR STRAIN
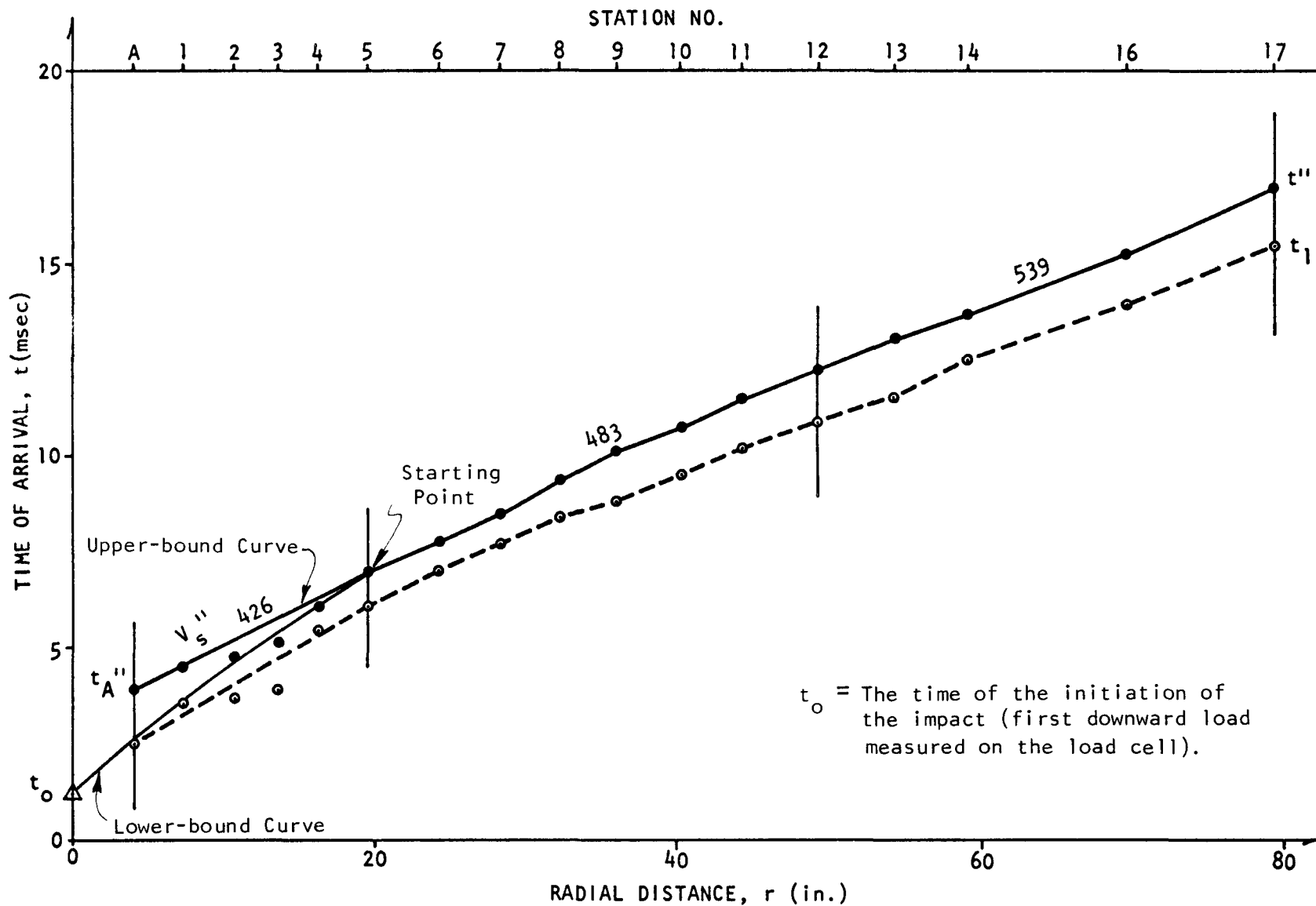
FIGURE 5-13   TIME-DISTANCE PLOTS.   TESTS 6.1 TO 6.7
ENERGY OF IMPACT, W = 58 lb x .5 ft.   JACK PRESSURE, σ_j = 3,500 psi

given by the slope of the straight line connecting times of maximum displacements of these two stations. This velocity, which is about 426 fps in this case, should be an upper bound value because slippage and higher stresses should delay the occurrence of maximum displacement of the anchor.

In the in situ test, described in Chapter 2, the record of the anchor is different from the records of the free field in that it may include slippage, it represents the superposition of pulses traveling through different paths in the mechanical system and it is part of the forcing functions that generate the waves. From the analyses of this and other tests, in the controlled conditions of the artificial fill, it seems that when firm coupling is achieved, the point of zero crossing, t", of the anchor record is a consistent upper bound point which relates well with the same points of the records of the free field. However, to use this point from the anchor record to obtain a corrected wave velocity at this point (rather than an upper value), the resultant velocity must be adjusted such that this point corresponds to stress conditions similar to those in the free field. This adjustment becomes especially significant when the applied radial stress is considerably different from the natural state of stress. The following correction may be used for this effect. Based on numerous laboratory tests on different types of soils (SW-AA, 1972), the shear modulus, G, has been found to be approximately proportional to the square root of the mean effective principal stress, $\bar{\sigma}_m$, or the shear wave velocity is proportional to the one-fourth power of the effective principal stress:

$$V_s = K_1 \bar{\sigma}_m^{\frac{1}{4}}$$

If $\bar{\sigma}_m$ is the mean principal stress in the free field and $\bar{\sigma}_A$ is the mean principal stress in the close range, a corrected shear wave velocity at the anchor or near anchor region can then be obtained from:

$$V_s \text{ corrected} = V_s" \times \left(\frac{\overline{\sigma}_m}{\overline{\sigma}_A} \right)^{\frac{1}{4}}$$

where $V_s"$ is the shear wave velocity determined from the time distance curve using times t" or times of maximum displacement.

Other defects incorporated within the anchor records, such as slippage and superposition of pulses cannot be readily assessed either quantitatively or qualitatively. As a result the corrected velocity, adjusted for different stress conditions must be considered as, at best, an estimate of the true shear wave velocity in this region.

5.5.4   Shear Strain at Anchor

The shear strain at the anchor has to be estimated somewhat arbitrarily since it is not possible to use the formula:

$$\gamma = \frac{\dot{w}}{V"}$$

because of the practical limitations of the record of the anchor and the theoretical limitations of the formula. Finite element results in general indicate that this ratio produces strains in the close in region which are low by 30 to 50 percent. However, this analysis does not include slippage and many of the other factors inherent in the "real" test. These factors, particularly slippage, tend to produce excessive particle velocities at the anchor. These higher values when used in the ratio, tend to compensate for this underestimate of strain.

The use of this ratio together with extrapolation of free field data to the higher range using dimensionless analysis as a second check both provide reasonable estimates of the shear strain at the anchor. In general, reasonable shear strain values

determined using similar equipment should produce shear strain values of the order of 10^{-1} percent or greater.

CHAPTER 6
PRODUCTION TEST DATA INTERPRETATION PROCEDURES

Section 2.4 describes in general terms the data handling
and graphical construction procedures for processing production
data. The desired parameters derived from this test at a given
depth are four shear wave velocities (or modulus) at four
different strain levels. To obtain these values, rational pro-
cedures had to be established for determining pertinent arrival
times from this data to compute propagation velocities. Also
practical methods for determining strain had to be provided both
for sensors positioned in the free field as well as at the anchor.
The experimental and analytical programs described in Chapters 4
and 5 treat this problem in considerable detail. From these
efforts, the following procedures are recommended for inter-
preting these points and completing the production test reduction
procedures.

6.1 FREE-FIELD STATIONS

Special tests and analytical support calculations show
that beyond twenty inches from the anchor, the shear wave travels
closely as a plane wave. Since the first station is generally
48 inches away, it and the more distant ones may be treated the
same. Arrival times are obtained by selecting common points
on each signature provided these points occur after the maximum
strain is reached. Maximum strain usually occurs at a time
corresponding approximately to the first positive peak on the
particle velocity records. Therefore either the time of the
first positive peak or the next point of zero velocity crossing
should be selected. Of these two points, the crossing point is
recommended, because it occurs when the velocity is changing
rapidly and is more readily identified. The first velocity peak
point while more theoretically applicable is occasionally
difficult to define precisely because the rate of velocity change

(acceleration) is small and therefore subject to minor distortions caused by imperfections in the signature. Also the zero crossing point corresponds to the time of peak displacement (i.e. the crest of the outward propagating wave). Close-in this is not true. The zero crossing/fit method in Chapter 4 is therefore recommended for determining shear wave velocities in the free field.

Shear strains can also be computed assuming that the propagating wave is a plane shear wave using the peak velocity/fit method (i.e. the shear strain = particle velocity amplitude divided by the shear wave velocity). Both theoretical and analytical data have shown that the error involved in such an assumption is of the order of less than about 10 percent for a distance beyond twenty inches from the anchor.

6.2   ANCHOR STATION

Within about twenty inches of the anchor, the horizontally propagating shear wave is ideally spherical or cylindrical in nature. Therefore, plane wave theory no longer applies, and treatment of close-in points involves more complex relationships. Fortunately, the only recording station within this range corresponds to the transducer mounted on the plate of the anchor.

When considering the use of corresponding points on this signature with the free field data, the problem becomes greatly complicated. Not only does the close-in soil region propagate waves as cylindrical waves rather than plane waves, but the actual measurement represents more nearly the motion of the anchor as well as slip at the interface. Therefore to theoretically treat this sensor and the record as a free field soil measurement, we not only must consider these factors but also must account for:

1) stress relief around the borehole occurring
   when the hole is made,
2) disturbance caused by drilling operations,
3) changes in stress by the application of radial
   jacking forces to achieve coupling.

Further, the anchor itself is not a rigid body and therefore the
recorded motion represents the real motion at only one point on
this complex mechanical structure. Thus the record corresponds
to a composite train of waves traveling through the complex
anchor. It is surprising, when considering all these factors,
that this signature so closely resembles those obtained in the
free field.

The only way to account for these factors was to perform
"close in" special tests under varying conditions and analytical
studies and together assess the problem empirically. The pro-
cedure consisted of bracketing the shear wave velocity making it
representative of an average zone of soil within 18 to 20 inches
of the anchor. From the experimental tests, if the same point
(specifically the point of second zero crossing) is selected on
the anchor signature as the free field signatures, an upper bound
value of time and shear velocity is obtained. This estimated
upper bound value may be modified to take into account the
different state of stress adjacent to the anchor. However, the
actual field installation conditions which may occur in an in
situ test have to be considered with first priority in the inter-
pretation of test results. Because of these problems, no
standard production procedure for use of the records of the
anchor can be recommended. The different approaches presented
in Chapter 5 may be used to obtain approximate values of wave
velocity and shear strain in this region, but they have to be
applied in close connection with field observations obtained
during the performance of the test.

6.3 FUTURE WORK

As a result of "close-in" experimental special testing and subsequent analytical calculations, much data has been collected, evaluated and has formed the basis upon which the in situ impulse test is founded. Now that procedures are developed, partial future work will consist of actually performing this test on a production basis. This work has been started by testing at accelerograph station sites to evaluate the geotechnical properties including the variation in modulus with strain. This work is planned to continue and will ultimately provide designers of nuclear plants with better geotechnical properties for establishing seismic design criteria.

Most research efforts in the past have been directed toward evaluating the shear modulus variation with shear strain. Future efforts will consist of utilizing this same experimental and analytical test data to evaluate other in situ soil properties such as material damping, P-wave velocities and possibly Poisson's ratio. If additional soil property data can be obtained using the same equipment, the flexibility of the test would be greatly increased.

Initial future efforts will include a thorough evaluation of material damping characteristics. Studies of existing close-in data reported herein including 1) attenuation rates from both experimental and analytical results, and 2) isolated anchor force and motion characteristics. From this study, potential approaches or the feasibility for estimating material damping using the in situ procedures and/or equipment will be evaluated. If in situ procedures for even estimating crudely the variation in material damping with strain could be developed, the state of the art of in situ testing for evaluating earthquake engineering problems would be greatly advanced.

REFERENCES

Mow, C. C. (1965)
"Transient Response of a Rigid Spherical Inclusion
in an Elastic Medium," Jour. Appl. Mech., September,
p. 637-642.

SW-AJA (1972)
"Soil Behavior Under Earthquake Loading Conditions:
State of the Art, Evaluation of Soil Characteristics
for Seismic Response Analyses," A Joint Venture of
Shannon & Wilson, Inc., and Agbabian-Jacobsen Associates,
Jan.

SW-AA (1973)
"Soil Behavior Under Earthquake Loading Conditions:
In Situ Impulse Technique for Determination of Soil
Shear Modulus," A Joint Venture of Shannon & Wilson, Inc.,
and Agbabian Associates, June.

SW-AA (1974)
"Soil Behavior Under Earthquake Loading Conditions:
In Situ Impulse Test for Determination of Shear Modulus
for Seismic Response Analyses, Progress Report," A
Joint Venture of Shannon & Wilson, Inc., and Agbabian
Associates, June.

Terzaghi, K. (1943)
Theoretical Soil Mechanics, 4th ed., John Wiley & Sons,
Inc., New York.

Troncoso, J. H. (1975)
"In Situ Impulse Test for Determination of Soil Shear
Modulus as a Function of Strain," Ph.D. Thesis,
University of Illinois.

Westergaard, H. M. (1940)
"Plastic State of Stress Around a Deep Well," Boston
Society of Civil Engineers, Vol. 27, January.

APPENDIX A

DESCRIPTION OF NONLINEAR SOIL MODEL

APPENDIX A

DESCRIPTION OF NONLINEAR SOIL MODEL

A mathematical model has been developed which is intended to represent the hysteretic shear stress vs. shear strain behavior of sand. The raw data from which this model was constructed consists primarily of the cyclic triaxial tests summarized in Appendix C. In addition, propagation velocities were available from in situ test data.

The model consists of a variable bulk modulus which depends on J_1, the first invariant of the stress tensor.

$$J_1 = \sigma_1 + \sigma_2 + \sigma_3 \tag{A.1}$$

where σ_1, σ_2, σ_3 are the normal stresses at a point in the soil. The sign convention for normal stresses is positive for tension, negative for compression. In addition, the shear modulus varies as a function of both J_1 and τ_p, the principal-shear-stress acting on an element of soil, where

$$\tau_p = \frac{1}{2} \left[(\sigma_1 - \sigma_2)^2 + (2\tau)^2 \right]^{\frac{1}{2}} \tag{A.2}$$

and τ is the shear component of stress with respect to the global coordinate axes.

The formula for computing bulk modulus, $K(J_1)$, is

$$K(J_1) = K_1 \left[1 - K_2 \exp(K_3 J_1) \right] \tag{A.3}$$

where K_1, K_2, and K_3 are parameters to be chosen to fit the available data. Eq. A.3 holds regardless of whether virgin loading, unloading, or reloading is taking place. This model, therefore, shows no hysteresis for cyclic loading in bulk.

However, since constitutive relations in shear are independent of bulk modulus, and since the inelastic finite element calculation consists primarily of shear loading, it is not particularly important to model completely the material behavior in bulk.

The variable shear modulus is expressed in terms of Poisson's ratio which, in conjunction with the bulk modulus, defines the shear modulus. Alternatively, one could have defined the variable shear modulus directly, ignoring any variation which might have occurred in Poisson's ratio. The objective is, however, that the shear modulus be represented realistically; and through Poisson's ratio, a realistic definition of the variable shear modulus is obtained. Therefore, the variable-Poisson's-ratio approach is used solely as a device to obtain shear behavior representative of the sand materials for which the triaxial measurements were obtained.

For virgin loading, Poisson's ratio is computed according to the following formula:

$$\nu_v(J_1, \tau_p) = \nu_{EL} + (\nu_{PL} - \nu_{EL}) \left[1 - \exp \frac{\alpha \tau_p}{J_1} \right] \qquad (A.4)$$

where ν_{EL}, ν_{PL}, and α are parameters to be chosen such that the material behavior agrees with the triaxial test data. Virgin loading occurs whenever τ_p exceeds all previously obtained values of τ_p. When τ_p is less than the previous maximum value of principal-shear-stress, τ_{max}, the unloading/reloading formula for Poisson's ratio applies.

$$\nu_u(J_1, \tau_p, \tau_o, \tau_{max}) = \nu_{EL} + \left[\nu_v(J_1, \tau_{max}) - \nu_{EL} \right] T^\beta$$

$$(A.5)$$

where β is a parameter to be chosen such that the triaxial data is satisfied and

$$T = \frac{|\tau_p - \tau_o|}{|\tau_o| + |\tau_{max}|} \qquad (A.6)$$

The function $\nu_v(J_1, \tau_{max})$ in Eq. A.5 is the virgin Poisson's ratio, defined by Eq. A.4. In Eqs. A.5 and A.6, τ_o is the value of the most recent relative-maximum principal-shear-stress. A sign is assigned to τ_o based on the criterion of whether or not the plane on which τ_p acts in a positive sense has rotated more than 45° from the plane on which τ_o acted in a positive sense. If τ_p and τ_o are opposite in sign, the unloading-Poisson's-ratio is prevented from exceeding the virgin Poisson's ratio which would exist for the same value of principal-shear-stress. This prevents the possibility of an element possessing a higher shear modulus in its second cycle of loading than it had in its first cycle under the same state of stress. Once the stress-dependent Poisson's ratio has been computed, the corresponding stress-dependent shear modulus is obtained by the following formula:

$$G = \frac{3K(1 - 2\nu)}{2(1 + \nu)} \qquad (A.7)$$

where G is the shear modulus, K is the bulk modulus, and ν is Poisson's ratio.

The parameters chosen for the representation of the sand used in the special tests are listed in Table A-1.

$$K_1 = 50,000 \text{ psi} \qquad \nu_{EL} = 0.34$$

$$K_2 = 0.98 \qquad \nu_{PL} = 0.48$$

$$K_3 = 0.019 \qquad \alpha = 10$$

$$\beta = 0.5$$

A-1 COMPARISON WITH CYCLIC TRIAXIAL TEST DATA

Two series of cyclic triaxial tests were carried out using the sand from the special tests. The triaxial tests consisted of cyclic loading and unloading at various strain levels with a constant confining pressure. A confining pressure of 6 psi was used in the first series of tests, while 18 psi was used in the second series. The finite element sand model was subjected to load histories intended to simulate these two test series. Comparisons of the finite element stress/strain paths with those of the triaxial tests are presented in Figs. A-1 and A-2.

Fig. A-1 shows the comparison between model behavior and triaxial data at a confining pressure of 6 psi. The model was subjected to a single load cycle corresponding to the loading of Test 1-B', followed by a portion of a load cycle corresponding to Test 1-C'. It should be noted from Fig. A-1a that for any value of stress, the slope of the stress/strain path for the first cycle of loading of the finite element model is approximately equal to the corresponding slope of the stress/strain path of Test 1-B', Cycle 2. This indicates that Young's modulus, as a function of stress, is modeled correctly at the stress level under consideration. In addition, the area contained in the hysteresis loop appears to be the same both for the model and the triaxial data.
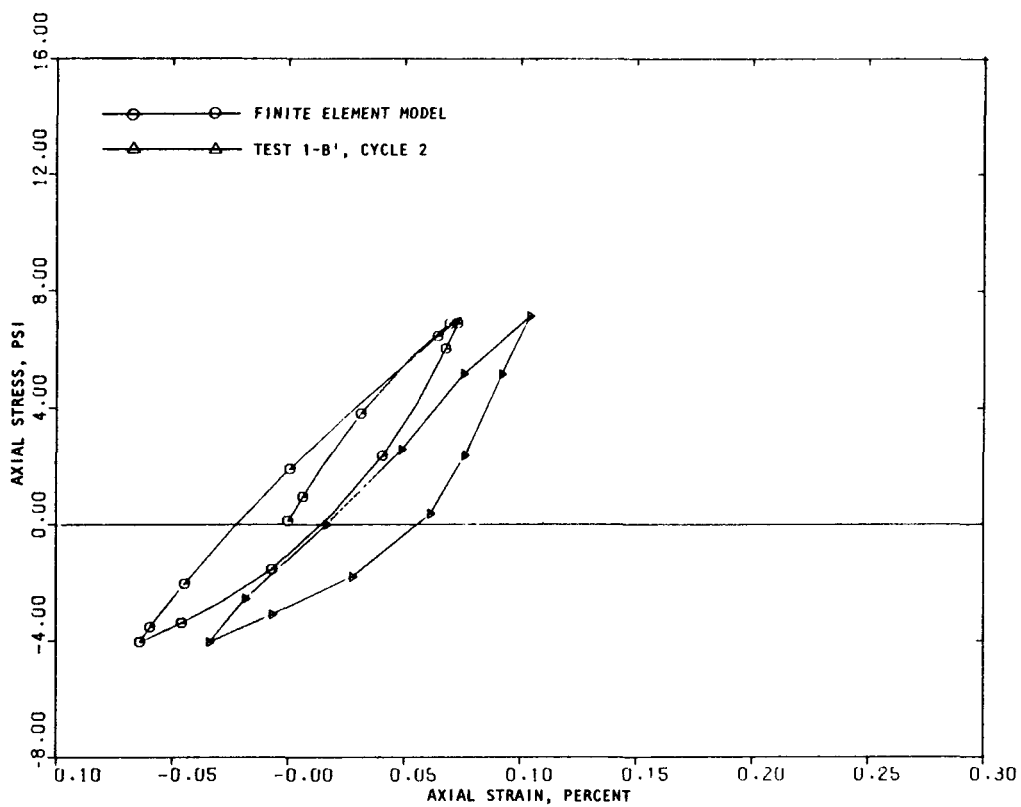
(a)   Comparison with Test 1-B'
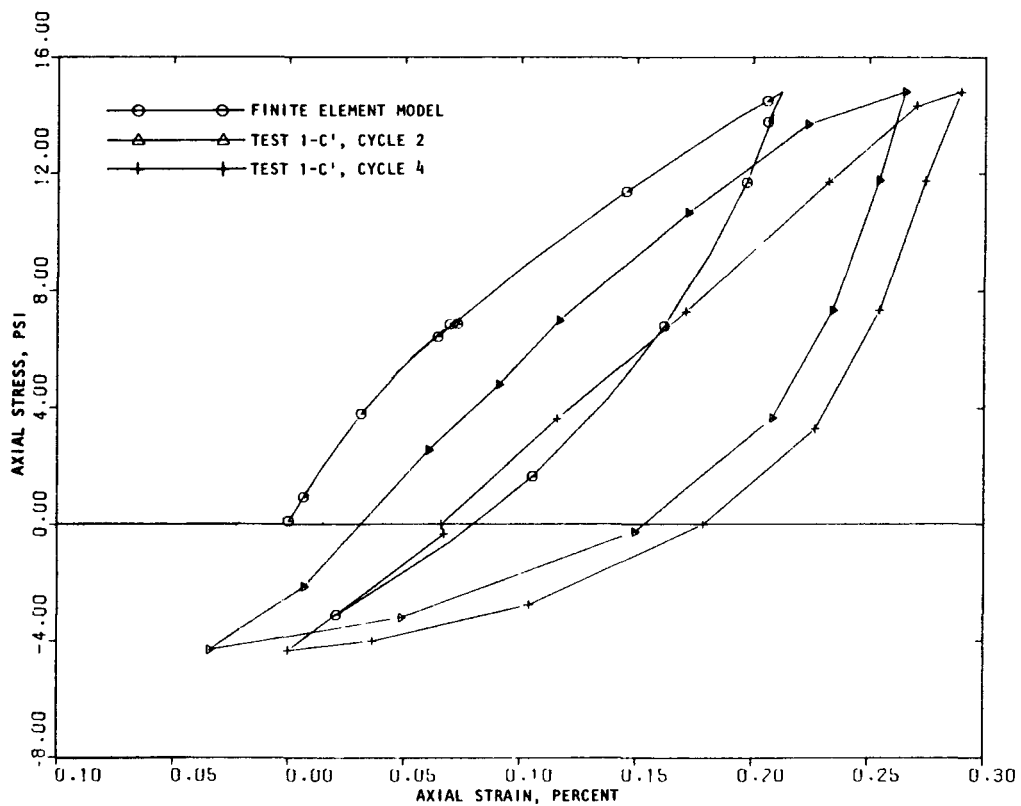
(b)   Comparison with Test 1-C'

FIGURE A-1.   COMPARISON OF FINITE ELEMENT MODEL WITH TRIAXIAL DATA
AT 6 PSI CONFINING PRESSURE

A-5
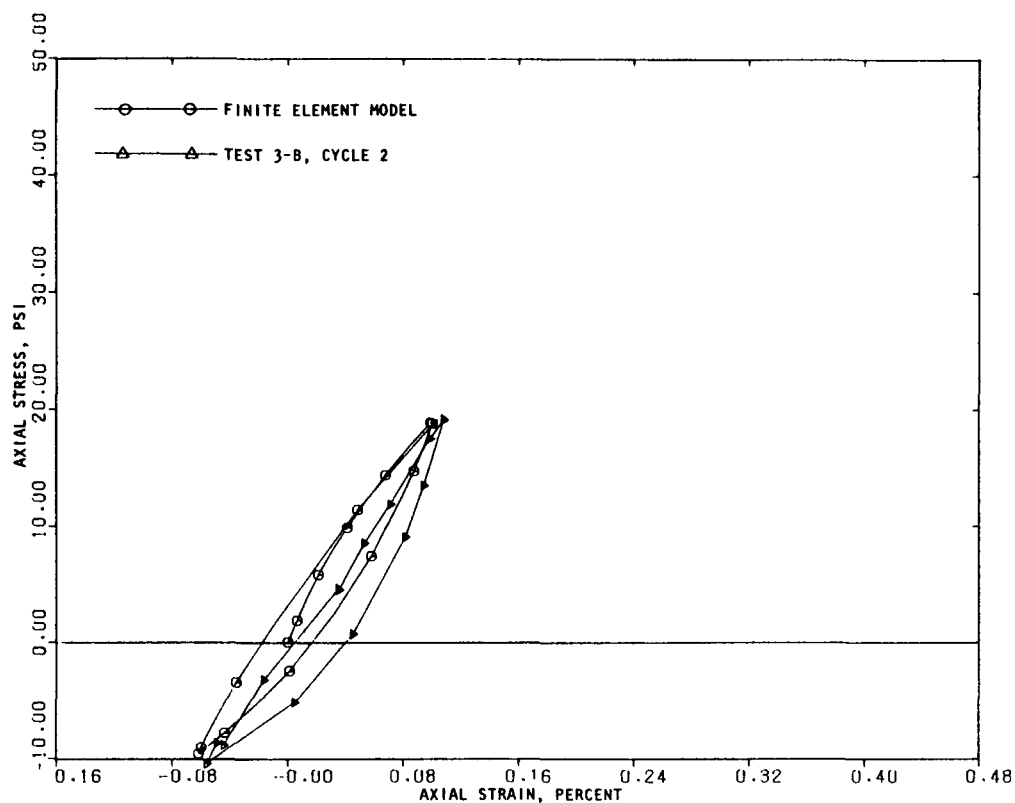
(a) Comparison with Test 3-B
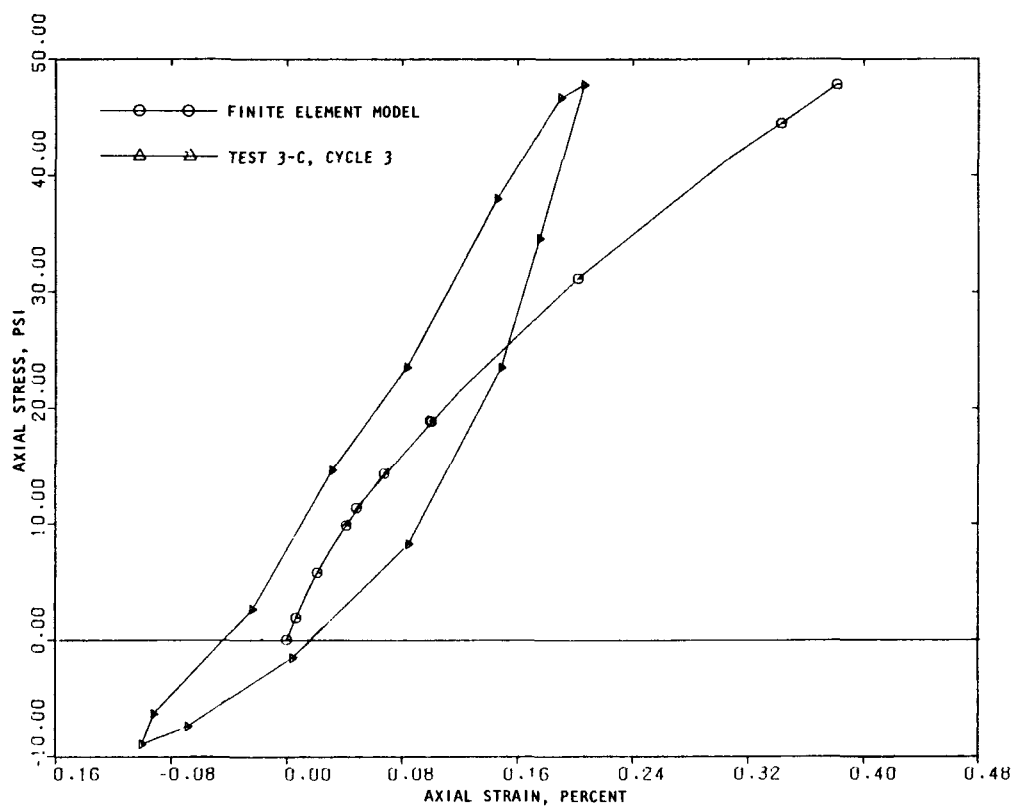
(b) Comparison with Test 3-C

FIGURE A-2.   COMPARISON OF FINITE ELEMENT MODEL WITH TRIAXIAL TEST DATA
AT 18 PSI CONFINING PRESSURE

A-6

The finite element model and the triaxial data are not in agreement as to the magnitude of the strain at any point in the load cycle. The triaxial data indicates that permanent compaction of the soil sample has taken place during the first load cycle. In the case of Test 1-B' (see Fig. A-1a) the test sample has compacted to the extent that the origin of the stress-strain coordinate system no longer lies within the hysteresis loop. The finite element model has not been designed to take this effect into account. However, the permanent compaction phenomenon appears to be related to the behavior of sand under the influence of normal stresses. It would appear that there should be no compaction at all due to the application or removal of shear stresses. In view of the fact that the sand model is used in a configuration which approaches loading in pure shear, the omission of this effect from the sand model appears justified. Furthermore, the values of shear modulus obtained from the finite element sand model are in reasonably good agreement with the state-of-the-art curve obtained from SW-AJA, 1972. This fact adds greater support for the hypothesis that permanent compaction under normal states of stress need not be considered in the finite element model.

In Fig. A-1b, the behavior of the finite element model is compared with Test 1-C'. As is the case in Fig. A-1a, the slope of the stress/strain path appears to be in good agreement among the three curves shown. The area contained in the hysteresis loop of the sand model appears to be slightly low, but comparison of Cycles 2 and 4 of Test 1-C' shows that the area of the loop is not consistent even between different cycles of the same test. Again the tendency for permanent compaction is evident in the triaxial data, and continues to take place to a considerable extent even between Cycles 2 and 4.

Fig. A-2 shows the comparison between model behavior and
triaxial data under a confining pressure of 18 psi. In that
the finite element calculation has been run at a confining pressure
of 6 psi, this comparison is of less interest than that of
Fig. A-1. Nevertheless, excellent agreement between the model
and Test 3-B is evident in Fig. A-2a. While Fig. A-2b shows
the finite element model to be too soft at a stress level of
50 psi, it should be kept in mind that this stress level is
much greater than any encountered in the finite element calcu-
lation.

A-2 BEHAVIOR OF MODEL UNDER CYCLIC SHEAR LOADING

The finite element sand model was subjected to cyclic
loading in pure shear at several strain levels. Throughout
these tests, the confining pressure was taken to be 6 psi.
The results of these tests are shown in Fig. A-3. Experimental
data does not accompany these curves in that the triaxial tests
did not measure the shear strain directly.

Note, particularly from Figs. A-3d and A-3e that for large
shear strains, the second cycle of loading reaches a higher
stress value than the first. It does so, however, while never
allowing the second cycle to possess a tangent shear modulus
which exceeds that of the first cycle at the same stress level.
Thus the phenomenon shown in these figures is not work hardening.
The higher stress obtained in the second cycle is due to the
large amount of plastic flow which takes place during the un-
loading phase of the first cycle. Reloading during the second
cycle, therefore, takes place over a much larger strain interval
than in the original loading of the first cycle. This allows
a higher stress to be attained, even though the modulus does
not exceed that of the first cycle.
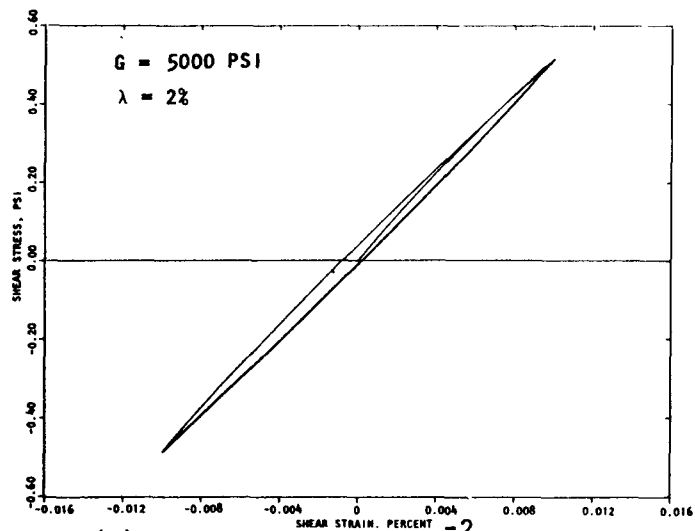
(a) Strain level = 10^{-2} percent
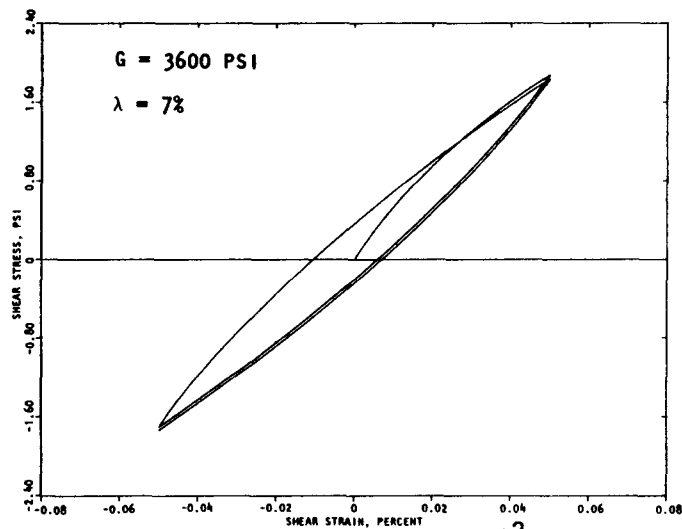
(b) Strain level = 5.0×10^{-2} percent
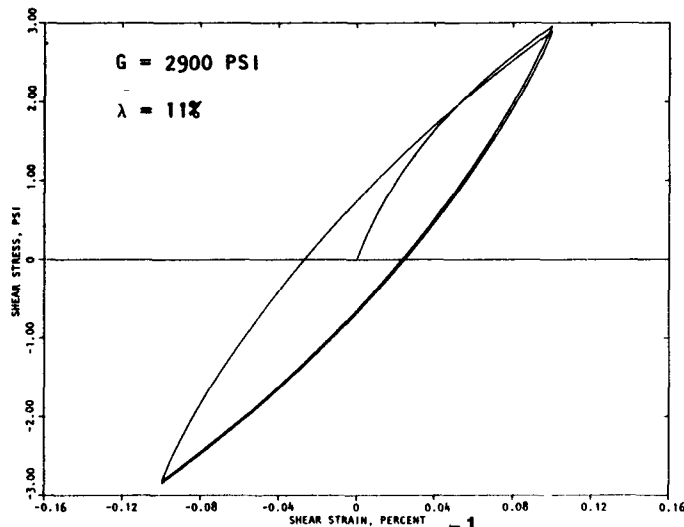
(c) Strain level = 10^{-1} percent

FIGURE A-3. CYCLIC SHEAR BEHAVIOR AT 6 PSI CONFINING PRESSURE

A-9
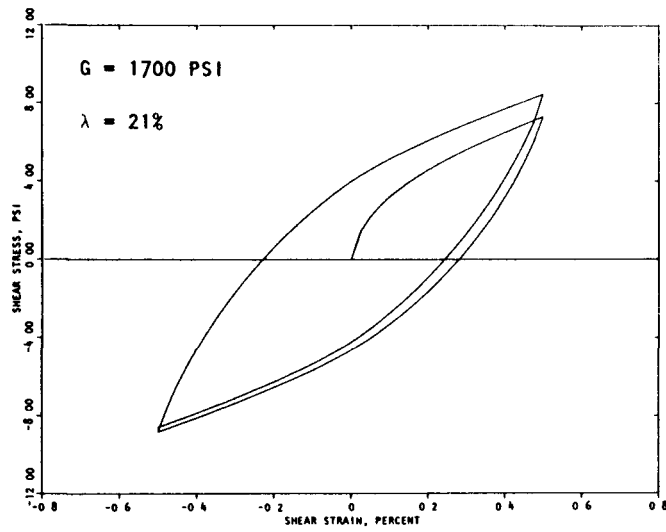
(d)   Strain level = 5.0×10^{-1} percent
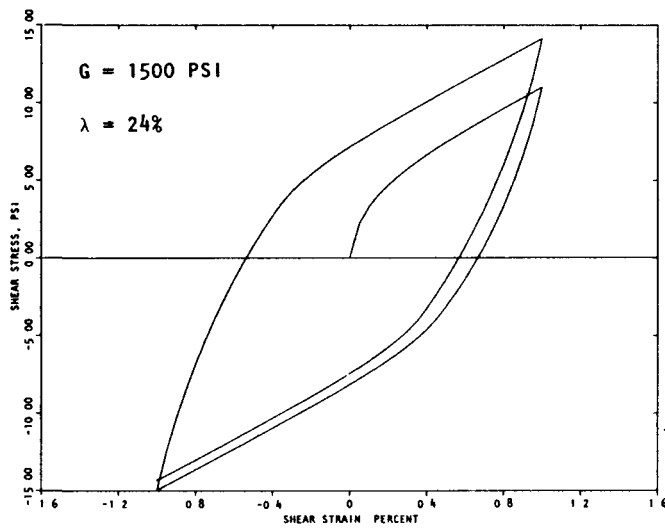
(e)   Strain level = 1 percent

FIGURE A-3. CYCLIC SHEAR BEHAVIOR AT 6 PSI CONFINING PRESSURE (CONTINUED)

A secant shear modulus, G, and a damping ratio, λ, have been measured for each of the stress/strain loops of Fig. A-3 according to the method outlined in Fig. A-4. These values are plotted in Fig. A-5 together with the state-of-the-art curves of SW-AA, 1972, and the interpretation of the triaxial data based on an assumed value of 0.3 for Poisson's ratio. The shear modulus comparison is presented in Fig. A-5a, and the damping ratios are compared in Fig. A-5b. The fact that the results using the finite element sand model, in most cases, fall within a range defined by the state-of-the-art curve and the constant Poisson's ratio interpretation of the triaxial data indicates that the values generated by the model are realistic at a confining pressure of 6 psi.

REFERENCES

SW-AJA (1972)
    "Soil Behavior Under Earthquake Loading Conditions: State of the Art, Evaluation of Soil Characteristics for Seismic Response Analyses," A Joint Venture of Shannon & Wilson, Inc., and Agbabian-Jacobsen Associates, Jan.

DEFINITIONS

SHEAR MODULUS, $G = \dfrac{G_2}{1}$

DAMPING RATIO, $\lambda = \dfrac{A_L}{4\pi A_T}$

A_L = AREA OF LOOP

A_T = AREA OF TRIANGLE

SHEAR STRESS

G_1

G_2

LOCUS OF TIPS OF
HYSTERESIS LOOPS

SHEAR STRAIN λ

SHEAR STRAIN
AMPLITUDE

NOTE:

DEFINITION OF MODULUS, DAMPING
AND STRAIN AMPLITUDE NOTED ON
FIGURE APPLIES TO LARGER
HYSTERESIS LOOP ONLY.
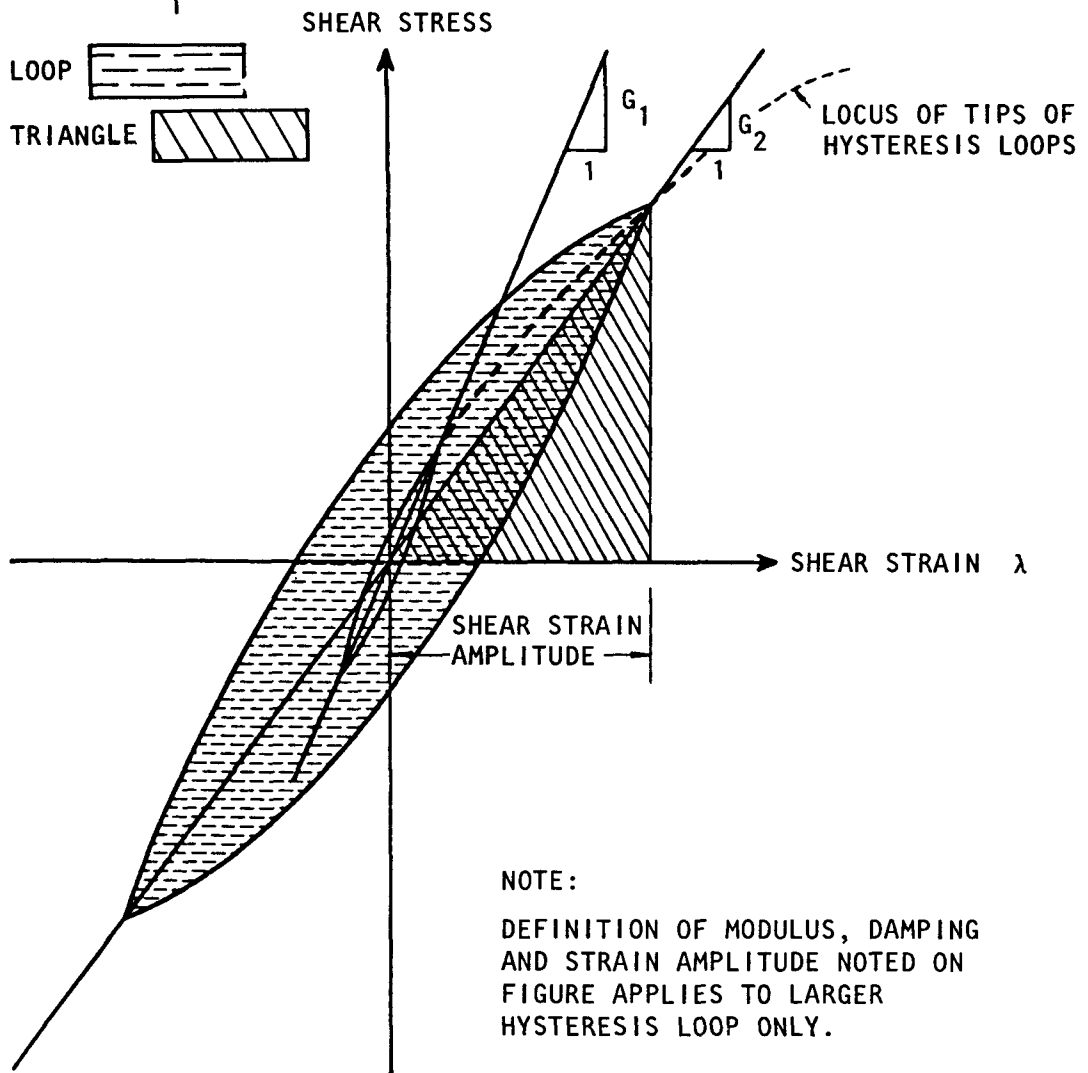
FIGURE A-4. HYSTERETIC STRESS-STRAIN RELATIONSHIPS AT DIFFERENT STRAIN AMPLITUDES
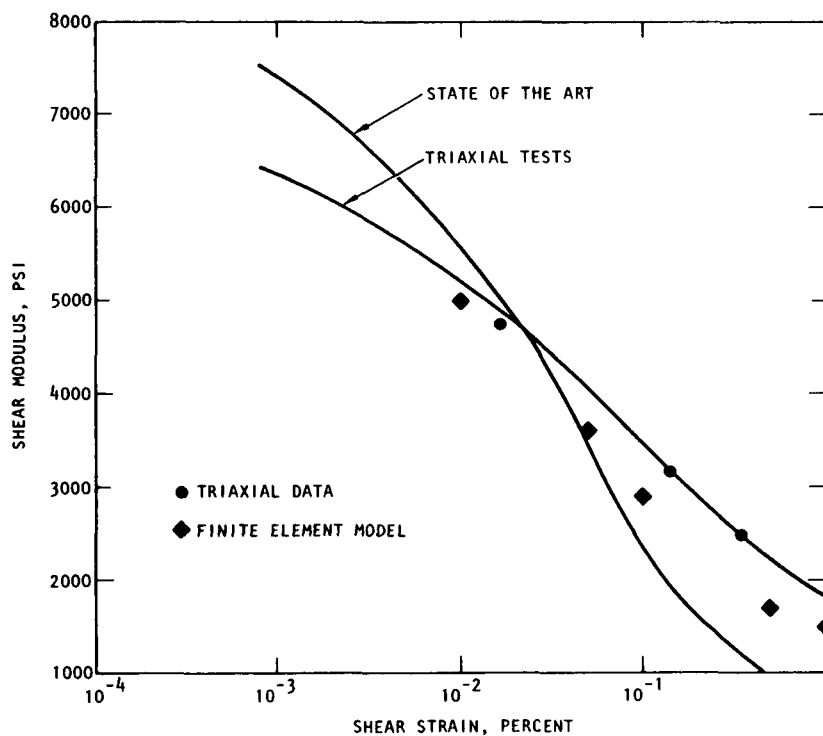
(a)   Shear modulus
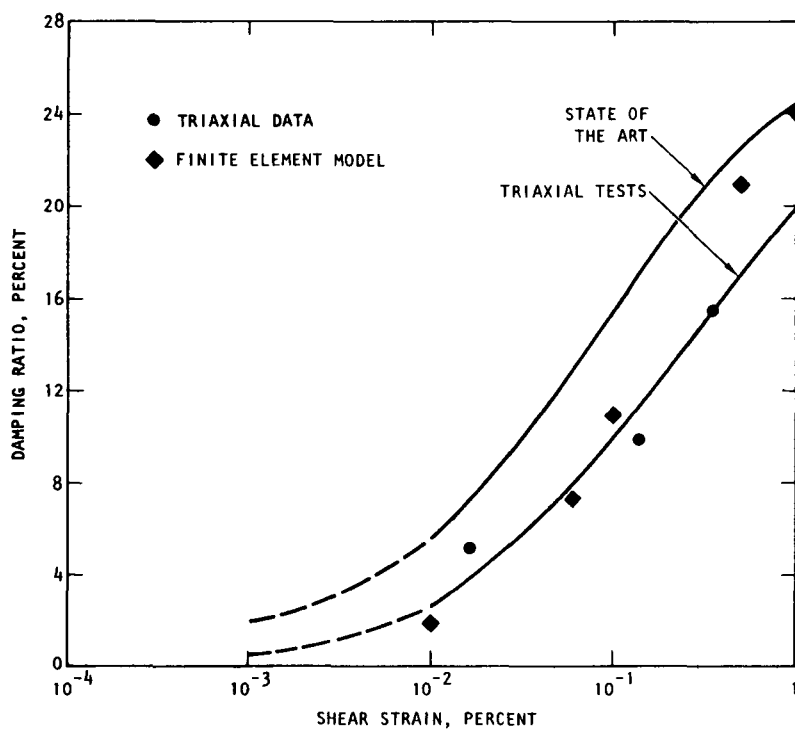
(b)   Damping ratio

FIGURE A-5.   COMPARISON OF FINITE ELEMENT SAND MODEL WITH TEST DATA AND
STATE-OF-THE-ART DATA FOR 6 PSI CONFINING PRESSURE

APPENDIX B

PNEUMATIC ANCHOR RESULTS

APPENDIX B

PNEUMATIC ANCHOR RESULTS

As pointed out in Chapter 5, primary waves are dominate
in the close range zone. These strong waves may be caused by
unavoidable imperfections in the design of the complex hydraulic
anchor assembly. The central hydraulic ram is of high mass and
when excited is thought to (by its inertia) produce a large
primary wave. To investigate this cause, a smaller diameter
prototype light-weight central mass anchor designed for use at
greater test depths was tested as a part of this program.

The new anchor shown in Chapter 2 was made up of three
rigid smooth cylindrical plates, cut from a 4-inch O.D., .636-inch
thick steel pipe, which were pressed against the soil mass by
an air inflated high pressure, reinforced pneumatic rubber packer.
The prototype used in these tests was placed in the hole left
by the hydraulic anchor after completion of this initial test
phase. Fill was placed around the anchor to fill in the extra
void space. Because the new anchor was smaller in diameter, about
4 to 5 inches in the fully retracted position, the spacing from
the wall to each recording station was slightly lengthened. The
vertical length of the anchor in contact with the soil was the
same, 4 feet, the lateral surface was smaller by approximately
50 percent, and the total weight was smaller by 30 percent.

The following paragraphs present the results of a series of
tests performed with this pneumatic anchor.

B-1 CHARACTERISTICS OF THE PULSE

The velocity-time histories obtained in six successive tests,
with the pneumatic anchor, showed that the general shape and
amplitude characteristics of the pulses follow the same trends
of those observed with the hydraulic anchor.

Comparisons of the ratios of main to primary components of
particle velocities and duration times in general verify that
the relative importance of the primary pulse is indeed smaller
for the pneumatic anchor than the hydraulic system. In fact,
the primary particle velocity amplitude is practically negligible
beyond Sensor No. 5 at a radial distance of 20 inches from the
center of the anchor. For a typical case of a 58 pound hammer
falling six inches, the primary particle velocity (P-wave)
decreases from 2.64 (in/sec) at station 1 to .01 (in/sec) in
station 13, while the main particle velocity (S-wave) decreases
from 3.38 (in/sec) in station 1 to .13 (in/sec) in station 17.
The ratio of the main to the primary particle velocities increases
from 1.28 at station 1 to 25 in station 5, while the ratio of the
corresponding duration times increases from 1.24 at station 1
to 8.23 at station 7. The time lag between primary and main
pulses increases from .97 (msec) at station 1 to 5.7 (msec) at
station 11.

This indicates that the hydraulic anchor system, while pro-
ducing a controlled wave rich in shear characteristics, is also
generating P-waves. The smaller anchor, tested because it
possibly represented a more ideal pure vertical shear impact in
general, demonstrated just that. Two major differences in the
two systems which probably account for this difference are 1) the
light central mass and 2) uniform vertical loading on the top
of the plates. The smaller weight of the internal packer units
is negligible when compared with the weight of the surrounding
plates. Because the energy is applied to the plates directly
internal movements and resisting inertia forces of the central
packer are likely to be small, minimizing the possibility of
transferring these internal forces laterally to the surrounding
soil as P-waves.

Since the diameter of the pneumatic anchor is smaller than
the hydraulic anchor, the striker plate is likewise smaller and
thus the possibility of achieving large eccentric loading con-
ditions is reduced. An eccentric loading on a plate segment can
produce bending and in effect induce lateral compression force
into the surrounding soil. This compressional stress wave will
occur as P-waves. As a result of this study, wedges were intro-
duced on top of each plate segment on both anchor assemblies
directly beneath the striker plate. The wedges produced point
loads between the striking plate and the centroid of each plate
segment. Subsequent production testing has demonstrated that the
P-waves were minimized significantly by this more uniform loading
condition.

B-2 WAVE VELOCITY COMPUTATIONS

The shear wave velocities were computed for the same series
of tests above by different methods, including both the waveforms
and various time history methods. The waveforms were computed
from the displacement pulses at time intervals of .1 msec. The
complete set of waveforms for these tests is plotted in Fig. B-1.
From these curves, plus additional intermediate ones, a new set
was formed to include only those waveforms whose crests were
located just at a given station. This set is shown on Fig. B-2.
The corresponding velocities are tabulated in Table B-1 along
with those velocities determined by the other various time
history methods.

The nomenclature for the wave velocities in this figure
are as follows:

V_1 = wave velocity for peak $\dot{w}_1$, t_1

V'' = same for second crossing t''
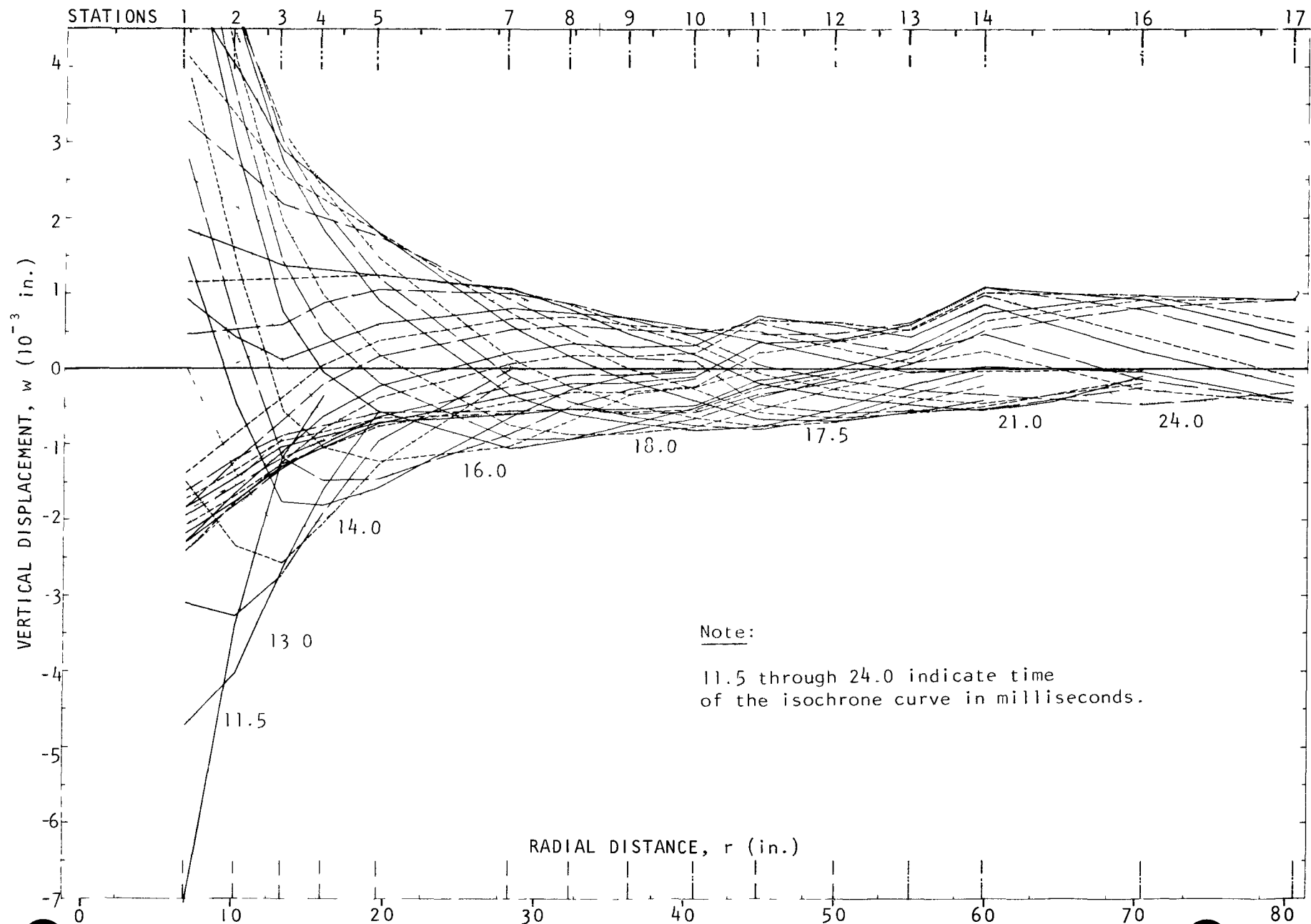
FIGURE B-1   WAVEFORMS FROM PNEUMATIC ANCHOR. TESTS 13.7 TO 13.12

B-4

Note:

11.5 through 24.0 indicate time
of the isochrone curve in milliseconds.

STATIONS

FIGURE B-2   WAVEFORMS FOR PNEUMATIC ANCHOR.   TESTS 13.7 TO 13.12, W = 58 lb x .5 ft, σ_j = 140 psi
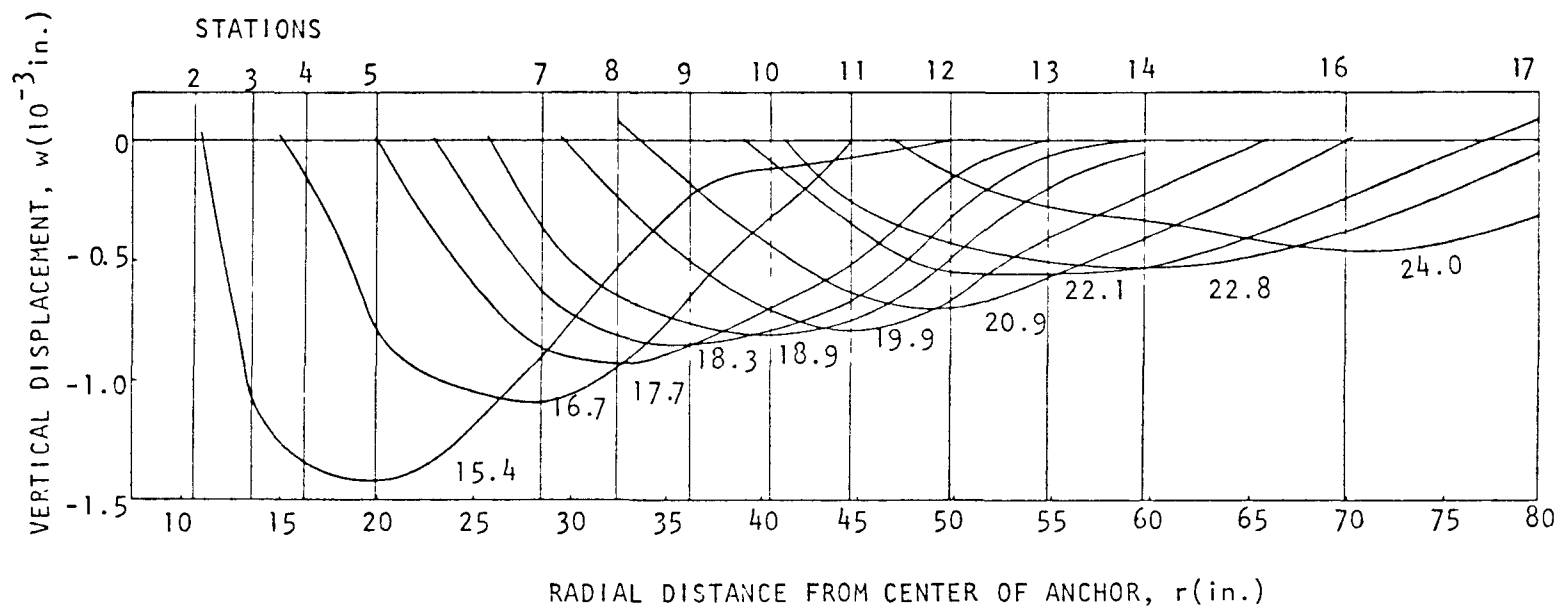
Notes:

1.   15.4 through 24.0 indicate time of the isochrone curve in milliseconds.

2.   Waveforms selected for crest just passing through a receiving station.

Table B-1

Wave Velocity Computed from Different Methods
Pneumatic Anchor
Tests 13.7-13.12, W = 58 x .5 lb/ft,
Wave Velocity (fps) and Average Wave Velocity (fps)

Station Number	Δr_t (ft)	V_1 (fps)		V'' (fps)		V_2 (fps)		V_c (fps)	
1-2	.266	329		324		302			
2-3	.25	431	380	281	302	510	406		
3-4	.218	303		307		234			
4-5	.302	254	280	340	324	408	321		
5-7	.715	533		441		(325)		550	
7-8	.328	746		444		(439)		328	
8-9	.322	596		430		460		537	
9-10	.354	466	587	485	450	506	432	590	501
10-11	.344	530		425		430		344	
11-12	.426	609		474		560		426	
12-13	.416	555	565	467	455	520	503	397	389
13-14	.406	(406)		384		(666)		581	
14-16	.864	540		546		579		720	
16-17	.825	(458)	468	594	508	546	598	(611)	637

V_2 = same for peak $\dot{w}_2$, t_2

V_c = velocity computed from the waveforms

The results show that for the precision of the measurements, including the spacing of the sensors, and the resolution of the time of peaks and crossings, all methods give velocity results that, when averaged for groups 3 to 4 respective sensors in the free field, are in reasonable agreement. The maximum difference in velocity between the various methods was 45 percent.

B-3 COMPARISON OF RESULTS FROM THE HYDRAULIC AND PNEUMATIC ANCHORS

The tests with the pneumatic anchor were not intended to provide a rigorous quantitative correlation between both anchors; therefore, the conclusions are limited to general characteristics of the results.

1.   The shear wave velocities given by both anchors in the free field are of the same order of magnitude and for both systems either method of computation of the wave velocity has been shown to give similar results with a general trend of increase of velocity with distance from the anchor.

2.   There is a considerable difference in the close range zone. The pneumatic anchor produces a purer shear input and thus generates a weaker primary wave, permitting reduction of the distance of the close range to approximately station 4, 16 inches from the center of the anchor.

These observations indicate that the nature or purity of the waves is dependent on the physical characteristics of the generating source. In the free field, however, where the main pulses are clearly defined, the properties of the soils are similarly well measured using either anchor system.

APPENDIX C

SOIL PROPERTIES

APPENDIX C

SOIL PROPERTIES

The sand encountered at the Ft. Lawton site and used as fill material is the Esperance sand member of the Vashon Drift, a comformable late Pleistocene sequence of interglacial and glacial sediments (Mullineaux et al, 1965). This sand member appears to be chiefly a preglacial fluval and lacustrine deposit, that was laid down about 15,000 years ago after the lake was mostly filled with deeper lying silts and clays. Following its deposition, ice overrode the locality, compacting this sand under the weight of the heavy overlying glaciers. This compaction accounts for the high density characteristics apparent in this sand member.

C-1 INDEX PROPERTIES

Two samples taken from depths of 3 to 4.5 feet and from 8 to 9.5 feet classify as brown, silty, fine to medium SAND and gray brown, silty fine to medium SAND, trace of fine gravel. Both samples have 16% silt and for both the 50% effective diameter is 0.26mm. Both samples are very similar, except for an additional 10% content of fine gravel, which is found in the deeper sample. Because gravel was removed during the construction of the fill, the shallower sample is more representative of the materials tested by the impulse test. The grain size distribution for this sample is shown in Fig. C-1. Its natural water content is 11.8% and the specific gravity was measured at 2.59. The shape of the particles is subangular.

C-2 MECHANICAL PROPERTIES

The maximum dry unit weight of this sand fill determined by the Modified Proctor compaction test (ASTM D-1557-58T), gave an average value of 115 pcf. The minimum dry unit weight

FIGURE C-1 GRAIN SIZE DISTRIBUTION. SOIL FOR ARTIFICIAL FILL TESTS.
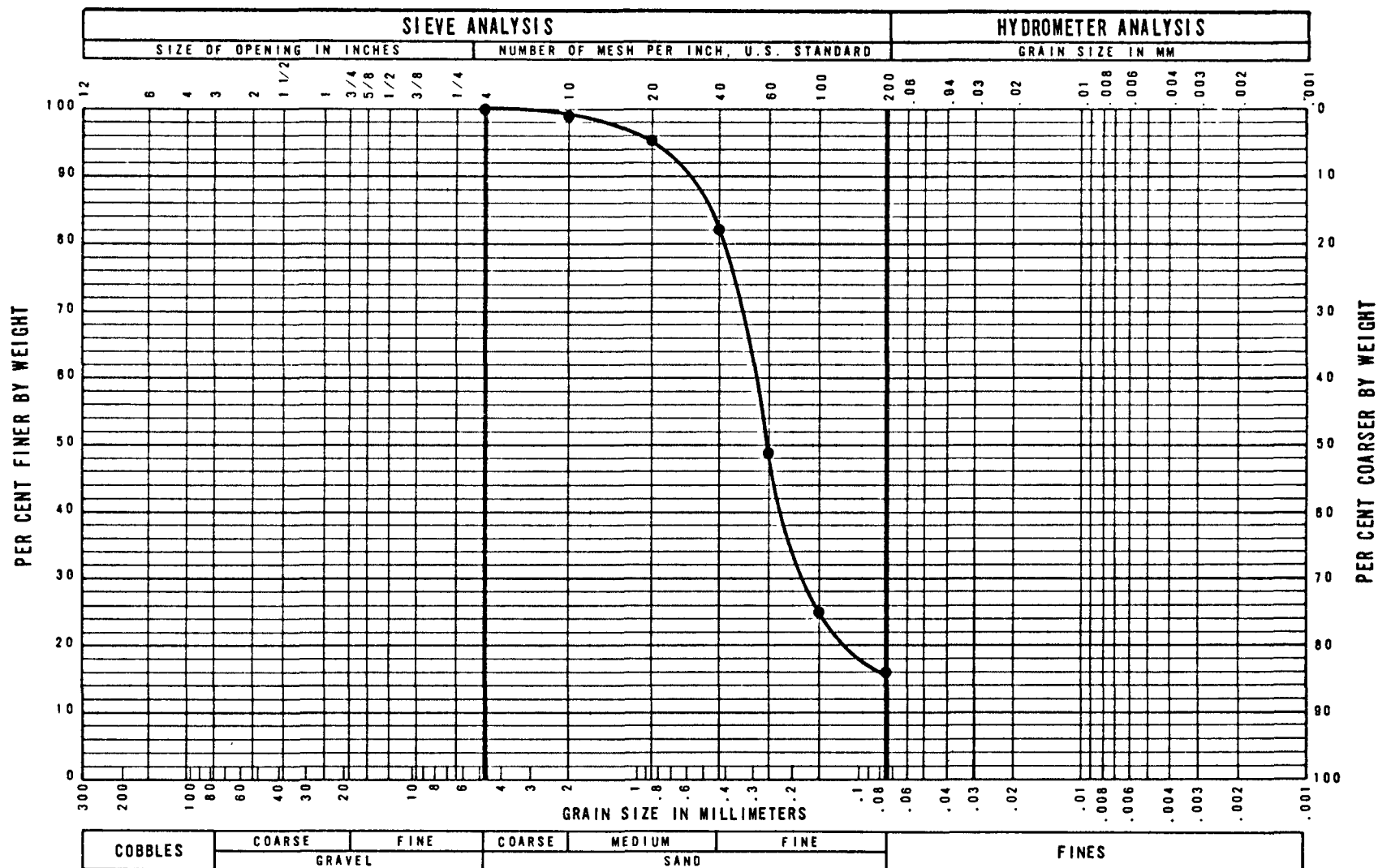
(ASTM D-2049-69) was 85.5 pcf. The average dry unit weight of
the soil as compacted in the artificial fill was 99.3 pcf.
This corresponds to 86% of the maximum Modified Proctor unit
weight. The maximum dry unit weight obtained by vibrations in
the laboratory (ASTM D-2049-69) was 107.8 pcf.

The shear strength of the dry soil, compacted to 106.3
pcf, or 92% of maximum Modified Proctor unit weight, was measured
in a slow triaxial compression test, performed at an average
rate of strain of .03% per minute. The angle of internal
friction for the range of confining pressures corresponding
to an element at the mid-plane of the fill, and close to the
anchor (confining pressures equal to .25 to .5 tsf) was 40
degrees, as shown in Fig. C-2.

The axial stress-strain curves for these triaxial tests
give the following initial tangent modulus:

Table C-1

Initial Tangent Modulus from Triaxial Compression Tests

Test No.	σ_3 (psf)	E (psf)	$(10^{-1}$ %)
101	860	705,600- 849,600	1.9-1.3
102	2,140	864,000-1,296,000	2.5- .9
103	4,300	1,569,600-2,332,800	3.0-1.0

C-3 DYNAMIC PROPERTIES

The dynamic properties of the compacted soils have been
measured in the laboratory by means of cyclic triaxial and
resonant column tests. The equipment for the cyclic triaxial
tests is shown in Fig. C-3. The testing cell is made of stain-
less steel with a special stainless steel top cover equipped
with a double-acting bellofram air cylinder connected to the

Deviator Stress, tsf

Axial Strain, %

STRESS vs. STRAIN
X = TOTAL DEVIATOR STRESS

S-101 S-102 S-103

Shear Stress, tsf

MOHR STRENGTH ENVELOPE
TOTAL STRESSES
$(\sigma_1-\sigma_3)$ MAX. FAILURE CRITERIA

45° 40°

S-103

S-102

S-101

Principal Stress, tsf
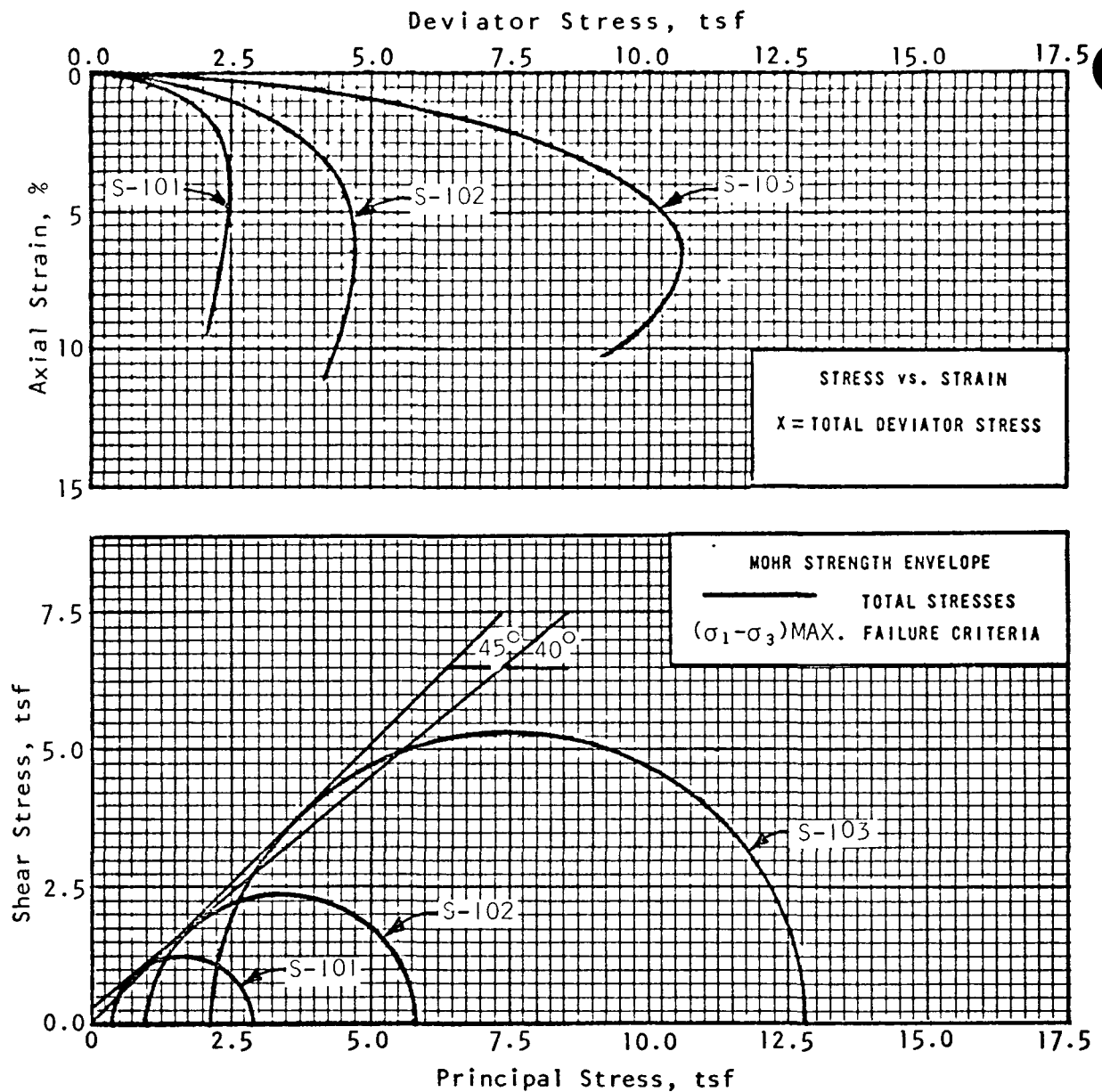
Test No.	101	102	103
Eff. Confining Pressure, tsf	.43	1.07	2.15
Ht., in.	6.36	6.36	6.40
Dia., in.	3.00	3.00	3.00
Dry Unit Wt.,pcf	106.2	106.2	106.6
Water Content, %* Before Test After Test			
Avg. % Strain/Min.	.037	.028	.024

Specimens Compacted
Strain Controlled Test
Classification:
    Gray, silty SAND

* Tests performed on oven-
  dried soil

FIGURE C-2   TRIAXIAL COMPRESSION TEST DRY, COMPACTED, SILTY SAND
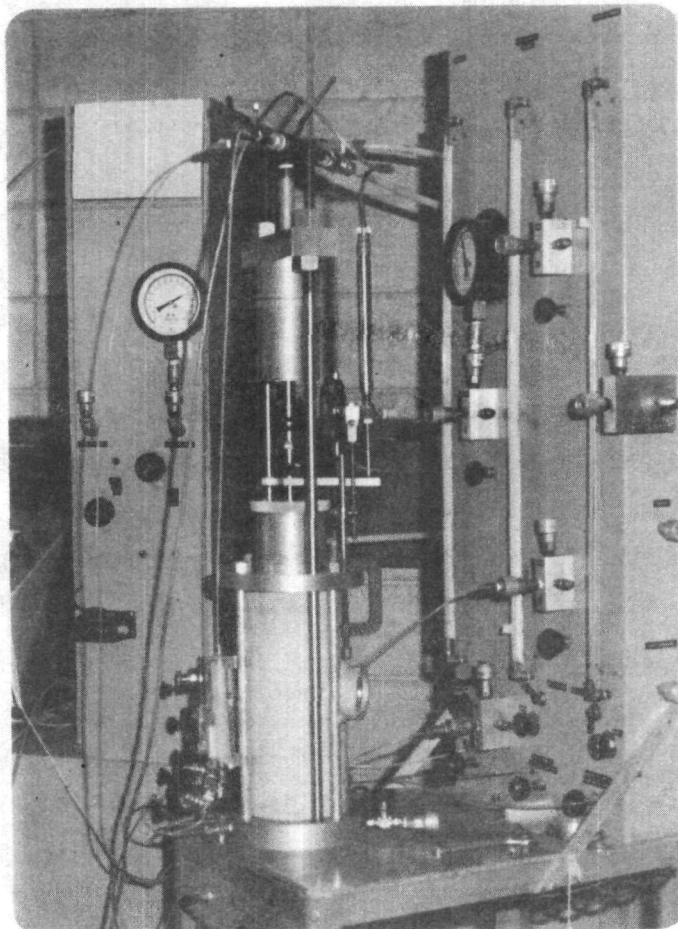
FIGURE C-3   LABORATORY EQUIPMENT FOR CYCLIC TRIAXIAL TEST

loading piston. The piston is fixed to the cap of the specimen
to permit the application of upward and downward axial forces
to the specimen.

The specimens are cyclically loaded as shown schematically
in Fig. C-4. The reversal of shear stresses is obtained by main-
taining the confining stress constant while adding and subtracting
an axial increment of stress σ_d. In this manner, the stress
conditions on a 45-degree plane are a normal stress $\sigma = \sigma_3 =$
constant and a shear stress, which cyclically reverses between
$\tau = + \frac{\sigma_d}{2}$ and $- \frac{\sigma_d}{2}$. The normal stress is always kept positive.
The reversal of shear stress is accomplished
by means of an air operated single solenoid valve which causes
the pressure acting on the bellofram to cycle between the equi-
valent maximum and minimum stress conditions. The result is an
approximately sinusoidal stress-time history applied to the speci-
men under a maximum stress σ_d at a frequency of 1 cycle per
second.

The axial strains are measured with a linear variable
differential transducer (LVDT) and the loads by a load cell
mounted on top of the specimen. In addition, a pressure trans-
ducer is connected to the pressure supply line of the double
acting bellofram to determine the magnitude of the pressure
supplied. This extra measurement provides a check of the
measurements of the load cell. The records of these measurements
are registered simultaneously on two Sanborn 321 dual channel
carrier amplifier-recorders.

The moduli and damping coefficients measured by the cyclic
triaxial tests, for the confining pressure of 6 psi, have been
summarized in the following table.

STAGES

a) CONSOLIDATION **b) COMPRESSION AND SHEAR** **c) TENSION AND SHEAR**

DESIRED CONDITION
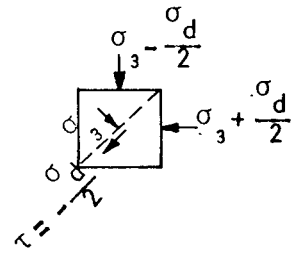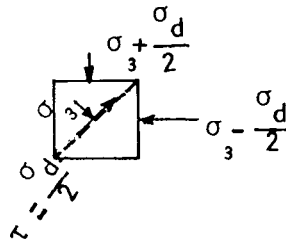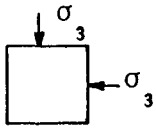
MOHR DIAGRAM
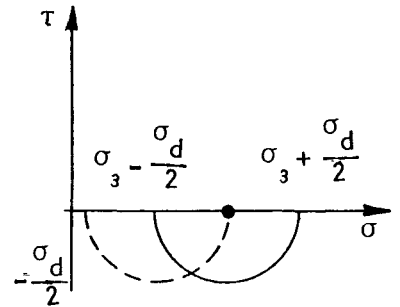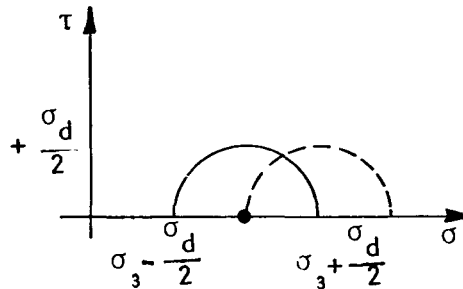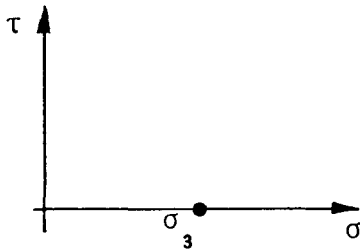
EQUIVALENT STRESS CONDITION
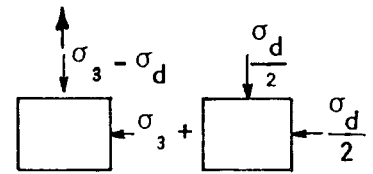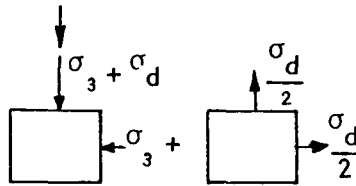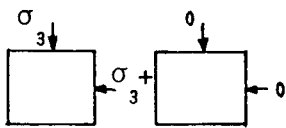
APPLIED STRESS IN TRIAXIAL TEST
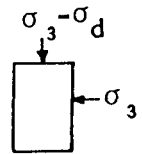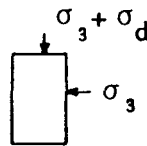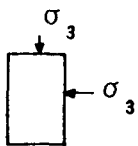
FIGURE C-4 CYCLIC TRIAXIAL TEST - $\overline{R}_{cy}$ — LOADING CONDITIONS

Table C-2

Cyclic Triaxial Test Results:
Shear Modulus and Damping Versus Strain

Laboratory Results for $\bar{\sigma}_3 = 6$ psi			Computed Properties for $\nu = 0.3$, $\rho = 3.4$ lb. sec.^{2}/ft.^{4}		
Axial Strain ε (%)	Young's Modulus E (psi)	Damping λ (%)	Shear Strain (%)	Shear Modulus G (psi)	Shear Wave Velocity V_s (fps)
.012	12,400	5.2	.016	4,760	450
.106	8,300	9.9	.14	3,190	368
.267	6,500	15.5	.35	2,500	326
			*.001	6,350	520

* Extrapolated value.

The variation of shear wave velocity with shear strain for confining pressures of 6, 12, 18, 24 and 36 psi is shown in Fig. C-5.

The resonant column tests were performed in the Combined Longitudinal and Torsional Modulus Device shown in Fig. C-6. The device subjects a cylindrical soil specimen to a sinusoidal vibration in a longitudinal or torsional mode such that the frequency corresponding to a state of resonance can be determined. For the specimen vibrating, as a fixed bottom, free top column, in the quarter-wave mode, the velocity of shear wave propagation is given by:

$$V_s = 4f_t L \qquad (C.1)$$

where f_t is the resonant torsional frequency in cycles per second, L is the length of the specimen in feet and V_s is the shear velocity in feet/second.

FIGURE C-5   SHEAR WAVE VELOCITY VERSUS SHEAR STRAIN
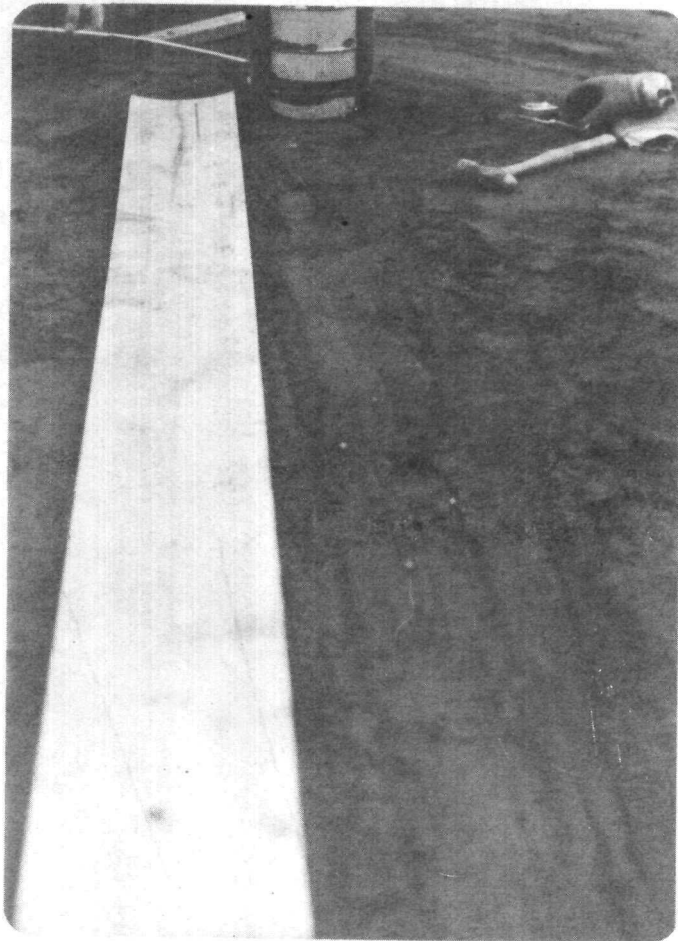
FIGURE C-6   RESONANT COLUMN

Resonant column tests were performed at confining pressures of 10, 20, 40 and 80 psi, in a dry sample of soil compacted to 108 pcf. The results are shown in Fig. C-7 and summarized as follows:

SHEAR MODULUS FROM RESONANT COLUMN TESTS

Confining Pressure $\overline{\sigma}_o$, psf	Shear Modulus G, psf	Shear Strain γ, %
1,440	1,238,400	9.5×10^{-4}
2,880	1,872,000	6.0×10^{-4}
5,760	2,448,000	4.1×10^{-4}
11,520	3,384,000	4.9×10^{-4}

The results of all the measurements of shear modulus determined in the laboratory may be conveniently summarized in a plot of shear wave velocity versus shear strain, normalized for effective confining pressure and density. Fig. C-8 shows this plot in the form of the parameter C versus γ, where γ is the shear strain, in percent, and C is the parameter from the equation:

$$V_s = C \; \overline{\sigma}_o^{-\frac{1}{4}} \; \rho^{-\frac{1}{2}} \qquad\qquad (C.2)$$

where: V_s is the shear wave velocity in (ft/sec)

$\overline{\sigma}_o$ is the effective confining pressure in (lb/ft^2)

ρ is the mass density in (lb.sec^2/ft^4)

and C is a parameter in (lb$^{\frac{1}{4}}$/ft$^{\frac{1}{2}}$)

100

Chamber Pressure, psi

F_T F_L G E

$\%\epsilon_T = 48.8 \times 10^{-5}$
$\%\epsilon_L = 36.2 \times 10^{-5}$

40

$\%\epsilon_T = 41.1 \times 10^{-5}$
$\%\epsilon_L = 40.4 \times 10^{-5}$

20

$\%\epsilon_T = 59.7 \times 10^{-5}$
$\%\epsilon_L = 20.8 \times 10^{-5}$

10

$\%\epsilon_T = 94.6 \times 10^{-5}$
$\%\epsilon_L = 37.1 \times 10^{-5}$

100   Frequency, cps   1000
                         10000   Modulus, psi   100000   1000000

Legend

F_T = Torsional Resonant Frequency, cps

F_L = Longitudinal Resonant Frequency, cps

G = Shear Modulus, psi

E = Modulus of Elasticity, psi

$\%\epsilon_T$ = Strain, Torsional Mode, percent

$\%\epsilon_L$ = Axial Strain, Longitudinal Mode, percent

Specimen Data

Height   6.40 in.
Diameter   3.10 in.
Dry Unit Weight   108.0 pcf
Test performed on oven-dried soil

Classification

Gray, silty SAND

FIGURE C-7   RESONANT COLUMN TEST DRY, COMPACTED, SILTY SAND
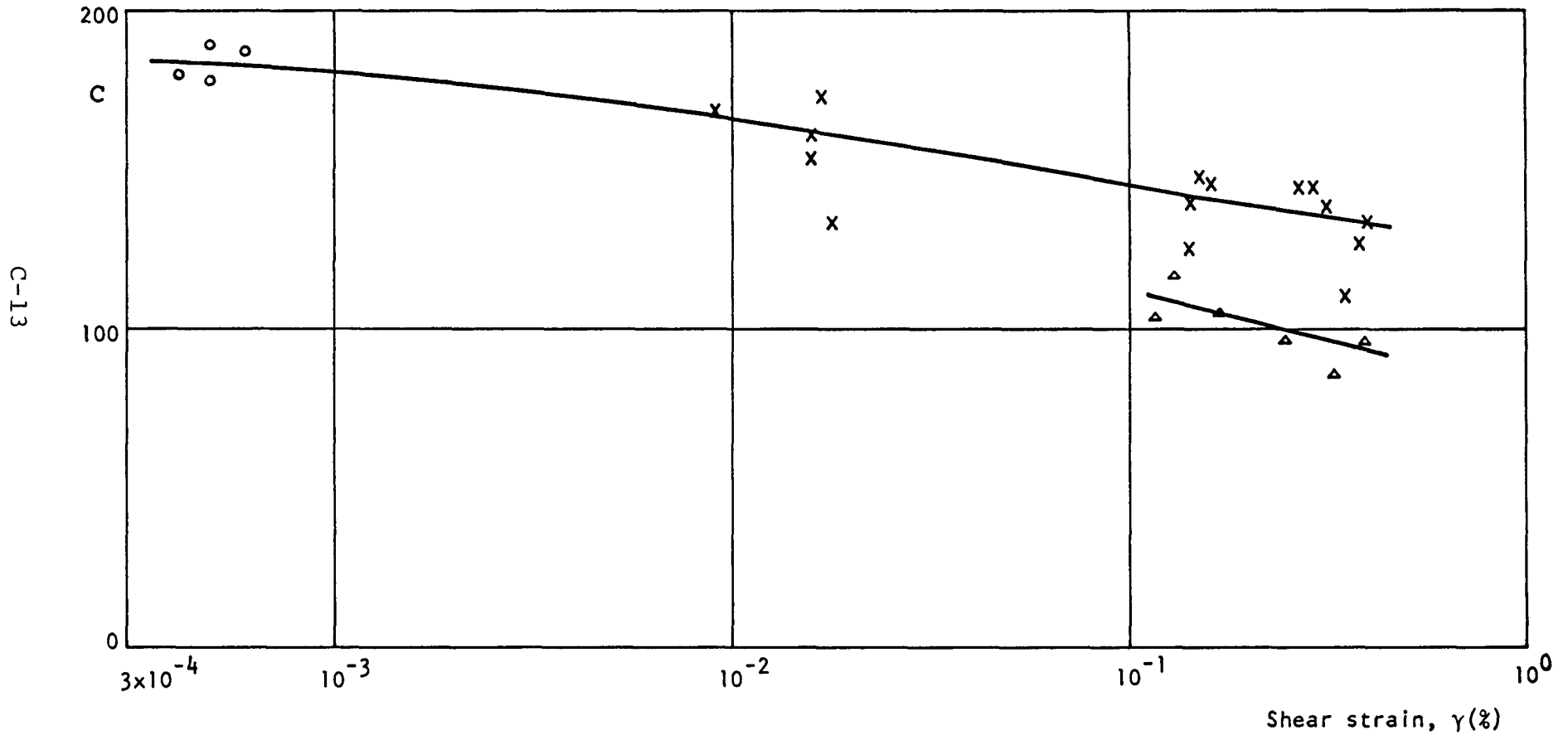
FIGURE C-8 SHEAR WAVE VELOCITY VERSUS STRAIN LABORATORY TESTS IN COMPACTED DENSE, SILTY SAND

It is observed that for the same confining pressure and density, the shear wave velocity decreases by 10 percent when the shear strain increases from 10^{-3} to 10^{-2} percent, and by 14 percent when the strain increases from 10^{-2} to 10^{-1} percent. It is also observed that the dynamic modulus is about 80 percent larger than the statically measured initial tangent modulus.

REFERENCES

Mullineaux, et al (1965)

    "Stratigraphy and Chronology of Late Interglacial and Early Vashon Glacial Time in the Seattle Area, Washington", Geological Survey Bulletin 1194-0.

APPENDIX D

FILL CONSTRUCTION AND EQUIPMENT INSTALLATION
AT FORT LAWTON

APPENDIX D

FILL CONSTRUCTION AND EQUIPMENT INSTALLATION
AT FORT LAWTON

A major part of the test program consisted of planning for and constructing an artificial fill to contain detailed instruments for performing the tests and making the evaluations presented in Chapter 5. This set up not only had to duplicate normal in situ test conditions, but preparation of the fill and installation of recording equipment had to be accomplished such that the body of material retained reasonable uniformity.

D-1 FILL CONSTRUCTION

The initial construction effort consisted of excavating with a rubber-tired tractor-mounted backhoe a large circular pit. The 10-foot deep pit was shaped like a truncated cone, 30 feet in diameter at the ground surface and 20 feet in diameter at the bottom. These overall dimensions were selected to avoid interferences of reflected waves from the boundaries.

During the excavation process removed soils were sorted into two general materials. Top soils and organic materials, as shown in Fig. D-1, were first stripped from the general test area. The remaining materials were removed and temporarily stockpiled as close as possible around the open excavation. This material was later used as backfill. The bottom of the pit was then leveled.

Backfilling operations were achieved in steps. Material was spread in six-inch or less loose lifts with shovels over the entire area of the bottom of the pit, and compacted using two walk-behind vibratory plates. The vibrators, shown in Fig. D-2, weighed 285 and 185 pounds and operated at 5500 rpm.
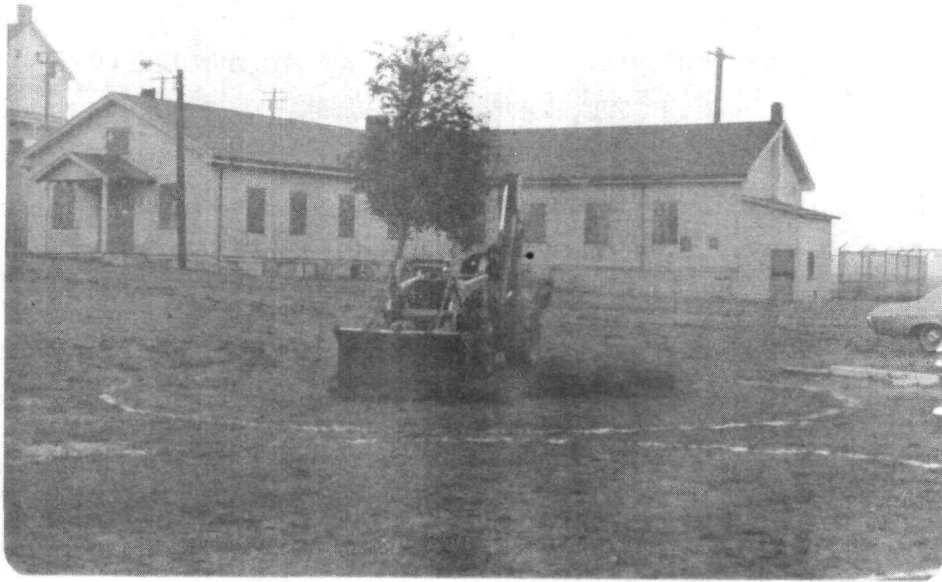
FIGURE D-1 INITIATION OF EXCAVATION

FIGURE D-2 COMPACTION

All gravel particles larger than 2 inches in diameter were removed by hand and eliminated from the test area. This operation was repeated for the entire depth of the fill.

Compaction was achieved by routing each vibrator in concentric and overlapping circles over the entire pit about three times. Compaction usually started at the outer boundary of the pit and proceeded to the center. The objective of the compacting effort was to obtain a reasonably homogeneous and uniform deposit of soil. A more uniform fill can usually be obtained if the materials are compacted in thin layers to a reasonably dense state.

At the most important depth zone (Elevation -5 feet) three in place density tests were performed in different parts of the pit to check the uniformity of the deposit. These tests produced densities of 90.4, 86.6 and 81.9 percent of the maximum Modified Proctor density. This corresponds to an average relative density of about 70 percent.

D-2 EQUIPMENT INSTALLATION

In conjunction with the backfilling operation, equipment was hand placed at predetermined points and eventually covered with subsequent soil layers. The general set up of the special tests in the artificial fill is shown in the Figs. 5-1 and D-3. The main plane of testing was defined at mid-depth of the fill (Elevation -5 feet).

The generating station, or anchor, was installed in the vertical axis of the pit. During backfilling, this heavy anchor was held in position and aligned vertically by suspending it from a portable tripod. To permit free vertical movement of the anchor and hammering equipment during testing, open cylindrical spaces, protected by one foot diameter corrugated
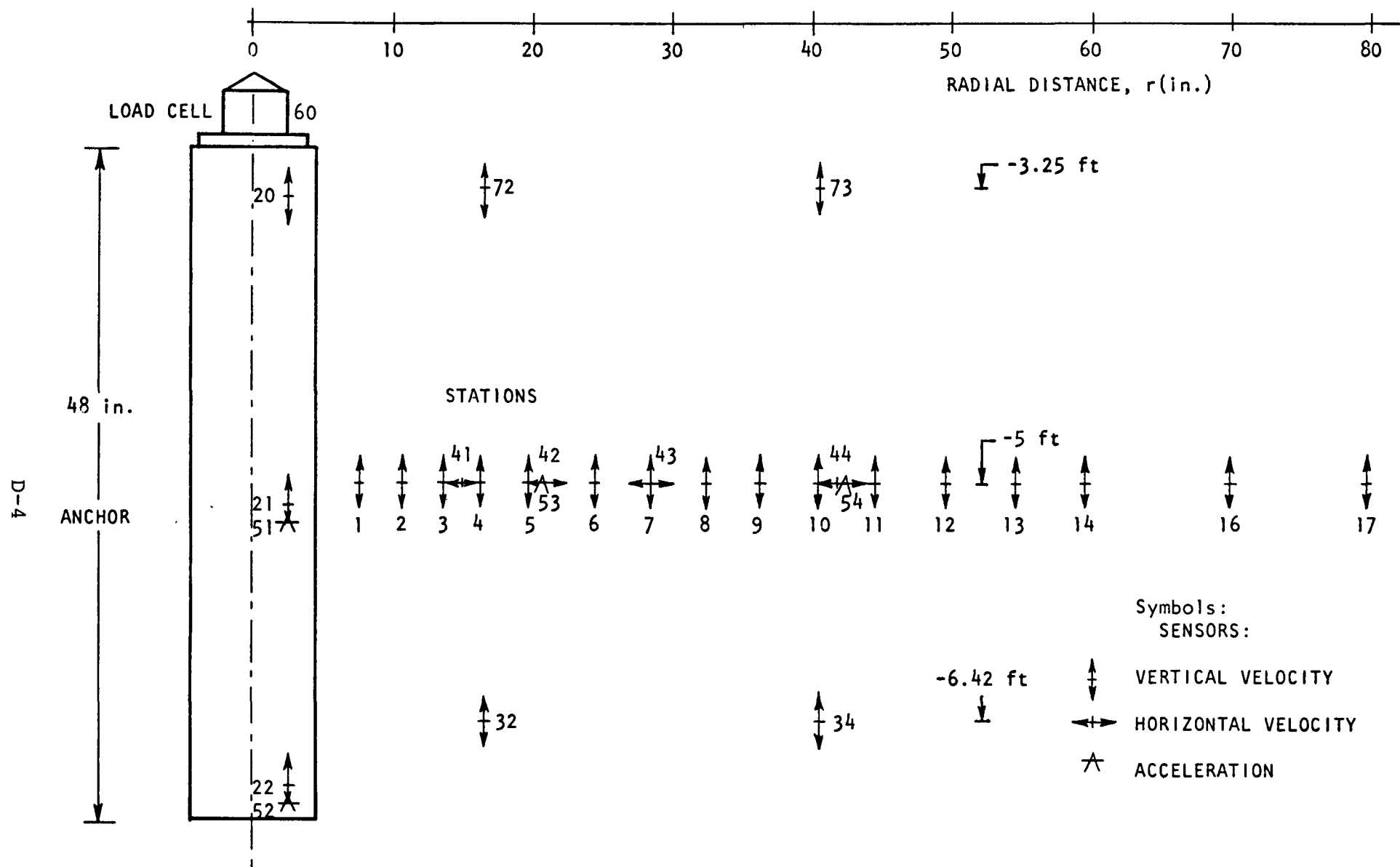
FIG. D-3   INSTRUMENTATION IN ARTIFICIAL FILL

casing were provided above and below the anchor (Fig. 5-1). This casing was placed to simulate the boundary conditions of the in situ test (i.e., open hole above and below the anchor).

The anchor was instrumented with:

a.   A 60 kip load cell, 4,000 hertz natural frequency, .0252 mV/lb sensitivity. As shown schematically in Fig. D-3, this load cell was installed on top of the anchor, between the Belleville spring and the striking plate.

b.   Three vertically oriented velocity transducers, type Mark Products L-10 AK, 30 hertz natural frequency, .63 V/in/sec sensitivity. These transducers were firmly fixed in cavities of one plate of the 48-inch anchor, 3.25, 25.25 and 45.5 inches from the top of the anchor.

c.   Two accelerometers, type Columbia 200-1, 4,000 hertz natural frequency, 40 mV/g sensitivity for 9 foot long cable. These sensors were attached to the same leg at distances of 26.5 and 46.75 inches from the top of the anchor.

Figs. D-4 and D-5 show the sensors mounted in the leg of the anchor.

The lower 3-foot long corrugated casing was aligned in position before starting the fill. The fill was then built up around it (Fig. D-6). When the fill reached elevation -7 feet, the anchor was suspended over the casing and aligned to permit free expansion of the anchor, as well as downward slippage, without transmitting direct forces to the casing during the tests. To avoid losses of ground around the anchor plates,
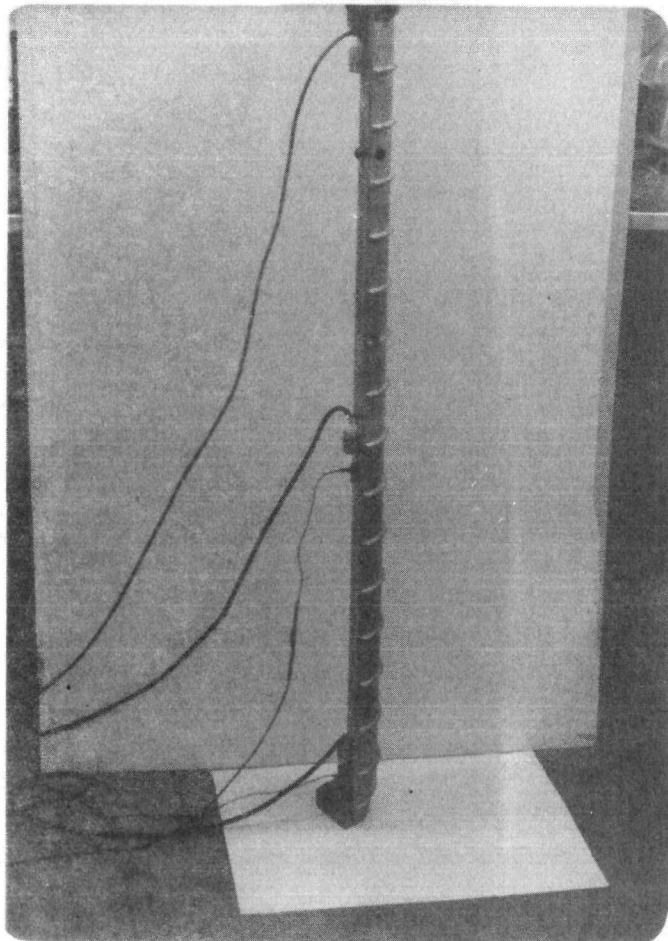
FIGURE D-4
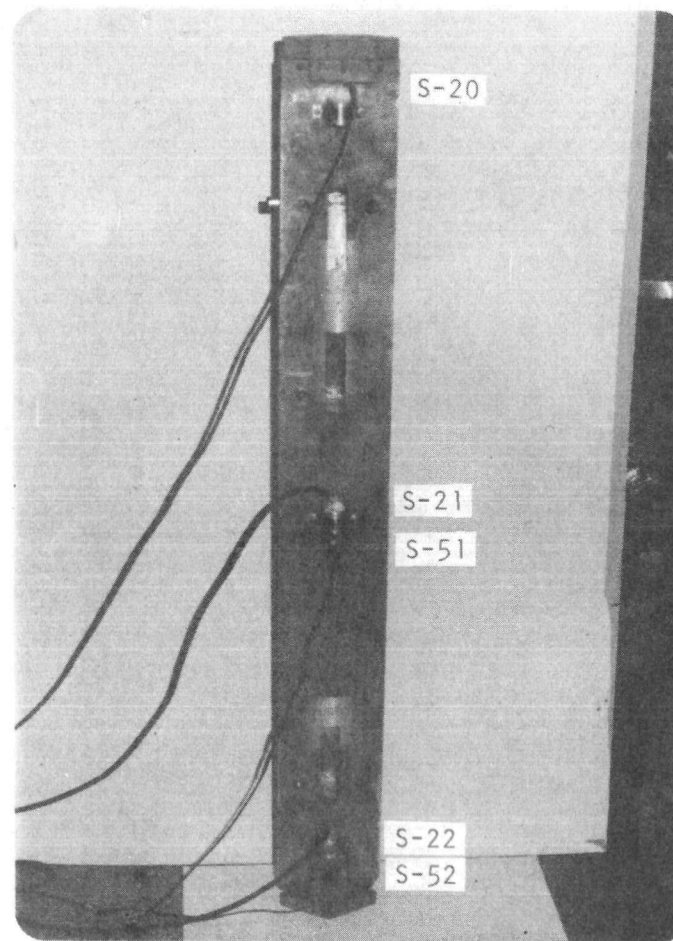
FIGURE D-5

SENSORS IN THE ANCHOR
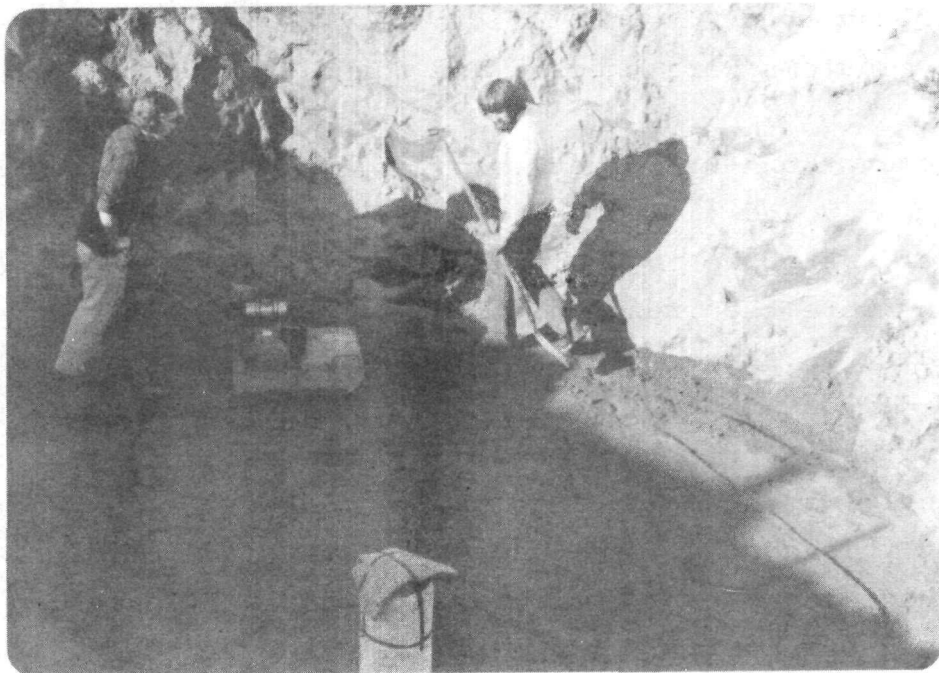
FIGURE D-6 SPREADING AND COMPACTION - FIRST LAYERS

interior void spaces in the core of the anchor were filled with compressible styrofoam. This styrofoam did not restrict the motions of the anchor and provided the minimum support necessary for the soil to develop arching around the narrow opening between the plates. This same compressible material was also placed at the bottom of the anchor and in the upper part of the lower casing to avoid the displacement of soil around the anchor into the lower cavity. After completion of the tests, both soil retaining systems were checked and found to have behaved adequately.

At elevation -6.75 feet, two vertical velocity transducers were placed 17 and 41 inches, respectively, from the center of the anchor, as shown in Fig. D-7. The fill and compaction operations were then resumed. Fig. D-8 shows construction details at this stage.

Elevation -5 feet was considered the main plane of testing. Consequently, as shown in Figs. D-3 and 5-2, 33 sensors were placed at this depth. Of these sensors, two were vertically oriented accelerometers, four were horizontally oriented velocity transducers and the remaining 27 were vertically oriented velocity transducers. When this elevation was reached, the soil along this plane was carefully leveled. A template made from a 1 x 6 wood board was next placed along the axis of the major band of sensors. Finishing nails were then inserted through the holes in the template and pushed into the soil to mark the precise center of each sensor. After this, the template was removed (Fig. D-9). Each nail was then removed and replaced by a transducer as shown in Fig. D-10. Each sensor is shown firmly seated into the soil fill. All sensors installed along this main band are shown in Fig. D-11. These sensors were staggered slightly to avoid interference or shadow effects from adjacent sensors. In general sensors were spaced at least three diameters apart (Appendix E). This staggering also enabled cables to be laid out in a pattern where discontinuity effects would be minimized.

FIGURE D-7   INSTALLATION OF SENSORS AT EL. - 6.75 FT.

FIGURE D-8   CONSTRUCTION BETWEEN EL. - 6.75 FT.
AND EL. - 5.00 FT.
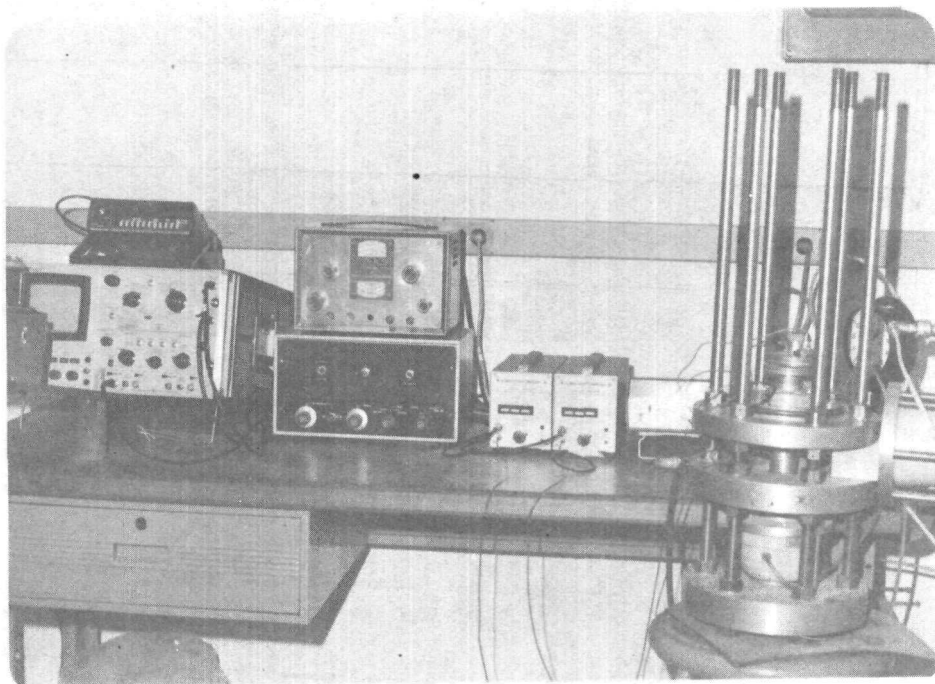
FIGURE D-9 INSTALLATION OF SENSORS AT EL. - 5 FT.
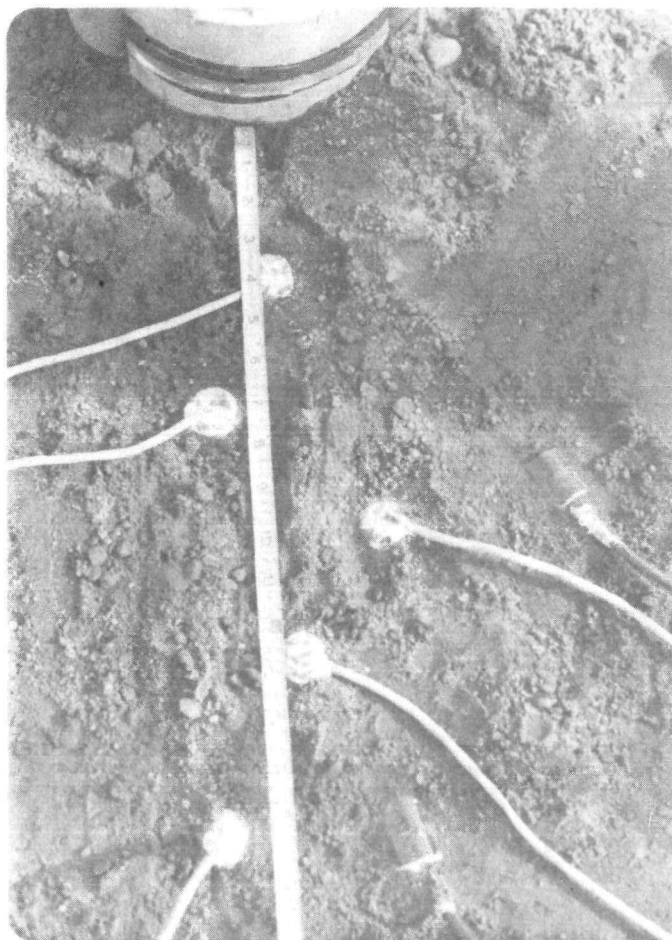
FIGURE D-10
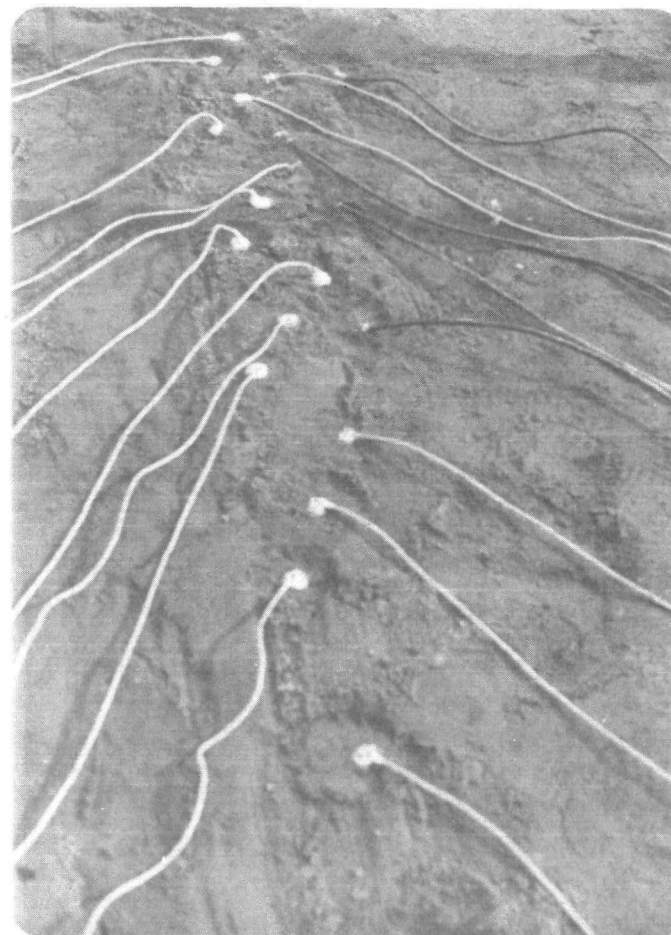
FIGURE D-11

INSTALLATION OF SENSORS AT EL. - 5 FT.

Other sensors were located and placed using a combination of simple geometric relationships and by taping. Installation procedures for these sensors were essentially the same as described above. All of these free-field sensors were the same types as used in the anchor. The velocity transducers used, depending upon their orientation, could measure either vertical or horizontal motions. They are cylindrical in shape, 1.25 inches in diameter and 1.28 inches long. The accelerometers were positioned to measure only vertical motion. They also are cylindrical units with both lengths and diameters of 0.5 inches.

After all sensors were placed, the distance between the anchor and each sensor was remeasured and recorded. To assure that these distances were correct and that individual sensors had not shifted during subsequent fill compaction, these distances were verified twice by measurements made during and at the completion of the test program. These were accomplished by digging a narrow trench down to the band of instruments and making check measurements. The distances were generally correct to within 1/16-inch.

Four types of casing were installed down to elevation -6 feet to measure casing effects. This casing was placed vertically and subsequently buried as the backfilling operation continued.

After completion of the installation and measurements of the distances of the sensors, the construction of the fill proceeded in the manner described previously. At elevation -3.25 feet, two vertical velocity transducers were installed at the same distances and in the same vertical plane as the two located at elevation -6.75 feet. These four sensors were to provide information about the characteristics of the motions of the particles and the propagation of wave fronts at different elevations around the anchor.

The top three feet of the fill was completed after installation of the upper corrugated pipe. This pipe served as protective casing permitting space for the hammer to operate.

In most cases, electrical cables from each transducer were generally run horizontally to the outer boundary of the pit. They were then collected at two main points and run vertically to the ground surface.

The first complete testing phase was accomplished using the large hydraulic anchor assembly shown in most of the photographs. At the completion of testing with this anchor assembly, it was retracted and removed through the upper corrugated casing. The smaller pneumatic anchor was then lowered into the same hole left by the bigger anchor and wedged against the soil face adjacent to the main band of sensors. Soil fill was then poured from the surface through the top corrugated casing around the outside of this anchor to fill the remaining void space. A high density was achieved by tamping each layer of soil in place with a long rod. Additional tests were then conducted with this anchor assembly. At the completion of this testing, all sensors were uncovered, the distance measurements rechecked, and the equipment removed. The results of these tests are discussed in Appendix B.

APPENDIX E

TRANSDUCER SPACING CRITERIA FOR SPECIAL TESTS

APPENDIX E

TRANSDUCER SPACING CRITERIA FOR SPECIAL TESTS

The objective of this appendix is to discuss the following two items: (1) spacing of transducers in the special tests to avoid interaction effects and (2) conditions by which the relative dynamic motion between the transducers and free field during these tests will be essentially eliminated. Static and dynamic closed-form solutions are applied to develop a criteria for spacing adjacent sensors as closely as possible without distortion of the soil response measurements due to shadow effects.

E-1 INCLUSION RESPONSE TO STATIC LOADS

The case of a uniaxial tension loading applied to a plate containing a circular hole with an elastic ring insert has been studied by Savin, 1961. The problem, as depicted in Fig. E-1a, can be considered analogous to the placement of transducers in an elastic soil medium, except for Poisson effects.

The circumferential stress concentration for a copper plate was studied for various ring materials and stiffnesses as shown in Fig. E-1b where H is the thickness of the ring and $D = 2R_1$. This figure indicates that there is essentially no interaction between the ring and the plate at a distance of 1.5D from the centerline of the ring. Similar conclusions can be made regarding the radial stress concentration factor for a rigid ring insert (Fig. E-1c).

E-2 INCLUSION RESPONSE TO INCIDENT PLANE WAVES

The response of a rigid spherical inclusion embedded in an elastic medium subjected to incident plane waves was studied by Mow, 1965, and Bagge, 1973. This study concluded that the medium/inclusion interaction is significant only within that
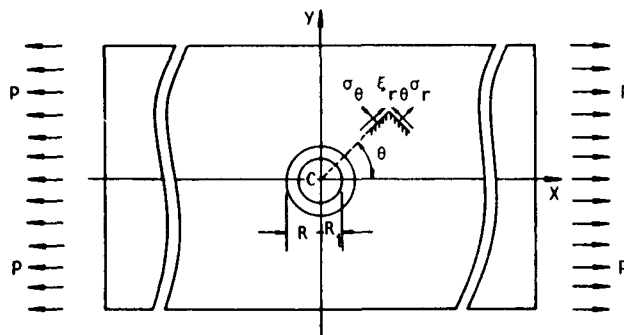
(a) Plate/ring configuration
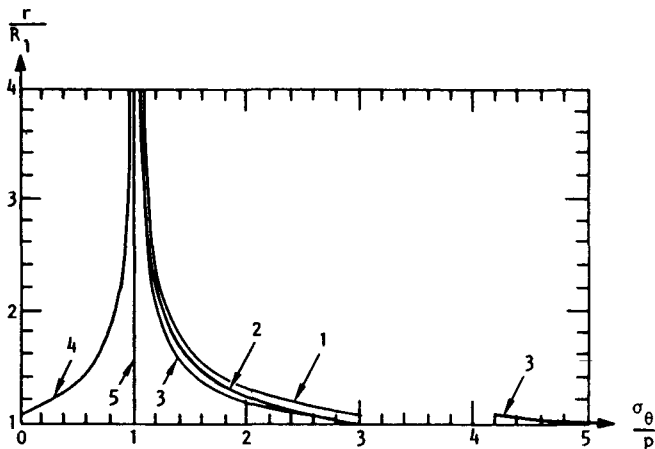
$$\alpha = \frac{H}{D} = \frac{1}{30}$$

NO.	PLATE	RING
1	COPPER	ABSOLUTELY FLEXIBLE
2	COPPER	COPPER
3	COPPER	STEEL
4	COPPER	ABSOLUTELY RIGID
5	PLANE (HOLE-FREE)	--

(b) Circumferential stress concentration

$\theta = 0$

$\nu_{PLATE} = 0.4$
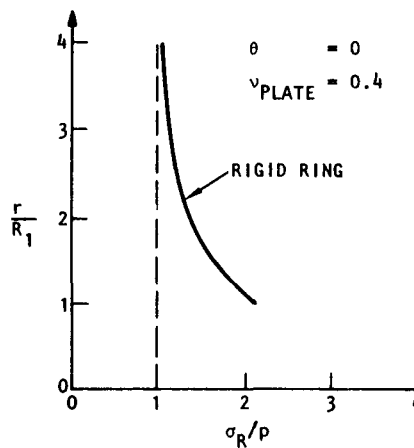
RIGID RING

(c) Radial stress concentrations -- rigid ring only

FIGURE E-1. STATIC STRESS CONCENTRATIONS FOR RING INSERT IN AN ELASTIC PLATE ELEMENT

portion of the medium that lies within a distance of roughly
one inclusion diameter from the medium/inclusion interface.
This suggests that placement of the transducers at center-center
distances of 3D in the in situ tests would eliminate interaction
effects between the transducers.

E-3 DYNAMIC INTERACTION OF SOIL/TRANSDUCER SYSTEM

The dynamic response of rigid spherical inclusions in
homogeneous elastic medium subjected to plane waves were studied
by Bagge, 1973. The results from this study can be used to
investigate dynamic interaction of the soil/transducer system
considered in the special tests.

From the study it was concluded that there will be less
than 10 percent error in measured response for frequencies that
satisfy the condition

$$\omega < \frac{\pi}{3} \frac{1}{t_e} \tag{E.1}$$

where ω is the frequency of the wave motion in rad/sec and

t_e = D/C = engulfment time of the spherical inclusion

D = inclusion diameter

C = compressional wave velocity of the medium

The cutoff frequency defined by Eq. E.1 is plotted in
Fig. E-2 for typical spherical inclusion diameters and effective
compressional wave velocities of soils. Since the problem is
analogous to the transducer/soil system in the special tests,
the studies of Bagge, 1973, can be used to evaluate the degree
to which the motion of a transducer might differ from that of
the surrounding soil medium.
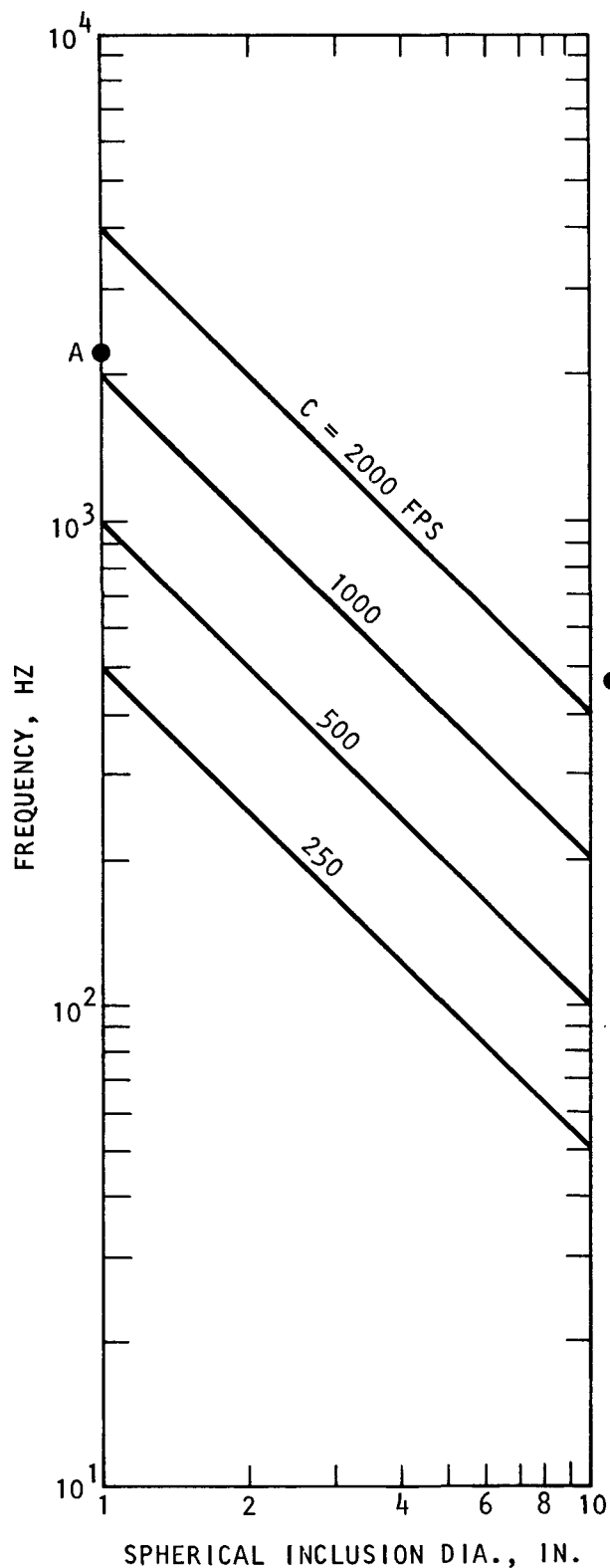
FIGURE E-2. CUTOFF FREQUENCIES BELOW WHICH SOIL/TRANSDUCER (SPHERICAL INCLUSION) INTERACTION HAS MINIMAL EFFECT ON SOIL MOTIONS (< 10% ERROR)

Point A in Fig. E-2 corresponds to the diameter of the transducer (1 in.) and an estimated P-wave velocity of the soil material of about 1100 fps. (This corresponds to an S-wave velocity of 450 fps, a Poisson's ratio of 0.4, and a density of 110 pcf, which are the approximate properties of the soil material used in the FY75 special tests.) Fig. E-2 indicates that for this case, signals with frequencies above about 2200 Hz will be affected by interaction effects; while for signals having frequencies below this level, soil/transducer interaction effects will have a negligible effect on the measured soil motions. Prior experience has indicated that the highest measured frequencies in the generated signal will be about 300 to 500 Hz (SW-AA, 1974); therefore, the results shown in Fig. E-2 indicate that soil/transducer interaction effects will be negligible for the special test program. It is noted that Fig. E-2 is based on the following assumptions: (1) elastic soil medium, (2) rigid transducer, and (3) weight of transducer equivalent to weight of equal volume of soil material.

E-4   CONCLUSIONS AND RECOMMENDATIONS FOR SPECIAL TESTS

Both static and dynamic studies indicate that interaction between transducers is virtually eliminated at a distance of 1D from interface of the transducer, or a distance of 1.5D to the center of the transducer. This implies that, in the special tests, the transducers should be spaced at distances not less than 3D center to center.

Analytical solutions have indicated that for a 1-inch diameter transducer and a soil medium with a P-wave velocity of 2500 fps, the cutoff frequency below which soil/transducer interaction will have minimal effect on free-field soil motions (error < 10%) is approximately 2200 Hz. Since this frequency is well above the highest significant frequencies expected in the soil response measurements, the relative motion between the

transducer and the free field should be negligible. Therefore, this information suggests that the use of 1-inch diameter transducers will not cause any significant modification of the shear wave propagation through the soil, during the in situ tests being conducted under the present program.

REFERENCES

Bagge, C. F. (1973)

    "Structure Medium Interaction", R-7243-1-2774,
    Agbabian Associates, El Segundo, CA, March

Mow, C. C. (1965)

    "Transient Response of a Rigid Spherical Inclusion
    in an Elastic Medium", Jour. Appl. Mech., September,
    p. 637-642

Savin, G. N. (1961)

    Stress Concentration Around Holes, translated by
    Eugene Gros, Permagon Press, New York, p. 249

SW-AA (1974)

    "Soil Behavior Under Earthquake Loading Conditions:
    In Situ Impulse Test for Determination of Shear Modulus
    for Seismic Response Analyses, Progress Report", A
    Joint Venture of Shannon & Wilson, Inc., and Agbabian
    Associates, June

APPENDIX F

STATISTICAL ASSESSMENT OF SPECIAL TEST RESULTS

APPENDIX F

STATISTICAL ASSESSMENT OF SPECIAL TEST RESULTS

F-1 PURPOSE AND SCOPE

As described in Chapter 5, a comprehensive special test program has been carried out to evaluate effects of various test parameters on the soil response measured during the in situ test. The test program was conducted in a pit containing a carefully controlled sand fill material within which sensors were hand-placed every few inches apart (Fig. F-1). Soil motions measured at the various sensors were then evaluated as a function of various test parameters associated with the loads applied to the anchor, the anchor jacking pressure, and the placement of the sensors in the soil.

The primary feature of part of this program consists of tests that were repeated a sufficient number of times to permit meaningful statistical evaluations of the resulting ensembles of soil response measurements. These statistical evaluations provide a basis for considering the effects that any scatter in the measurements might have on the trends associated with the above indicated variations in certain test parameters. The purpose of this appendix is to report the results of these statistical evaluations and, from these results, to draw con- clusions regarding the effects of the various test parameters on the measured in situ responses of the soil materials.

A large part of the special test program is indicated in Table F-1. From this table, it is seen that the following test variables have been evaluated statistically

    a.   Repeatability effects

    b.   Symmetry and shadow effects

(a) Cross section

(b) Plan view at elevation -5 ft

FIGURE F-1. LAYOUT OF SENSORS FOR SPECIAL TEST PROGRAM

TABLE F-1.   MEASUREMENTS FOR SPECIAL TEST PROGRAM

Group	Case No.	Purpose	Sensors	Hammer Weight, lb	Drop Height, ft	Jacking Pressure psi	No. of Repeated Tests
A*	1	Symmetry and Shadow Effects	1, 1a, 2, 2a	58	0.5	3500	12
	2		3, 3a, 8, 8a	58	0.5		12
B*	1		21, 3, 5, 7	58	0.5	3500	12
	2		7, 9, 11, 14	58	0.5	3500	12
	3		21, 1, 2, 3	58	1.5	3500	12
	4		4, 5, 7, 8	58	1.5	3500	12
	5		9, 11, 12, 14	58	1.5	3500	12
	6		21, 1, 2, 3	150	0.58	3500	12
	7	Prior Load History and Variations in Hammer Weight and Drop Height	4, 5, 7, 8	150	0.58	3500	12
	8		9, 11, 12, 14	150	0.58	3500	12
	9		21, 1, 2, 3	16.4	5.3	3500	12
	10		4, 5, 7, 8	16.4	5.3	3500	12
	11		9, 11, 12, 14	16.4	5.3	3500	12
	12		21, 1, 2, 3	58	0.5	3500	12
	13		4, 5, 7, 8	58	0.5	3500	12
	14		9, 11, 12, 14	58	0.5	3500	12
C	1	P-Wave Effects	21, 41, 42, 43	58	0.5	3500	2
	2		21, 41, 42, 43	58	1.5	3500	2
D	1	Casing Effects	21, 71, 72, FF_1	58	0.5	3500	2
	2	(FF_1, FF_2 = free-field velocity	21, 73, 74, FF_2	58	0.5	3500	2
	3	transducer between 71-72 and	21, 71, 72, FF_1	58	1.5	3500	2
	4	73-74, respectively)	21, 73, 74, FF_2	58	1.5	3500	2
E*	1		21, 1, 2, 3	58	0.5	2000	12
	2	Jacking Pressure Effects	4, 5, 7, 8	58	0.5	2000	12
	3		21, 1, 2, 3	58	0.5	5000	12
	4		4, 5, 7, 8	58	0.5	5000	12
F	1		60, 20, 51, 52	58	0.5	3500	2
	2		60, 20, 51, 52	58	1.5	3500	2
	3	Anchor Responses	60, 20, 51, 52	150	0.58	3500	2
	4		60, 20, 51, 52	29	3.0	3500	2
	5		60, 20, 51, 52	58	0.5	2000	2
	6		60, 20, 51, 52	58	0.5	5000	2

*Data considered in statistical analysis phase of special test program.

c.   Prior load history

d.   Variations in hammer weight and drop height for
     a given input energy level

e.   Jacking pressure

Other test variables indicated in Table F-1, such as casing
effects, P-wave effects, and anchor responses have not been
evaluated statistically and are therefore not included in this
appendix. These tests, together with additional supplemental
tests, were performed to study some of these same effects, as
well as these other effects, on a non-statistical basis. An
evaluation of this data is presented in Appendix G.

   The remainder of this appendix is divided into three
sections. A description of the data processing approach and
analytical procedures used to develop the statistical results
is contained in Section F-2. These results are described and
evaluated in Section F-3, while Section F-4 contains a summary
and conclusions regarding this work.

F-2   DATA PROCESSING APPROACH AND ANALYTICAL PROCEDURES

   Prior to presenting the results of the statistical evalua-
tions, it is appropriate to first discuss the approach philosophy
associated with the processing of the test data and the analytical
procedures used to carry out this processing. This discussion
is contained in the remaining paragraphs of this section.

   F-2.1   Data Processing Approach

       As noted in Table F-1, ensembles of repeated soil
response measurements were obtained at a large number of the
sensors used in the special tests. Upon examination of these
measurements, it was judged appropriate to carry out statistical
processing of the measurements at selected sensors that represent

the soil response at different ranges of distances from the anchor. Measurements at the remaining sensors could then be used as backup, in case additional investigation of the trends related to the various test parameters was required. Therefore, to assess symmetry and shadow effects, soil responses measured at Sensors 1, 2, 3, and 8 were processed. The repeatability assessments and evaluations of the effects of prior load history, hammer weight-drop height variations and jacking pressures were carried out by processing response measurements at Sensors 21, 1, 3, 7, and 14. Locations of these various sensors relative to the anchor and a complete summary of the data processed in this statistical evaluation are provided in Table F-2.

The results from the repeatability assessments are presented in the form of overlaid plots of velocity time histories. Results from the assessments of the other test variables are provided as mean velocity time histories and in addition, as velocity history bands that represent mean ⁺ one standard deviation (MSD) bounds. The mean time histories indicate the general trends associated with the effects of each test variable, while the MSD bounds indicate to what extent these trends might be affected by scatter in the data. It is noted that the probability level associated with these MSD bounds is dependent on the assumed probability distribution that can be associated with the in situ soil tests. For example, if the data follows a normal (Gaussian) distribution, then 68% of the total population of velocity histories will fall within the MSD bounds. Other probability distributions will result in a slightly different estimate of this percentage of the total population of test results contained within these MSD limits.

F-2.2 Analytical Procedure

Two processing packages were used in evaluating this data. The first was a specially written interface program that

TABLE F-2. DATA PROCESSED IN STATISTICAL EVALUATIONS

Sensor No.	Distance from Edge of Anchor, In.	Effect	Tests to Compare
21	At Anchor	Repeatability Prior Load History Different Combinations of Drop Height and Hammer Weight for Same Energy Level Jacking Pressure	Selected Tests B-1, B-12 B-3, B-6, B-9 B-12, E-1, E-3
1 1A	2.94 2.43	Repeatability Symmetry and Shadow Effects Prior Load History Different Combinations of Drop Height and Hammer Weight for Same Energy Level Jacking Pressure	Selected Tests A-1 A-1, B-12 B-3, B-6, B-9 B-12, E-1, E-3
2 2A	6.13 5.07	Symmetry and Shadow Effects	A-1
3 3A	9.13 8.5	Repeatability Symmetry and Shadow Effects Prior Load History Different Combinations of Drop Height and Hammer Weight for Same Energy Level Jacking Pressure	Selected Tests A-2 A-2, B-12 B-3, B-6, B-9 B-12, E-1, E-3
7	23.93	Repeatability Prior Load History Different Combinations of Drop Height and Hammer Weight for Same Energy Level Jacking Pressure	Selected Tests B-1, B-13 B-5, B-7, B-10 B-13, E-2, E-4
8 8A	27.86 27.79	Symmetry and Shadow Effects	A-2
14	55.11	Repeatability Prior Load History Different Combinations of Drop Height and Hammer Weight for Same Energy Level	Selected Tests B-2, B-14 B-5, B-8, B-11

carried out the following initial data reduction and formatting
operation:

a. Read the magnetic tapes containing the
    field data
b. Scale the velocity data using factors pro-
    vided in the tape label record that precedes
    each test
c. Integrate the velocity time histories, where
    required
d. Label the test channels
e. Write a new data tape according to a format
    suitable for direct input into MAC/RAN

The second processing package used in this study
was MAC/RAN, a comprehensive system of digital computer programs
for complete reduction of time series data. MAC/RAN was applied
in the special test program in two different ways. First, to
assess the repeatability of the data, velocity time histories
measured at each sensor and corresponding to repeated appli-
cations of each test condition were multiple-plotted. In this,
ten of the twelve repeated tests for each case (Table F-1) were
utilized. The scaled data from the interface program were merged
to form files of data that were grouped by sensor number rather
than test number. These files were then multiple-plotted using
consistent amplitude and time scales, so that the repeatability
could be easily assessed.

In addition to multiple-plotting of the individual
velocity history measurements, MAC/RAN was also used to perform
statistical analyses of the ensembles of data. In this, ten
data channels for each selected sensor and each test condition
were processed to obtain velocity time histories corresponding
to the ensemble mean and the ensemble MSD bounds. The multiple-
plot capabilities of MAC/RAN were then used to overlay the

time histories corresponding to different variations of each test parameter.

F-3   RESULTS OF STATISTICAL ASSESSMENTS

The results of the statistical assessment of the special test results are described and evaluated in this section. The section is organized into separate subsections that consider the repeatability assessment, and the evaluation of symmetry and shadow effects, the effects of prior load history, hammer weight-drop height combinations, and jacking pressures.

F-3.1   Repeatability Assessment

Assessments of the repeatability of velocity histories recorded at the various sensors indicated in Table F-2 are summarized in Figs. F-2 to F-6. These figures indicate that, on the whole, the velocity measurements are very repeatable. The only clear exception to this general trend is the results corresponding to the 150-lb hammer drop (Test Groups B-6 to B-8 in Table F-1). For this case, the velocity measurements obtained at or near the anchor appear to have a relatively high degree of variability; however, for sensors located at increased distances from the anchor, the variability of the measurements diminishes substantially and the results become quite repeatable. This overall trend may be attributed to the sensitivity of the near-anchor measurements to the details of the applied loadings, such as the orientation of the hammer as it strikes the Belle-ville springs, the manner in which the anchor plates bear against the sides of the borehole, and the ability to manually obtain the same exact drop repeatedly. The soil response at sensors located away from the immediate vicinity of the anchor tends to be less sensitive to such load details.
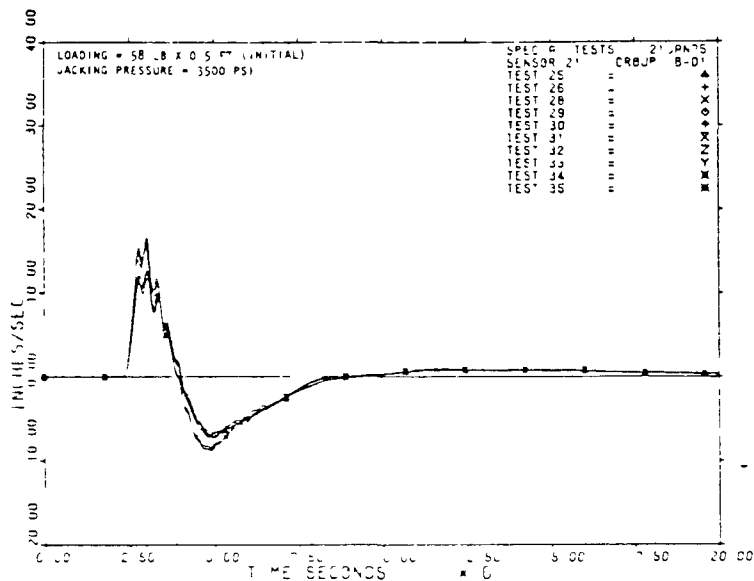
(a) Test Group B-1
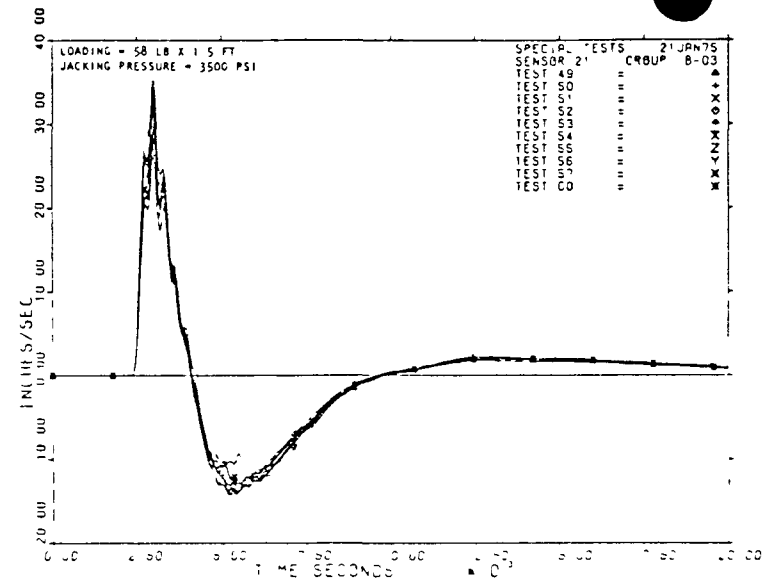
(b) Test Group B-3
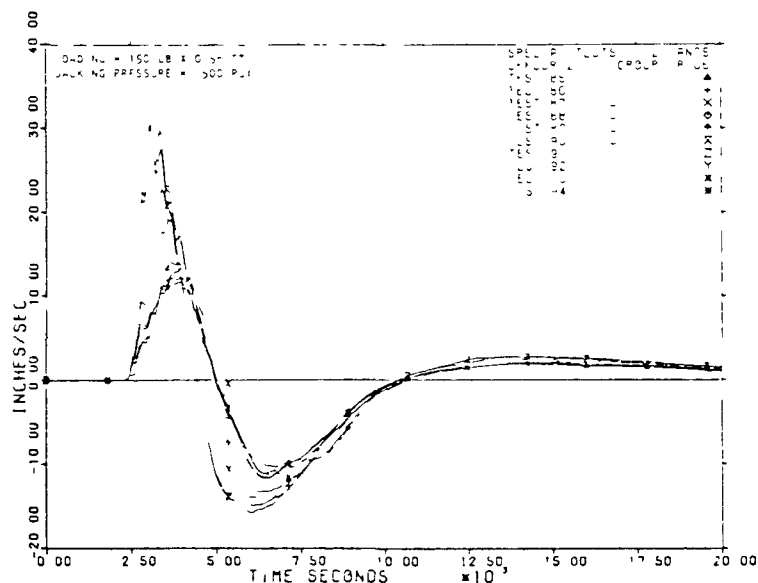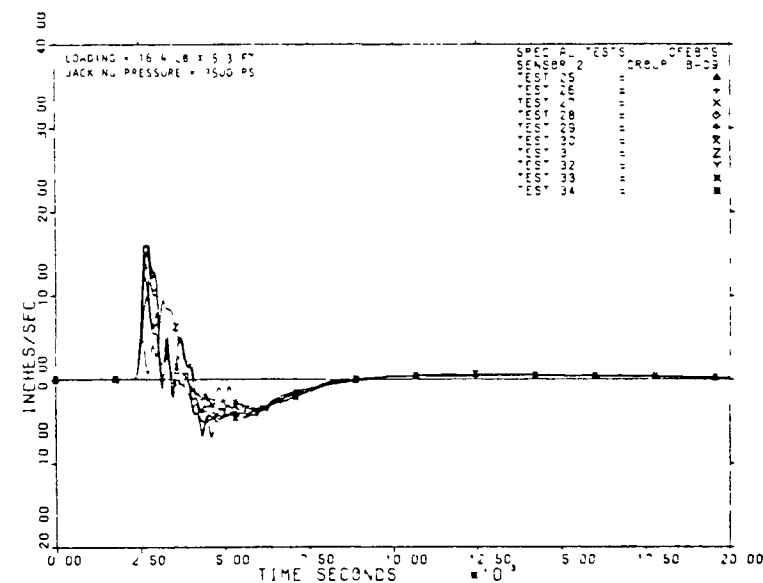
(c) Test Group B-6

(d) Test Group B-9

FIGURE F-2.   REPEATABILITY OF VELOCITY HISTORIES AT ANCHOR
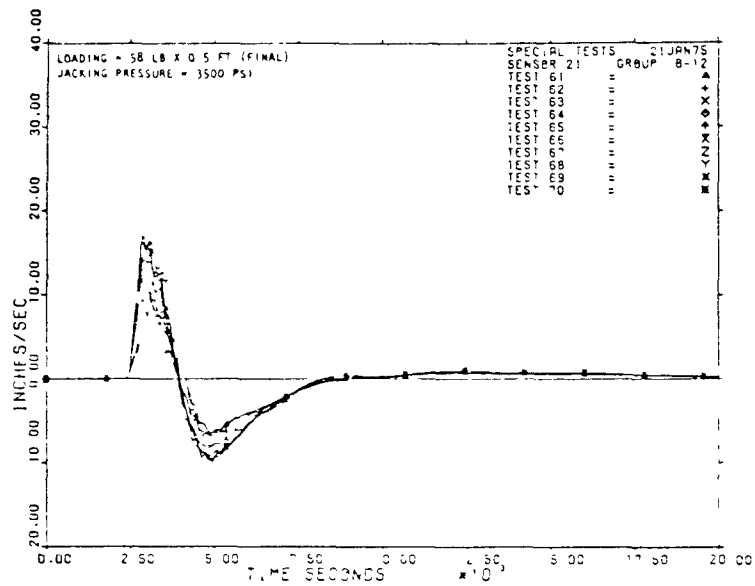
(e) Test Group B-12
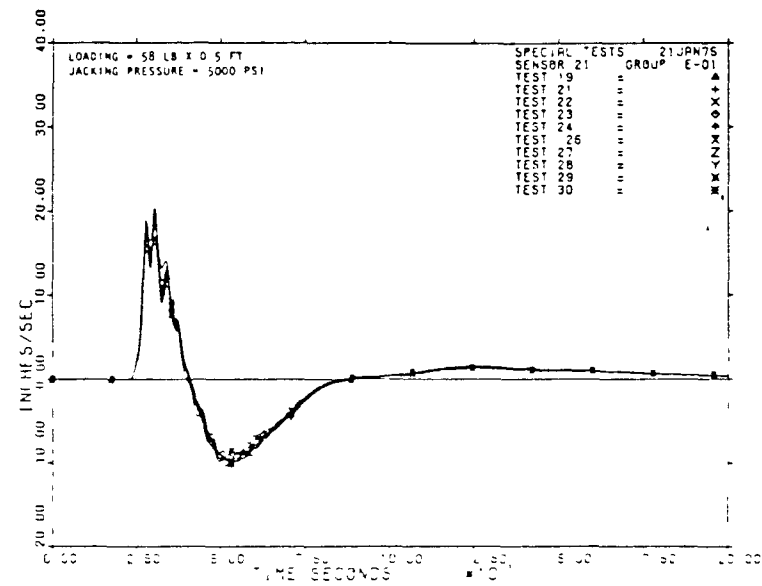
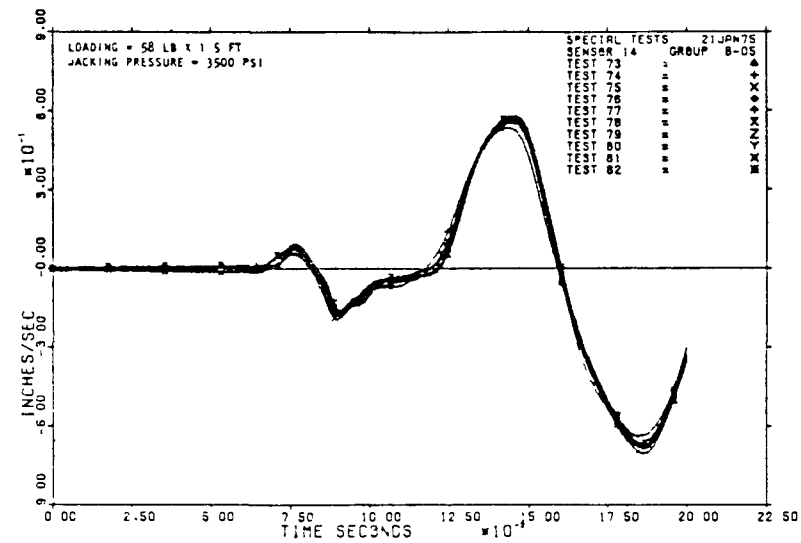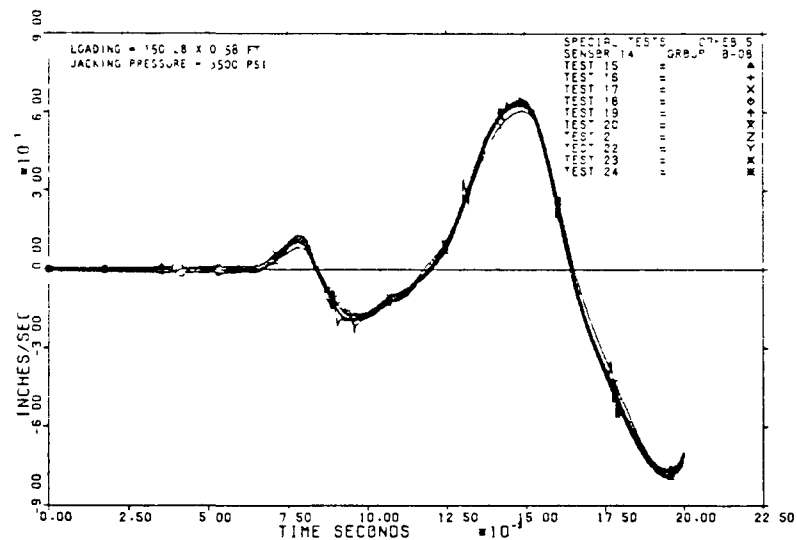(f) Test Group E-1
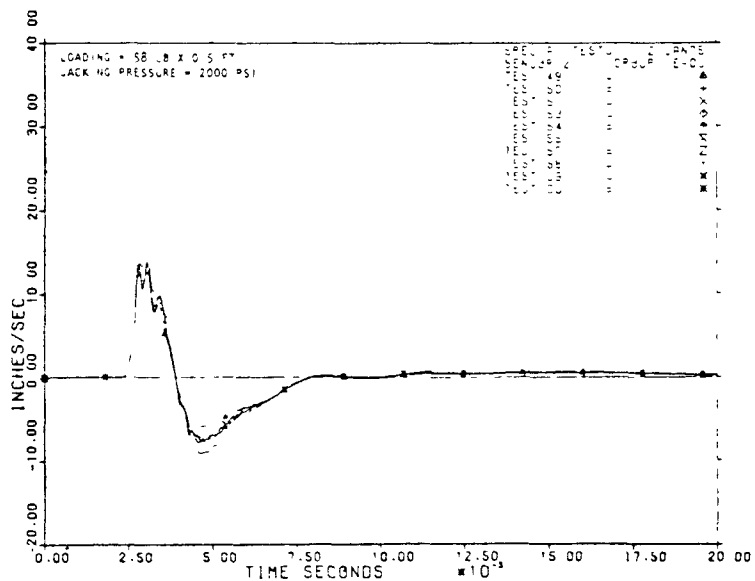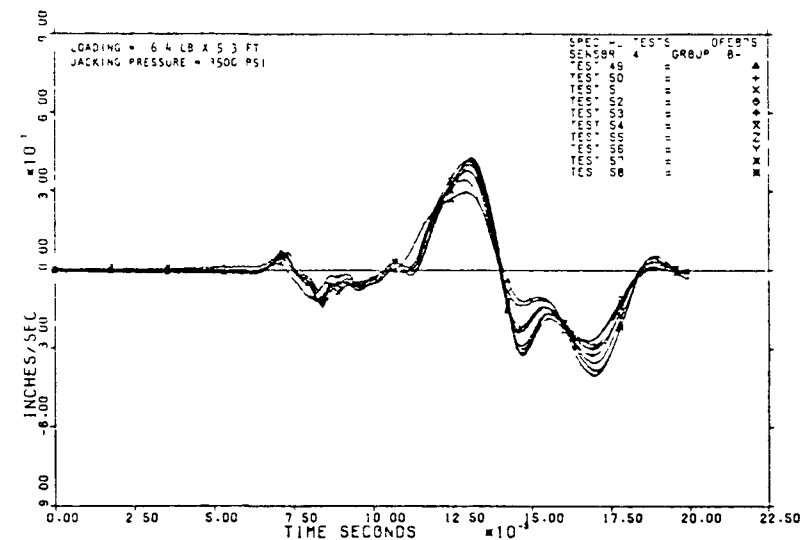

(g) Test Group E-3

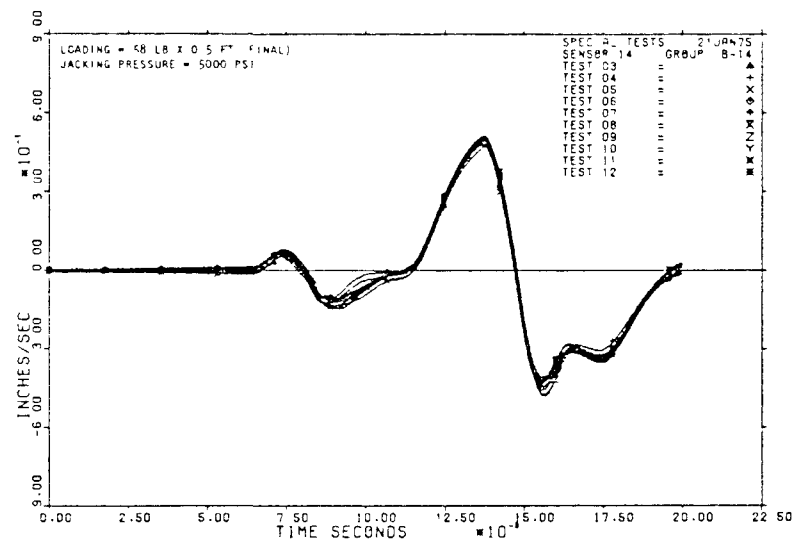FIGURE F-2.   (CONCLUDED)
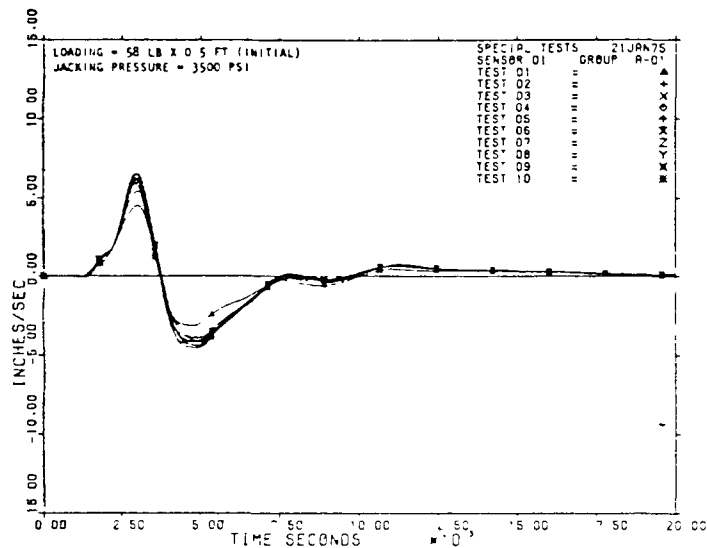
(a) Test Group B-1
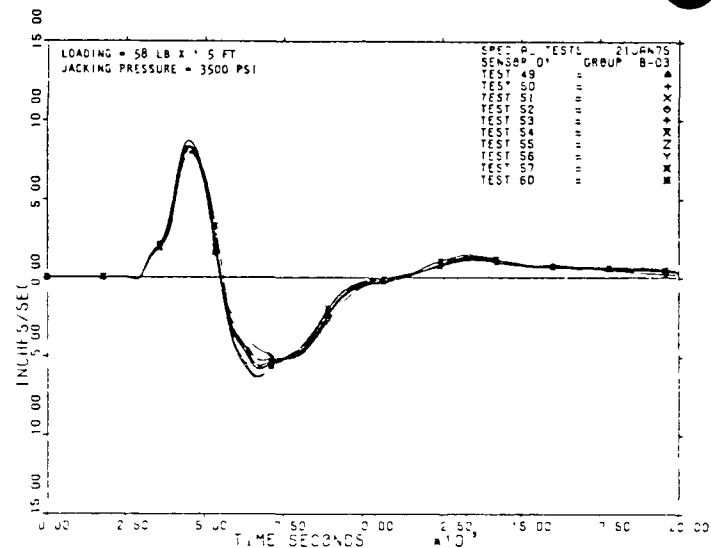
(b) Test Group B-3
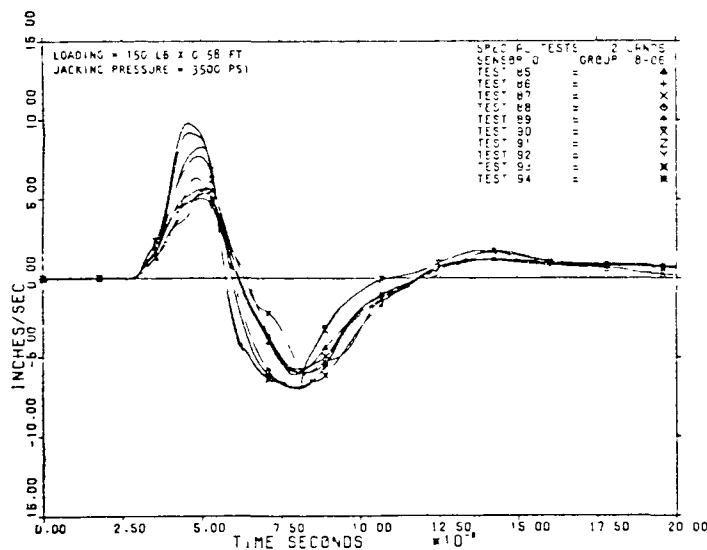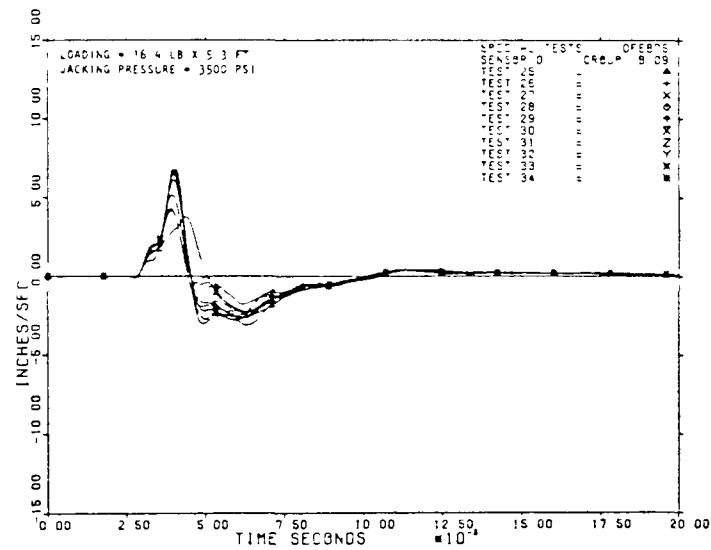
(c) Test Group B-6

(d) Test Group B-9

FIGURE F-3. REPEATABILITY OF VELOCITY HISTORIES AT SENSOR 1 -- 3 IN. FROM ANCHOR EDGE

(e) Test Group B-12

(f) Test Group E-1
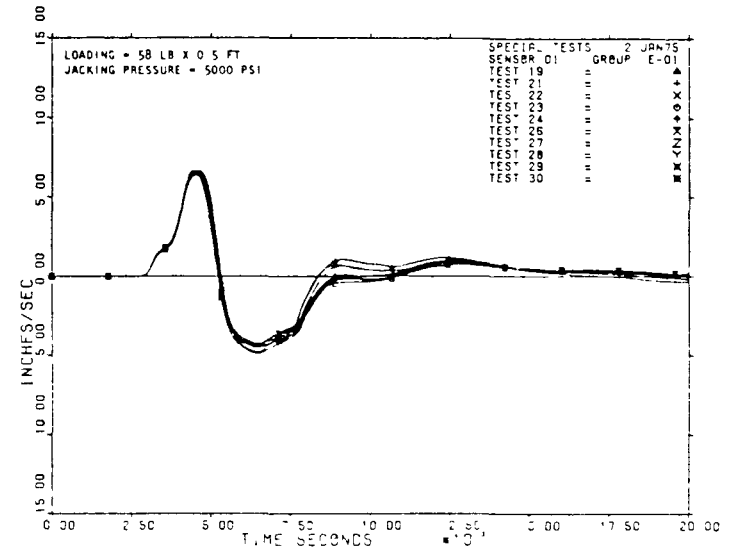
(g) Test Group E-3
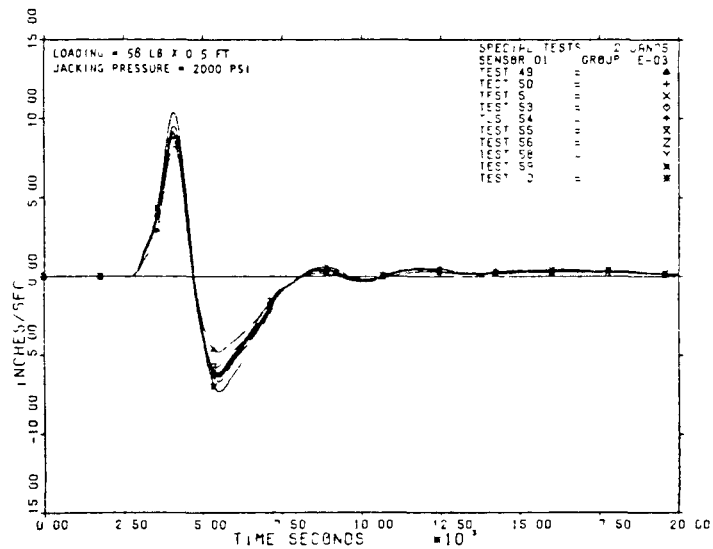
FIGURE F-3. (CONCLUDED)
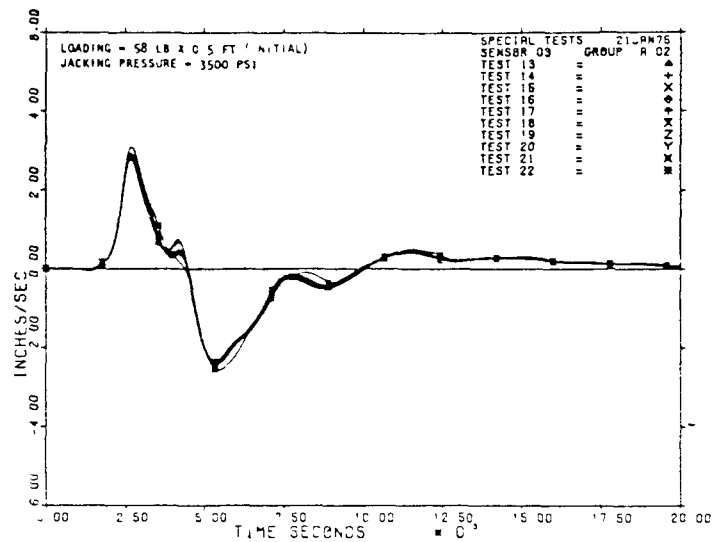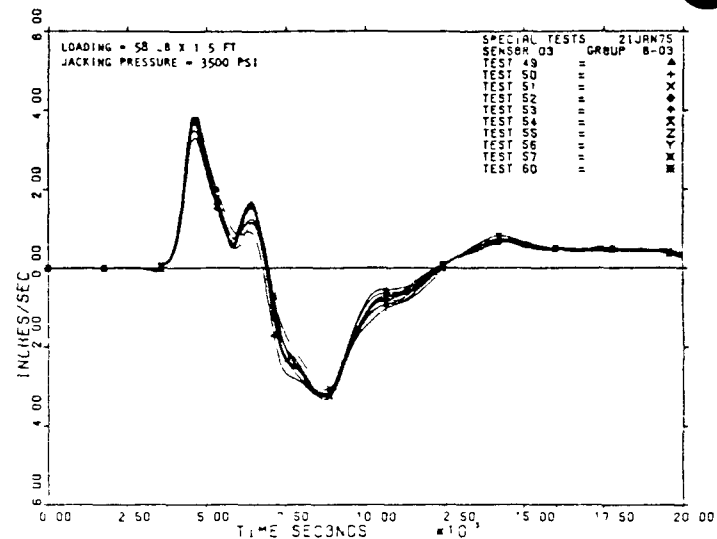
(a) Test Group A-2

(b) Test Group B-3
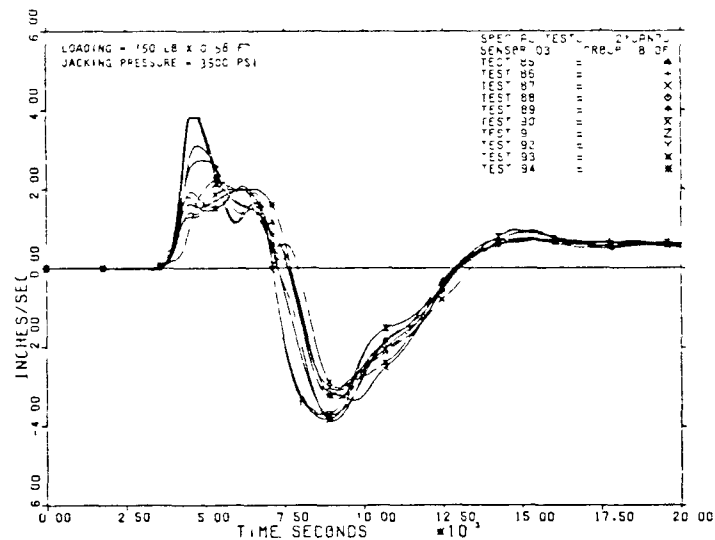
(c) Test Group B-6
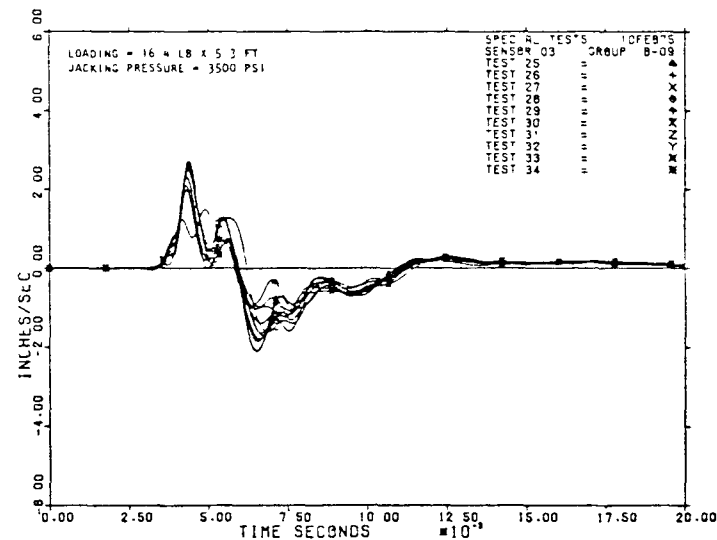
(d) Test Group B-9

FIGURE F-4.   REPEATABILITY OF VELOCITY HISTORIES AT SENSOR 3 -- 9 IN. FROM ANCHOR EDGE
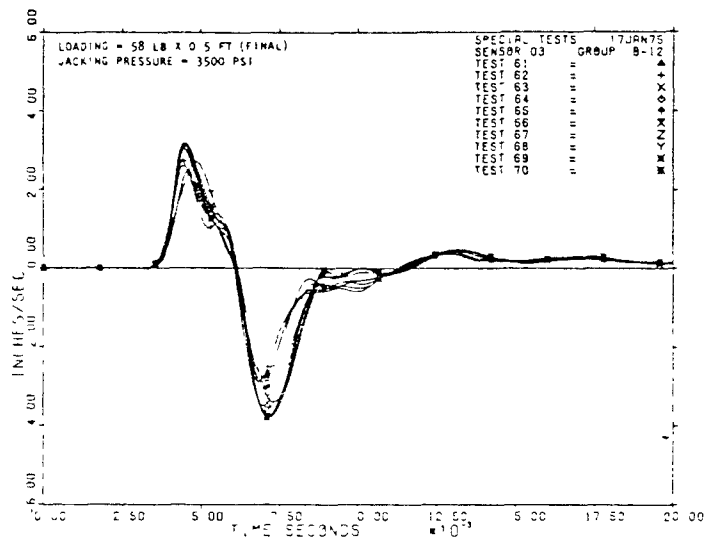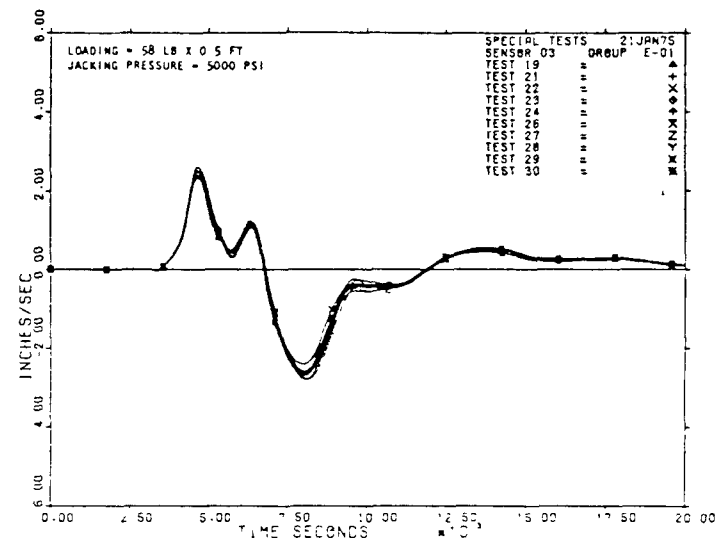
(e)   Test Group B-12
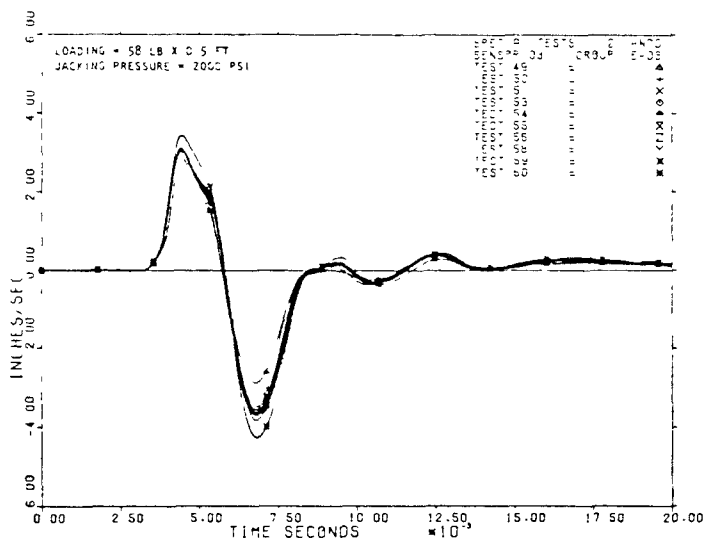
(f)   Test group E-1

(g)   Test Group E-3

FIGURE F-4.   (CONCLUDED)
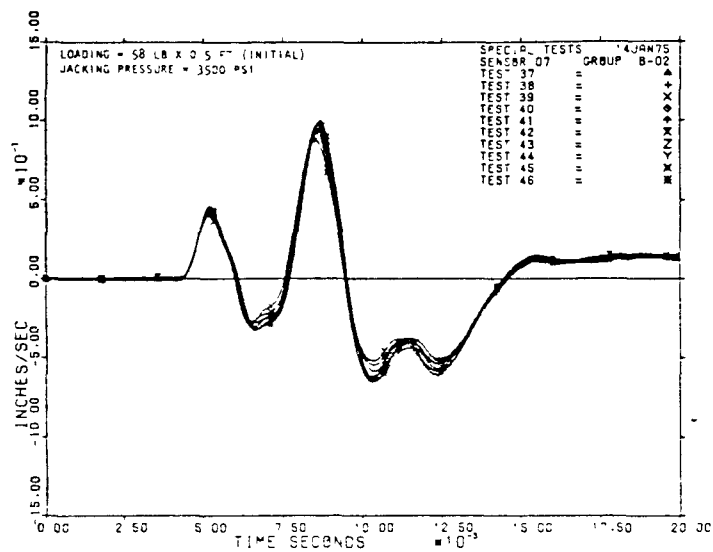
(a) Test Group B-2
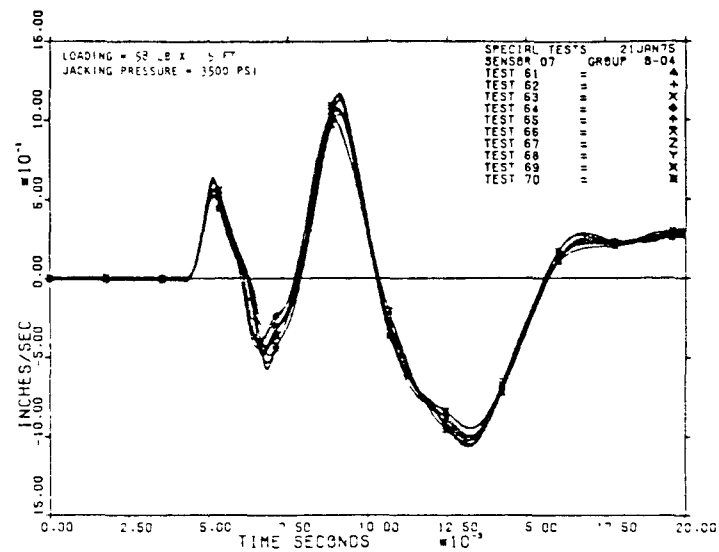
(b) Test Group B-4
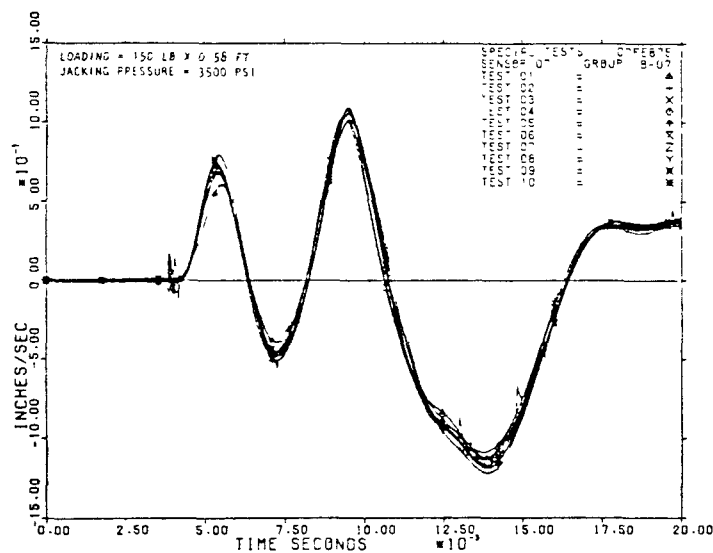
(c) Test Group B-7
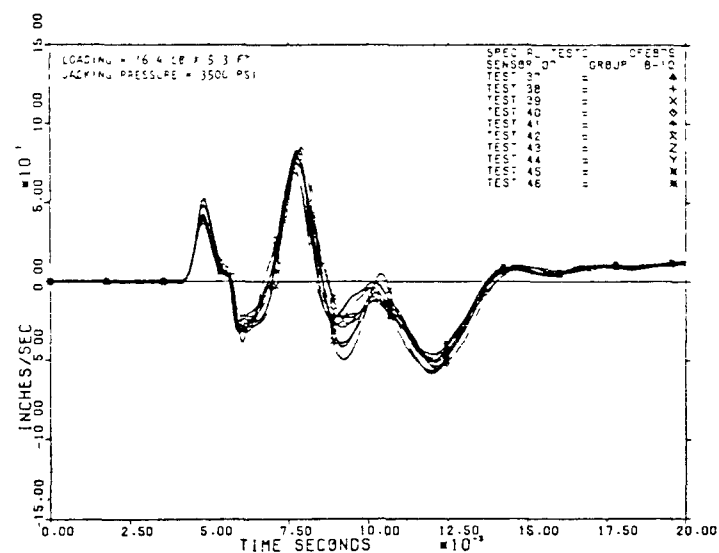
(d) Test Group B-10

FIGURE F-5. REPEATABILITY OF VELOCITY HISTORIES AT SENSOR 7 -- 24 IN. FROM ANCHOR EDGE
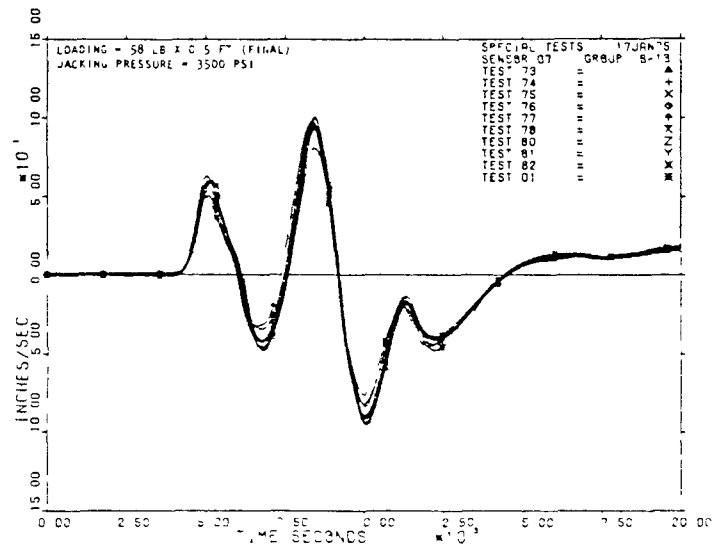
(e)   Test Group B-13
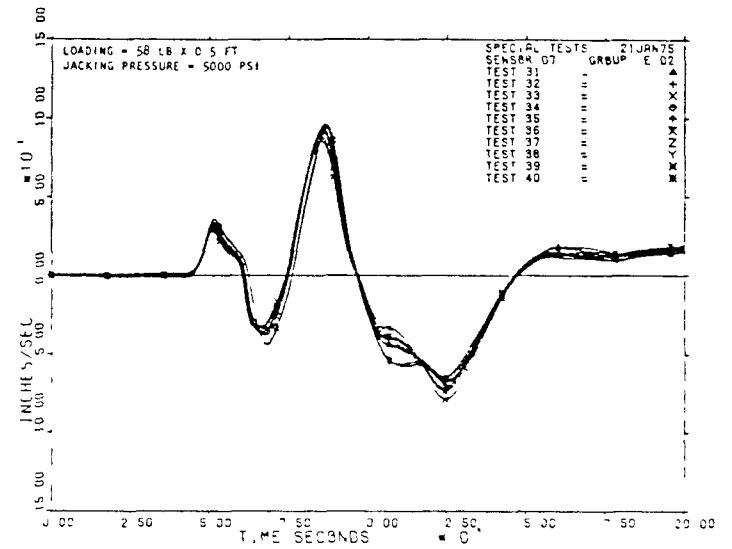
(f)   Test Group E-2
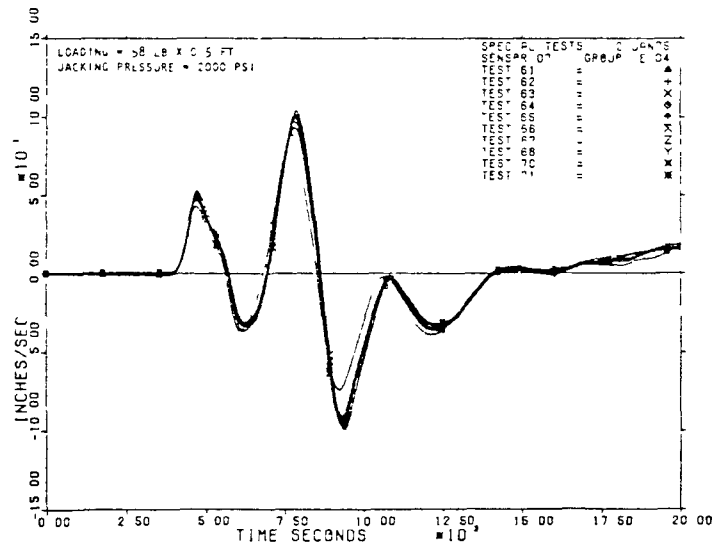
(g)   Test Group E-4

FIGURE F-5.   (CONCLUDED)
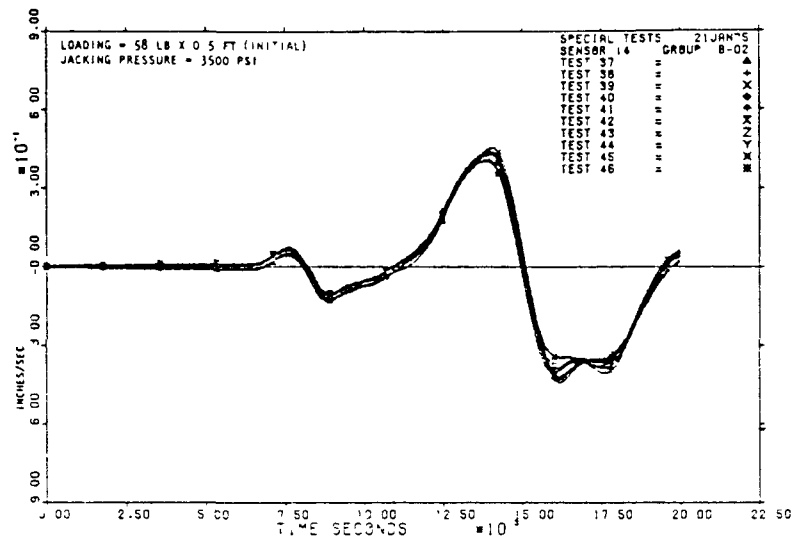
(a) Test Group B-2

(b) Test Group B-5

(c) Test Group B-8

(d) Test Group B-11

FIGURE F-6. REPEATABILITY OF VELOCITY HISTORIES AT SENSOR 14 -- 55 IN. FROM ANCHOR EDGE

(e) Test Group B-14

FIGURE F-6. (CONCLUDED)

F-3.2 Symmetry and Shadow Effects

In this subsection, assessments of the effects of
the position of the sensor are assessed. Two aspects of this
problem have been investigated. The first deals with the spacing
of a series of sensors along a line (which corresponds to axis
X-X in Fig. F-1b). For the special tests, it was desired to
place these sensors as closely as possible to one another in
order to obtain the maximum refinement in the response measurements.
However, if the sensor spacing was too small, adjacent sensors
may have interacted with one another and could have distorted
the resulting soil response measurements. Therefore, it was
required to determine an optimum sensor spacing that avoids these
"shadow" effects while still providing a sufficiently fine
network of response measurements.

A second phase of this problem dealt with possible
variations in the soil response measurements due to differences
in the circumferential position of the sensors. This may be
due to inhomogenities in the soil or non-uniform bearing of
each of the anchor plates against the side of the borehole.
An assessment of this problem was judged to be particularly
important, since production tests have in the past typically
utilized sensors placed at different circumferential positions,
as shown in Fig. 1-1.

To investigate these potential effects, two different
approaches were used. First, analytical solutions were used
to define an optimum spacing for the special tests. These
analyses are presented in Appendix E and were used to guide
the actual placement of the sensors along axis X-X in Fig. F-1b.
As noted in this figure, these sensors were staggered so that
they were at least three diameters apart, which is well within
the guidelines indicated in Appendix E.

A second approach for assessment of these effects utilized field tests in which velocity measurements were obtained at sensors located at near equal radial distances from the anchor but at different circumferential positions. An ensemble of these measurements, as generated from repeated applications of a 58-lb hammer and a 0.5-ft drop height were analyzed statistically to obtain mean and MSD velocity histories. Comparisons of these statistical results were used to indicate the presence of any non-symmetries in the circumferential distribution of the waves propagating from the anchor.

Results of these comparisons are shown in Fig. F-7. They indicate that the peak velocity amplitudes and corresponding wave shapes are generally similar regardless of the circumferential position of the sensor; however the rise times to peak velocity or the arrival times are not. In general, the sensors placed along axis X-X (Fig. F-1b) tend to arrive later in time or have a longer rise time to peak velocity than do those sensors at the same radial position but offset circumferentially. This minor difference in arrival times was due, at least in part, to the distances of the sensor in the radial pattern being slightly closer to the center of the anchor than the corresponding sensors along the axis (see Table F-2). Except for this difference, the remainder of each velocity history does not seem to be substantially affected by the circumferential position of the sensor. It is noted that differences between the upper bound and lower bound MSD curves are quite small, indicating that the data is quite repeatable and that the above trends are not obscured by data scatter.
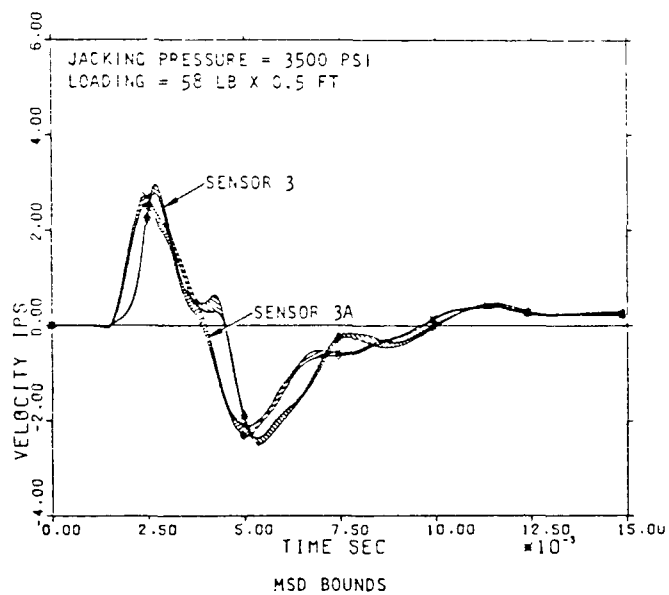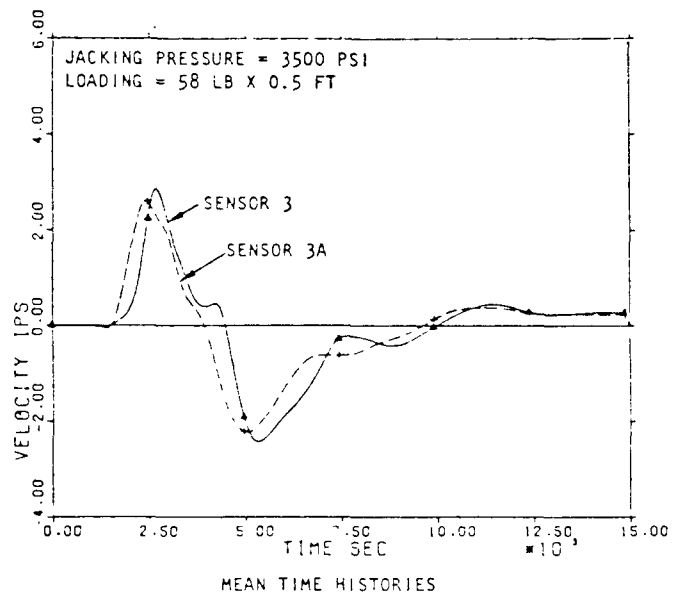
F-3.3 Prior Load History Effects

In the in situ soil testing approach, the soil layers at a particular depth may be subjected to repeated load applications corresponding to different energy levels, in order to
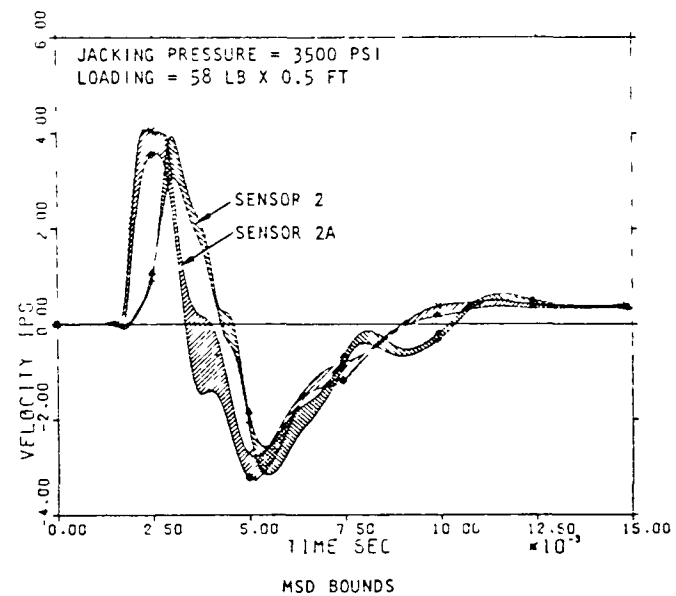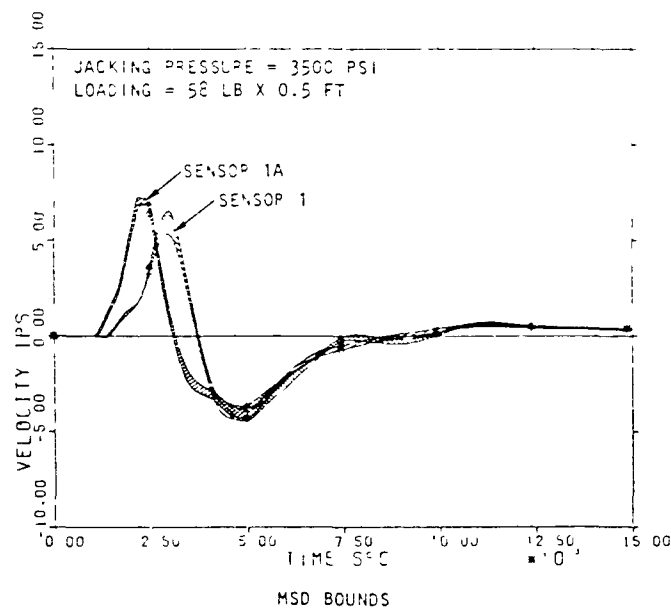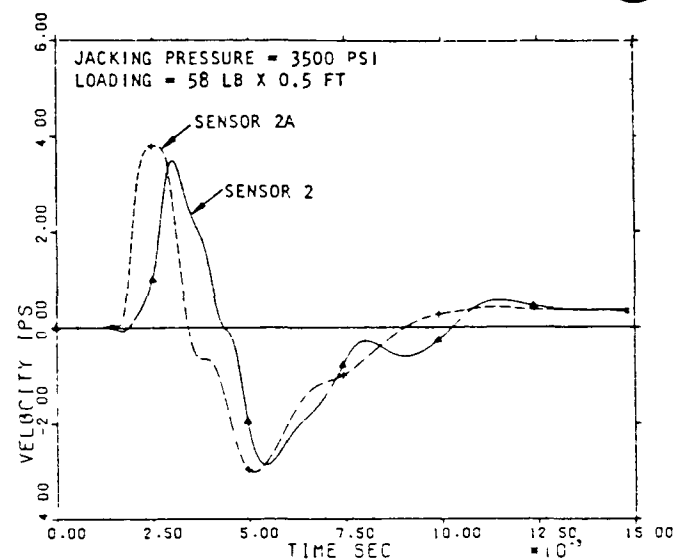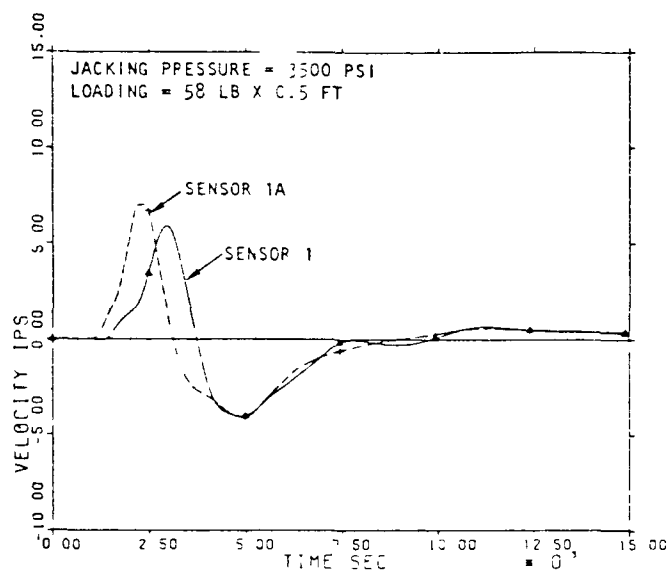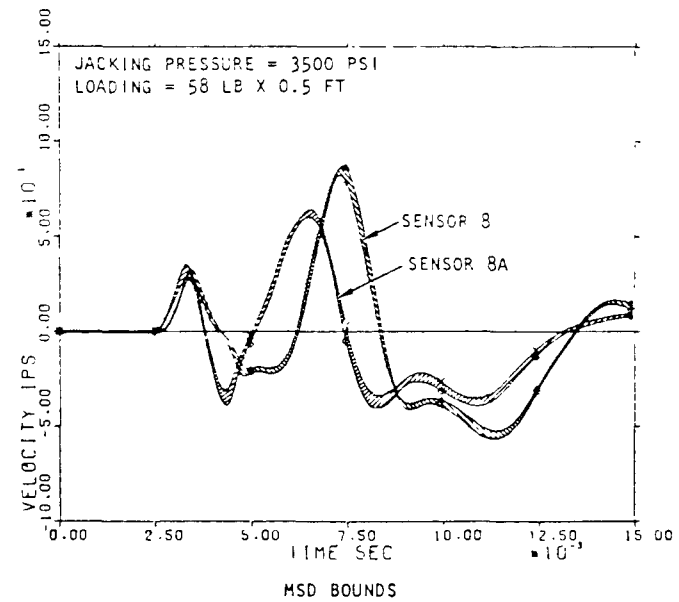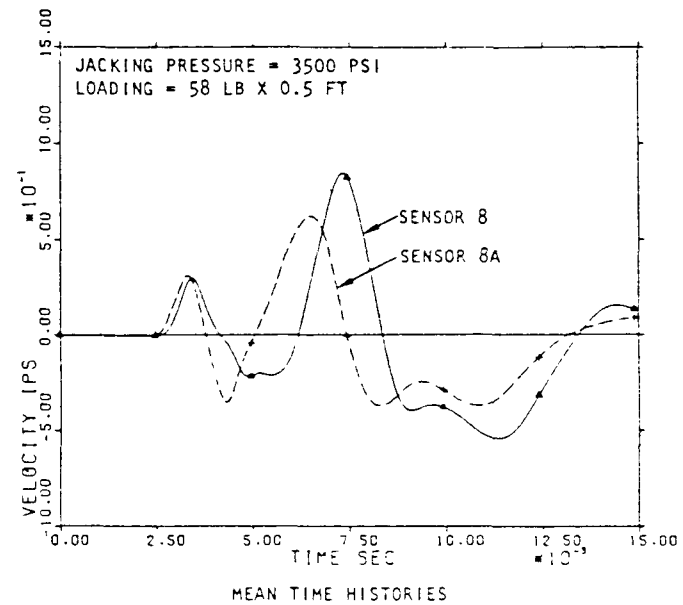
(a) Sensors located 3 in. from edge of anchor (b) Sensors located 6 in. from edge of anchor

FIGURE F-7. STATISTICAL ASSESSMENT OF SYMMETRY AND SHADOW EFFECTS

(c) Sensors located 9 in. from edge of anchor

(d) Sensors located 28 in. from edge of anchor

FIGURE F-7. (CONCLUDED)

obtain a wide spectrum of shear modulus vs. shear strain
measurements. However, it is conceivable that for some soil
materials, the measured responses during a given test may be
affected by the number and magnitude of prior loadings to which
the soil has been subjected. Therefore, it is important to
investigate whether such prior load history effects have a
significant influence on subsequent soil response measurements.

To investigate this effect, a series of initial
tests were conducted during which a 58-lb hammer was dropped
0.5 ft onto the Belleville springs. These correspond to Tests
A-1, A-2, B-1, and B-2 in Table F-1. Then a large number of
tests were conducted at higher energy levels (Tests B-3 to B-11),
and these were followed by a series of tests corresponding to
the initial loading conditions (Tests B-12 to B-14). To investi-
gate prior load history effects, mean and MSD velocity histories
corresponding to the initial and final sets of the 58-lb x 0.5-
ft loadings were compared.

The above indicated comparisons at various sensors
within the in situ soil test network are shown in Fig. F-8.
They indicate that, regardless of the sensor location, prior
load history effects are negligible. The mean velocity time
histories may indicate some minor differences related to prior
load history effects; however these differences are completely
masked by the small amounts of data scatter observed in these
test groups, as indicated by the comparisons of the MSD time-
history bounds.

F-3.4 Variations in Hammer Weight and Drop Height
       for a Given Energy Level

In the in situ soil test program, the input loads are
typically specified in terms of an input energy level, deter-
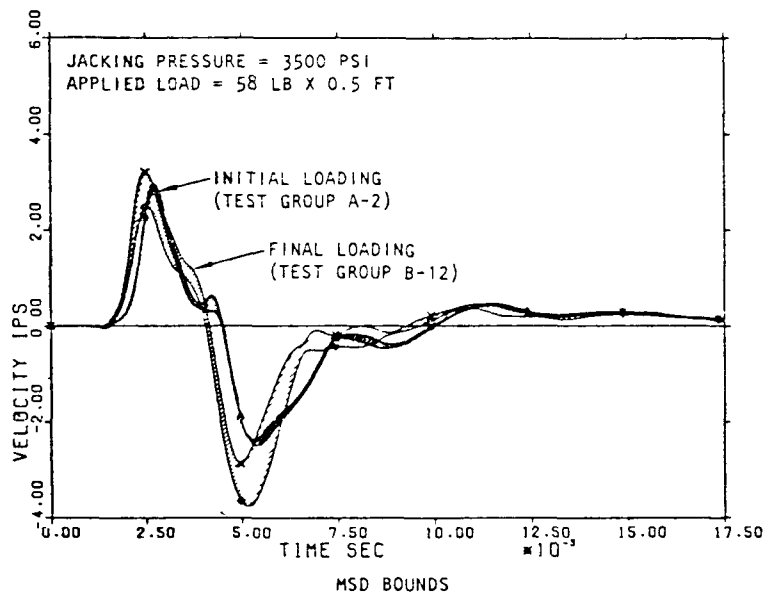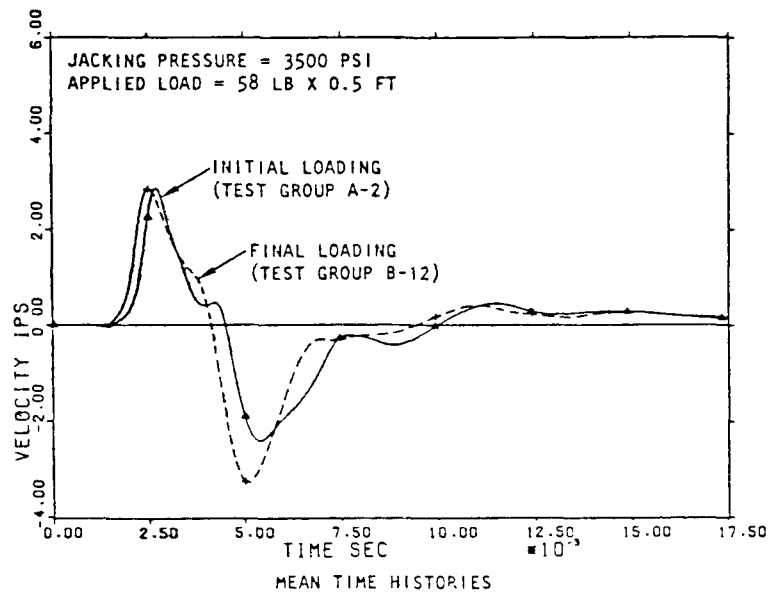mined as the product of the hammer weight and its height of free
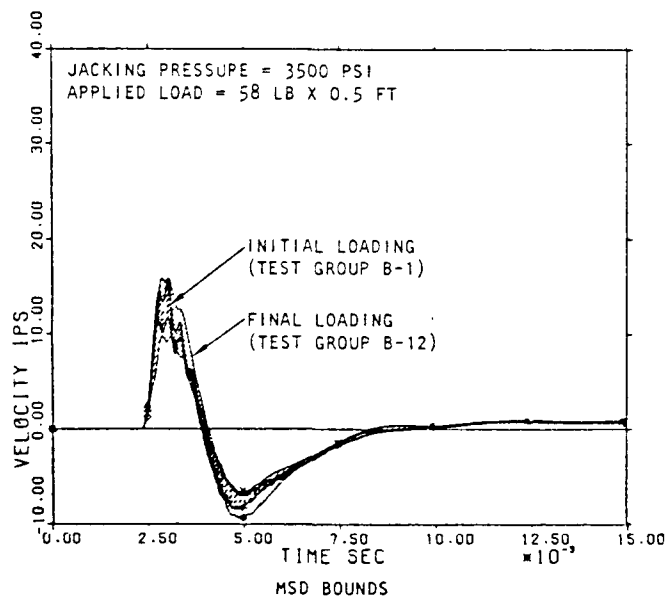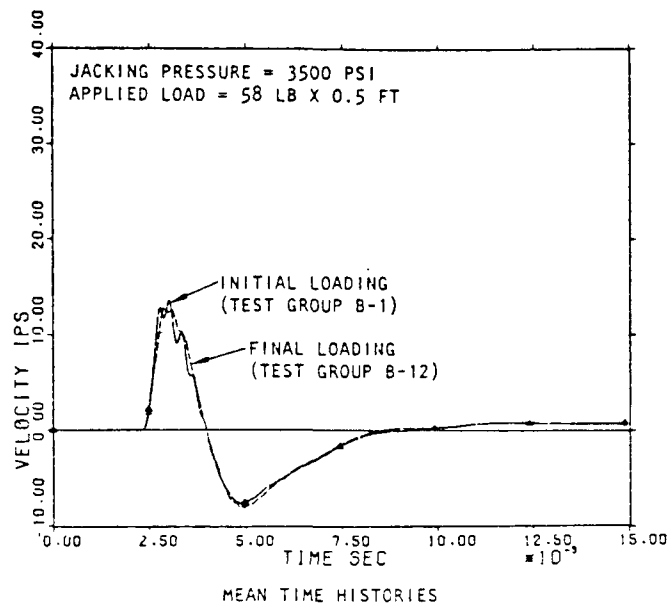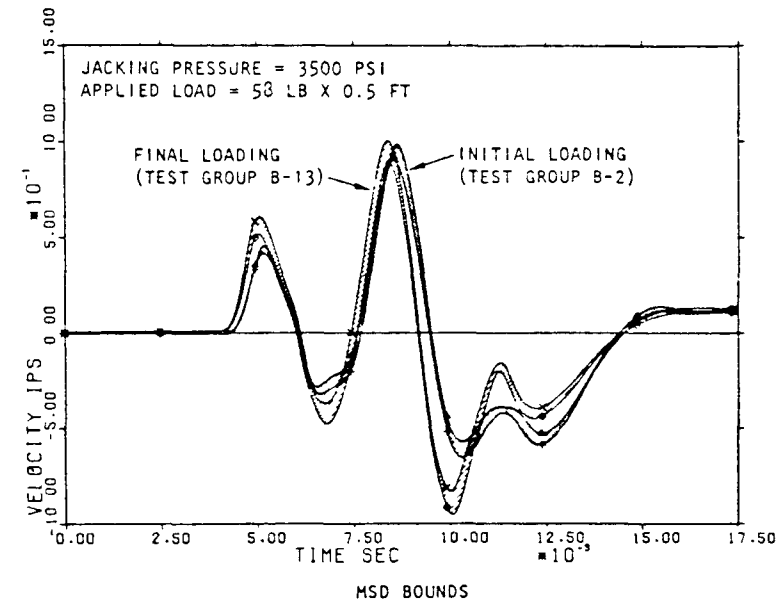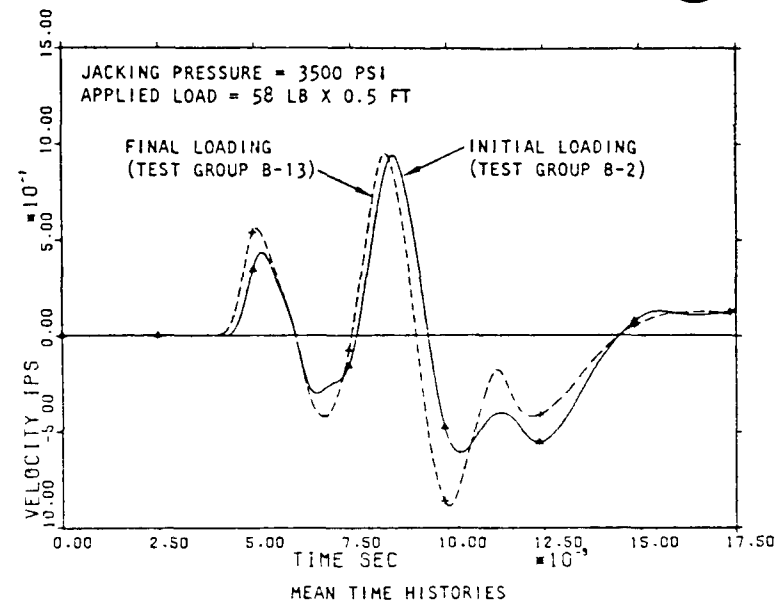
(a) Sensor 21 -- at anchor
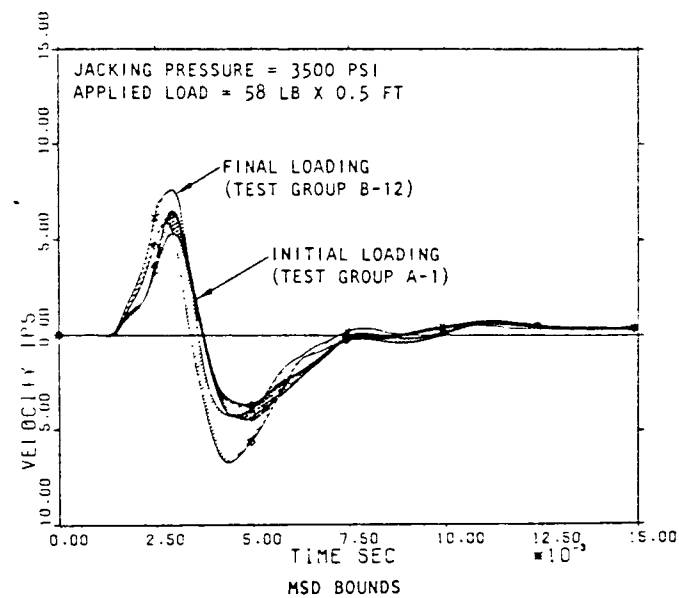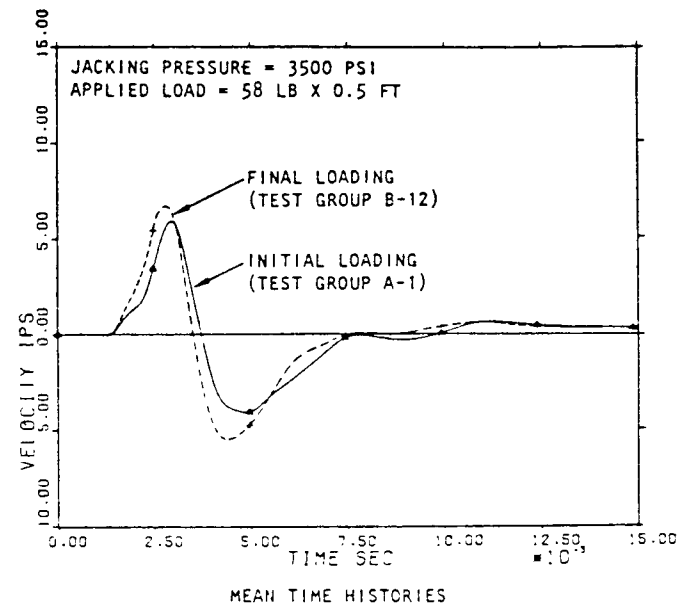
(b) Sensor 1 -- 3 in. from anchor edge

FIGURE F-8. STATISTICAL ASSESSMENT OF PRIOR LOAD HISTORY EFFECTS
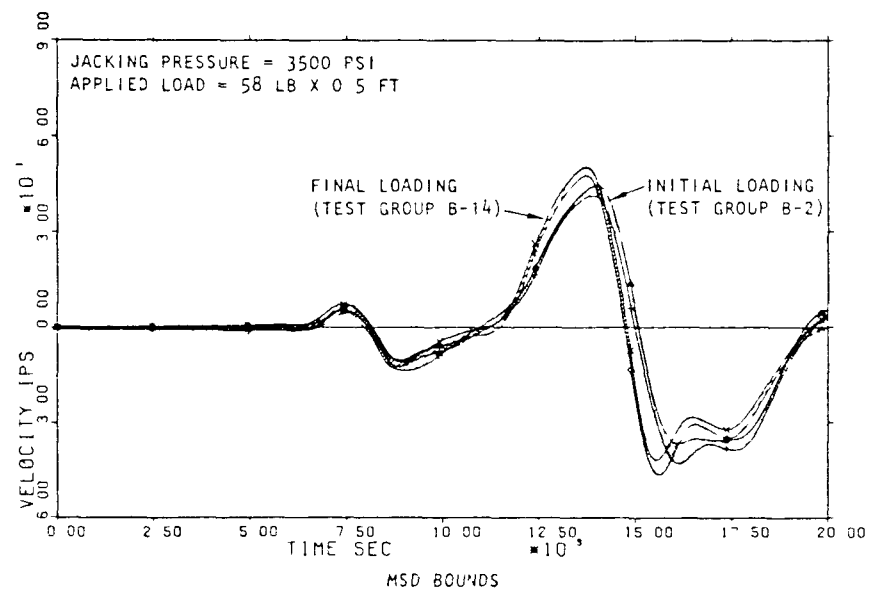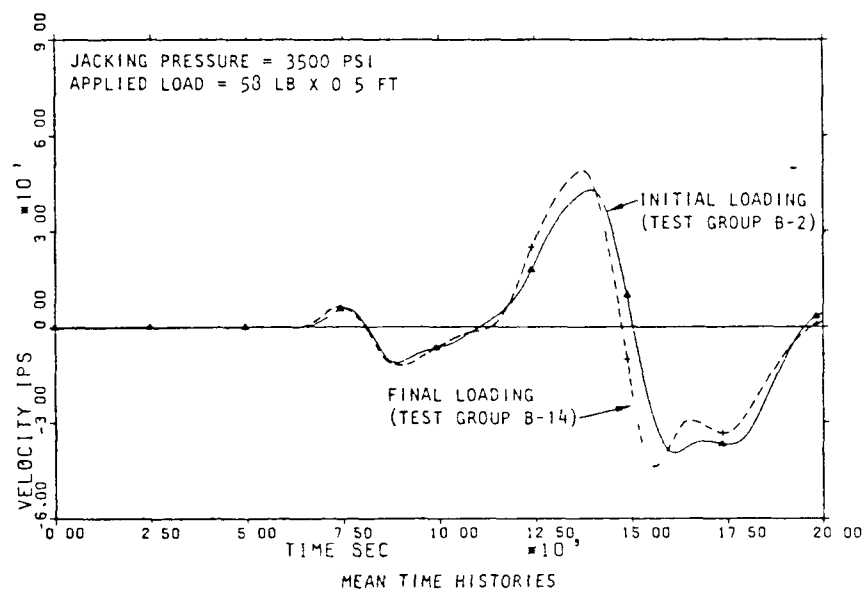
(c) Sensor 3 -- 9 in. from anchor edge

(d) Sensor 17 -- 24 in. from anchor edge

FIGURE F-8.   (CONTINUED)

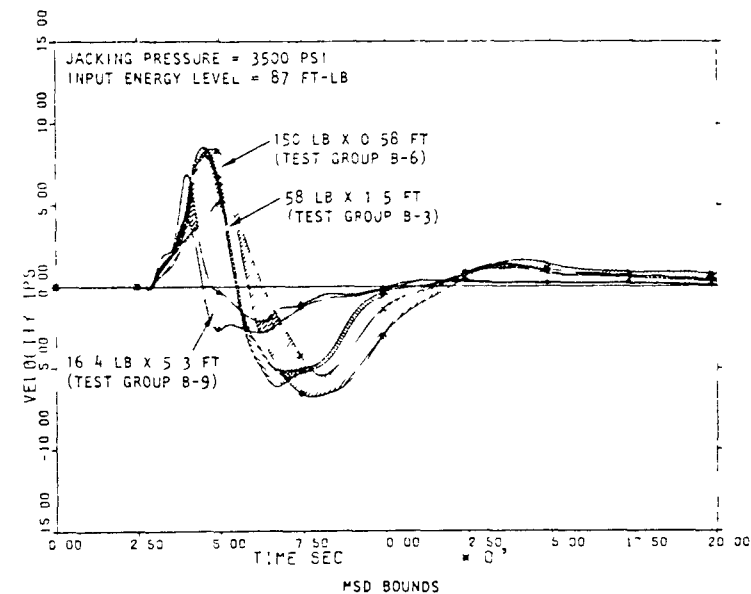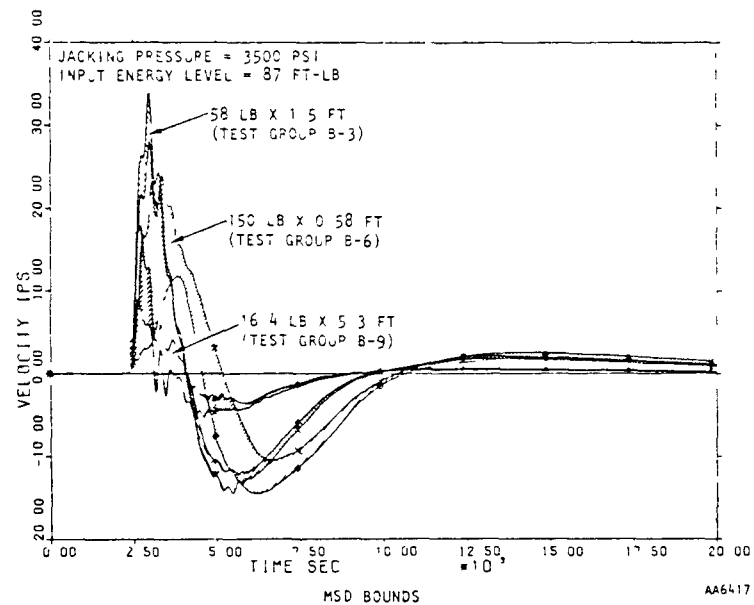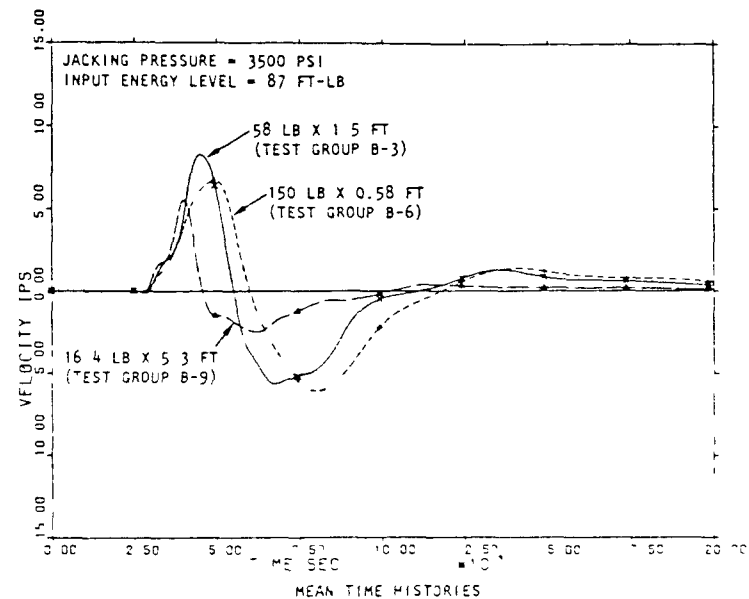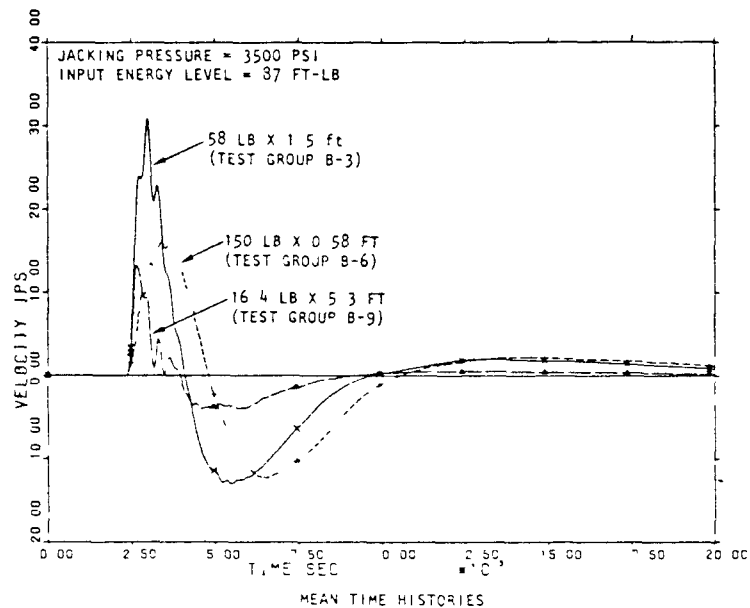(e)   Sensor 14 -- 55 in. from anchor edge

FIGURE F-8.   (CONCLUDED)

fall onto the Belleville springs. However, it is clear that a given energy level can be comprised of any combination of hammer weights and drop heights, and that each combination will represent a different dynamic system with different response characteristics.* Therefore it is important to investigate the degree to which these various combinations might affect the in situ soil response measurements and to gain some insight into those particular ranges of combinations that might be most advantageous for use in subsequent tests.

To investigate these effects as part of the special test program, three groups of tests were conducted. Each test consisted of a different hammer weight-drop height combination whose product corresponded to a total energy level of 87 ft-lb. These three combinations are, respectively, 58 lb x 1.5 ft, 150 lb x 0.58 ft, and 16.4 lb x 5.3 ft. Soil response measurements corresponding to each of these combinations are compared in Fig. F-9.

The results compared in Fig. F-9 show a number of interesting trends. First of all, as expected, the measured soil responses corresponding to each hammer weight-drop height combination are quite different, particularly in the immediate vicinity of the anchor. The largest peak velocity amplitudes tend to correspond to the 58-lb x 1.5-ft combination, while the smallest amplitudes generally occur when the 16.4-lb x 5.3-ft combination was applied. These differences in the peak amplitudes were generally greatest at the anchor and tended to decrease with increasing distance from the anchor.

---

* Changes in the weight of the hammer will affect the total mass of the coupled hammer-Belleville spring-anchor-soil system, while the variations in height of free fall of the hammer will influence its initial velocity as it first strikes the Belleville spring.

(a)   Sensor 21 -- at anchor

(b)   Sensor 1 -- 3 in. from anchor edge

FIGURE F-9.   STATISTICAL ASSESSMENT OF EFFECTS OF VARIOUS HAMMER WEIGHT-DROP HEIGHT
COMBINATIONS FOR GIVEN ENERGY LEVEL
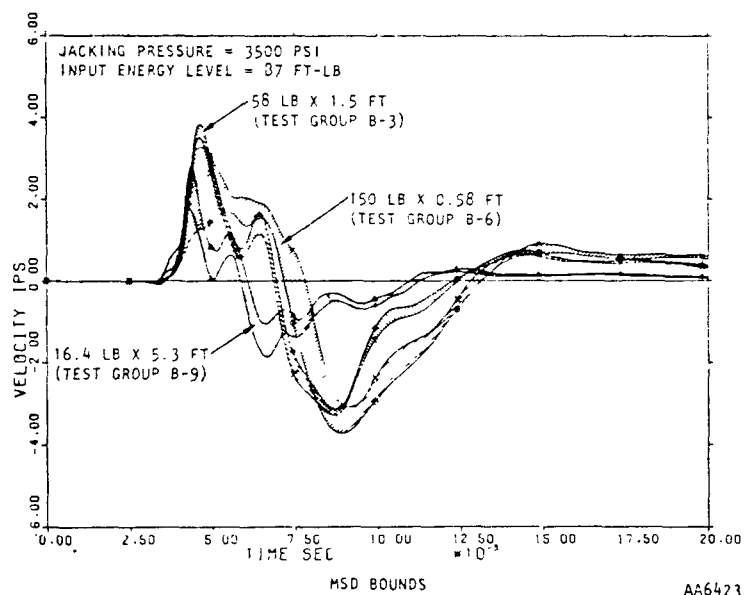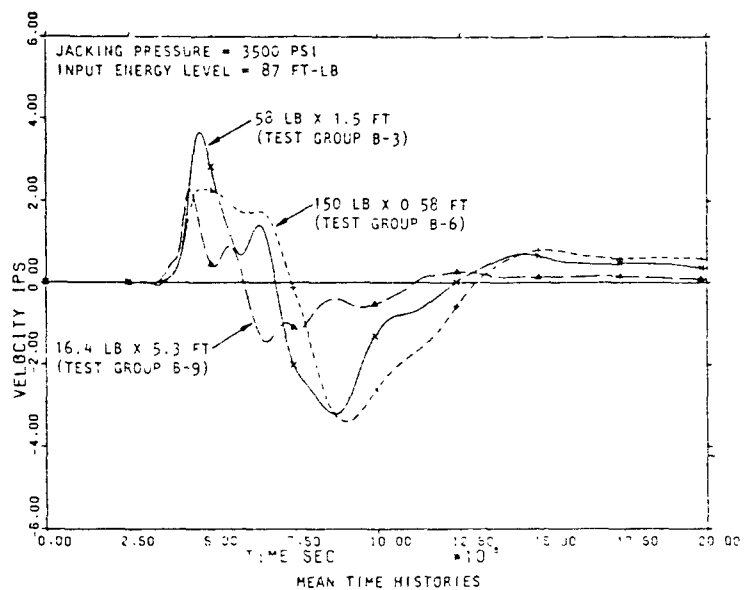
(c) Sensor 3 -- 9 in. from anchor edge   (d) Sensor 7 -- 24 in. from anchor edge

FIGURE F-9.   (CONTINUED)

(e)   Sensor 14 -- 55 in. from anchor edge

FIGURE F-9.   (CONCLUDED)

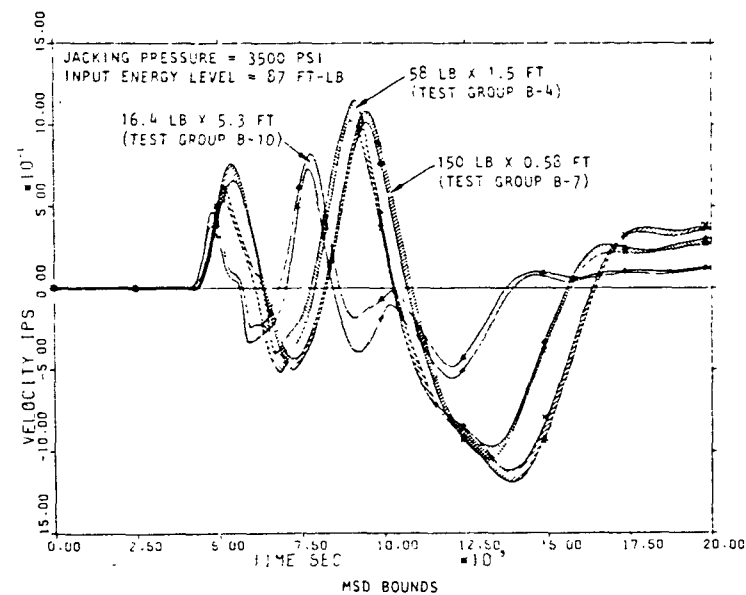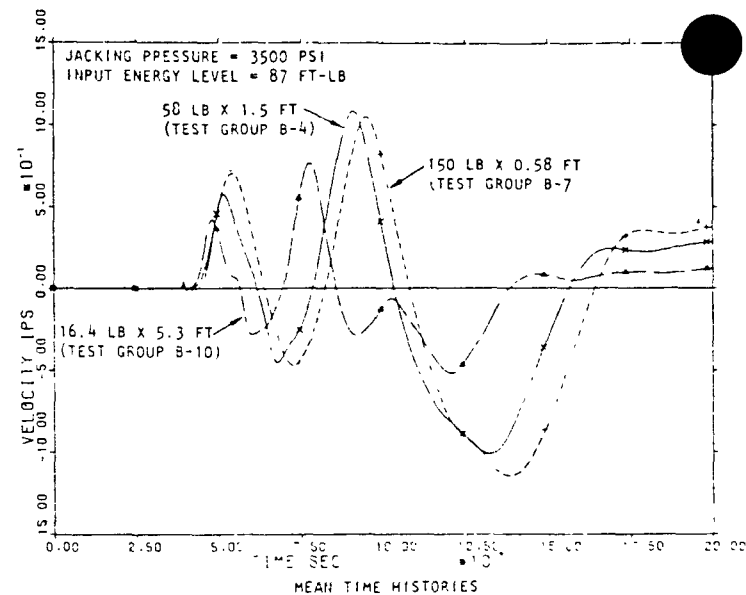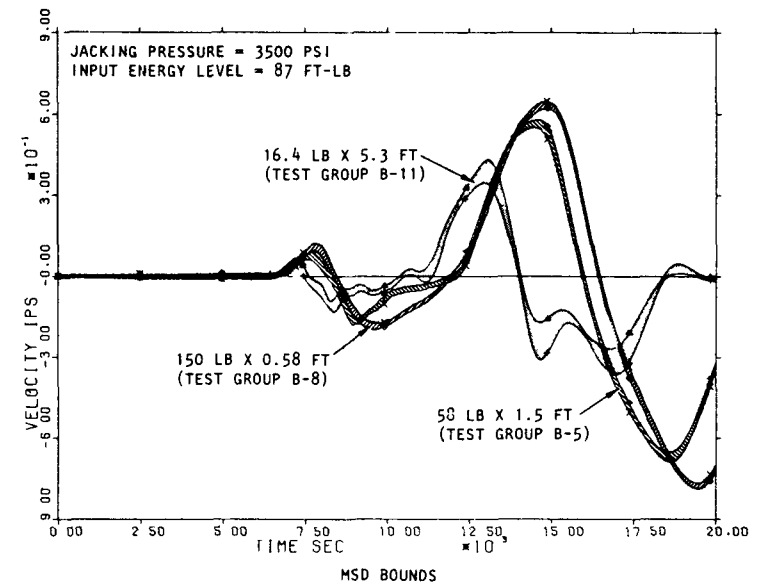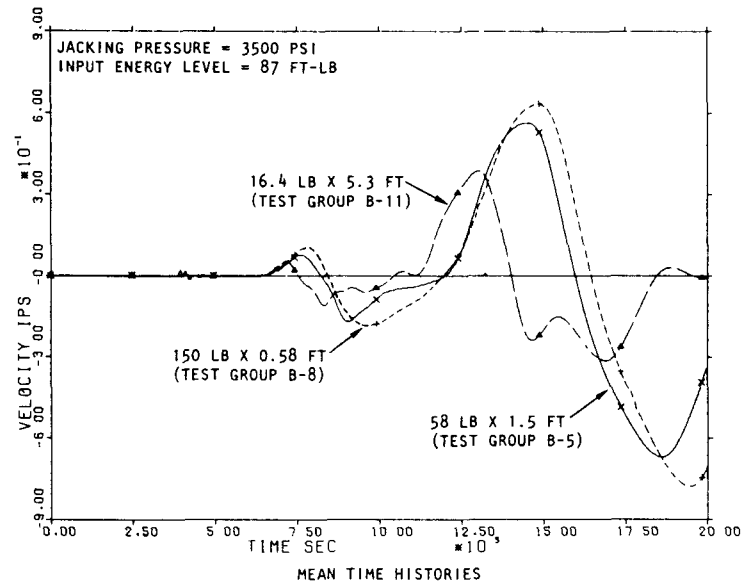Another important trend relates to the width of the various velocity peaks measured during each set of tests. The widest peaks, which correspond to the lowest characteristic frequencies of the soil response, occur when the largest hammer weight, 150 lb, is applied. In contrast, the sharpest peaks, which correspond to the highest characteristic frequencies, correspond to application of the smallest weight, 16.4 lb. This follows from the fact that the characteristic frequencies of the soil response are related to the inverse of the total mass of the system. An increase in the weight of the hammer obviously increases the total system mass, which in turn, will tend to widen the peak response peaks (i.e., reduce the characteristic response frequencies of the system).

A third trend relates to the scatter in the data. In the near-anchor regions, the substantial differences between the MSD time-history bounds from the 150-lb hammer tests indicates substantial scatter, while the widths corresponding to the smaller hammer weights are relatively narrow. However, at sensors located further from the anchor, these differences become small, indicating that the data from the 150-lb hammer tests are quite repeatable in this range. These differences in scatter over different regions of the soil may be attributed to the non-uniformities in the load applied by the heavy hammer, which might occur, for example, if the hammer is not flush when it first strikes the Belleville springs. Apparently, tests conducted using a heavier hammer are more prone to such non-uniformities than are tests with lighter hammers, possibly due to increased difficulty in handling the heavy hammer in the field. As the distance from the anchor increases, the soil response measurements become less sensitive to these non-uniformities.

As a final point, it is appropriate to compare the results from initial tests at a low energy level of 58 lb x 0.5

ft (Fig. F-8) to the results indicated for the higher energy level (Fig. F-9). To carry out and interpret these comparisons, it must first be noted that the hammer weight influences the measured soil responses in two ways. First it affects the input energy level and dynamic loads to which the soil is subjected. Second, once the hammer makes contact with the Belleville springs, a coupled dynamic system is formed that consists of the hammer, springs, anchor, and soil. The weight of the hammer affects the inertial characteristics of this coupled system and thereby affects the manner in which this system responds to dynamic loads.

With this in mind, a comparison of the results from the high-energy and low-energy tests that correspond to the same hammer weight (58 lb) can first be made. This comparison indicates that the 58-lb x 1.5-ft loading (Fig. F-9) results in soil velocity amplitudes that are consistently higher than the soil velocity amplitudes corresponding to the 58-lb x 0.5-ft loading (Fig. F-8). These differences are as much as a factor of 2.5 at the anchor (e.g., a mean velocity of over 30 ips in Fig. F-9a vs. about 12 ips in Fig. F-8a) and range from about 25 to 35% at the various soil sensors. However, when the hammer weight used in the high-energy tests differs from that used in the low-energy tests, no such consistent trends can be observed. Figs. F-8 and F-9 indicate that, at a given sensor, the peak velocities from the high-energy tests using the 16.4-lb hammer and 150-lb hammer were not necessarily greater than those from the low-energy tests using the 58-lb hammer; in fact, at some sensors (e.g., Sensor 3) the low-energy tests produced higher peak velocity amplitudes than did the high-energy tests using the different hammer weights. These comparisons indicate that:

a. An increase in the input energy level caused
    by changing the hammer weight will not
    necessarily result in increased soil response
    amplitudes. This is because the change in
    inertial characteristics of the coupled hammer-
    spring-anchor soil system due to the changed
    hammer weight may in some cases be more important
    than the corresponding change in input energy
    level and may not tend to increase the soil
    response.

b. An increase in the input energy level caused
    by maintaining the same hammer weight and
    increasing the drop height will increase the
    soil response amplitudes. For this case, the
    inertial characteristics of the coupled system
    are unchanged; only the initial velocity of the
    hammer as it strikes the Belleville springs is
    increased because of its increased drop height.

F-3.5 Jacking Pressures

     In order for loads to be transmitted from the anchor
to the borehole, adequate coupling must be maintained along
the anchor-soil interface. As described in Chapter 2, this
coupling is developed by means of a vertically oriented hydraulic
piston within the anchor. This piston, when expanded, forces a
system of arms against the curved anchor bearing plates, forcing
them outward and pressing them tightly against the sides of the
borehole. A pump and gage located at the ground surface controls
and maintains the hydraulic jacking pressures in the piston.

     It is clear that the jacking pressures, applied as
indicated above, represent a key component of the in situ soil
test system. If these pressures are too low, slippage of the

anchor will occur and adequate energy will not be transmitted to the soil medium. Alternatively, if the pressures are too high when compared to the dynamic stresses induced in the soil during the in situ test, they could affect the subsequent shear modulus measurements and, in the extreme, could induce shear failures in the soil surrounding the borehole.

The above discussion indicates the necessity of establishing a range of jacking pressures that will result in adequate coupling of the anchor to the soil, while not affecting the dynamic properties of the soil medium or inducing shear failures along the borehole. Therefore it is important to first define reasonable ranges of jacking pressures that can be applied by the hydraulic piston, and then to determine the extent to which the soil response measurements are affected by these ranges of pressures.

To carry out the statistical evaluation of this part of the special test program, three sets of tests were conducted, corresponding to radial jacking pressures of 2000 psi, 3500 psi, and 5000 psi. For each set of tests, repeated loadings corresponding to a 58-lb hammer dropped 0.5 ft were applied, and soil velocity time histories were recorded during each application of these loadings. The resulting ensembles of time histories, measured at each sensor and corresponding to each jacking pressure level, were then analyzed statistically to develop composite time histories corresponding to a mean and to MSD bounds. These composite time histories at each sensor were then compared to indicate the sensitivity of the soil response to the assumed variations in jacking pressure.

Comparisons of the various composite time histories for the different jacking pressures and different sensors are shown in Fig. F-10. These comparisons indicate the following trends:
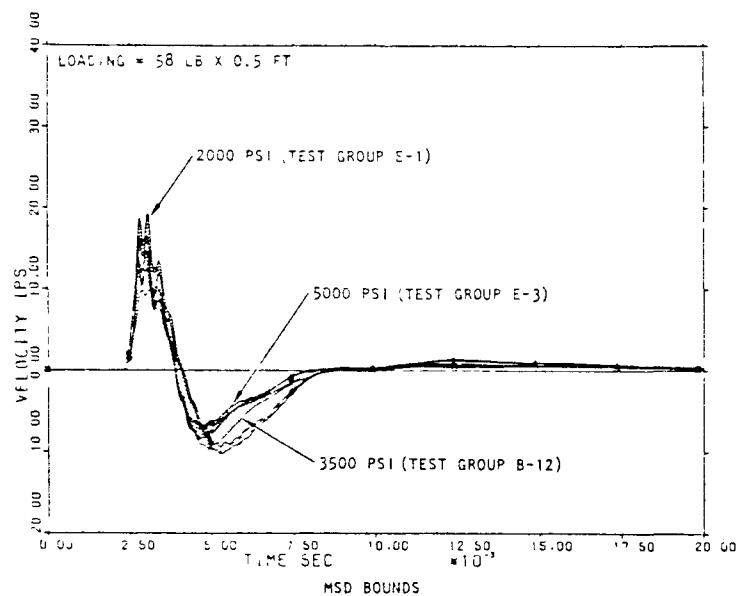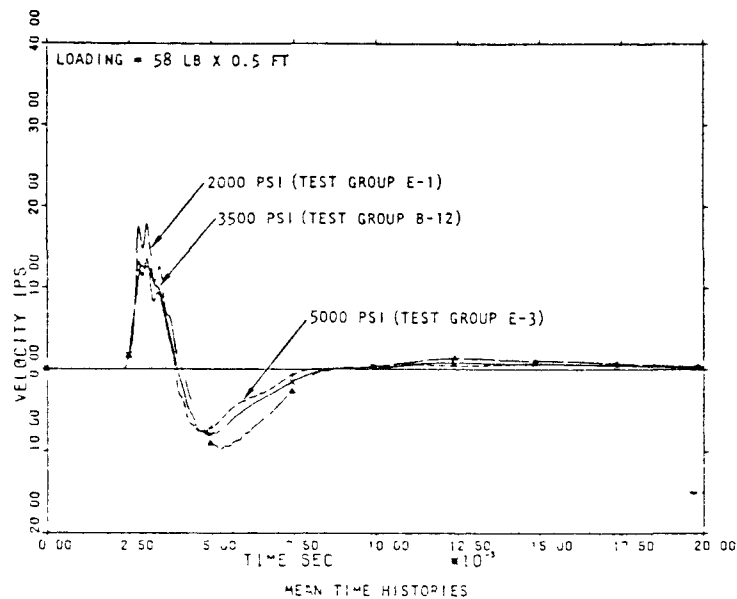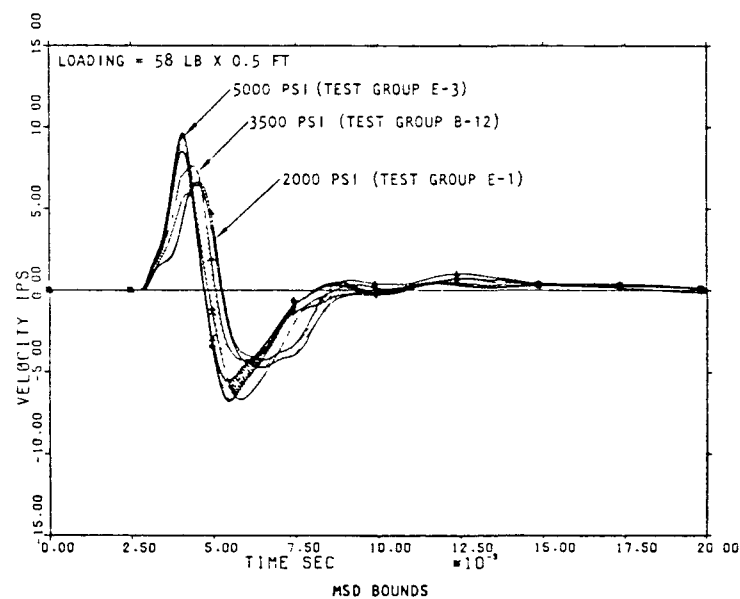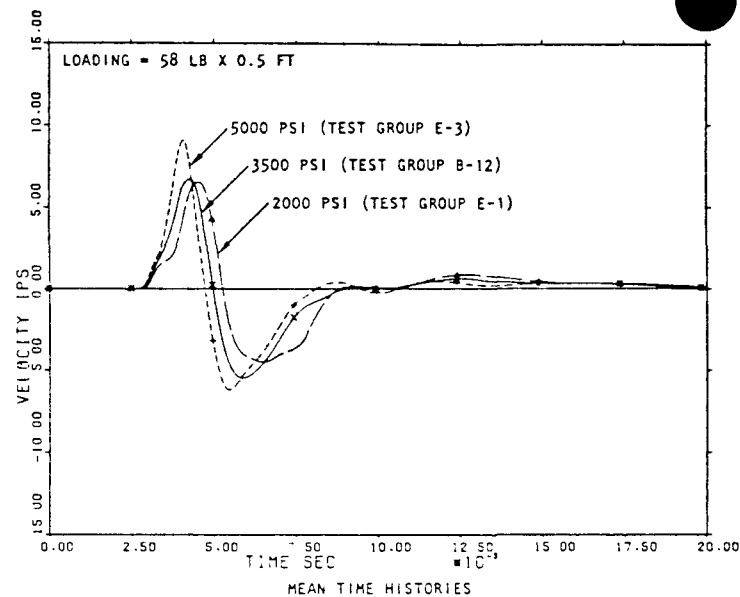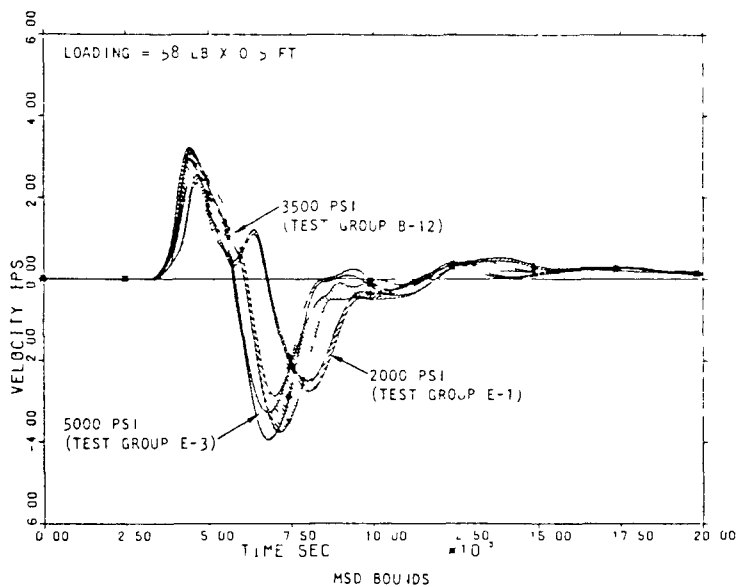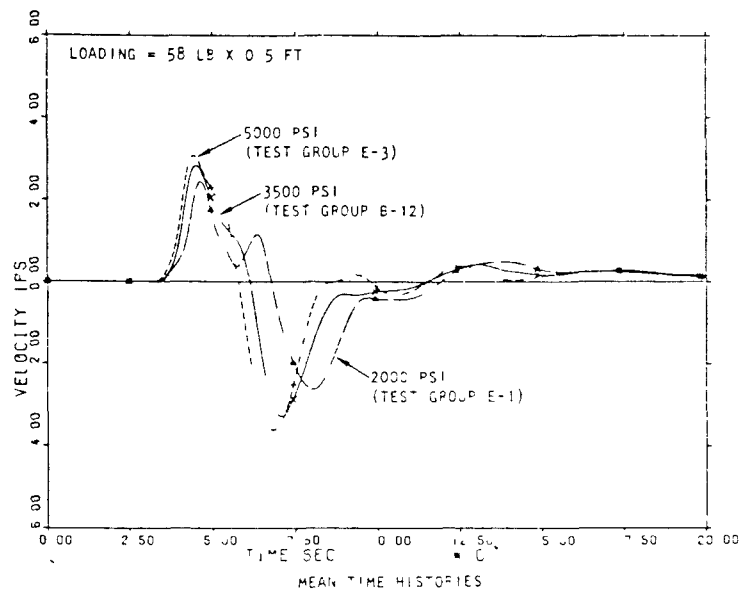
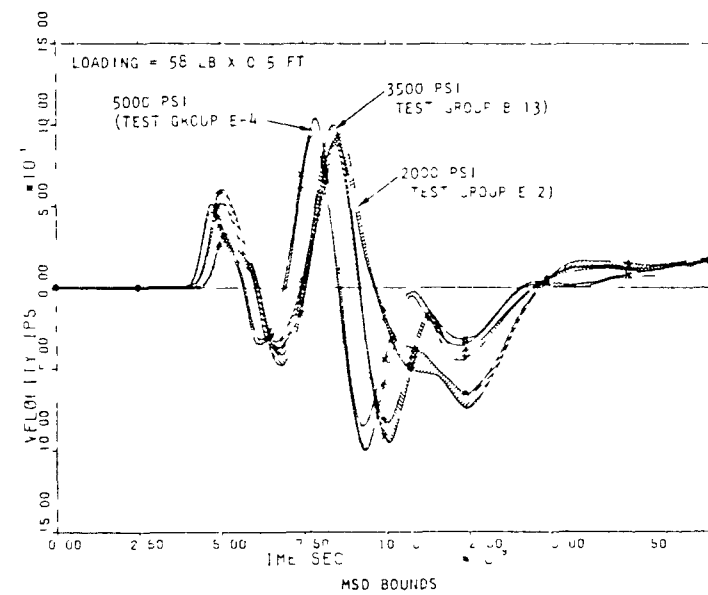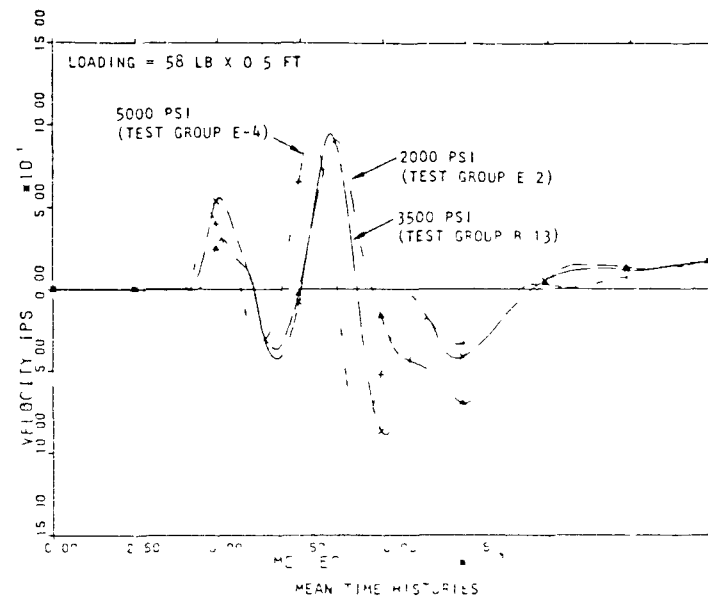(a)   Sensor 21 -- at anchor   (b)   Sensor 1 -- 3 in. from anchor edge

FIGURE F-10.   STATISTICAL ASSESSMENT OF EFFECTS OF JACKING PRESSURE

(c) Sensor 3 -- 9 in. from anchor edge   (d) Sensor 7 -- 24 in. from anchor edge

FIGURE F-10. (CONCLUDED)

a. At the anchor, the velocity histories corresponding to the 2000 psi level exhibit slightly larger peak velocity amplitudes; in contrast to this, the peak velocity amplitudes corresponding to this low jacking pressure that were recorded at Sensors 1 and 3 exhibited somewhat lower peak velocity amplitudes. At Sensor 7, differences in peak velocity amplitudes corresponding to the three jacking pressure levels are negligible. This suggests that greater slippage occurs along the anchor-soil interface during the tests conducted at the lower jacking pressure; however differences between the velocity amplitudes from the three jacking pressure levels were not substantial, suggesting that any slippage that might have occurred is small. Furthermore, effects of this slippage appear to be confined to a region only in the immediate vicinity of the anchor.

b. No significant trends could be observed regarding differences in velocity histories due to changes in jacking pressure of from 3500 psi to 5000 psi. Only slight, highly localized differences between the velocity histories corresponding to these two jacking pressures could be observed (see Fig. F-10b corresponding to the Sensor 1 measurements), but these are not significant in view of the negligible differences between the measurements at the other sensors.

The above trends suggest that for the input loading conditions, soil properties, and ranges of jacking pressure considered in these special tests, the variations in jacking pressure have a negligible effect on the soil response measurements. The potential effects of jacking pressure should be kept in mind when using the in situ soil test at other soil conditions and possibly for larger loads; however the special test results suggest that, for reasonable ranges of jacking pressures and input loads, the effects of jacking pressure on

the in situ dynamic soil properties will be confined to a highly
localized region around the anchor. Reasonable jack pressures
should not affect the overall free-field soil response
measurements to any substantial degree as long as slippage is
not excessive producing, in effect, distorted wave shapes.

F-4   SUMMARY AND CONCLUSIONS

This appendix contains results of a statistical assessment
of results obtained during a comprehensive special test program,
whose purpose was to investigate the effects of certain key test
parameters on the in situ soil response measurements. The para-
meters investigated correspond to repeatability of the data,
symmetry and shadow effects, prior load history effects, the
effects of variations in hammer weight and drop height for a
given input energy level, and jacking pressure effects.

The use of statistical assessments of an ensemble of test
results, as described in this appendix, provides a meaningful
basis for evaluating trends that arise from variations in the
test parameters. They offer one advantage over nonstatistical
studies based on a limited number of tests, since they indicate
to what extent scatter in the data may influence apparent trends
that are observed. Since any number of systematic or random
effects can lead to data scatter in a complex testing approach
of this type, it is important that this scatter be considered
in this manner. If, as shown, the statistical data indicates
a high level of repeatability and small scatter of data, non-
statistical studies can be conducted also to evaluate these
same effects in greater detail, as well as other effects not
included herein. The results of these additional studies are
presented in the next appendix.

Results of this statistical assessment have indicated
certain clear-cut trends regarding the effects of the various

test parameters on the soil response measurements. Of course, judgement must be exercised when extrapolating these particular trends to other site conditions and other load applications; nevertheless, the results contained in this appendix serve to increase our understanding of the overall in situ soil testing approach.

The particular trends observed from this statistical assessment of the special test data are as follows:

a.   The measured velocity histories are generally quite repeatable, as evidenced by the close correlations between the overlaid time histories and the relatively narrow widths of the composite velocity histories corresponding to MSD bounds. The only lack of repeatability occurred at near-anchor soil response measurements when an extremely heavy hammer (150 lb) was used; this suggests that, in future in situ soil test applications, hammers of a more moderate weight should be used to avoid this potential source of data scatter.

b.   Except for minor differences in rise times to peak velocity caused at least in part by minor differences in sensor distances from the anchor, symmetry and shadow effects did not appear to influence the soil response measurements to any substantial degree. It is noted, however, that in these studies, sensors located along axis X-X in Fig. F-1b, were deliberately staggered so that their clear spacing was within guidelines set by prior analytical solutions for avoiding shadow effects (Appendix E).

c.   For the conditions considered in these special tests, prior load history effects were shown to have a negligible effect on the soil response measurements.

d.   The particular hammer weight and drop height used
to represent a given input energy level could have an important
effect on the resulting soil response measurements, particularly
near the anchor. An increase in the input energy level, by
changing the hammer weight and drop height relative to prior
tests conducted at lower energy levels, will not always result
in increased soil response amplitudes relative to these low
energy tests. Therefore, it is important to utilize the parti-
cular hammer weight-drop height combination that maximizes the
near-anchor soil response for a given energy level; trial-and-
error field tests or analytical solutions may be required to
establish these combinations.

e.   The range of jacking pressures considered in these
special tests resulted in only highly localized effects on the
near-anchor soil responses and did not affect the overall soil
response characteristics to any noticeable degree.

APPENDIX G

GENERAL ASSESSMENT OF SPECIAL TEST RESULTS

APPENDIX G

GENERAL ASSESSMENT OF SPECIAL TEST RESULTS

When a test procedure is being studied with experimental testing, there are always minor adjustments or measurements that can be readily incorporated or accomplished which can provide greater insight into a number of test conditions or parameters. A number of these parameters were evaluated statistically in the previous appendix. From these studies, it was generally shown that from repeated tests, there is a high level of data repeatability and that with few exceptions the scatter of data is generally small. As a result, it was considered desirable to study some of this same data together with supplemental test data using a non-statistical approach. This approach was necessary because these supplemental tests were not repeated a large number of times and were originally obtained under the assumption that the data, as indicated in the previous appendix, is repeatable. Rather, these tests are fewer, but cover a wider range of test variables. In particular, those parameters or conditions studied in this appendix include:

    a.   Casing effects.

    b.   Anchor coupling effects.

    c.   Symmetry effects.

    d.   Studies of sensors at different elevations.

    e.   Horizontal motion characteristics (P-wave effects).

    f.   Attenuation of motions.

Most of these results are based on a direct review of the data followed by a semi-empirical evaluation of the results.

G-1 CASING EFFECTS

One objective was to determine if casing could be used with the production test primarily to retain soils highly subject

to caving. For this program, four types of casing were
systematically hand placed within the backfill material along
with adjacent free field sensors. These casings consisted of
3-inch ABS plastic casing, 3-inch aluminum casing, 3-inch corru-
gated (vac-u-flex) hose, and 3-inch standard steel casing.
Two groups consisting of two casings and a free field sensor
as shown in the plan, Fig. 5-1, were positioned together each
about 45 inches from the closest part of the anchor. This
distance was considered representative of that distance between
the anchor and the first sensor location in the conventional
test. Then sensors were lowered inside each casing and coupled
at the depth (elevation -5 feet) immediately adjacent to each
free field sensor. Simultaneous measurements from sensors
in the anchor, the free field, and each of the two adjacent
casings were then made. Comparisons of corresponding signal
shapes, amplitudes and times of arrival could then be accom-
plished, studied and evaluated.

From these tests the following results were obtained:

a) Average variation of particle velocity amplitudes
with free field measurements:

Plastic Casing   Amplitude of signal in casing was   7% low
Aluminum Casing   Amplitude of signal in casing was 35% low
Corrugated Casing   Amplitude of signal in casing was 26% high
Steel Casing   Amplitude of signal in casing was 29% low

b) Time lag between free field sensors and sensors in
casing:

Plastic Casing   Signal arrived .46 msec later in casing
Aluminum Casing   Signal arrived .68 msec later in casing
Corrugated Casing   Signal arrived .03 msec later in casing
Steel Casing   Signal arrived .73-1.77 msec later in casing

These data in general reflect the logical conclusion that the more resistant or stiffer the casing to vertical motion, the smaller is the resulting amplitude of the measured signal and the greater is the lag in time from the free field condition.

In addition to these results, the shape of the primary velocity signal recorded in the casings was only slightly altered from the signal recorded by the free field sensors. As a result of this and the above results, a valid conclusion would be that any of the four casings could be used in sensor holes provided adjustments in time and amplitude are accomplished, when applying the data with sensors on the anchor. When considering all of the above factors, the plastic or the corrugated casing appears to be the best of these casings for practical use with this test. Of these two, the plastic casing is probably the better primarily because it is far easier to handle and install. The steel casing produced the largest variation in time. Since time is a very sensitive parameter, much more so than amplitude, these large variations or lags in time are not desirable and therefore the steel casing is the least desirable of the four casings.

Based on the above data, the following time and amplitude adjustments are recommended for use with the in situ test:

Casing	Time (msec)	Amplitude % Increase
Plastic	.4	0
Aluminum	.6	35
Corrugated	0	-25
Steel	1.2	30

The adjustment in time is only made for the sensors within casing (i.e., the Equivalent Free Field Time = Measured Time in casing less the above adjustment).

To study the importance of anchor coupling effects in the near-anchor region, a number of tests were conducted to obtain measurements at or near the anchor under different jack pressures. By comparing force and response characteristics of the anchor and the response of the first "close-in" adjacent sensor (Sensor No. 1) as a function of jack pressure, the importance or influence of this parameter on the near-anchor responses can be shown.

To study this effect in relation to the forcing character-istics applied to the anchor, the jack pressure is first compared in Fig. G-1 with the load measurements obtained at the top of the anchor with the load cell. Significant measurements from the typical triangular or parabolic load pulse are the peak load value, F_1, the total load pulse duration time, T_d, and the rise time of the pulse, T_r. For this comparison, the drop height and mass are held constant while the jack pressure is varied over five different values.

In the upper plot, the applied load first increases as the jack pressure increases, reaching a maximum for $\sigma_j = 3,500$ psi, and then decreases for higher jack pressures. These results would indicate that the anchor-soil system becomes more rigid as the radial stress applied to the soil increases within the limits of the elastic state. This fact is to be expected, since a higher radial stress in general increases the resistance to slippage. However, excessive jack pressures cause higher radial stresses which combined with the stresses generated from the impact may exceed the bearing resistance of the soil, thus explaining the drop in the applied load at higher jack pressures. The rise and the duration times of the load pulses follow the same trend as the maximum load. The total impulse defined as the area of the load-time curve also has a maximum value for
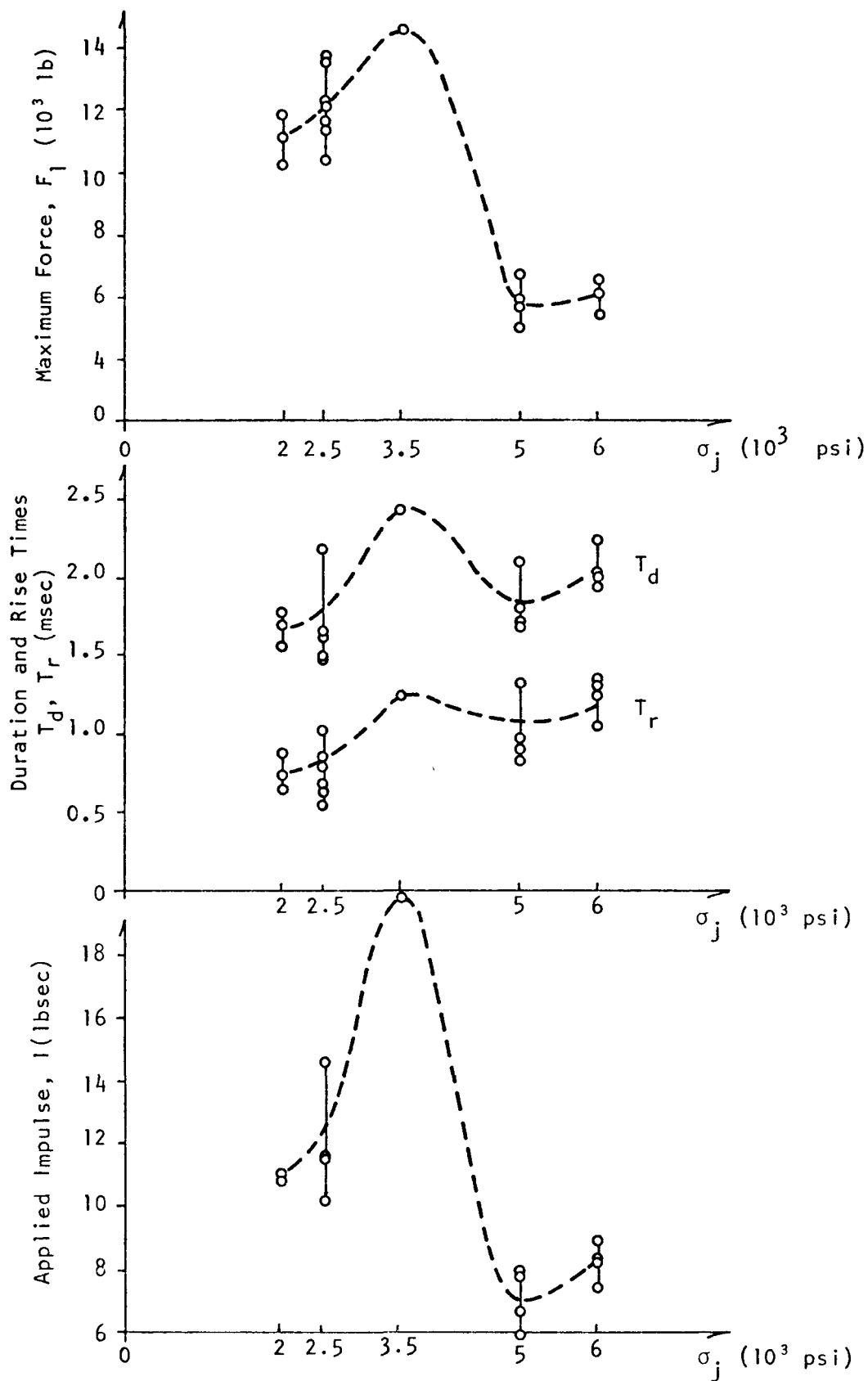
FIG. G-1   EFFECT OF JACK PRESSURE ON APPLIED LOAD FOR
CONSTANT ENERGY.   W = 58 x 0.5 lb ft

σ_j = 3,500 psi.

The skewing constant $\sigma = T_r/T_d$ of the load pulse has an average value of .51 for these tests with a tendency to increase from .4 for smaller to .6 for larger jack pressures. These values indicate that the load pulse is symmetrical for the intermediate pressure of 3,500 psi, it has a steeper rise time for smaller pressures and it decays faster for larger pressures. For the tests performed at the constant jack pressure of 3,500 psi the average σ is .48.

The response characteristics of the anchor to an impact also depend on the degree of coupling with the soil mass. Fig. G-2 shows the effects of increasing the jack pressure, from 2,000 psi to 6,000 psi, on the velocity and displacement of the anchor, and Sensor No. 1 under a constant hammer weight and height of drop. It is observed that the velocity and the displacement at the anchor decrease to minimum values for σ_j = 3,500 psi and then slightly increase for the higher σ_j = 5,000 and 6,000 psi. This agrees with the results obtained in the load measurements, in that the anchor-soil system increases in rigidity as the jack pressure increases to a certain limit and then it becomes softer as the bearing capacity of the soil is exceeded. Therefore, based on this trend, there appears to be an optimum jack pressure (in this case 3,500 psi) which makes the anchor-soil system most rigid and, permits the most efficient transmission of higher shearing stresses to the soil mass. This important effect of the jack pressure is further confirmed by comparing the maximum displacement of the anchor with the maximum displacement of Sensor No. 1, located 3.19 inches from the edge of the anchor. In the lower plot of Fig. G-2 it is shown that the differences in peak displacements decrease and the two curves tend to converge as the jack pressure increases. This indicates that as the radial stress is gradually increased less slippage at the interface occurs.
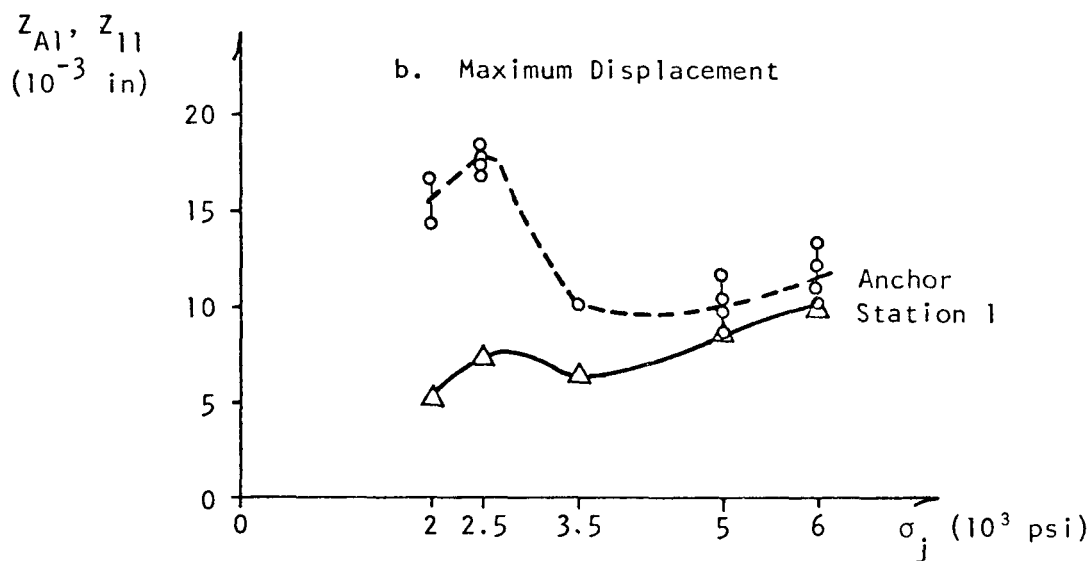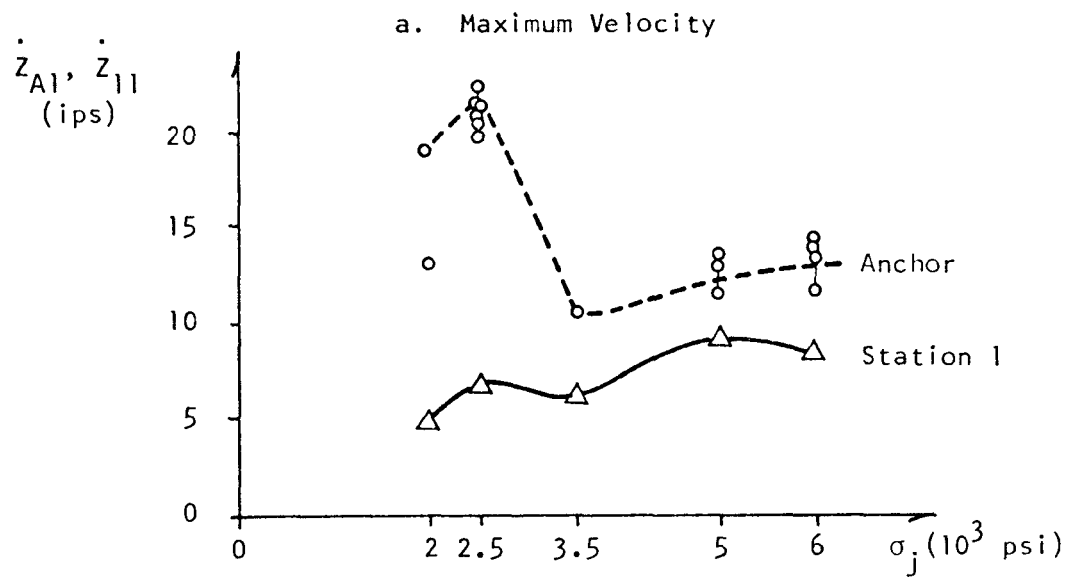
FIG. G-2   MOTIONS OF THE ANCHOR AND STATION NO. 1 FOR
            DIFFERENT JACK PRESSURES.   IMPACT ENERGY W =
            58 x 0.5 lb ft

These two curves, because they do not converge even at the
very high pressures indicate that 100 percent coupling, for
even this moderate drop height and hammer weight, is probably
not possible and that some permanent displacement or anchor
slippage occurs with each impact.

G-3   SYMMETRY EFFECTS

This part of the testing program was conducted to establish
the importance of placing holes along a single axis or band
versus on a radial pattern 120 degrees apart. Practically, a
radial pattern is desirable for two reasons. First, closely
spaced boreholes are less likely to become interconnected either
physically or hydraulically because they are drilled farther
apart. Finally shadow effects of holes between the anchor
boring and more distance holes do not become a consideration.

For data interpretation, the holes placed in a line have
the distinct advantage of measuring velocities along one vertical
plane, eliminating the possibility of encountering different
soil types if measurements are made along different radial paths.

For this evaluation, sensors were positioned at different
points radially throughout the test fill as shown in the plan
Fig. F-1. In general, the borings designated A were compared
with their twin sensor located in the main band. Simultaneous
measurements obtained from these sensors of near equal distance
from the anchor but along different radial patterns were made
for this study.

Comparisons of amplitudes of two near equal distant "close
in" sensors (within one foot of the anchor) produced variations
in peak particle velocity amplitudes by as much as 20% at res-
pective stations. For these close-in distances, this is not
unusual and was partly due to minor differences in the travel

distance (Appendix F) and to the fact that in this region, the measured signature is the result of two waves (P & S waves) superimposed upon each other. Because these two waves are traveling at very different speeds (Section 5.2), each component of the wave is tending to separate rapidly producing a highly distorted signal. This distorting effect greatly influences the measured peak amplitudes, especially if the travel distances are slightly different. At greater distances, the difference in amplitudes was not this large. Comparison of decay rates of peak particle velocities with distance at two simultaneous stations each on two different radial planes indicated nearly identical values (i.e., where the "close-in" particle velocity was lower along one radial plane than another, it was always lower at other points along that same plane. This suggests that the anchor is sending consistent trains of waves that behave the same in all directions, however, the strength or amplitude of the signal leaving the anchor may be slightly different. In later production tests, simultaneous measurements of the particle velocity on different plate segments of the anchor also produced amplitudes that varied in amplitude by as much as 20%. This variation is probably due to the inability to make two flat masses (the hammer and striking plate) hit evenly every time especially when these masses are usually located deep below the ground surface within a heavy drilling mud.

Fortunately, the particle velocity amplitude close-in is not a sensitive parameter, because at high strains (10^{-1}%) the modulus change is not large. As a result, if the amplitude or the strain computed from this amplitude is off by 20% or even larger, the end result of a modulus versus strain plot is altered an essentially insignificant amount.

Comparisons of travel time between sensors equal distances from the anchor but along different horizontal lines were also conducted as also described in Appendix F. Since time is used

directly to compute velocities and thus moduli, it is considered much more sensitive to minor variations. Because of distortions in the composite signals "close-in", the only repeatedly consistent point on the signature was the first arrival. At more distant recording stations (i.e., greater than about one foot from the soil anchor interface) the conventional point of zero crossing was used because the first arrival points were not discernable. Data of arrival times from nine different tests (36 time histories) using the same impact energy were all normalized with respect to the closest station and each point plotted with respect to distance regardless of the radial position of the station. The close-in data produced one smooth curve with all points falling on the line. A scatter in the points was almost undetectable.

For the more distant sensors, the typical variation in time at similar stations was of the order of ±.2 msec. However, data from any successive test, when compared with other tests produced only a small change in the average velocity (determined as the slope of the line between those stations). This variation therefore, reflects that in this fill, measurements taken along different propagation paths through different soils can produce differences in the propagation velocity. It was determined from the different wave velocities measured along the single line of sensors that local soil differences could account for slight variations in velocities. These facts, therefore, lead to the conclusion that where possible for production testing, sensor holes should be accomplished along a single plane to obtain the best data possible. Where it is not possible, the radial pattern should produce reasonable results, however any local variations in the soil at random depths may produce slight time shifts which will not always produce a consistent change in velocity with strain. In such cases averaging of velocities may be required at some depths.

G-4 STUDIES OF SENSORS AT DIFFERENT ELEVATIONS

Two vertical sensors were located on the plane at
Elevation -3.25 feet, or 1.75 feet above the main plane of
testing, and two others at Elevation -6.42 feet, or 1.42 feet
below that plane. The radial distances from the anchor were about
the same as those of the sensors No. 4 and No. 10 on the band.
The location of these sensors is shown in Fig. G-3.

Measurements with these sensors were accomplished to obtain
a preliminary picture of the waves around the anchor, to compare
with results obtained in the finite element calculations (Chapter
4) and to observe the distribution of deformations with time at
the approximate levels of the top, middle and bottom of the
anchor. Tests for this study were performed with both the
hydraulic and pneumatic anchor.

For the hydraulic anchor, the vertical displacement-time
histories of the top, middle and bottom stations at the radial
distances of 16.39 to 16.64 inches are shown in Fig. G-4. The
vertical displacements using the pneumatic anchor are presented
in Fig. G-5. Sensor No. 34 failed at the beginning of the tests
and the records obtained could not be used.

At the closer distances, displacements using the hydraulic
anchor are large at the middle and bottom sensors and much
smaller at the top. This ununiform distribution of displacements
indicates that the motions of the stations correspond to the
superposition of pulses from different waves propagating outward
and downward from the anchor.

The displacements obtained from the pneumatic anchor appear
more representative of a pure shearing condition and typical of
the data obtained from the finite element analysis. In general
at both the closer sensors and the more distant ones, the recorded
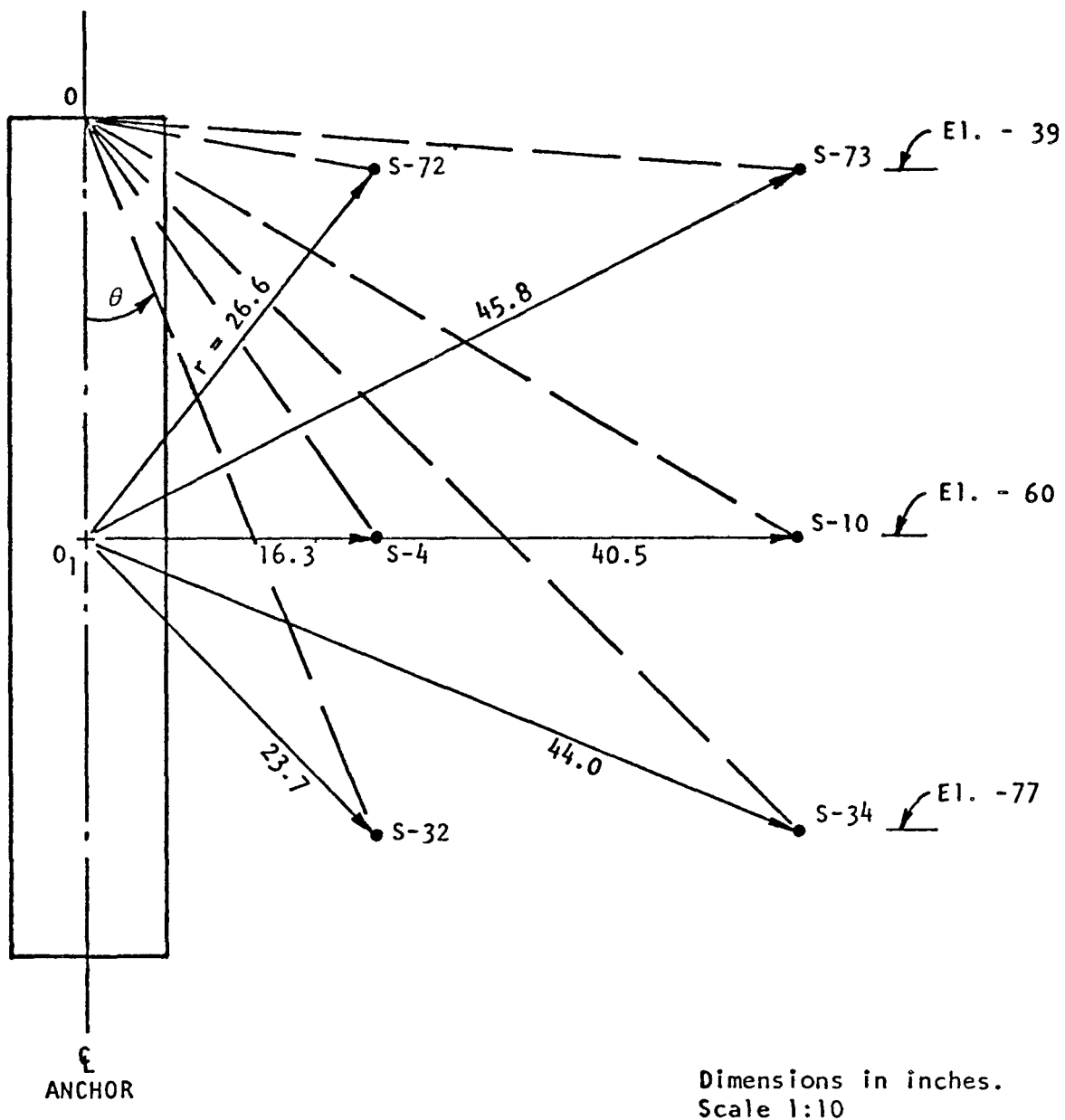
Dimensions in inches.
Scale 1:10

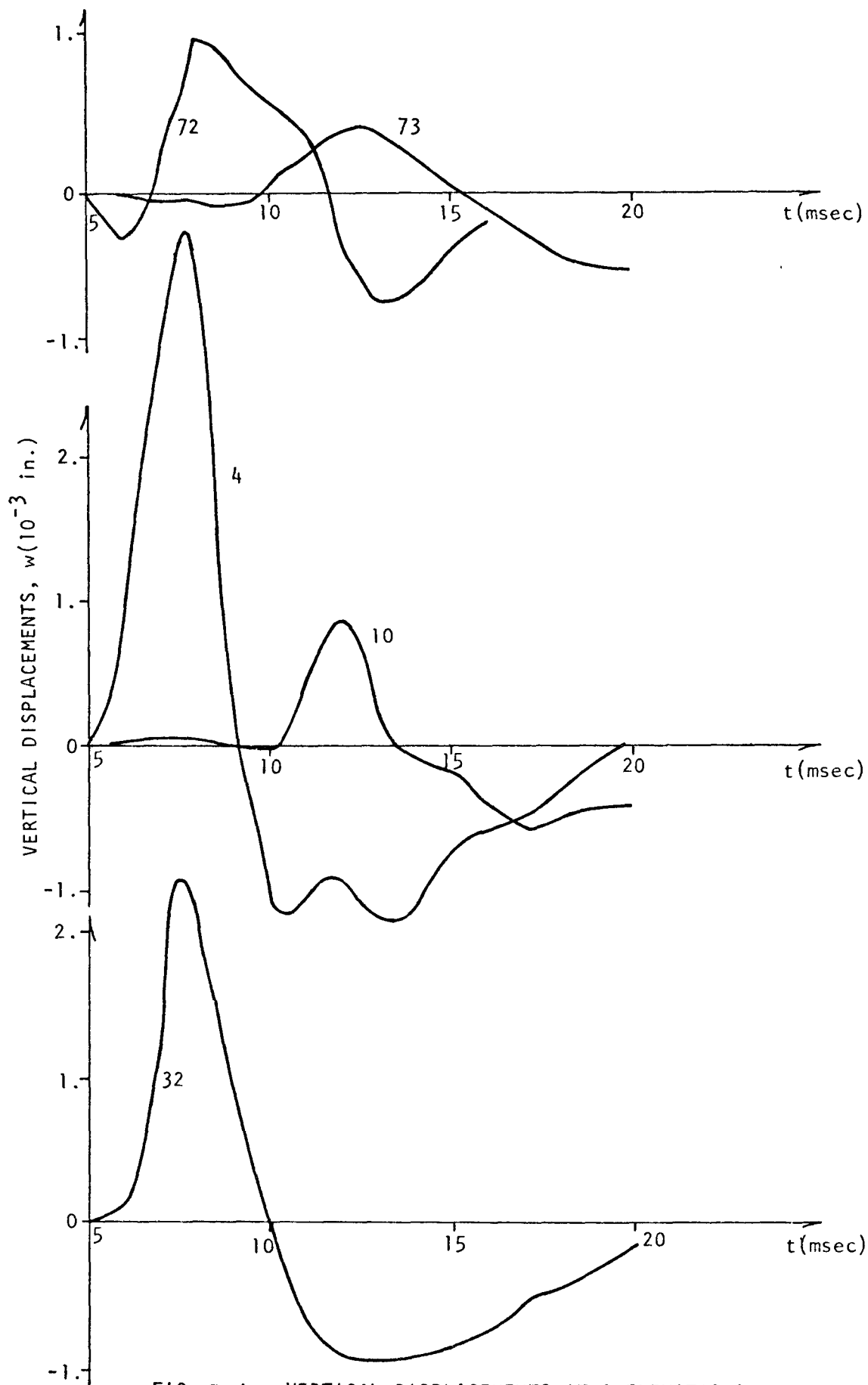FIG. G-3   SENSORS AT DIFFERENT ELEVATIONS

FIG. G-4   VERTICAL DISPLACEMENTS AT 3 ELEVATIONS
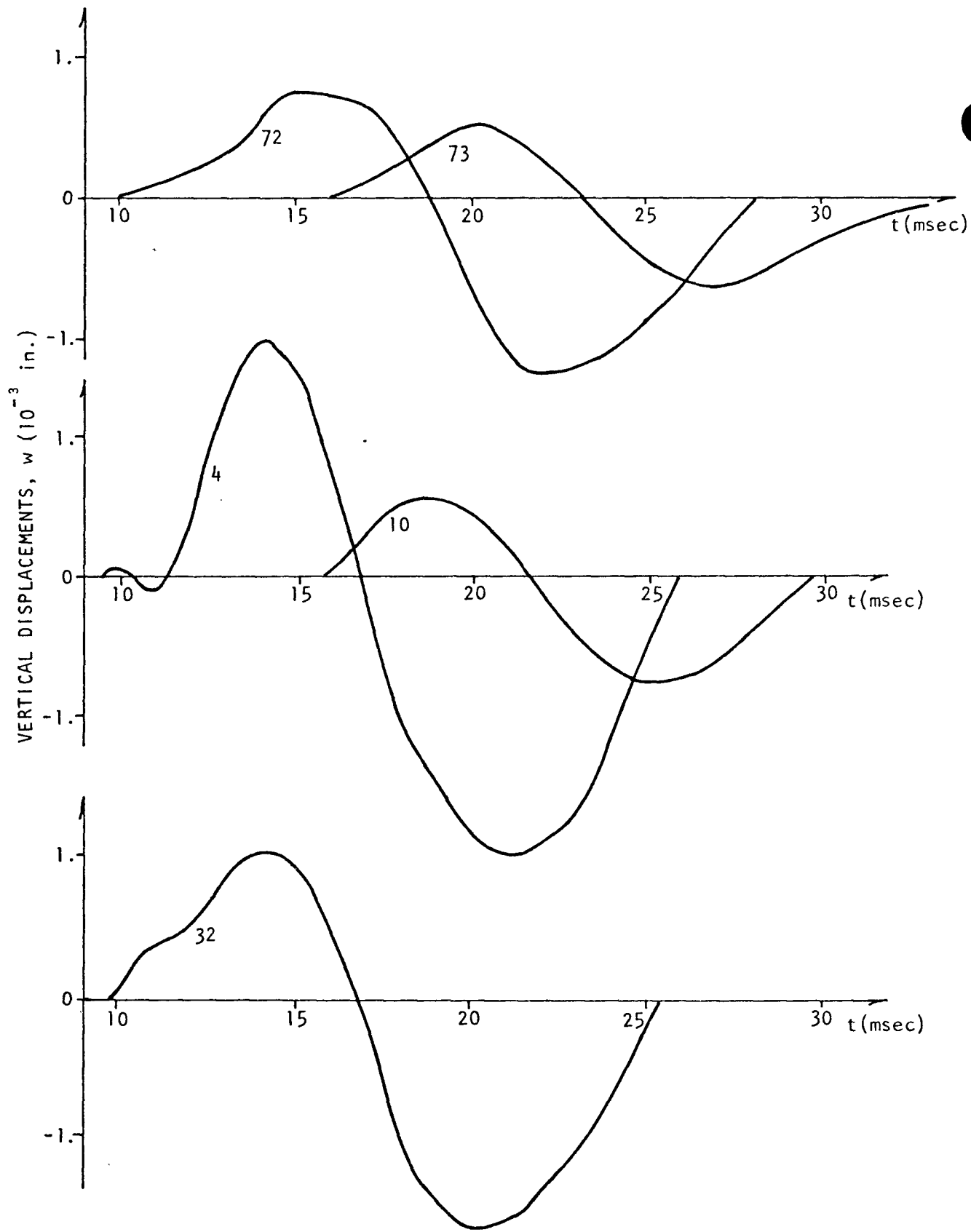TESTS 8.3 & 8.4 HYDRAULIC ANCHOR

FIG. G-5 VERTICAL DISPLACEMENTS AT 3 ELEVATIONS
TESTS 15.5 AND 15.6 PNEUMATIC ANCHOR

distribution in Fig. G-5 at five sensors is more uniform. The maximum value appears to be along the mid-depth horizontal plane. The shear velocity of the waves estimated from the travel times of the peaks is an average 416 fps for the upper sensors, and 465 fps for the middle.

The shape of the wave front cannot be disclosed from the few measurements available. However, the fact that the displacements are not similar at corresponding times for sensors at the same radial distance, from the axis of the anchor in the closer range, indicates that the front is not exactly cylindrical or plane in this zone. In the free field the front appears as a plane shape, or sphere of infinite radius. This is suggested by the records of the sensors at the 40-inch radius which show more similar time histories.

G-5 HORIZONTAL MOTION CHARACTERISTICS

As a part of the special test program, four velocity sensors, designated 40 through 44, were placed in horizontal positions directly opposite vertical sensors 3, 5, 7 and 10. These sensors shown in Fig. G-6 were located 13.6, 19.9, 28.4 and 40.5 inches from the center of the anchor respectively. By making simultaneous measurements from all horizontal sensors together with combined vertical and horizontal velocity measurements, horizontal response characteristics could not only be studied but horizontal and vertical components could be compared. Unfortunately, the most distant sensor (44) was damaged and did not work. In the absence of measurements from this sensor, for lack of many tests and because the remaining three horizontal sensors were in the complex distance range where the primary and main values were rapidly separating, interpretation of this data is at best somewhat sketchy especially the determination of consistent propagation velocity trends.
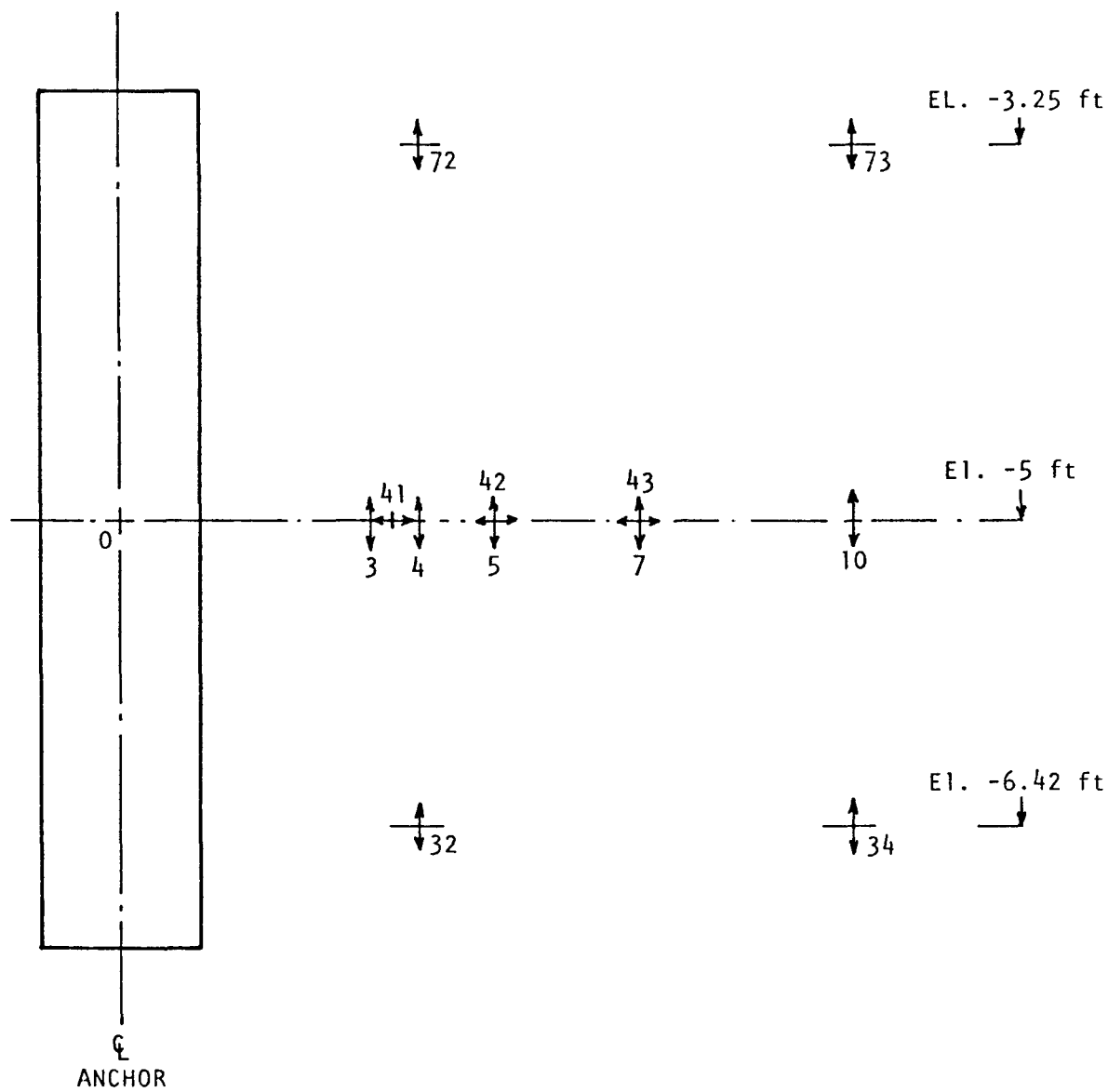
SCALE 1:10

LEGEND
SENSORS:

VERTICAL

HORIZONTAL

FIG. G-6   LOCATION OF HORIZONTAL AND VERTICAL SENSORS

For studying these data, two tests consisting of six time histories for the three couples of sensors have been normalized for time shifts and are superimposed in Fig. G-7. A clear correspondence in time of the first positive peak of the vertical sensor with the first negative peak of the horizontal sensor is observed for the three couples. Also the amplitudes are about the same. This correspondence indicates a first motion downward and away from the anchor. The velocity of propagation of this first disturbance is about 1,300 fps.

The second (positive) peak of the horizontal sensors seems to match the unloading trough or second (negative) peak shown characteristically by all vertical sensors close to the anchor. Since the trough in the vertical sensors is the combined result of the unloading pulse and the starting of a main loading pulse, there is not a well defined point in all three sensors. However, Fig. G-7 indicates that there is correspondence between times of second peaks or troughs. This velocity would be in order of 950 (fps), between sensors 3-5 or 41-42, and 1,300 (fps) between sensors 5-7 and 42-43.

It is further observed in Fig. G-8 that correspondence exists between the positive peaks at time t_1 and T_2 for couples 5 and 42, and 7 and 43; if the corresponding travel times and velocities are computed, using these points and including sensors 3 and 41, the disturbance is found to be traveling with a much slower velocity of the order of 480 fps.

A separate comparison of significant time points of the horizontal and vertical time histories was accomplished for a second series of tests. The resulting average wave velocities are summarized in Table G-1. Because the wave shapes are changing and separating rapidly at these distances, as indicated in Chapter 5, the computed velocities using station to station results are expected to vary; however, it is apparent that the
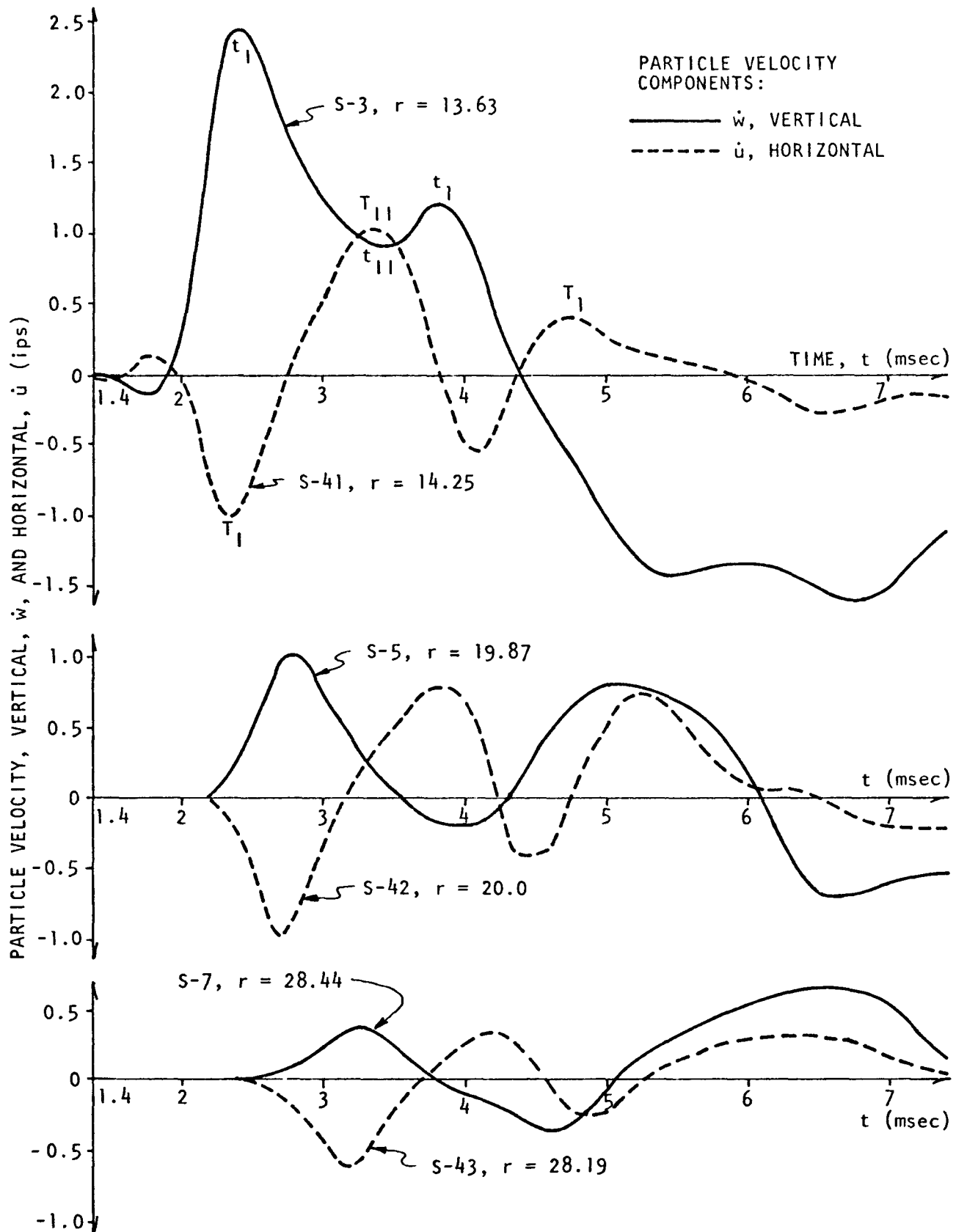
FIG. G-7 VERTICAL AND HORIZONTAL COMPONENTS OF PARTICLE VELOCITY
TIME-HISTORIES. TESTS 5.5 AND 5.6. W = 58 lb x 0.5 ft,
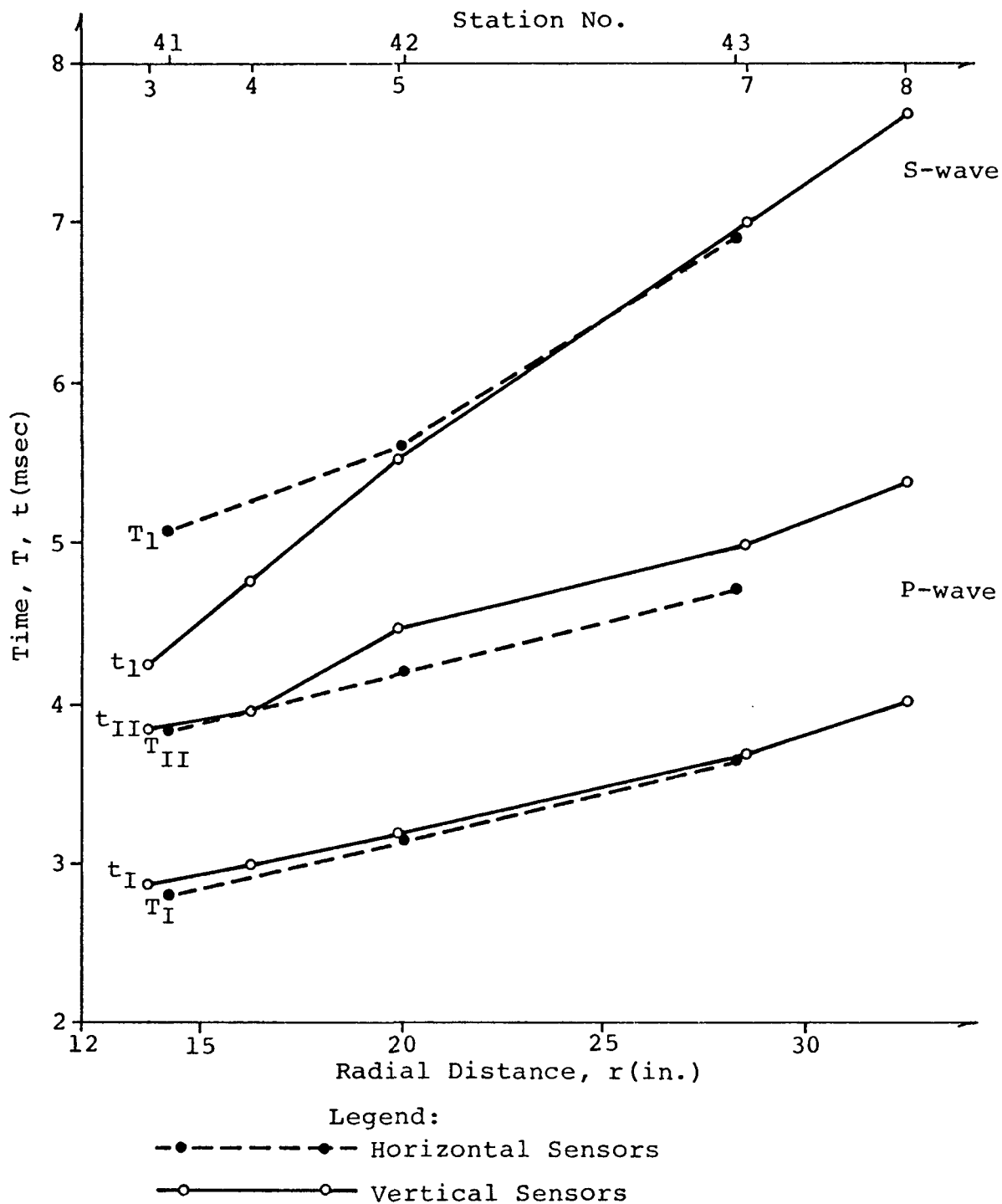σ_j = 2,500 psi.

FIG. G-8   TIME - DISTANCE PLOT
FOR HORIZONTAL AND VERTICAL
SENSORS. TESTS 5.1 to 5.4

Table G-1

Wave Velocities Computed from Tests 5.1 - 5.4

Stations Vertical- Horizontal	R_T(ft)	Wave Velocities (fps)					
		V_{tI}	V_{TI}	V_{tII}	V_{TII}	V_{tl}	V_{Tl}
3-4	.218	1,680		2,180		411	
4-5	.302	1,590		580		398	
41-42	.479		1,370		1,260		904
42-43	.681		1,390		1,340		524
5-7	.714	1,400		1,190		476	
7-8	.328	1,020				504	

first positive peak of the vertical velocity and the first nega-
tive peak of the horizontal velocity pulses travel at approximately
the same velocity of 1,400 fps. It seems that the second
significant peaks also travel at a similar velocity. The peaks
that follow, in both pulses, travel at a much smaller velocity,
which is about 450 fps. The change in velocities of these
points is illustrated by the change in slopes in Fig. G-8.

Using the same points for the tests shown in Fig. G-7, the
same approximate results or trends are obtained. Here the
velocity of first peaks is 1,300 fps, for second peaks it is
about 1,150 fps, and 400 fps for later peaks in vertical motion
and 720 fps average for horizontal motions.

Therefore, it may be concluded that the hydraulic anchor
creates both P-waves and S-waves in this region. Based on common
time points identified on both the vertical and horizontal
velocity histories, these waves travel at approximate velocities
of 1,300 to 1,400 and 450 to 700 fps, respectively, in this
close-in region. Using these velocities in Eq. 5.1 produces
values of Poisson's ratio of the order of .35 to .4.

A series of tests with horizontal velocity measurements
was also performed with the pneumatic anchor, at an internal
pressure of 140 psi. The degree of coupling of this anchor
with the soil was smaller than that corresponding to tests with
the hydraulic anchor, because the applied effective radial stress
was smaller, the contact surface was smoother and the compaction
of the backfill soil around this anchor was weaker. Therefore,
larger slippages were observed after each test.

For the pneumatic anchor, the resulting particle velocity-
time histories in horizontal and vertical direction were very
ragged and difficult to interpret. However, similar differences
in wave velocities, as found for the hydraulic anchor, determined

from corresponding peaks in the pulses, were obtained in these tests.

The periods of the same pulses in horizontal motions have been compared for the two anchors. In general, the pneumatic anchor generates pulses about four times longer than the hydraulic anchor.

The following preliminary conclusions are derived from these above observations:

a.   The main source of the precursor pulses is a primary, dilatational wave which travels two to three times faster than the shear wave.

b.   The physical characteristics of the originating energy source influence significantly the shapes of the pulses. The hydraulic anchor generates primary pulses of much higher amplitude than the pneumatic anchor possible due to, 1) better coupling with the soil, 2) the presence of wedges extending from the plates and 3) greater eccentric loading.

c.   The significant points of the pulses which indicate unloading do not lead to a significantly different wave velocity than that computed from the positive loading peaks. This data indicates that the inelastic behavior of the soils does not have an important influence on the shape of the pulses.

Because the interpretation of horizontal motions in this program was limited to a somewhat small distance range (between 13 and 28 inches from the center of the anchor), a fuller treatment of the subject was not possible. To provide greater insight into horizontal motions and P-wave characteristics subsequent horizontal measurements concurrent with vertical measurements were made at several production test sites as a

routine part of this test. This data was generally obtained
at a number of depth intervals at distances of 4, 8 and 16 feet
from the anchor. It is anticipated that this data can be
studied in future efforts.

G-6   ATTENUATION OF MOTIONS

The components of particle motions generated by impulse
tests, attenuate with distance from the source. This attenuation
is caused by geometrical spreading of the energy of the waves
and by hysteretic damping. The geometrical effect (sometimes
called geometrical damping), as recorded by an arrangement of
receiving stations, is dependent upon the shape of the wavefront
and the direction in which it propagates, relative to the
orientation of the stations. The hysteretic damping is a pro-
perty of the material through which the waves propagate and
it depends upon the strain amplitude of the motions.

Fig. G-9 summarizes the results of three series of tests
performed with the same impact energy of 58 lb x 0.5 ft. The
jack pressure was different, in each series: 2,000, 3,500 and
5,000 psi. Both P and S-pulse peak particle velocities are
plotted versus radial distance in the figure.

It is first observed that higher jack pressures lead to
higher particle velocities throughout the soil mass. This is
consistent with the fact that higher jack pressures produce
better coupling of anchor and soil, and therefore, more efficient
transmission of energy from the impact source into the soil.

Second, the attenuation rates for P-pulses are higher than
for S-pulses. In effect, the slopes of the log-log lines
representatives of the general trends of attenuation for P and
S-particle velocities are, approximately, -2.4 and -1.4,
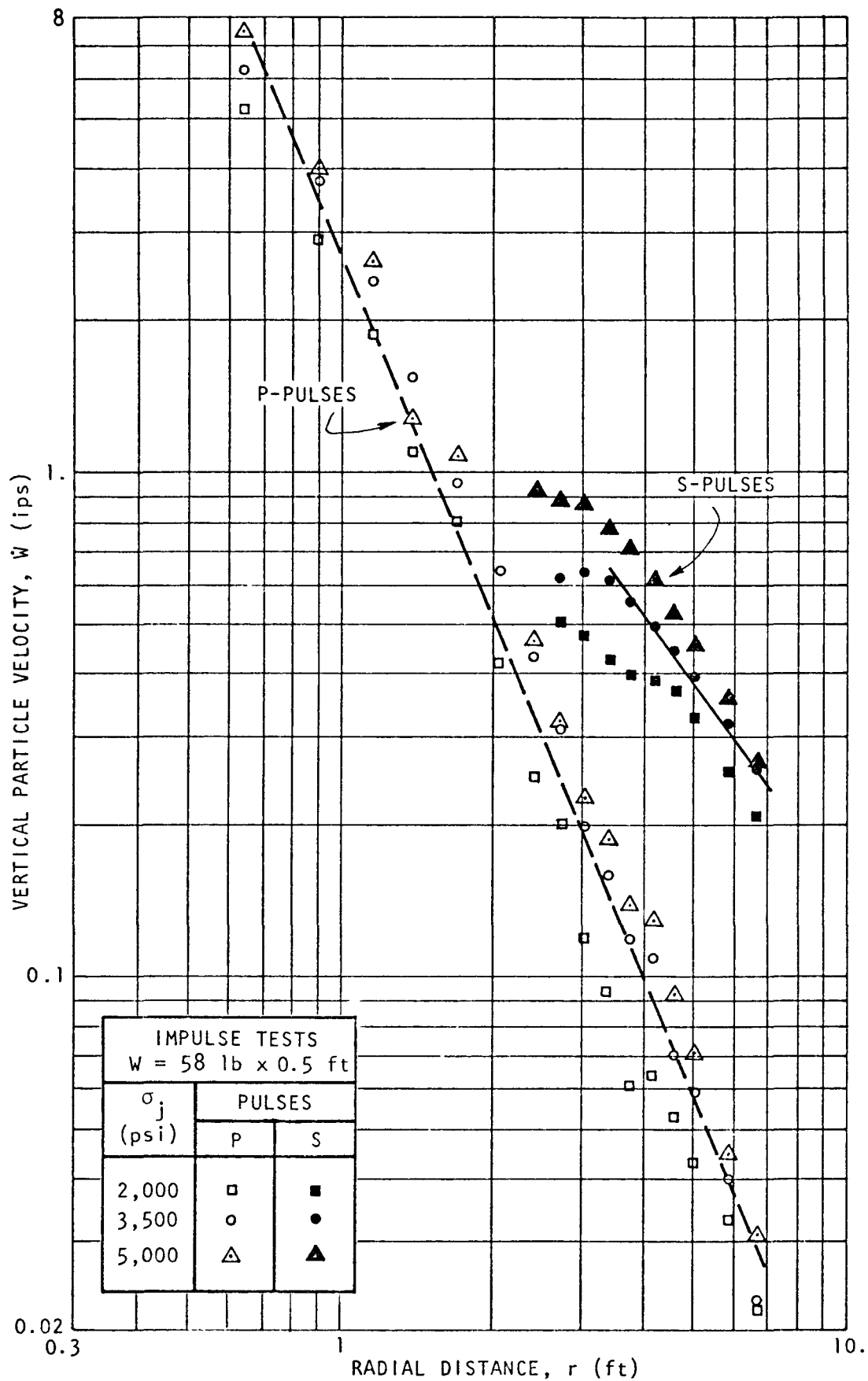respectively. Because of the superposition of pulses in the

FIG. G-9 PARTICLE VELOCITY ATTENUATION - P & S PULSES

close range, these rates of attenuation are only approximate.
The differences in the rates between P and S pulses may be due
to a different geometrical pattern of propagation of the waves.
P waves traveling in an inclined direction, outward and downward
from the source, will produce decreasing vertical components
of motions, as distance increases, in stations aligned on a
mid-depth horizontal plane. S waves may travel more preferably
in a horizontal direction, outward from the source, thus
generating predominant vertical components of motion in the mid-
depth plane.

Hysteretic damping can be estimated from the rate of
attenuation of the waves after deducting the effect of geometrical
damping from the total rate of attenuation. At this point, a
method for converting these results to a useful form for esti-
mating material damping has not yet been established. This pro-
cedure, however, introduces one possible avenue for future
work in evaluating damping in situ.